

**PHOTOSENSITIZING EFFECTS CHLORIN E6 – POLYVINYLPIRROLIDONE
FOR FLUORESCENCE GUIDED PHOTODYNAMIC THERAPY OF CANCER**

WILLIAM CHIN WEI LIM

BSc (Hons), University Malaysia Sabah

A THESIS SUBMITTED

FOR THE DEGREE OF DOCTOR OF PHILOSOPHY

DEPARTMENT OF PHARMACY

NATIONAL UNIVERSITY OF SINGAPORE

2009

This study was conducted in the Tan Chin Tuan Laboratory of Optical Imaging and Photodynamic Therapy of Cancer, National Cancer Centre Singapore and the Department of Pharmacy, National University of Singapore.

Supervisors:

Associate Professor Paul Heng Wan Sia

Associate Professor, Department of Pharmacy, National University of Singapore;
Principal Investigator, GEA-NUS Pharmaceutical Processing Research
Laboratory

Professor Malini Olivo

Principle Investigator, Laboratory of Optical Imaging and Photodynamic Therapy
of Cancer, National Cancer Centre Singapore
Principle Investigator, Biophotonics Laboratory, Singhealth
Adjunct Professor, Department of Pharmacy, National University of Singapore
Head of Bio-optical Imaging, Singapore Bioimaging Consortium, A*STAR,
Singapore

DEDICATION

To BD,

*There is no feeling more comforting and consoling
than knowing you are right next to me
in this whole journey.*

ACKNOWLEDGEMENTS

This thesis is the result of four years of work whereby I have been accompanied and supported by many wonderful people. I have now the opportunity to express my gratitude to all of them.

First, I would like to thank my advisor, Prof. Malini Olivo, for giving me the opportunity to pursue a PhD and be a part of this challenging team. Her advice and constant motivation has kept me moving forward. She has also trained me in manuscript writing, grantsmanship and all other aspects of scientific research. Prof. Malini's overall enthusiasm and integral view on research and her mission for providing only high-quality work have made a deep impression on me. I owe her lots of gratitude for having shown me this way of research.

I would like to thank Associate Prof. Paul Heng WS who kept an eye on the progress of my work, and always was available when I needed an advice. If it were not for his willingness to give me the opportunity to pursue my PhD candidature in the Department of Pharmacy, this thesis would not exist.

I would like to thank A/Prof Weber Lau from Dept of Urology, SGH and Prof Soo Khee Chee for providing valuable support from a clinician standpoint.

My thanks are also to my labmate Ms Bhuvana Shridar, who has also embarked in the pursuit of PhD together with me. Throughout the six years of working together, she has become more than just a colleague. She has not only cheerfully participated in many experiments described in this thesis but she has

also been a source of encouragement and unwavering support during my ups and downs. Your friendship is priceless and a blessing to me.

I also would like to thank my current lab members and others who have left this lab for greener pastures: Thank you to Dr Patricia Thong for valuable scientific discussions and help with experimental setup and advice; Ms Lucky Sasidharan for helping out in lab administration work during my thesis writing; Mr Kho Kiang Wei for all the help on laser light sources, Ms Karen Yee and Ms Vanaja Manivasager whom initially mentored me in cell culture and animal work, Dr Praveen Thoniyot from Singapore Bioimaging Consortium for labeling PVP with FITC, Dr Sirajudeen from Nanyang Technological University for rendering help in some of the image analysis and Dr Constance Saw for her kind friendship.

Thanks to the following students who have rendered their help throughout the course of my research work: Mr Fan Ming Wei, Mr Camillus, Ms Lim Pei Li, Ms Christine, Ms Maryam Jameelah and Mr Lin Yingbo.

Special thanks to Dr Othmar Dill from Targetmed, GmbH, Germany for numerous stimulating discussions, and Dr Manfred Haupt from Haemato-science, GmbH, Germany who provided the photosensitizer that was investigated in this study.

And last but not least, thank you to my mom, Mdm. Pomaney Chelladurai, and my dad, Mr. Chin Chee Keong for encouraging the pursuit of my education.

*William Chin
February 2009*

TABLE OF CONTENTS

DEDICATION.....	iii
ACKNOWLEDGEMENTS.....	iv
SUMMARY.....	x
LIST OF TABLES.....	xii
LIST OF FIGURES.....	xiii
GLOSSARY OF ABBREVIATIONS.....	xxi
CHAPTER 1: Literature Review.....	1
1.1 Historical perspective.....	1
1.2 Photodynamic Therapy.....	2
1.3 Photosensitizer for fluorescence diagnosis of cancer.....	5
1.4 Photochemistry and photophysics of PDT and fluorescence imaging.....	7
1.5 Current issues in PDT: Delivery of photosensitizer to mucosal tissue.....	8
1.6 Chlorins as a promising photosensitizer.....	11
1.7 Polyvinylpyrrolidone.....	13
1.8 Novel association of polyvinylpyrrolidone with chlorin e6.....	14
1.9 Experimental purpose and hypothesis.....	16
CHAPTER 2: Biodistribution And Pharmacokinetic Profile Of Chlorin e6 – Polyvinylpyrrolidone In The Murine Model.....	18
2.1 Summary.....	18
2.2 Introduction.....	20
2.3 Materials and methodology.....	24
2.3.1 Preparation of photosensitizers.....	24
2.3.2 Cell culture conditions and xenograft tumor model.....	24
2.3.3 Serum uptake of Ce6–PVP.....	25
2.3.4 Fluorescence imaging.....	26
2.3.5 Spectroscopic measurement using fiber optics-based fluorescence spectrometer.....	27
2.3.6 Determination of Ce6-PVP concentrations in tissues in mice.....	27
2.3.7 Confocal fluorescence microscopy and image analysis.....	28
2.3.8 Statistical analysis.....	29
2.3.9 Experimental design for PDT.....	29
2.3.10 Assessment of tumor response post PDT.....	30
2.4 Results and discussions.....	32
2.4.1 Fluorescence distribution in serum.....	32
2.4.2 Qualitative assessment of Ce6-PVP accumulation in MGH tumor xenograft.....	33
2.4.3 Qualitative assessment of Ce6-PVP accumulation in CNE2 tumor xenograft.....	36
2.4.4 Fluorescence imaging in normal organs in mice.....	38
2.4.5 In vivo fiber optic spectrofluorometric measurement.....	42
2.4.6 Quantitative assessment of Ce6-PVP accumulation in human nasopharyngeal tumor (CNE2) xenograft.....	45
2.4.7 A comparison of Ce6-PVP induced fluorescence quantification using image processing and tissue extraction method in human bladder tumor (MGH) xenograts.....	49
2.4.8 Comparison of fluorescence distribution of Ce6-PVP versus Ce6 only in MGH tumor and normal tissue.....	51
2.4.9 Fluorescence monitoring in skin.....	53

2.4.10 Tumor response post PDT.....	56
2.4.11 Toxicity effects.....	62
2.4.12 Correlation of Ce6-PVP uptake in serum and percentage of tumor necrosis at post PDT.....	67
2.5 Conclusion.....	69

CHAPTER 3: New formulation of chlorin e6 – polyvinylpyrrolidone shows improved selectivity and specificity for fluorescence diagnostic imaging and photodynamic therapy of human cancer.....	71
3.1 Summary.....	71
3.2 Introduction.....	73
3.3 Materials and methodology.....	75
3.3.1 Photosensitizers and chemicals.....	75
3.3.2 In vitro photosensitizing efficacy.....	75
3.3.3 Bladder tumor model.....	76
3.3.4 Cell culture.....	77
3.3.5 Chick chorioallantoic membrane (CAM) tumor xenograft.....	77
3.3.6 Fluorescence imaging and image analysis.....	78
3.3.7 Nonlinear regression and statistical analysis of fluorescence intensity.....	79
3.3.8 Statistical analysis of fluorescence image.....	80
3.3.9 Chemical extraction and spectrofluorimetry analysis.....	81
3.3.10 PDT treatment on murine xenograft model.....	82
3.3.11 Assessment of tumor response post PDT.....	83
3.4 Results and discussions.....	84
3.4.1 HPLC chromatogram of two formulations of Ce6-PVP and Ce6.....	84
3.4.2 In vitro photosensitizing efficacy.....	85
3.4.3 Biodistribution of Ce6 formulations.....	88
3.4.4 Sensitivity and specificity of Ce6 formulations.....	92
3.4.5 <i>In vivo</i> photodynamic therapy on tumor xenografts.....	94
3.4.6 Ce6-PVP induced fluorescence on human lung carcinoma.....	99
3.4.7 Ce6-PVP induced PDT on human lung carcinoma.....	106
3.5 Conclusion.....	109

CHAPTER 4: Membrane transport enhancement of chlorin e6 - polyvinylpyrrolidone and its photodynamic efficacy on the chick chorioallantoic model.....	110
4.1 Summary.....	110
4.2 Introduction.....	111
4.2.1 Theory: Fick's Law of diffusion.....	114
4.3 Materials and methodology.....	117
4.3.1 Photosensitizer preparation.....	117
4.3.2 Preparation of chick chorioallantoic membrane (CAM) tumor model.....	117
4.3.3 Administration of photosensitizer.....	119
4.3.4 Fluorescence intensity imaging on CAM tumor model.....	120
4.3.5 Statistical analysis of fluorescence image.....	121
4.3.6 Transport of photosensitizer across CAM.....	122
4.3.7 Laser confocal fluorescence microscopy.....	122
4.3.8 Photodynamic therapy of CAM model.....	123
4.3.9 Flow cytometry analysis.....	123
4.4 Results and discussions.....	125
4.4.1 Multicellular spheroids on the CAM model.....	125
4.4.2 Fluorescence imaging of Ce6-PVP in normal CAM.....	127

4.4.3 Fluorescence imaging of Ce6-PVP in CAM tumor xenografts.....	130
4.4.4 Membrane transport study.....	138
4.4.5 Fluorescence confocal microscopy imaging.....	141
4.4.6 Photodynamic therapy efficacy of Ce6-PVP.....	143
4.5 Conclusion.....	145
CHAPTER 5: Effect of polyvinylpyrrolidone on the interaction of chlorin e6 with plasma proteins and its subcellular localization.....	146
5.1 Summary.....	146
5.2 Introduction.....	147
5.3 Materials and methodology.....	149
5.3.1 Photosensitizer and serum proteins.....	149
5.3.2 Determination of photosensitizer stability using fluorescence spectrometry.....	149
5.3.3 Preparation of photosensitizer–protein complex and measurement.....	149
5.3.4 Determination of partition coefficient.....	150
5.3.5 Labelling of PVP with fluorescein isothiocyanate (FITC).....	151
5.3.6 Intracellular localization by confocal laser scanning microscopy.....	152
5.4 Results and discussions.....	153
5.4.1 Partition coefficient.....	153
5.4.2 Fluorescence properties of Ce6-PVP in various biological media.....	155
5.4.3 Effect of different plasma lipoproteins on spectral properties of Ce6 and Ce6-PVP.....	158
5.4.4 Association binding measurement.....	162
5.4.5 Subcellular localization.....	167
5.7 Conclusion.....	170
CHAPTER 6: Evaluation of clinical response of chlorin e6 – polyvinylpyrrolidone mediated photodynamic therapy of refractory bladder cancer.....	171
6.1 Summary.....	171
6.2 Introduction.....	173
6.3 Materials and methodology.....	174
6.3.1 Angiosarcoma patients.....	174
6.3.2 Bladder cancer patients.....	174
6.3.2.1 Clinical history for patient received intravenous administration of Ce6-PVP.....	175
6.3.2.2 Clinical history for patient received intravesical administration of Ce6-PVP.....	176
6.3.4 Light source and fiber positioning.....	177
6.3.5 Light irradiation.....	178
6.3.5.1 Intravenous drug administration.....	178
6.3.5.2 Intravesical drug administration.....	178
6.3.6 Laser confocal fluorescence microscopy studies.....	181
6.3.7 Analysis of serum and urine uptake.....	181
6.3.8 ELISA detection of human inflammatory cytokines.....	182
6.4 Result and discussion.....	183
6.4.1 Fluorescence imaging of angiosarcoma lesions in patients.....	183
6.4.2 Ce6-PVP mediated PDT response for refractory bladder carcinoma patients.....	186
6.4.3 Analysis of serum and urine uptake of Ce6-PVP.....	188
6.4.4 Fluorescence imaging and laser confocal microscopy study of refractory bladder carcinoma patients.....	191
6.4.5 Analysis of cytokines at post PDT.....	195
6.5 Conclusion.....	198

CHAPTER 7: Conclusion and future direction	199
7.1 Conclusion.....	199
7.2 Future perspective.....	203
BIBLIOGRAPHY.....	205
APPENDIX A: LIST OF PUBLICATIONS.....	218
APPENDIX B: LIST OF CONFERENCE PARTICIPATION.....	220
VITA.....	223

SUMMARY

Photodynamic therapy and fluorescence diagnosis of cancers can realize their full clinical potential if photosensitizers could be delivered specifically to tumor tissue at optimal rates and concentrations. An improvement of photophysical and pharmacokinetic parameters of existing photosensitizers can be achieved by either chemical or non-covalent modifications of photosensitizing molecules with polymers. In particular, polyvinylpyrrolidone (PVP), a water soluble and nontoxic polymer, is widely used to modify water solubility and bioavailability of various biologically active compounds. Thus, the photosensitizer-polymer formulation of chlorin e6 – polyvinylpyrrolidone (Ce6-PVP) was developed with the rationale of providing a new photosensitizer with a high photochemical stability, good solubility both in aqueous and in biological fluids, high affinity to the target tissue, large depth of necrosis, efficient generation of the reactive oxygen species that cause destruction of the pathologically changed tissue, low phototoxicity in normal tissue as well as to provide a method of preparation of such photosensitizer. In this thesis, photodynamic therapy consists in systemic or topical administration of Ce6-PVP that selectively accumulates in the tumor tissue of a human or an animal. Following exposure to light of 665 nm wavelength, the photosensitizer produces cytotoxic species that destroy tissues. Destruction of cells by cytotoxic species, via necrosis or apoptosis leads to destruction of the tissue. Simultaneously, the irradiation at 400 nm wavelength induces fluorescence of the photosensitizer that is a sensitive diagnostic tool suitable for detecting the regions of the body which are abnormal in terms of their structural and functional condition or where intense biological processes occur, including formation of benign and malignant neoplasms. The scope of this study includes in vitro and in vivo evaluation of Ce6-PVP formulations human tumor

xenograft in murine and chick chorioallantoic membrane (CAM) tumor model. In addition, we have investigated on how the polymer PVP has affected the mechanisms of penetration of Ce6 and its binding distribution to various lipoproteins. Using CAM as a drug transport model, we have demonstrated that the presence of PVP facilitates the transport of Ce6 across a biological membrane. This formulation has also been tested in selected patients in a pilot clinical trial to determine depth of penetration, specificity and selectivity of the photosensitizer for angiosarcoma and bladder cancer. It is hope that this new association of PVP with Ce6 with enhanced penetration, selectivity and photosensitizing properties towards cancer tissue will be developed as a potential photosensitizer in photodynamic therapy and diagnostics in the area of oncology.

LIST OF TABLES

Table 2.1 In order to study the in vivo selectivity of the photosensitizers in MGH tumor, the ratio of drug fluorescence in tumor over normal tissue were tabulated. Each time point represents a mean of 5 animals for Ce6-PVP and 4 animals for Ce6.

Table 2.2 Percentage of tumor necrosis evaluated at 48 h post PDT after treatment with Ce6-PVP using various parameters.

Table 2.3 Percentage of tumor necrosis evaluated at 48 h post PDT after treatment with Ce6 using various parameters.

Table 2.4 The survival of mice was expressed as the number of mice that recovered from treatment 24 h post treatment with Ce6 alone. Mice were subjected to various parameters such as differing drug-light intervals, fluences, fluence rates and drug doses.

Table 2.5 The survival of mice was expressed as the number of mice, which recovered from treatment 24 h post treatment with Ce6-PVP. Mice were subjected to various parameters such as differing drug-light intervals, fluences, fluence rates and drug doses.

Table 3.1 Comparison of tumor to normal tissue ratio in various organs after intravenous administration of 5 mg/kg Ce6-PVP, Ce6 or Ce6-DMSO. Ratio was calculated by dividing the fluorescence intensity span of tumor to the fluorescence intensity span of the various tissues from 1 to 6 h post drug administration. The span was tabulated using nonlinear regression analysis.

Table 3.2 A comparison of the percentage of necrotic tumor and survival of mice evaluated at 48 h post PDT after administration of 5 mg/kg Ce6-PVP, Ce6 or Ce6-DMSO with irradiation at a fluence and fluence rate of 100 J/cm² and 85 mW/cm² respectively. Each data point represents a mean of 3 – 5 animals.

Table 3.3 A comparison of areas under the ROC curves between NSCLC and SCLC at various time post drug administration.

Table 4.1 Non-linear regression of time-dependent changes in fluorescence was used to estimate the decay rate constant (K) and half-life from 1 to 5 h post topical administration of Ce6 and Ce6-PVP in MGH tumor and normal CAM. Half-life = 0.69/K; CI = confidence interval; *p < 0.0001.

Table 5.1 The influence of different concentrations of three lipoproteins on the protein binding affinity of Ce6 and Ce6-PVP.

Table 6.1 A summary of PDT treatment parameters were administered to the patients.

Table 6.2 Comparison of span, rate constant decay (K) and half-life (t_{1/2}) of Ce6-PVP in serum and urine sample from clinical patients.

LIST OF FIGURES

Figure 1.1 Principles of photodynamic diagnosis and therapy.

Figure 1.2 Molecular structure of Ce6 and PVP (C_6H_9NO) and the absorption spectra of Ce6-PVP formulations and Ce6 in 0.9% NaCl measured from 400 to 800 nm. Binding of PVP to Ce6 did not affect the Ce6 absorption spectra.

Figure 2.1 Subcutaneous injection of tumor cells onto the flank

Figure 2.2 Light irradiation procedure on mouse

Figure 2.3 Serum uptake of Ce6-PVP at various time points post drug administration. Each time point represents a mean of 5 animals \pm SE.

Figure 2.4 Upon intravenous administration of Ce6-PVP, tumor fluorescence at 2, 3, 6 and 27.5 h was observed under blue light illumination (A-D). The intensity of the fluorescence kinetics can be monitored in a fluorescence intensity distribution map, with red regions being hot spots for localization of Ce6-PVP followed by yellow and green (EH). Normal bladders of mice (arrow) were imaged at 2, 3, 4 and 6 h post drug administration (I-L) and their corresponding intensity distribution images were acquired (M-P). No fluorescence was observed at 2 and 6 h post drug administration. Mild fluorescence was observed at 3 and 6 h post administration.

Figure 2.5 Ce6-PVP macroscopic fluorescence of NPC tumor xenografted on mouse and the surrounding tissue captured at various time points.

Figure 2.6 Macroscopic white light and fluorescence imaging in skin, heart, lung, gall bladder, liver, spleen, kidney and gastrointestinal tract at 1 h post-intravenous administration of 5.0 mg/kg Ce6-PVP.

Figure 2.7 Macroscopic white light (A, C, E) and fluorescence (B, D, F) imaging in normal bladder, liver, gall bladder, and gastrointestinal tract at 6 h post-intravenous administration of 5.0 mg/kg Ce6-PVP.

Figure 2.8 Comparison of emission spectra of bladder tumor xenograft, normal bladder and muscle of the murine model at 1 and 3 h post administration of Ce6-PVP using 400 nm excitation. The spectral signatures showed a peak at the wavelength 665 – 670 nm in tumor while the fluorescence intensity of normal bladder and muscle is weaker than that of the tumor tissue.

Figure 2.9 Comparison of emission spectra in the 650 – 700 nm region using 410 nm excitation in various normal organs at 1 and 3 h post Ce6-PVP administration. Except for skin and gall bladder, it is evident that the emission spectra of normal organs were lower compared to the emission spectra of tumor.

Figure 2.10 (A) Quantification of Ce6-PVP fluorescence intensity in tumor and normal tissue in CNE2 tumor model as a function of time as determined by fluorescence imaging technique. Each time point represents a mean of at least 3

animals \pm SE. (B) The selectivity of Ce6-PVP was determined by tabulating the relative tumor to normal fluorescence ratio.

Figure 2.11 Fluorescence confocal microscopy of Ce6-PVP localization in tumors at various time points.

Figure 2.12 A comparison of fluorescence quantification using image processing and tissue extraction method. (A) Fluorescence intensity tabulated as the ratio of red to blue pixel intensity in normal (■) and tumor (●) tissue at various time points post drug administration using the fluorescence image processing technique. (B) Fluorescence intensities expressed as per gram of tissue using the tissue extraction technique. The best-fit logarithmic trend line were plotted in order to compare the correlation coefficient value between two methods of quantification. Each time point represents a mean of at least 3 animals \pm SE.

Figure 2.13 The kinetics of fluorescence intensity of Ce6-PVP (A) and Ce6 (B) in normal tissue of femoral muscle and tumor tissue at various time points post drug administration based on fluorescence image analysis. Each time point represents a mean of 5 animals \pm SE.

Figure 2.14 Fluorescence intensities of (A) Ce6-PVP, (B) Ce6 alone and (C) Photofrin measured over time in skin of Balb/c nude mice. For Ce6-PVP and Photofrin, mice were given a dose of 2.5, 3.5 and 5 mg/kg whereas for Ce6, mice were given 5 mg/kg only. Each plot represents a mean of at least 8 animals. Bars = standard deviation.

Figure 2.15 Cross-section of tumors xenografted on mice stained with Evans Blue dye at 48 h post PDT after treatment with various drug and light dose at 1 h drug-light interval.

Figure 2.16 Cross-section of tumors xenografted on mice stained with Evans Blue dye at 48 h post PDT after treatment with various drug and light dose at 3 h drug-light interval.

Figure 2.17 Short term evaluation of MGH tumor growth post PDT using various drug and light dosimetry. Mice were treated with the following parameters: Group 1 = 100 J/cm²; 85 mW/cm² at 1 h DLI, Group 2 = 150 J/cm²; 125 mW/cm² at Group 3 h DLI, 3 = 200 J/cm²; 165 mW/cm² at 3 h DLI, Group 4 = 300 J/cm²; 167 mW/cm² at 3 h DLI and Group 5 = 300 J/cm²; 167 mW/cm² at 6 h DLI. (A) Tumor volumes at 7 days post PDT and (B) tumor volumes at 14 days post PDT, with each point represent the mean of 4 animals. Bars = SE.

Figure 2.18 Cross section images of tumor and kidneys stained with Evan's Blue dye using a camera mounted on a stereomicroscope. The white area represents necrotic tissue whereas the blue area represents viable tissue. (A) The depth of necrosis in tumor was found to be around 8 mm. (B) Control tumor was administered with photosensitizer but not irradiated with light. (C) The kidney located underneath the irradiated side of the flank, showed necrosis (white line) after PDT, indicating that the depth of necrosis could reach more than 1 cm. (D) The kidney located on the opposite site of irradiation did not show any necrosis effect at post PDT. Bar = 1 mm.

Figure 2.19 Ce6-PVP induced depth of necrosis on the rat tumor model. Drug-light interval: 3 h; drug dose: 2.5 mg/kg for Rat 1 and 5 mg/kg for Rat 2; light dose: 200 J/cm² and 165 mW/cm².

Figure 2.20 Correlation of percentage of necrosis post PDT and level of Ce6-PVP in serum. The fluorescence intensity measured spectrometrically determined the level of Ce6-PVP in serum. Drug dose: 5.0 mg/kg, light dose of 200 J/cm² at 165 mW/cm². Each bar represents a mean of 3 animals. Bars = SE.

Figure 3.1 HPLC chromatogram describing the chemical purity of 75% Ce6-PVP and 99% Ce6-PVP and Ce6-Na.

Figure 3.2 (A) Representative of flow cytometry analysis of PDT induced apoptosis and necrosis for PMN blood (normal) cells (left panel) and K562 leukemic cells (right panel) after treated with Ce6 and Ce6-PVP. Induction of apoptosis and necrosis, was detected through the accumulation of Annexin – V and propidium iodide (PI) stained cells respectively. Cells were incubated with a concentration of 10 μM of either Ce6 or Ce6-PVP for 30 min before light irradiation of 1 J/cm². Three main subpopulations, corresponding to viable cells (lower left quadrant), apoptotic cells stained with Annexin – V (upper right quadrant), and dead/necrotic PI-stained cells (lower right quadrant), can be readily differentiated. (B) In terms of apoptosis, both Ce6 and Ce6-PVP demonstrated lower percentage of apoptotic cell death in PMN cells compared to K562 leukemic cells. However, Ce6 displayed higher photocytotoxicity in both PMN and K562 cells compared to Ce6-PVP, indicating the potency of Ce6. (C) When the total percentage of cell death (apoptosis and necrosis) was tabulated, Ce6 was found to induce significant cell death in PMN cells compared to Ce6-PVP, indicating toxicity to normal cells, while for K562 cells photocytotoxicity was comparable between the Ce6 and Ce6-PVP. For K562 cells, data for Ce6-PVP represent a mean value of 6 replicates while data for Ce6 represents a mean value of 3 replicates. For PMN cells, data for Ce6-PVP represent a mean value of 15 replicates taken from 5 volunteers while data for Ce6 represents a mean value of 6 replicates taken from 2 volunteers. Bars = SD. * p < 0.05 and ** p < 0.01 with respect to Ce6-PVP).

Figure 3.3 Comparison of biodistribution of Ce6-PVP, Ce6 and Ce6-DMSO in tumor, muscle and skin at 1, 3 and 6 h post drug administration respectively using chemical extraction method. For all data points, n = 4 ± SD. Statistical significance was calculated by two-way ANOVA with Bonferroni post hoc test (* p < 0.05; ** p < 0.01, *** p < 0.001 with respect to Ce6). All Ce6-DMSO data points were statistically significant with respect to Ce6.

Figure 3.4 ROC curves comparing fluorescence intensities of Ce6-PVP, Ce6 and Ce6-DMSO for classifying tumor from peritumoral muscle. The areas under the curve (AUC) were then compared in order to make a fair judgment of the effectiveness of Ce6 formulations without being constricted to single values of sensitivity and specificity, which largely depend on the cut-off fluorescence intensity value chosen to distinguish normal from malignant tissue. The closer the curve comes to the 45-degree diagonal solid line, the less accurate the fluorescence diagnostic. The following is a rough guide for classifying the

accuracy of fluorescence intensities based on the AUC: 1 – 0.9 = excellent; 0.9 – 0.8 = good; 0.8 – 0.7 = fair; 0.7 – 0.6 = poor; and 0.6 – 0.5 = fail. The AUC for Ce6-PVP, Ce6 and Ce6-DMSO were 0.98 ± 0.02 , 0.95 ± 0.05 and 0.83 ± 0.1 respectively. The ROC curves also potentially demonstrate how the fluorescence diagnostic scheme can be adjusted to obtain the desired degree of sensitivity at the cost of specificity. Ce6-PVP induced fluorescence showed the highest sensitivity and specificity in detecting tumor from peritumoral muscle.

Figure 3.5 A representative macroscopic view of whole MGH tumor xenograft stained with Evans Blue dye at 48 h post PDT after treatment at 1 h drug-light interval mediated PDT with Ce6-PVP (A) and control tumor (with Ce6-PVP, no light irradiation) (B). Necrotic tumor tissue appeared white and was almost devoid of vital staining. Shrinkage of tumor blood vessels was observed on the surface of tumor (arrow).

Figure 3.6 Extent of tumor vascular destruction following treatment with PDT post injection of Ce6 and Ce6-PVP at 1 (A, B) and 3 h (C, D) drug-light interval. The fractal dimension analysis was performed to evaluate the damage of tumor blood vessels post PDT. Shrinkage of tumor blood vessels was observed at post PDT. Control tumor with no light irradiation (E).

Figure 3.7 Preliminary analysis of tumor blood vessel fractal dimension on PDT treated tumor xenografts. Columns indicates the amount of space-filled by blood vessels; bars, standard deviation. Data analysis was only based on 1 animal for each treatment group.

Figure 3.8 Fluorescence imaging of lung cancers xenografted on the CAM model. Representative of white light images of NSCLC and SCLC grafted on CAM before administration of photosensitizer (A, C). Before incubation of Ce6-PVP, the CAM tumor xenografts were imaged under blue light illumination, to confirm that there was no autofluorescence. Tumor fluorescence images at 3 h post-topical administration of 1 mg/kg of Ce6-PVP under blue light illumination (B, D).

Figure 3.9 Fluorescence kinetics of Ce6-PVP on NSCLC (▲) and SCLC (■) xenografted on CAM examined up to 24 h post topical drug administration. Values are expressed as red-to-blue intensity ratio of fluorescence images post administration of drug normalized with images before drug administration. For tumor, each point represents a mean of 5 eggs whereas for normal (●), each point represents a mean of 10 eggs. Bars = standard error of the mean. Non-linear regression analysis demonstrated that all the curves were statistically different with each other. The elimination rate constant for NSCLC, SCLC and normal CAM was in the following order: NSCLC < SCLC < normal CAM.

Figure 3.10 Receiver operating characteristic curves illustrating the ability of Ce6-PVP to separate NSCLC (solid line) and SCLC (dotted line) from normal chorioallantoic membrane in the CAM model. The ROC curve of two indistinguishable populations (i.e. abnormal versus normal region), represented by the 45-degree line (area under the ROC curve = 0.5), is included for comparison. Area under the ROC curve was 0.82 ± 0.04 ($p < 0.0001$) and 0.70 ± 0.05 ($p = 0.0009118$) for NSCLC and SCLC respectively.

Figure 3.11 A morphologic study of NSCLC and SCLC tumor damage efficiency using the method of vital staining with Evans blue at 48 h post Ce6-PVP mediated PDT. Strong homogeneous staining was observed in the untreated controls (Fig. 5A, B), whereas in the treated tumor at 3 h drug-light interval (DLI) (Fig 5C, D) and at 6 h DLI (Fig 5E, F). Tissues damage was clearly distinguishable as an unstained area in the tumor. Drug dose: 2.0 mg/kg; light dose: 150 J/cm²; 125 mW/cm². Each data point is an average of at least 5 animals, Bars = standard error of the mean. *The mean difference is significant at the 0.05 level compared to the NSCLC group.

Figure 4.1 A diagrammatic representation of a photosensitizer transport model using CAM. The concentrations across the cells are represented in the top part of the figure. The concentration gradient across the membrane of thickness h is shown at steady state. C_g is not expected to equal C_1 unless the partition coefficient of the drug into the membrane from the donor phase is unity.

Figure 4.2 (A) Egg incubator and (B) Xenograft tumor on the CAM.

Figure 4.3 Topical administration of photosensitizer on CAM.

Figure 4.4 Xenografting of tumor spheroids on the CAM model. (A) MGH tumor (*tu*) was xenografted on the CAM. (B) Formation of neovasculature (arrow) surrounding the implanted cells after 2 days of xenografting. (C). Formation of spheroid like structure of the tumor on the CAM.

Figure 4.5 Representative images of normal CAM before and after administration of the Ce6-PVP. CAM before administration of the photosensitizer under white light and blue light mode (A-B). CAM fluorescence at 0.5, 4 and 24 h after systemic (C-E) and topical (F-H) administration of the photosensitizer.

Figure 4.6 The Ce6-PVP fluorescence kinetics on normal CAM examined up to 24 h post drug systemic administration (■) and topical administration (▼). Values are expressed as fluorescence intensities after normalization with CAM before drug administration. Each point represents a mean of 5-measurements/6 eggs/time point. Bars = SE.

Figure 4.7 Fluorescence imaging of MGH human bladder tumor xenografted on the CAM model. (A) White light image of the tumor before drug administration, (B) Ce6-PVP induced red fluorescence in tumor imaged under blue light illumination at 3 h post drug administration. Minimal fluorescence was observed in the adjacent normal CAM. (C) By displaying the fluorescent image in a pseudo color using simple image processing technique, a clear discrimination of the tumor border can be visualized.

Figure 4.8 The Ce6-PVP fluorescence kinetics on normal CAM (●) and bladder tumor cell xenografts on CAM (■) plotted against time. The CAM was topically incubated with the drug for 30 min prior to the fluorescence measurement. A logarithmic trendline (solid line) was used to best fit a curve to the data. Higher fluorescence intensity was observed in the tumor xenografts compared to the normal CAM tissue. Each point represents a mean of 7 eggs. Bars = SE.

Figure 4.9 A scatter plot comparing the fluorescence intensity in tumor and the adjacent normal CAM tissue was compiled from 1 – 5 h post topical drug administration. The points on the scatter plot are normalized individual measurements from 24 eggs. The dotted line is the cut-off fluorescence intensity threshold derived from the ROC curve to classify tumor from normal tissue with a sensitivity and specificity of 70.8% (95% CI 48.9% to 87.4%) and 83.3% (95% CI 62.6% to 95.3%) respectively.

Figure 4.10 (A) Representative images of MGH tumor (tu) xenografted on the CAM under white light. (B) Selective red fluorescence was observed on the MGH tumor at 3 h post topical administration of Ce6-PVP while no fluorescence was observed on the normal CAM tissue. (C) Receiver operating characteristic (ROC) curves illustrating the ability of various drug dose of Ce6-PVP to separate MGH tumor from adjacent normal chorioallantoic membrane ($p < 0.0001$). The ROC curve of two indistinguishable populations (i.e. tumor versus normal region), represented by the 45-degree line (area under the ROC curve = 0.5), is included for comparison. Area under the ROC curve was 0.83 ± 0.02 , 0.78 ± 0.02 and 0.79 ± 0.03 for 0.0625 and 0.0313 and 0.016 mg/mL respectively. The y axis represents the specificity of the Ce6-PVP induced fluorescence and the x axis represents the sensitivity of the Ce6-PVP induced fluorescence.

Figure 4.11 Optical coherence tomography (OCT) imaging of the CAM. OCT is a high-resolution noninvasive imaging technique based on laser interferometry, used to assess CAM thickness. The chorionic epithelium, mesoderm and allantoic epithelium layers can be visualized in the OCT structural image. The thickness of the CAM was estimated to be around $100 \pm 1.9 \mu\text{m}$.

Figure 4.12 Drug transport study comparing Ce6 and Ce6-PVP in the CAM model. (A) Uptake studies of Ce6 and Ce6-PVP in the receptor chamber, (B) comparison of diffusion coefficient of Ce6 and Ce6-PVP across the CAM. $*p < 0.05$ and (C) uptake studies of Ce6 and Ce6-PVP in the chick embryo.

Figure 4.13 Fluorescence confocal microscopy imaging in the CAM. Different increase in fluorescence on CAM treated with Ce6 or Ce6-PVP captured by confocal microscopy and its corresponding topographical contouring image. Confocal images of (A) CAM with no photosensitizer showed some autofluorescence; (B) CAM incubated with Ce6 for 2 mins showed a minimal fluorescence; and (C) CAM incubated with Ce6-PVP for 2 mins showed a 14-fold fluorescence increase after correction for background autofluorescences. Scale bar, 100 μm .

Figure 4.14 CAM with bladder tumor xenografts after topical administration of Ce6-PVP (0.625 mg/mL) and exposed to increasing light doses (1, 10, 15 and 20 J/cm^2) at 665 nm. The efficacy of Ce6-PVP mediated PDT for eradication of bladder tumor in the CAM model seems to be inversely proportional to the light dose used. $*p < 0.05$ compared to 1, 15 and 20 J/cm^2 .

Figure 5.1 Partition coefficients of the Ce6 and Ce6-PVP between 2-octanol and PBS at various pH values.

Figure 5.2 Graphs showing representative emission spectra of Ce6-PVP in (A) water, (B) PBS (C) 5% fetal calf serum (D) 10% fetal calf serum at room temperature assessed as a function of time (from 0 to 27 days).

Figure 5.3 The effect of (A) water, (B) phosphate buffered saline (PBS), (C) 5% fetal calf serum (FCS) and (D) 10% fetal calf serum (FCS) on the emission intensity of Ce6-PVP (0.5 mg/mL) at room temperature (RT 21 °C) (■), 37 °C (▲) and 4 °C (▼) for a period of up to 27 days. Each data point represents the average of 3 measurements. Experiments were repeated twice and showed similar trends.

Figure 5.4 The fluorescence emission spectra of Ce6 dissolved in saline with (A) HDL, (B) LDL and (C) VLDL at concentrations of 0% (red), 0.005% (green) and 0.05% (blue). The fluorescence emission spectra of Ce6-PVP dissolved in saline with (D) HDL, (E) LDL and (F) VLDL at concentrations of 0% (red), 0.005% (green) and 0.05% (blue).

Figure 5.5 The equilibrium titration of Ce6 (■) and Ce6-PVP (▼) in various lipoprotein buffer solutions at pH 7.0. Low concentration (0.01mg/mL) of the photosensitizers combined with (A) HDL, (B), LDL and (C) VLDL and high concentration (0.06 mg/mL) of the photosensitizers combined with (D) HDL, (E), LDL and (F) VLDL. Curves were fitted and constants derived from one site binding equation and are presented in the main text. Y axis units are relative fluorescent units per mL of the solution. On graphs (A) and (F) trendlines are not presented for some of the data sets because the data did not fit in the binding equation.

Figure 5.6 MGH cells were incubated with PVP-FITC (green) for 30 min and co-stained (A) rhodamine-phalloidin (red) and, (B) DAPI (blue). Cells were also incubated with (C) Ce6 (red) and (D) Ce6-PVP (red) for 30 min and and co-stained with rhodamine-phalloidin (yellow).

Figure 5.7 Determination of Ce6 and Ce6-PVP fluorescence intensities distribution in MGH cells by image analysis. Each bar represents average intensities of 10 cells divided by the area of the cell. Error bars represent the standard error of the mean.

Figure 6.1 (A) Ultrasound image of the position of the fiber tip (white arrow) and balloon (red arrow) in the bladder (red circle). (B) Schematic diagram of the intensity output of the fiber for various bladder volumes was prepared for the clinician.

Figure 6.2 White light image (A) and its corresponding fluorescence image (B) of angiosarcoma lesion and the surrounding normal skin at 3 h post intravenous administration of Ce6-PVP. Spectra kinetic of Ce6-PVP intensity at 1 hr (C) and 3 hr (D) in normal skin and angiosarcoma lesions from patient. The fluorescence spectra from the cancerous lesion were found to be higher than the surrounding normal skin.

Figure 6.3 Scatter plot of red-to-blue intensities in normal skin and angiosarcoma lesions plotted against time from 3 patients after intravenous administration of

Ce6–PVP. Red fluorescence from the cancerous lesion was found to be higher than the surrounding normal skin.

Figure 6.4 Urine sample collected before and after PDT from patient given intravenous administration of Ce6-PVP. Blood was observed after 24 h post treatment. There was no blood detected at 48 h post treatment.

Figure 6.5 Emission spectra of Ce6-PVP in serum at 1 h post drug administration, recorded with a spectrophotometer after excitation at 400 nm. Ce6-PVP was not detected in the serum of patient that received intravesical administration (red line), indicating that no systemic absorption of the photosensitizer was observed.

Figure 6.6 Uptake kinetic of Ce6-PVP in serum (A) and urine (B) from patient after intravenous administration as determined using spectrofluorimetry. Fluorescence emission was measured from 665 nm – 670 nm ($\lambda_{\text{ex}} = 400 \text{ nm}$). For urine, triplicates sample/time point was analysed for each data point while for serum, 4 replicates/time point for each data point were analysed.

Figure 6.7 Representative images of optical detection of human bladder carcinoma using Ce6-PVP as a fluorescent marker. (A) Normal bladder under white light illumination and (B) its corresponding image taken using blue light excitation. (C) Carcinoma of the bladder under white light illumination and (D) its corresponding image using HAL fluorescence cystoscopy (B). Lesion was clearly visualized under blue light.

Figure 6.8 Laser confocal microscopy and histopathology of cross section of biopsy sample of bladder wall. Laser confocal microscopy of cryo-section of bladder biopsy; images show Ce6 fluorescence for acute and chronic inflammation (A), low grade papillary urothelial carcinoma (B) and high grade papillary transitional cell carcinoma C). Bar = 100 μm .

Figure 6.9 Fluorescence kinetics of different histopathological grades of bladder biopsies. Error bars represent the standard error of the mean of 6 patients.

Figure 6.10 Cross section of fluorescence image (A, B) and corresponding hematoxylin–eosin-stained image (C, D) and measurement of fluorescence intensity and depth of penetration of Ce6-PVP (E, F) in bladder tumor biopsy tissue at 2 h after oral administration of Ce6-PVP.

Figure 6.11 Serum cytokines (IL-1 β , IL-8, IL-10, IL-12, IFN- γ and TNF- α) levels after PDT. Serum samples were obtained before PDT and 24 h post PDT for patient treated with intravenous mediated PDT (A – F). Results are presented as average of duplicate experiments.

Figure 6.12 Comparison of IL-6 for patient treated with intravenous or intravesical Ce6-PVP mediated PDT. Results are presented as average of duplicate experiments.

GLOSSARY OF ABBREVIATIONS

AMD = Age macular degeneration

ALA = 5-aminolevulinic acid

BPD-MA = benzoporphyrin derivative monoacid ring A

Ce6 = Chlorin e6

CAM = Chick chorioallantoic membrane

CI = Confidence interval

CIS = Carcinoma *in situ*

EA = Embryo age

CCD = Charge-coupled device

CLSM = Confocal laser scanning microscopy

DMSO = Dimethyl sulfoxide

FCS = Fetal calf serum

HBSS = Hank's buffered saline solution

HSA = Human serum albumin

HPMA = N-(2-hydroxypropyl) methacrylamide

LCLC = Large cell lung carcinoma

NSCLC = Non small cell lung carcinoma

NMP = N-methyl-pyrrolidone

MACE = Mono-L-aspartyl chlorin e6

MTT = 3-(4,5-dimethylthiazol-2-yl)-2,5-diphenyltetrazolium bromide

OSCC = Oral squamous cell carcinoma

PI = Propidium iodide

PVP = Polyvinylpyrrolidone

PDT = Photodynamic therapy

PBS = Phosphate buffered saline

ROS = Reactive oxygen species

SOSGR = Singlet oxygen sensor green reagent

SCLC = Small cell lung carcinoma

SCID = Severely combined immuno-deficient

CHAPTER 1

Literature review

1.1 Historical perspective

Light alone or in combination with chemical compounds has been used for a long time to induce therapeutic effects. Light was used in ancient India, China and Egypt for the treatment of vitiligo and light alone was often used for the treatment of psoriasis [1; 2]. However, the first experimental evidence of photosensitization was reported around the turn of the last century from von Tappeiner's laboratory in Munich; one of his medical students, Oscar Raab, observed that low concentrations of acridines in the presence of light could be lethal to the protozoan paramecium [3]. Thus, the term 'photodynamic reaction' was coined for such reactions in the presence of molecular oxygen. Today, photodynamic therapy (PDT) is an approved treatment modality against some forms of cancers, precancerous lesions and age-related macular degeneration (AMD). The earliest attempts to exploit the phenomenon of photosensitization for potential antitumor therapy were made by Jesionek and Tappeiner by light exposure of tumor in the presence of eosin [4]. The modern interest in PDT as a treatment modality for cancer therapy began around 1960 with Lipson et al. and Schwartz et al., who used a fluorescent tumor-localizing mixture of porphyrins termed 'haematoporphyrin derivative'. Since their pioneering work, compounds including photofrin, purpurins, xanthenes, phthalocyanines, oxazines, cyanines, chlorines and others have been tested in vitro and in vivo with some degree of success; however, in the clinical setting, porphyrins or porphyrin-related compounds continue to form the bulk of the photosensitizers used in PDT.

1.2 Photodynamic therapy

Photodynamic therapy (PDT) is a treatment modality for premalignant and malignant conditions that depends on the dynamic interaction of light, oxygen, and a photosensitizer to induce oxidative damage in target tissues [5]. PDT has emerged as a promising modality for the treatment of cancer [6]. The molecular and pharmacological basis for photodynamic therapy is well known [7].

Essentially, the therapeutic effect is mediated through the generation of reactive oxygen species (ROS), a process dependent on the intracellular interaction of the photosensitizer with light and oxygen. ROS generated by this photochemical mechanism have an irreversible damaging effect on tumor cells. The specificity and selectivity of the photosensitizer is mainly based on its mechanism of accumulation in cellular or vascular compartments of the tumor and clearance from its normal cells. PDT is now well established as a clinical treatment modality for the treatment of lung, esophagus, bladder, skin and head and neck cancers [3; 8; 9]. It involves the administration of a photosensitizer, followed by light irradiation in the presence of molecular oxygen in the target tissue. The combined action of these results in the formation of singlet oxygen, which is thought to be the main mediator of cellular death induced by PDT [7; 8]. In addition, fluorescence diagnosis based on the accumulation of the photosensitizer which emits fluorescence upon light excitation, is also emerging as a promising tool for the detection of small or poorly differentiated neoplastic

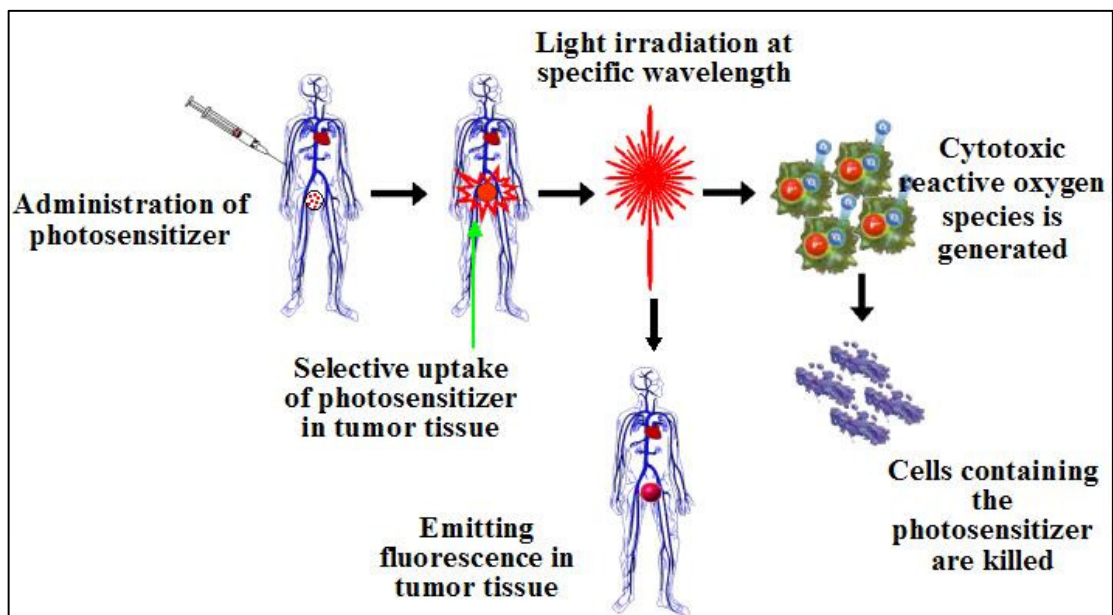


Figure 1.1 Principles of photodynamic diagnosis and therapy

changes. The significance of PDT is that there is a degree of treatment selectivity that allows tumor destruction with minimal involvement of healthy tissue. This is achieved by a combination of selective accumulation of photosensitizer within the tumor and by control of the light geometry and illumination parameters [10].

Many new generations of photosensitizers are being introduced and discovered regularly. Photosensitizers can be categorized by their chemical structures and origins. In general, they can be divided into three broad families: (i) porphyrin-based photosensitizers (e.g., Photofrin, 5-aminolevulinic acid (ALA), benzoporphyrin derivative monoacid ring A (BPD-MA), (ii) chlorophyll-based photosensitizers (e.g., chlorins, purpurins, bacteriochlorins), and (iii) dyes (e.g., phthalocyanine, naphthalocyanine) [2, 12]. With the advent of improved photosensitizers and the availability of information from well-controlled, randomized phase III clinical trials, PDT has gained a niche in the

comprehensive cancer care regime [13], 14]. The most widely used sensitizer in PDT is haematoporphyrin derivative with Photofrin being approved in U.S., Japan, Canada and eleven European countries [15]. However, these complex mixtures of porphyrin oligomers have substantial limitations. This has led to a search for improved photosensitizers, thus allowing production of a second and third generation of efficient photosensitizers. Such photosensitizers are actively being sought among chlorin, bacteriochlorin, purpurin, benzoporphyrin, texaphyrin, etiopurpurin, naphthalocyanine, phthalocyanine and perylenequinones derivatives.

1.3 Photosensitizer for fluorescence diagnosis of cancer.

As with most cancers, early diagnosis is critical to achieve favorable prognosis. Currently, surveillance biopsy is the existing gold standard for the identification of lesions in pre-neoplastic conditions. However this method is prone to sampling error, time-consuming, subjective and cost-inefficient. A diagnostic method that could provide rapid, automated classification of cancer lesions would increase the efficiency and comprehensiveness of malignancy screening and surveillance procedures. A variety of optical techniques have recently been utilized for the diagnostic study of cancerous tissue. These include fluorescence spectroscopy [16], Raman spectroscopy [17], light scattering spectroscopy [18], and Fourier-transform infrared spectroscopy [19]. These optical spectroscopic techniques are capable of providing both biochemical and morphological information within short integration times, and may be adapted for automated diagnosis on intact tissue. However, in order to be useful as a comprehensive screening procedure, the optical technique must allow rapid real time imaging of a large area of tissue rather than point by point measurements, such that suspicious regions could be identified accurately and biopsied for histopathologic correlation [20].

With the advent of molecular probes, imaging methods such as ultrasound, microCT (Computed Tomography), microMRI (Magnetic Resonance Imaging), and microPET (Positron Emission Tomography) can be conducted not only to visualize gross anatomical structures, but also to visualize substructures of cells and monitor molecular dynamics [21]. Imaging of endogenous or exogenous fluorochromes has several important advantages over other optical approaches for tumor imaging. This imaging technique relies on fluorochrome induced fluorescence, reflectance, absorption or bioluminescence as the source of

contrast, while imaging systems can be based on diffuse optical tomography, surface-weighted imaging, phase-array detection, intensified matrix detector and charged-coupled device camera detection, confocal endomicroscopy, multiphoton imaging or microscopic imaging with intravital microscopy [22] [23]. Fluorescence ratio imaging is a method widely used for optical diagnosis of cancer after administration of a photosensitizer [24] [25]. Enhanced contrast between tumor and adjacent normal tissue can be obtained based on calculating the ratio between red intensity of the photosensitizer (600–700 nm) over the blue/green intensity of the back-scattered excitation light or tissue autofluorescence (450–550 nm). Many investigations have confirmed good agreement with the histopathological extent of the tumor, implying that this technique can be applied as a useful tool for indicating tumor boundary [26].

A number of fluorochromes such as fluorescein, toluidine blue, cyanine dyes and indocyanine green have been described with variable stabilities, quantum efficiencies, and ease of synthesis. However, most of the fluorochromes are not tumor specific and are rapidly eliminated from the organism. Chemically and endogenously synthesized fluorochromes such as porphyrin-based photosensitizers have properties that may be utilized both experimentally and clinically. Porphyrins have been known to naturally localize in malignant tissue where they emit light when irradiated at certain wavelengths, providing a means to detect tumor by the location of its fluorescence. However, one of the major limitations is its relative long half-life causing prolong skin photosensitivity. Moreover, the porphyrin's core absorbs light too short for optimal penetration in tissue. However, by reducing a pyrrole double bond on the porphyrin periphery, a chlorin core compound can be generated with a high absorption at longer

wavelengths of 660 – 670 nm that can penetrate deeper in human tissue than those of porphyrins.

1.4 Photochemistry and photophysics of PDT and fluorescence imaging

With the advent of quantum theory and modern photochemistry, it has become obvious that the rate-limiting factor in the success of a photodynamic reaction is the inherent ability of the photosensitizer to get excited to a higher, long-lived energy rich triplet state upon exposure to light. Organic photosensitizers exist in the ground state in the dark with no unpaired electron spin; however, upon absorption of a photon, an electron in the sensitizer shifts to a higher orbit that could undergo fast spin inversion to generate the triplet state containing two unpaired electrons (type I reaction) [27]. In this metastable state, the photosensitizer could then collide with molecular oxygen with the subsequent transfer of energy (type II reaction) and the return of the photosensitizer to the ground state to start another round of excitation.

The type II reaction results in the formation of a highly toxic activated oxygen molecule, singlet oxygen ($^1\text{O}_2$), with a very short lifetime (< 40 nsec) in biological systems and a short radius of action (< 0.02 μm) [28]. Depletion of molecular oxygen at the site of the photodynamic reaction during high-fluence rate irradiation has been reported to counteract the effectiveness of PDT. However, the major impediment to this is the fact that light delivered at high fluence rates generates $^1\text{O}_2$ at a rate that depletes molecular oxygen faster than can be replenished, thereby limiting the cellular and tissue damage derived from $^1\text{O}_2$ [29].

One of the strategies under investigation to circumvent this problem is by using fractionation of the excitation light. This has been observed to allow for re-oxygenation during dark periods has been shown to increase the effectiveness of PDT under some conditions. Another factor that limits the efficacy of PDT is the diverse optical property of tissues, which influences the penetration depth of activating light, its scattering and absorption properties as well as the intensity of light that can be tolerated to produce only non-thermal effects [28]. The penetration of visible and near-infrared light as a function of wavelength of light through bovine muscle has been described in terms of the 1/e depth (approximately 37% of the incident light density). The depth of penetration doubles from the 4 mm observed between 500 and 600 nm to 8 mm at 800 nm, which defines the 600 – 800 nm range where light penetration is most effective. Biological effects can still be observed at two to three times the 1/e depths, which correspond to 3 – 10% of the incident light intensity and a depth of penetration of nearly 2.5 cm.

Thus, for an optimal photodynamic effect, the prerequisites are: (i) optimal concentration of the photosensitizer; (ii) abundant supply of molecular oxygen; and (iii) delivery of light at a fluence rate that allows for resupply of molecular oxygen within the target tissue.

1.5 Current issues in PDT: Delivery of photosensitizer to mucosal tissue

Currently, the main photosensitizers used in the clinical setting belong to the porphyrin sodium family [30]. They are a highly complicated chemical composition, containing porphyrin elements, whose coupling is secured by ether bondings (simple and complex polyhaemoporphyrinether PHP). However, the stability of this

preparation is not sufficient. It tends to develop macroparticles, which can be explained by the fact that ether bonds easily break up when stored at room temperature. Consequently, the preparation needs to be stored and transported under cool conditions only. One of the most important features of porphyrin is its intensive absorption peaks, both in the UV and in the visible (red and green) spectrum, which is particularly important for PDT. However, the extinction coefficient is relatively low and therefore a high concentration of the preparation is needed for a successful PDT. Its usage has been hampered by the potentially serious and prolonged skin photosensitivity due to the long half-life of the drug in the body after intravenous administration [31]. Even though the photosensitizer has preferential uptake in the tumor cells after intravenous administration, extensive distribution of the photosensitizer to other non-targeted area is unavoidable.

Topically applied photosensitizers are preferred for dermatological, oral and bladder PDT because of the reduced risk for prolonged skin photosensitivity, which is often the case after systemic administration. This form of delivery appears to offer a series of advantages, including localized treatment area, quick and easy removal of the dosage form, relatively good drug absorption, and satisfactory patient acceptance and compliance. Even so, the conventional topical formulation has its limitation because of the difficulty in reaching therapeutic levels due to impediment in penetration effect of the photosensitizer in deep-seated tumors. The varying degrees and depths of the tumors might contribute to the large variation in the distribution of the photosensitizer and thus could be one of the reasons for the poor tumor response observed in most clinical trials of PDT. Limited penetration depth of photosensitizer such as ALA

might pose a risk of not accurately recognizing the infiltration depth of solid tumors [41]. Therefore, the results of ALA mediated PDT in invasive cancers are less satisfactory, mainly because the PDT effect is too superficial [42]. Therefore, there is a need for the development of an effective topical drug delivery system to overcome these problems.

1.6 Chlorins as a promising photosensitizer

Chlorins are reduced forms of porphyrins. The core of porphyrin is oxidatively stable, which has allowed for numerous derivatives to be prepared and examined. However, the porphyrin's core absorbs wavelengths of light too short

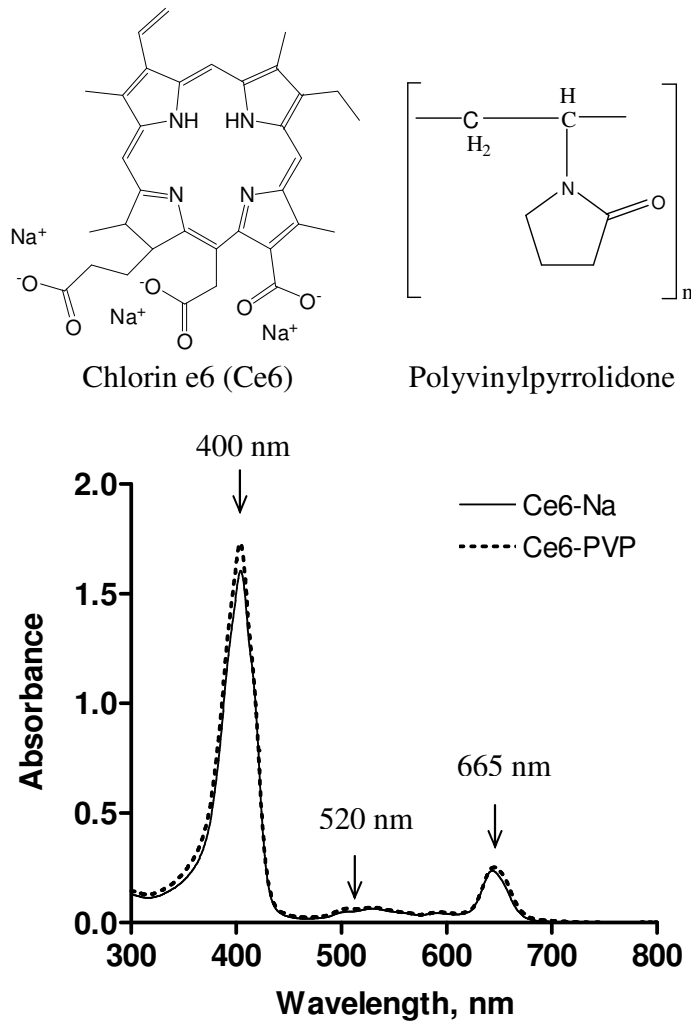


Figure 1.2 Molecular structure of Ce6 and PVP (C₆H₉NO) and the absorption spectra of Ce6-PVP formulations and Ce6 in 0.9% NaCl measured from 400 to 800 nm. Binding of PVP to Ce6 did not affect the Ce6 absorption spectra.

for optimal penetration in tissue. The reduction of a pyrrole double bond on the porphyrin periphery gives the chlorin core a high band I absorption at longer wavelengths of 650-670 nm than those of porphyrins and yet remaining efficient in generating singlet oxygen. Chlorins are actively being investigated for their photodynamic activity in cancer treatment. These photosensitizers have improved efficacy and have lesser known side effects compared to first generation photosensitizers from porphyrin derivatives. The advantages of this group of photosensitizers are: (i) they exhibit deeper penetration of PDT induced necrosis as their absorption wavelength is at the “phototherapeutic window” of 600 - 670 nm, where meaningful PDT activity can be achieved without the interference of absorption by endogenous biomolecules, (ii) they accumulate preferentially in the tumor rather than in normal tissue, and (iii) they clear faster from the skin. Chlorins also exhibit a large extinction coefficient in the red region of the visible spectrum that is one order of magnitude higher than the corresponding extinction coefficient for porphyrins [47]. In addition, it has been shown that molecules with a chlorin-type structure are able to sensitize the generation of singlet oxygen with a high quantum yield [48]. The more widely used chlorin derivatives are tetrahydroxyphenyl chlorin (mTHPC, Foscan) and monoaspartyl-Ce6 (NPe6).

Water-soluble derivatives of chlorophylls were first introduced as potential photosensitizer by E. Snyder (USA) in 1942. Since then, several chlorins based water soluble preparations have been developed [43, 44]. Of particular interest among the evaluated chlorin is the naturally occurring Ce6 [45]. Ce6 has improved efficacy and has decreased side effects compared to first generation photosensitizers from hematoporphyrin derivatives. It is also known to

preferentially accumulate in tumor tissue, exhibiting a deeper penetration of PDT induced necrosis since its absorption wavelength is between 600 – 670 nm. In addition, Ce6 exhibits a faster clearance from skin tissue. A number of other Ce6 derivatives, including mono-L-aspartyl chlorin e6 (MACE), diaspartyl Ce6, monoseryl Ce6 and other amino acid derivatives, exhibit a better retention ratio in tumors and sensitize the photodynamic destruction of tumors better than Ce6 itself [46]. Subsequently, MACE was patented as prospective photosensitizer for clinical PDT in Japan.

Various approaches were undertaken to improve tumor targeting and selectivity of chlorin-based photosensitizers. Bachor *et al.* reported that in comparison to free Ce6, conjugation of Ce6 to microspheres were found to be highly specific for the MGH-U1 human bladder carcinoma cells [49]. Other methods of delivery include the usage of covalent low-density lipoprotein conjugates [50], peptide-based intracellular vehicles [51], antibody mediated targeting [52], chemical alteration such as introduction of a hydrophilic group [53], liposomes [54] and others. Polymer conjugation has also been explored to improve the photosensitizer solubility as well as to alter the biodistribution, elimination and pharmacokinetic profiles [55]. Among the polymers that are currently known to have been used with chlorin derivatives are polyethyleneglycol [56, 57] and N-(2-hydroxypropyl)methacrylamide (HPMA) copolymers [58].

1.7 Polyvinylpyrrolidone

Polyvinylpyrrolidone (PVP) is a macromolecular polymer of N-vinylpyrrolidone. It is metabolically inert in rat, dog and man as shown by experiments using ¹⁴C- or ¹³¹I-labelled PVP [59]. It has been widely used as plasma expander [60]. The

excretion of PVP is inversely related to increasing molecular weight. The glomerulus can excrete all PVP of molecular weight 40 000 Dalton or below within a few days [59]. Low molecular weight PVP adsorbs various substances, e.g. bacterial toxins, inorganic poisons, barbiturates, vitamins and hormones in the blood, either reducing their toxicity or prolonging their activity [59]. The reticuloendothelial system retains PVP with a molecular weight in excess of about 100 000 Dalton for a long time [59]. PVP is also accumulated in the mitochondria of the kidneys [61]. Transfer of intravenously injected PVP to the brain or through the placenta was not observed [59]. PVP of molecular weight 11 500 Dalton is not absorbed from the intestinal tract by man or by rat and PVP of molecular weight 16 000 Dalton is not absorbed from the gastrointestinal tract by guinea-pigs [59].

1.8 Novel association of polyvinylpyrrolidone with chlorin e6

In parallel with the development of second-generation photosensitizers, this thesis was aimed at investigating a new preparation containing Ce6 (as a trisodium salt) and the polymer PVP. This formulation was a mixture of the active ingredient of Ce6 combined with PVP with mass fraction ratio of 1:1. Ce6 was obtained from the plant *Spirulina platensis*. PVP (molecular mass = 12000) is a synthetic, water-soluble, neutral polymer with low toxicity and high degree of biocompatibility that is commonly used in pharmaceutical formulations as a water-soluble polymeric carrier to improve solubility of lipophilic drugs [62]. The highly polar amide group of PVP monomer confers its hydrophilic and polar-attracting properties, whereas the apolar methylene and methyne group in the backbone and the ring contribute to its hydrophobic properties. PVP acts as a carrier to modify the distribution of the drug. The use of PVP is based on the

principle that polymer conjugated drugs are passively and preferentially absorbed by tumors due to the enhanced permeability and retention effect [63]. It has been reported that drugs bioconjugated with PVP demonstrated longer mean resident time in the blood [64, 65]. Such macromolecular conjugates can potentially prolong the blood accumulation of drugs and thus preferentially accumulate in solid tumors through enhanced permeability and retention effects [66]. PVP has also been shown to inhibit drug crystallization in solution as well as in the solid state [67] and protects against drug degradation in solution. Another formulation using the photosensitizer Hypericin and PVP was reported to show improved water solubility as well as high affinity for cellular membranes [39]. In parallel with the development of second-generation photosensitizers using polymers, this report investigates a new preparation consisting of Ce6 (as a sodium salt) and the polymer polyvinylpyrrolidone (PVP) (Figure 1.2). This formulation was prepared as a mixture of at least 75% active ingredient of Ce6 (18-carboxy-20-(carboxymethyl))-8-ethenyl-13-ethyl-2,3-dihydro-3,7,12,17-tetramethyl-21H,23H-porphin-2-propionic acid) and PVP with mass fraction ratio of 1:1.

Currently Ce6-PVP is being used for palliative photodynamic treatment of head and neck squamous cell carcinoma lesions in patients not curable with surgery and/or radiotherapy in the scientific research centre of Belarus and Russian Federation. In its original form, Ce6 is unstable in aqueous solutions at room temperature. Aggregation of Ce6 observed in aqueous solutions is known to reduce the fluorescence quantum yield. In order to overcome Ce6's insolubility, PVP was used as a hydrophilic carrier. PVP is a synthetic, water-soluble, neutral pharmaceutical polymer with low toxicity, used commonly to improve drug dissolution. Mixture of Ce6 with PVP was found to prevent Ce6 aggregation in

aqueous media and led to an enhancement of Ce6 fluorescence quantum yield, while keeping the quantum yield of the intersystem crossing essentially unchanged [68].

1.9 Experimental purpose and hypothesis

In the field of photomedicine, there is a continuing need for a drug delivery system that is simple, non-toxic, chemically inert, economical and can easily be used for formulating different types of photosensitizers. Requirements for a photosensitizer formulation include not only maintaining the drug in a stable form, but also to achieve effective delivery of a therapeutic dose to target site. The underlying aim of this thesis is to evaluate the efficacy of association of polymer PVP blends for the photosensitizer, Ce6. It is hypothesized that the Ce6-PVP formulation are expected to have increased hydrophilicity, enhanced penetration and accumulation at tumor sites, where upon irradiation of laser light, Ce6-PVP will cause destruction in the cellular and vasculature within the tumors. They are also likely to be rapidly cleared from normal tissue thereby reducing normal tissue photosensitivity effect.

The efficacy of Ce6-PVP was evaluated as a topical formulation in a multicellular tumor spheroid in the chick chorioallantoic membrane (CAM) model in order to have a better understanding of formulation effects in terms of penetration and uptake distribution. The CAM tumor model was chosen as this allowed for an easy evaluation of the formulation for screening purposes. The use of CAM model to culture tumor spheroids and model for photosensitizer transport study was a relatively novel concept in this study.

In vitro and *in vivo* preclinical tumor models were next employed to determine selectivity of the new Ce6-PVP formulations by measuring its pharmacokinetics and photodynamic efficacy and biological responses. The effect of PVP on the interaction of Ce6 with plasma proteins and its subcellular localization was also investigated to explore the possible mechanisms that had contributed to the accumulation of photosensitizer in the tumor.

The final objective of this thesis was to evaluate the efficacy of Ce6-PVP in a selected sample of angiosarcoma and bladder cancer patients using fluorescence endoscopy imaging and *in vivo* spectrofluorometric technique. This was to enable the quantification of Ce6-PVP in lesions and normal tissue of patients. Confocal microscopic imaging on bladder biopsy samples was carried out after topical administration of Ce6-PVP to determine the depth of Ce6-PVP penetration into the mucosal and submucosal layers within the bladder tissue. Measurement of cytokine after Ce6-PVP mediated PDT in bladder cancer patients was also performed to evaluate for inflammatory response that was considered important for the activation of antitumor immunity at post PDT.

CHAPTER 2

Pharmacokinetic profile of chlorin e6 – polyvinylpyrrolidone in the murine model

2.1 Summary

This chapter describes the biodistribution and pharmacokinetics profile of Ce6–PVP on poorly differentiated human bladder and nasopharyngeal carcinoma murine models with the following specific aims: (i) to qualitatively evaluate the fluorescence accumulation in human bladder and nasopharyngeal tumor, (ii) to correlate the fluorescence distribution of Ce6–PVP using tissue extraction technique and fluorescence imaging technique, (iii) to compare the fluorescence distribution of Ce6, Ce6–PVP and Photofrin in skin of nude mice and (iv) to evaluate tumor response at post Ce6-PVP mediated PDT. The results presented here demonstrated that this formulation had a rapid accumulation in tumor tissue within 1 h post intravenous administration. The fluorescence of Ce6–PVP determined either by fluorescence imaging or by chemical extraction from the tissues displayed similar trends of distribution. It was also confirmed that Ce6–PVP had a faster clearance from the skin of nude mice compared to Ce6 alone or Photofrin. The photodynamic activity of Ce6-PVP and its acute toxicity effect induced by different parameters such as drug-light interval, drug dose, irradiation fluence rate and total light fluence were also investigated. It was demonstrated that Ce6–PVP had less *in vivo* phototoxic effect compared to Ce6 alone. The phototoxicity revealed a strong dependence on the drug and light dosimetry as well as on the drug-light interval. Ce6–PVP was most toxic at 1 h drug-light interval, irradiated at 200 J/cm², while Ce6 alone was most toxic at a light dose of more than 50 J/cm² at the 1 and 3 h drug-light interval PDT. Although high

selectivity in tumor tissue was found between the period of 3 and 6 h, the efficacy of Ce6–PVP mediated PDT was best at 1 h drug-light interval. It was observed that the extent of tumor necrosis post PDT was dependent on the plasma concentration of Ce6–PVP, implying a vascular mediated cell death mechanism. In conclusion, the Ce6–PVP formulation appeared to be a promising photosensitizer for fluorescence imaging and PDT of cancer.

2.2 Introduction

PDT is gradually becoming a widely used medical tool and has received regulatory approval for the treatment of a number of diseases worldwide, particularly age-related macular degeneration and certain solid tumors [69]. However, the use of PDT in clinical applications is frequently limited by associated side effects, such as nonspecific biodistribution and prolonged accumulation in non-neoplastic tissue. First-generation PDT photosensitizers, such as Photofrin[®], exhibited prolonged skin photosensitivity and lacked long wavelength absorption. Therefore, there is a need for increased selectivity of photosensitizers for tumor tissue over healthy tissue. The synthesis of improved second-generation photosensitizers which have longer wavelength absorption moved towards modified tetrapyrrolic compounds, such as benzoporphyrin (Visudyne[®]), chlorin (Temoporfin[®]) and porphycene (ATMPn) to metallated derivatives such as AlPcS₄, SiNC (Nc—naphthalocyanine); and SnEt₂. More recently, targeting strategies using nanoparticles have been shown to increase the affinity of photosensitizer for tumor tissue [70]. Conjugating a targeting component, such as an antibody (directed against the tumor antigens), towards the photosensitizer allows the drug to localize, accumulate and bind selectively at the diseased site [71]. The photosensitizer bioconjugate is then able to photodynamically inactivate in tumor cells expressing the tumor-associated antigen, and could greatly improve PDT's therapeutic margin with minimal side effects. Other alternative approaches include the use of a molecular carrier such as a liposome or targeted nanospecies [72, 73].

The chemical structure of a photosensitizer plays a key role in the success of the compound as a PDT agent. A number of promising photosensitizers exhibit poor

solubility in aqueous media, thus preventing intravenous delivery into the bloodstream and affecting their efficacy and use in physiological media in the clinic. Photosensitizer needs to be soluble in physiological media as the degree of photosensitizer hydrophilicity and amphiphilicity directly affects its route of administration and its pharmacokinetic profile [74]. Lipophilic photosensitizers were found to accumulate in high amounts in the vessels, especially in the endothelial cells, whereas hydrophilic photosensitizers are cleared from the plasma more quickly and accumulate in the tumor cells after a short incubation time [75]. Photosensitizers with anionic substituents, such as sulphonate or carboxyl groups, have been observed to localize preferentially in the cytoplasm and relocate to the nucleus upon illumination, whereas lipophilic photosensitizers functionalized with cationic groups are believed to traverse the mitochondrial membrane and accumulate in the mitochondrion. However, it remains to be established whether total drug distribution to neoplastic tissues or concentration in specific subcellular sites is the more important factor for an efficient PDT effect [76]. Exactly which physicochemical/structural properties and mechanisms behind these specific distributions and localizations and how to maximize tumor tissue selectivity over normal tissue accumulation are issues still under investigation [77].

During the past decade much research has been focused on developing effective drug delivery systems for the preparation of chlorins as potential photosensitizers for PDT. Ce6, a second-generation photosensitizer has been reported to have significant efficacy in killing cancer cells *in vivo* [78]. In its original form, Ce6 has the disadvantage of having poor solubility in aqueous solutions at room temperature. Aggregation of Ce6 observed in aqueous solutions is known to

reduce the fluorescence quantum yield as well as its cytotoxic effect. This provided the rationale for the development of Ce6 using PVP, an alternative water-soluble formulation with which the monomeric form of Ce6 can be administered intravenously. A spectroscopy study using multiple scattering experiments have shown that Ce6-PVP was present in the monomeric form in whole blood [79]. This is important as the ability to introduce the drug in a monomeric form into the circulation has been proven to correlate well with the efficacy of the photosensitizer in tumor destruction in the murine tumor model [80].

The photochemical generation of singlet oxygen and other reactive oxygen species is responsible for the cytotoxicity induced by PDT. Lethal toxicity induced by various photosensitizers has been documented and systemic toxicity has been reported following whole body and abdominal light exposure of porphyrin PDT in mice. In previous studies, high levels of acute lethality in mice were reported using the photosensitizer Photofrin II-mediated PDT [81] and it was suggested that the localized PDT elicits systemic toxicity in the form of a traumatic shock syndrome. Traumatic shock can be produced by tissue injury, which in turn leads to inadequate peripheral perfusion that leads to circulatory collapse. The characteristics of traumatic shock includes induction of significant levels of ischemia or hypoxemia, the release of prostaglandins and kinins, as well as production of large amounts of cell necrosis.

In this chapter, the ability of PVP to enhance the accumulation of Ce6 on the human bladder (MGH) and nasopharyngeal (CNE2) tumor model was investigated. Using fluorescence imaging and tissue extraction methods, the

fluorescence distribution in tumor and normal tissue were made by comparing the fluorescence distribution of Ce6, Ce6-PVP and Photofrin in the skin of nude mice. Visual presentation on Ce6-PVP induced fluorescence in tumor and gross anatomical structure of normal organ of a murine model were made.

Fluorescence spectroscopy measurements were also performed to characterize emission spectra from these tissue samples as well as to corroborate results from fluorescence images. Comparisons were also made on the therapeutic efficacy of the formulation Ce6-PVP against Ce6 in a human bladder tumor xenograft model. Experiments were designed to evaluate effects of drug and light dose rate on Ce6 or Ce6-PVP mediated PDT on tumor and its lethal toxicity response in mice.

2.3 Materials and methodology

2.3.1 Preparation of photosensitizers

Ce6-PVP also known as Fotolon or Photolon preparation was prepared at RUE Belmedpreparaty, Minsk, Belarus by our collaborator [114]. For each experiment, the photosensitizer stock solution was freshly prepared by dissolving 1 mg of Ce6-PVP in 1 mL of 0.9% sodium chloride while 1 mg of Ce6 (Frontier Scientific, USA) was dissolved in 0.5 mL dimethyl sulfoxide (Sigma, USA) to constitute a stock concentration of 2 mg/mL. During administration of Ce6, the stock solution was further diluted with 0.9% sodium chloride to obtain the desired dose. Photofrin was obtained from Sinclair Pharmaceuticals, UK. Photofrin was prepared by dissolving 1 mg of drug in 1 mL of 0.9% sodium chloride, to constitute a stock concentration of 1 mg/mL.

2.3.2 Cell culture conditions and xenograft tumor model

Male Balb/c nude mice, 6 – 8 weeks of age, weighing an average of 24 g were obtained from the Animal Resource Centre, Western Australia. The epithelial-like carcinoma of the human bladder cell, MGH, and nasopharyngeal carcinoma cells, CNE-2, were used to establish the tumor xenograft model. The cells were cultured as a monolayer in RPMI-1640 medium supplemented with 10% fetal bovine serum, 1% non-essential amino acids (Gibco, USA), 1% sodium pyruvate (Gibco, USA), 100 units mL⁻¹ penicillin–streptomycin (Gibco, USA) and incubated at 37 °C, 95% humidity and 5% CO₂. Before inoculation, the cell layer was washed with phosphate-buffered saline, trypsinized, and counted using a hemocytometer. Approximately 3.0 × 10⁶ cells suspended in 150 µl of Hanks' Balanced Salt Solution (Gibco, USA) were injected subcutaneously into the lower flanks of the mice (Figure 2.1). All procedures were approved by the Institutional

Animal Care and Use Committee, SingHealth, Singapore, in accordance with international standards.



Figure 2.1 Subcutaneous injection of tumor cells onto the flank

2.3.3 Serum uptake of Ce6–PVP

A dose of 5 mg kg^{-1} of the photosensitizer was administered intravenously through the tail vein. The mice were anaesthetized with $120 \text{ }\mu\text{L}$ cocktail of ketamine hydrochloride (50 mg/mL , Trittau, Germany), dormicum (5 mg/mL Midazolam HCl, David Bull Laboratories) and deionized water ($1 : 1 : 2$ volume/volume) through intraperitoneal injection. Blood was collected by cardiac puncture at 1, 3 and 6 h time points. Following this, the mice were sacrificed by cervical dislocation. Serum was collected by allowing blood to coagulate at room temperature and centrifuged at $3500 \text{ rev min}^{-1}$ for 15 min. $100 \text{ }\mu\text{L}$ of serum was added to $1900 \text{ }\mu\text{L}$ of Solvable™ (Packard Instrument, USA). The mixture was incubated at $50 \text{ }^\circ\text{C}$ for 16 h. Subsequently, 1 mL of the solution was placed in a cuvette and the fluorescence emission at 665 nm was detected upon excitation at 400 nm using the spectrofluorophotometer RF-5301 PC (Shimadzu).

2.3.4 Fluorescence imaging

A fluorescence endoscope system (Karl Storz, Tuttlingen, Germany) was used to perform the macroscopic fluorescence digital imaging. A modified xenon short arc lamp (D-Light system, Karl Storz) filtered by a band pass filter (375 – 480 nm) was used for excitation of Ce6–PVP in tissue. Fluorescence was captured via a sensitive CCD camera (Tricam SL PAL, Karl Storz) attached to a modified endoscope integrated with a long pass filter (cut-off wavelength 560 nm). The red channel registered the photosensitizer's fluorescence and the blue channel captured the diffusely back-scattered excitation light. Mice were administered with various doses of the photosensitizers. At various time points, mice were anaesthetized and the skin overlaying the tumor was carefully removed to expose the tumor and normal peritumoral muscle. Fluorescence images of the tumor, muscle and dorsal skin were then captured. The distance between tissue surface and probe lens was standardized before imaging. This was done to minimize variations due to geometrical factors such as fluorescence excitation and collection angles. In addition, a short exposure of the surface of tumor and muscle to the excitation light (10 seconds) was performed to avoid excessive photobleaching effects. The intensities of the red and blue channels of the fluorescence images were quantified using the software MicroImage (Olympus Optical Co. (Europa) GmbH, Germany). By applying the red-to-blue pixel ratio of the same tissue of interest, the relative photosensitizer kinetics based on fluorescence intensity was determined. The red-to-blue pixel ratio algorithm is independent of the observation geometry, the distance between the endoscope tip and the observed tissue as well as the fluctuation of the excitation irradiance. This allowed for a more accurate quantitative assessment of the drug kinetics in

the tissue. The red-to-blue pixel ratios of all tissue were normalized with the red-to-blue pixel ratio of the tissue before drug administration.

2.3.5 Spectroscopic measurement using fiber optics-based fluorescence spectrometer

The spectral measurement was performed on mice sacrificed at 1 and 3 h post Ce6-PVP administration. A fiber optics-based fluorescence spectrometer (Spex SkinSkan, JY Inc., Edison, NJ, USA) was used for the measurement of fluorescence intensity of Ce6-PVP. A monochromator with a 150-W Xenon lamp was used as the excitation light source. The excitation light (400 nm) was guided to illuminate samples by one arm of a Y-type quartz fiber bundle, and the emission fluorescence was collected by another arm of the fiber bundle, guided to another motor-controlled monochromator. The resulting emission spectra were recorded from 650 to 750 nm, in 1 nm increments, collected using the DataMax version 2.20 (Instruments SA, Inc.) software package. The optical fiber tip was placed on the measuring sites and fluorescence intensity spectra were measured. After each measurement, the optical fiber tip was carefully cleaned to remove the possible remaining drug on the tip.

2.3.6 Determination of Ce6-PVP concentrations in tissues in mice

For analyzing the fluorescence intensity distribution in skin, mice were intravenously injected with 5 mg/kg with all three different photosensitizers (Ce6, Ce6-PVP and Photofrin). Fluorescence images of dorsal skin were taken in unanaesthetized mice at different time points over 42 h. For the analysis of the distribution of Photofrin, chemical extraction method was used because the fluorescence endoscope system was not suitable to detect Photofrin

fluorescence. Skin tissue samples were placed with 2 mL of Solvable™ (Packard Instrument, USA) tissue solubilizer and incubated at 50 °C for 16 h in the dark. The level of fluorescence of the solubilized samples were measured by a spectrofluorophotometer (model RF-5301 PC, Shimadzu) with $\lambda_{\text{ex}} = 400$ nm, slit width 1.5 nm and $\lambda_{\text{em}} = 665$ nm, slit width 1.5 nm.

2.3.7 Confocal fluorescence microscopy and image analysis.

After administration of Ce6-PVP and macroscopic imaging, the animals were sacrificed and the tumor tissue was harvested at various time points (15 min, 30 min, 1 h, 3 h and 6 h). The tumors were then snapped frozen in liquid nitrogen. Cryo sections with a thickness of 15-20 μm were obtained using Microtome Cryostat (Cryo-Star HM 560MV, Germany). The sections were mounted on microscope slides covered with fluoromount (Ingram and Bell, USA). Fluorescent microscopic images were obtained from these sections. A laser confocal fluorescence microscope (Meta LSM 510, Carl Zeiss, Germany) was used to obtain the fluorescence microscopic images. An argon laser was used as an excitation source of 488 nm. Fluorescence emissions in the wavelength range of 600 – 670 nm were split by a dichroic filter and detected through a band-pass filter (BP-610 nm, Omega Optical, USA). Voltage gain, PMT voltage and sensitivity (contrast, brightness and filters) were fixed for all fields and slides imaged. The images were stored on an optical disk and analyzed using an image analysis software package.

2.3.8 Statistical analysis

Fluorescence half-life ($t_{1/2}$) values were derived by non-linear fitting to one phase exponential decay equation and comparison of fits was performed using Graph-Pad Prism™ (San Diego, USA) and results were expressed as mean $t_{1/2}$ with 95% confidence interval (95% CI). Statistical evaluation on the $t_{1/2}$ values was performed using the nonparametric Friedman test to compare the matched groups for each time points whereas multiple comparison of Bonferroni post hoc test was used to compare the effect of various PDT parameters on tumor response. All the mean differences were significant at the 0.05 level.

2.3.9 Experimental design for PDT

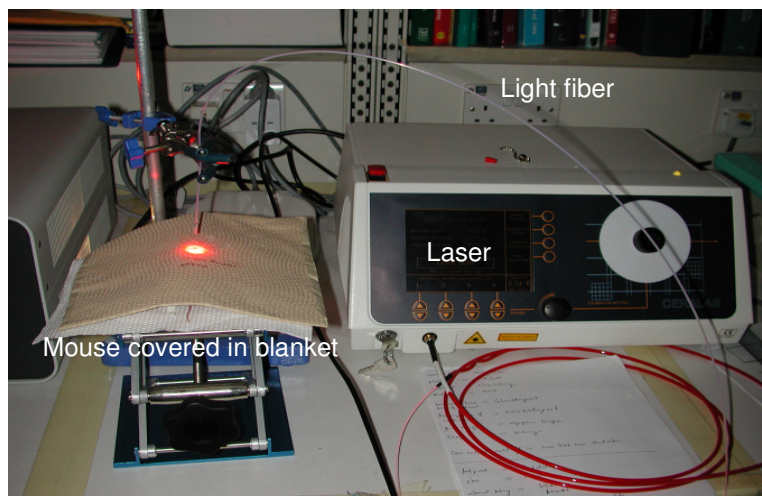


Figure 2.2 Light irradiation procedure on mouse

A portable diode laser (Ceralas PDT 665, Biolitec) emitting at a wavelength of 665 ± 3 nm was used for irradiation (Figure 2.2). The peak power output was calibrated to 1.75 – 1.85W at the fiber tip before commencement of irradiation. The laser energy was delivered to the surface of the tumor via a silica fiber

frontal light distributor (FD model, Medlight, Switzerland). The fiber was positioned to produce a 0.5 – 1.0 cm² circular spot of uniform light irradiation. Fluence rate was measured using a power meter (LaserCheck, Coherent). PDT treatment was performed at various parameters on anaesthetized mice bearing MGH tumors. Experiments were designed to study the effect of variation of four variables: the drug dose (2.5, 3.5 and 5 mg kg⁻¹), the drug-light interval (DLI, the time from the bolus injection of drug to the start of light delivery at 1, 3 and 6 h), the fluence (from 50 – 200 J cm⁻²) and the fluence rate (from 41.7 – 165 mW cm⁻²). Prior to irradiation, animals were wrapped in aluminum foil layered with brown paper towel in order to avoid irradiation to the other parts of the body. After illumination, the animals were kept in microisolator cages wrapped in aluminium foil to avoid light exposure.

2.3.10 Assessment of tumor response post PDT

The evaluation of tumor necrosis was performed using Evans Blue (Merck, Germany) vital staining. At 48 h post PDT, 1% Evans Blue in PBS was injected intraperitoneally at a volume of 0.4 mL in mice. Six hours later, animals were sacrificed and the tumors were excised. Around 2 – 3 mm thick cross-section slices were cut and imaged under a stereoscopic microscope (Stemi 2000C, Zeiss, Germany). The unstained area was attributed to tissue necrosis, whereas the stained area indicated viable tissue. Digital images were saved in JPEG format, and all analyses were carried out using NIH Image v1.62 software. Each image captured had the same calibration values to allow uniformity in the processing of the images. The tumor was outlined using the freehand drawing tool to measure the total tumor area. Similarly the necrotic area of the tumor was measured. The percentage of necrosis was calculated as the necrotic area

divided by the total tumor area multiplied by 100. In addition, a short-term tumor growth evaluation was performed to evaluate the efficacy of the treatment. Tumor volume was determined in a double-blinded manner at 7 and 14 days post PDT through caliper measurements using the formula: $V = \pi/6 \times d1 \times d2 \times d3$ where V represented volume (mm³) and d1, d2 and d3 represented the three mutually orthogonal diameters (mm) of the ellipsoid tumor. For evaluation of lethal toxicity effects of the photosensitizers, the evaluated endpoint was survival of the animals at 24 h post PDT.

2.4 Results and discussions

2.4.1 Fluorescence distribution in serum

The uptake kinetics of Ce6-PVP in serum was determined spectrofluorimetrically as shown in Figure 2.3. The fluorescence level of the photosensitizer in serum peaked after 1 h post administration. Subsequently, the concentration of the drug decreased steadily over the next few hours and approximately 4 % of its maximum concentration was retained in serum at 24 h. The calculated $t_{1/2}$ value of Ce6-PVP in serum was 1.4 h (95% CI 0.8 – 3.7).

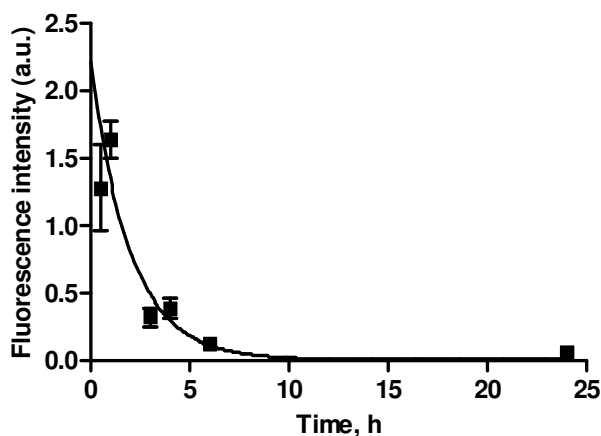


Figure 2.3 Serum uptake of Ce6-PVP at various time points post drug administration. Each time point represents a mean of 5 animals \pm SE.

PVP alone was effectively retained in the blood and showed little tissue-specific localization following its intravenous administration [82]. Previous research has demonstrated that drugs bioconjugated with PVP demonstrate a decreased minimum volume of distribution and longer mean resident time in the blood [64, 65]. Such macromolecular conjugates may prolong the residency of drugs in blood and therefore preferentially accumulate in solid tumors through enhanced permeability and retention effects [66].

2.4.2 Qualitative assessment of Ce6-PVP accumulation in MGH tumor xenograft

Fluorescence imaging approaches are increasingly being used as a medical diagnostic procedure to assess tissue malignancy over conventional methods because they do not use potentially harmful ionizing radiation [84]. In situations where discrimination of suspicious lesion is clinically problematic, fluorescence imaging may provide added advantage in demarcating abnormal tissue. The development of photosensitizer based fluorescence imaging is hindered by problems such as skin photosensitivity, poor selectivity of the photosensitizer, and formulation issues. For these reasons, Ce6 was formulated with PVP to address these issues. Formulations using biocompatible polymers such as PVP are increasingly being used in the pharmaceutical industry for enhancing drug solubility and bioavailability. Figure 2.4 shows fluorescence images of the bladder tumor (A-D) post Ce6-PVP administration and their fluorescence intensity distribution images (E-H). The red fluorescence is an indicator of Ce6-PVP accumulation. The fluorescence intensity distribution map monitored the intensity of the fluorescence kinetics whereby red regions represented the hot spots for localization of Ce6-PVP followed by yellow and green. Intense fluorescence observed in the tumor indicated a tumor specific uptake of the compound. When compared to the images of normal bladder, no evident fluorescence was observed, demonstrating a clear fluorescence contrast between bladder tumor tissue and the normal bladder tissue. Only mild fluorescence was observed at 3 and 4 h post administration. At 6 h post drug administration, fluorescence was not detected, indicating clearance of the photosensitizer from normal bladder tissue.

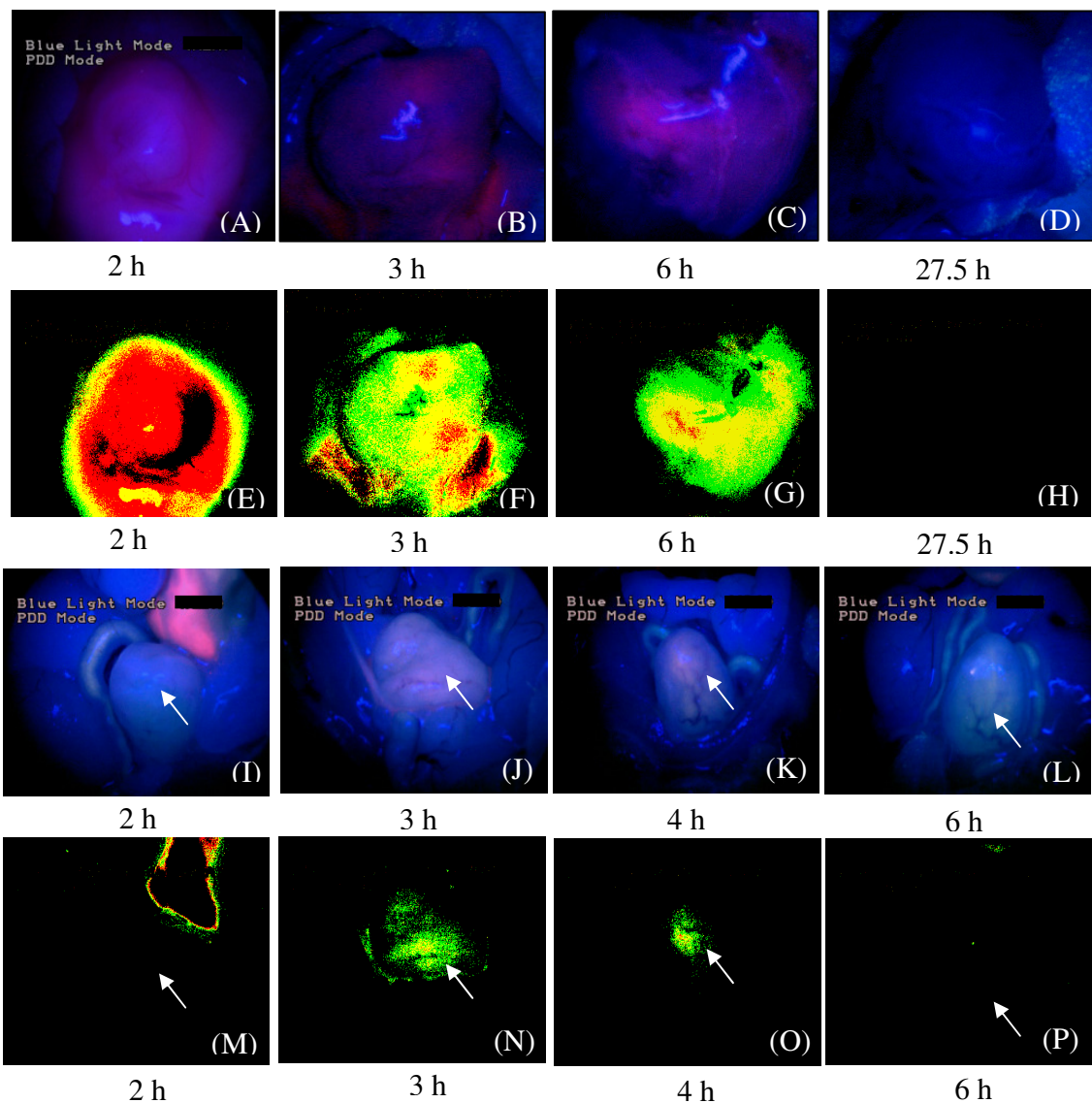


Figure 2.4 Upon intravenous administration of Ce6-PVP, tumor fluorescence at 2, 3, 6 and 27.5 h was observed under blue light illumination (A-D). The intensity of the fluorescence kinetics can be monitored in a fluorescence intensity distribution map, with red regions being hot spots for localization of Ce6-PVP followed by yellow and green (E-H). Normal bladders of mice (arrow) were imaged at 2, 3, 4 and 6 h post drug administration (I-L) and their corresponding intensity distribution images were acquired (M-P).

The use of preferential accumulation of photosensitizers in neoplastic lesions is already approved for detection of bladder cancer and undergoes further development for the detection of other cancer diseases [85]. However, PDT is

also associated with significant rates of bladder contracture because of the nonspecific accumulation of photosensitizers in the detrusor muscle. Selectivity of the photosensitizer between layers of hollow organs such as the bladder is one area in which PDT can demonstrate a therapeutically important advantage [38]. Even though, the selectivity of the photosensitizer is relatively poor at times, optimizing this selectivity using an improved formulation such as Ce6-PVP could provide a useful alternative to currently used photosensitizer.

2.4.3 Qualitative assessment of Ce6-PVP accumulation in CNE2 tumor xenograft

Macroscopic fluorescence images of CNE2 tumors were obtained using the fluorescence endoscopy system (Figure 2.5). Fluorescence intensity in tumor and tumor vasculature of nude mice xenografts was observed as early as 15 min post drug administration. Higher fluorescence was observed in tumor and adjacent normal tissue at 30 min and at 1 h. The tumor fluorescence selectivity was highest at 3 h. The overall fluorescence started to decrease from 6 h, and by 24 h, the fluorescence was negligible. These results were consistent with the results of the bladder tumor xenografts, demonstrating good fluorescence contrast was observed between tumor and normal tissue.

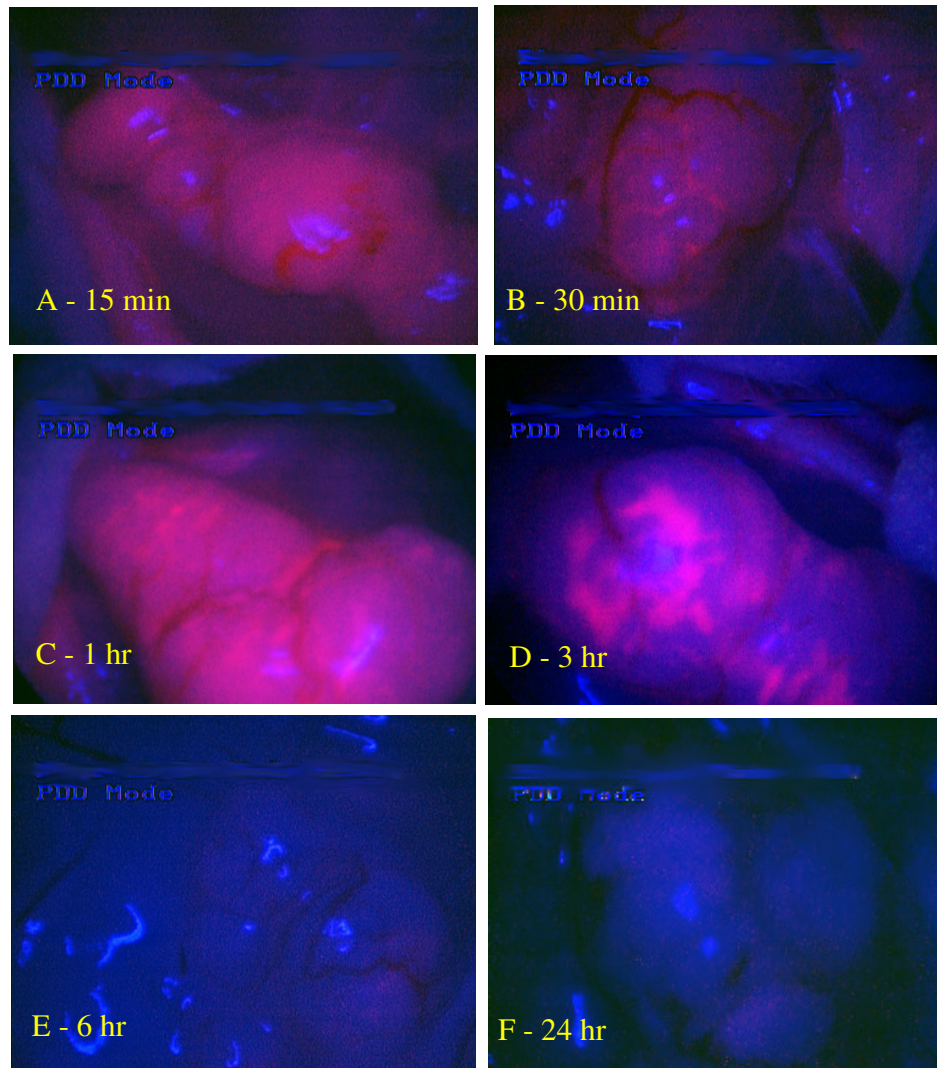


Figure 2.5 Ce6-PVP macroscopic fluorescence of NPC tumor xenografts and the surrounding tissue captured at various time points.

2.4.4 Fluorescence imaging of normal organs in mice

Representative fluorescence images of skin and various internal organs taken at 1 h post Ce6-PVP administration are presented in Figure 2.6. The internal organs were found to yield substantial fluorescence especially the gall bladder, liver, stomach, small and gastrointestinal tracts. Minimal fluorescence was observed in the heart and spleen. The fluorescence intensity in skin, lung, liver, and bladder dropped at 3 h post drug administration. There was little or no fluorescence remaining in heart and spleen. In contrast, the tumors showed sustained fluorescence intensity at 3 h post drug administration. By 6 h post drug administration, minimal fluorescence was detected in the gastrointestinal tract, liver and bladder (Figure 2.7).

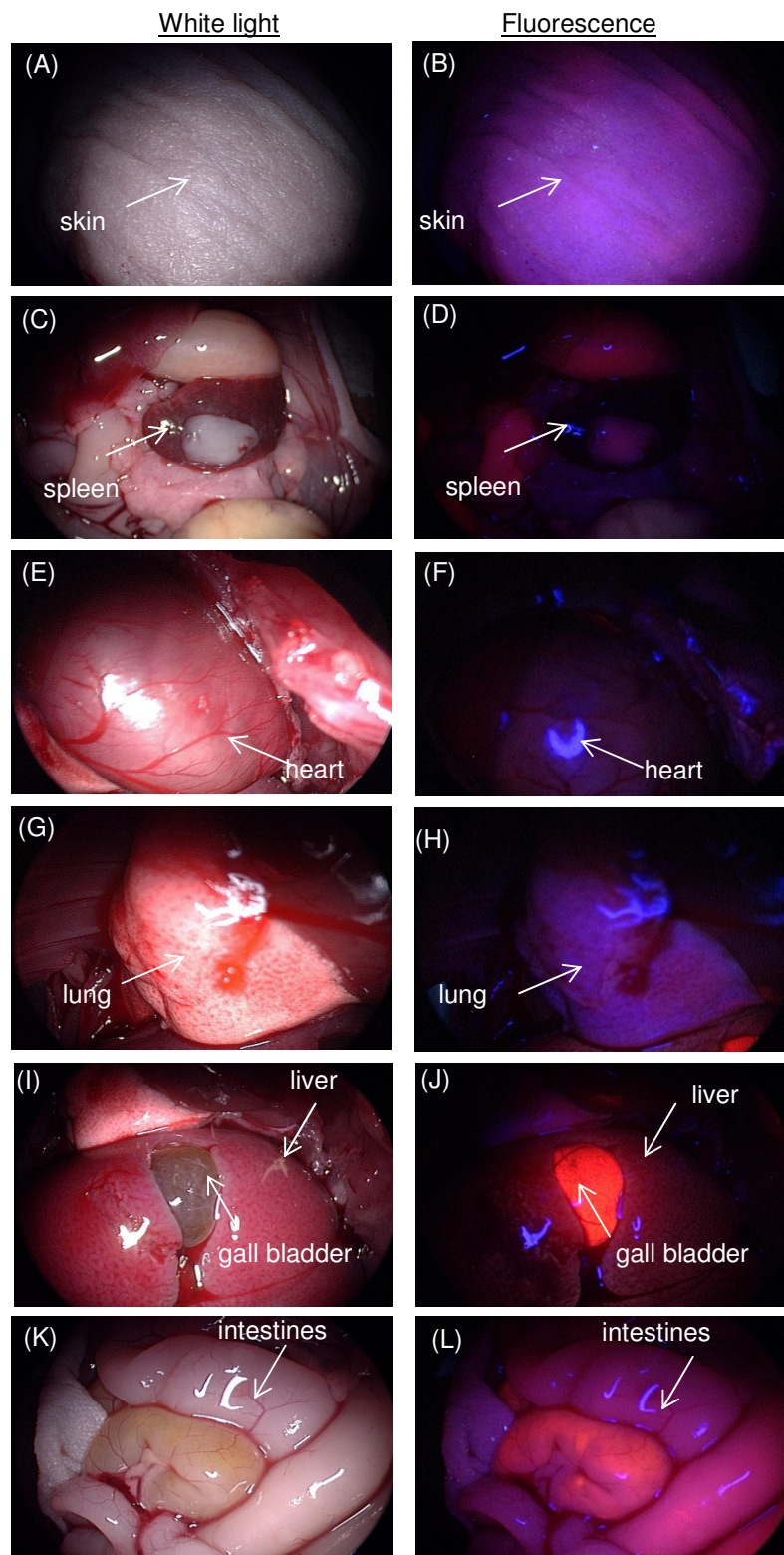


Figure 2.6 Macroscopic white light and fluorescence imaging in skin, heart, lung, gall bladder, liver, spleen, kidney and gastrointestinal tract at 1 h post-intravenous administration of 5.0 mg/kg Ce6-PVP.

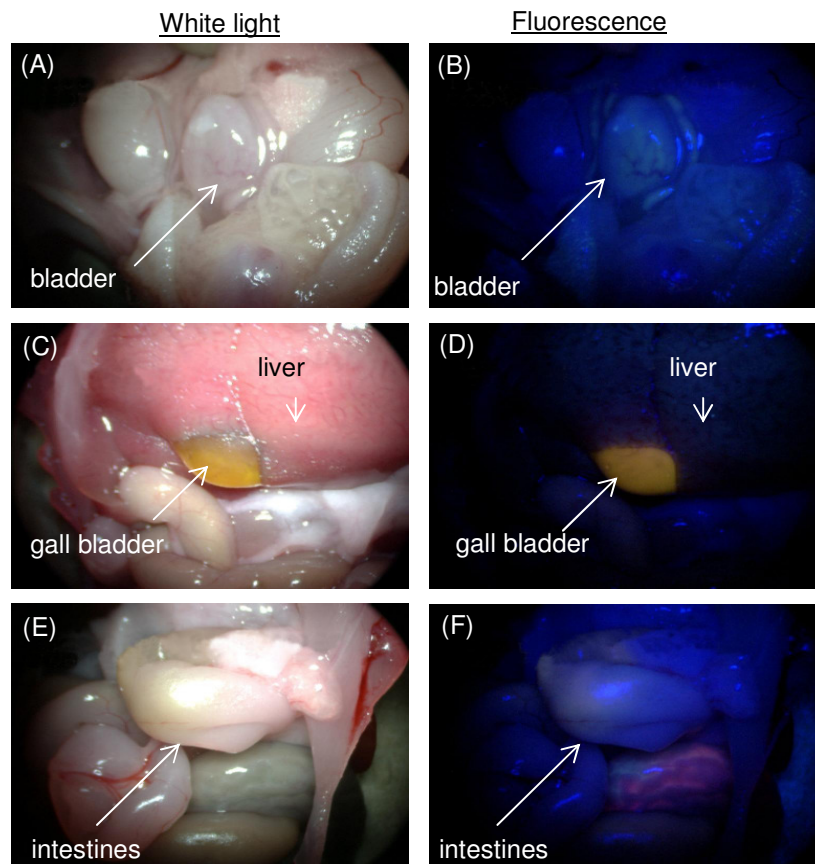


Figure 2.7 Macroscopic white light (A, C, E) and fluorescence (B, D, F) imaging in normal bladder, liver, gall bladder, and gastrointestinal tract at 6 h post-intravenous administration of 5.0 mg/kg Ce6-PVP.

Macroscopic fluorescence imaging showed that there was considerable distinction in the localization of fluorescence in tumor compared to other organs that could enable discrimination between tumor and normal organs. Organs of elimination and detoxification such as skin, gall bladder and gastrointestinal tracts were characterized by high photosensitizer accumulation efficiency. In contrast, all other normal organs such as muscle and bladder had much lower photosensitizer accumulation at 1 h post drug administration. Blood vessels growing on the tumor can also be observed because they contrast with the

fluorescence of the tumors. At 3 - 6 h post drug administration, a decrease of fluorescence intensity became evident on all normal organs, confirming that Ce6-PVP has fast clearance rate from normal organs. In some instances, variability of fluorescence intensity on the surface tissue such as stomach and lung was observed. This is possibly attributed to the variations of the tissue optical properties of the organs given by their color, density and composition.

2.4.5 In vivo fiber optic spectrofluorometric measurement

Typical fluorescence emission spectra from tumor, adjacent peritumoral muscle and normal bladder after i.v. administration of Ce6-PVP are shown in Figure 2.8. In general, the peak fluorescence intensities of tumor were higher than those of normal sites. The greatest intensity occurred in the region between 660 – 670 nm. When the spectra were normalized to baseline value, changes in peak intensity became evident. The line-shape differences were predominantly due to increased Ce6-PVP accumulation of tumor in the red region (emission peak at 665 nm).

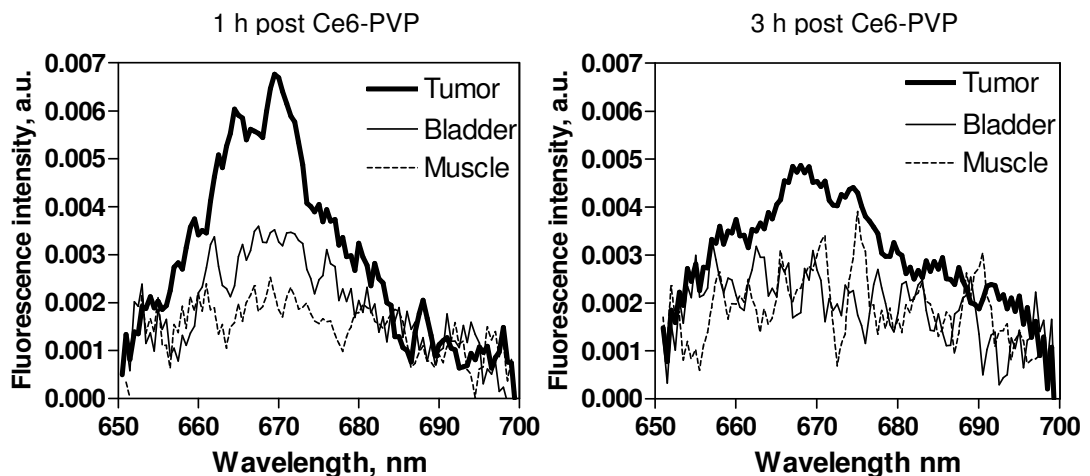


Figure 2.8 Comparison of emission spectra of bladder tumor xenograft, normal bladder and muscle of the murine model at 1 and 3 h post administration of Ce6-PVP using 400 nm excitation. The spectral signatures showed a peak at the wavelength 665 – 670 nm in tumor while the fluorescence intensity of normal bladder and muscle is weaker than that of the tumor tissue.

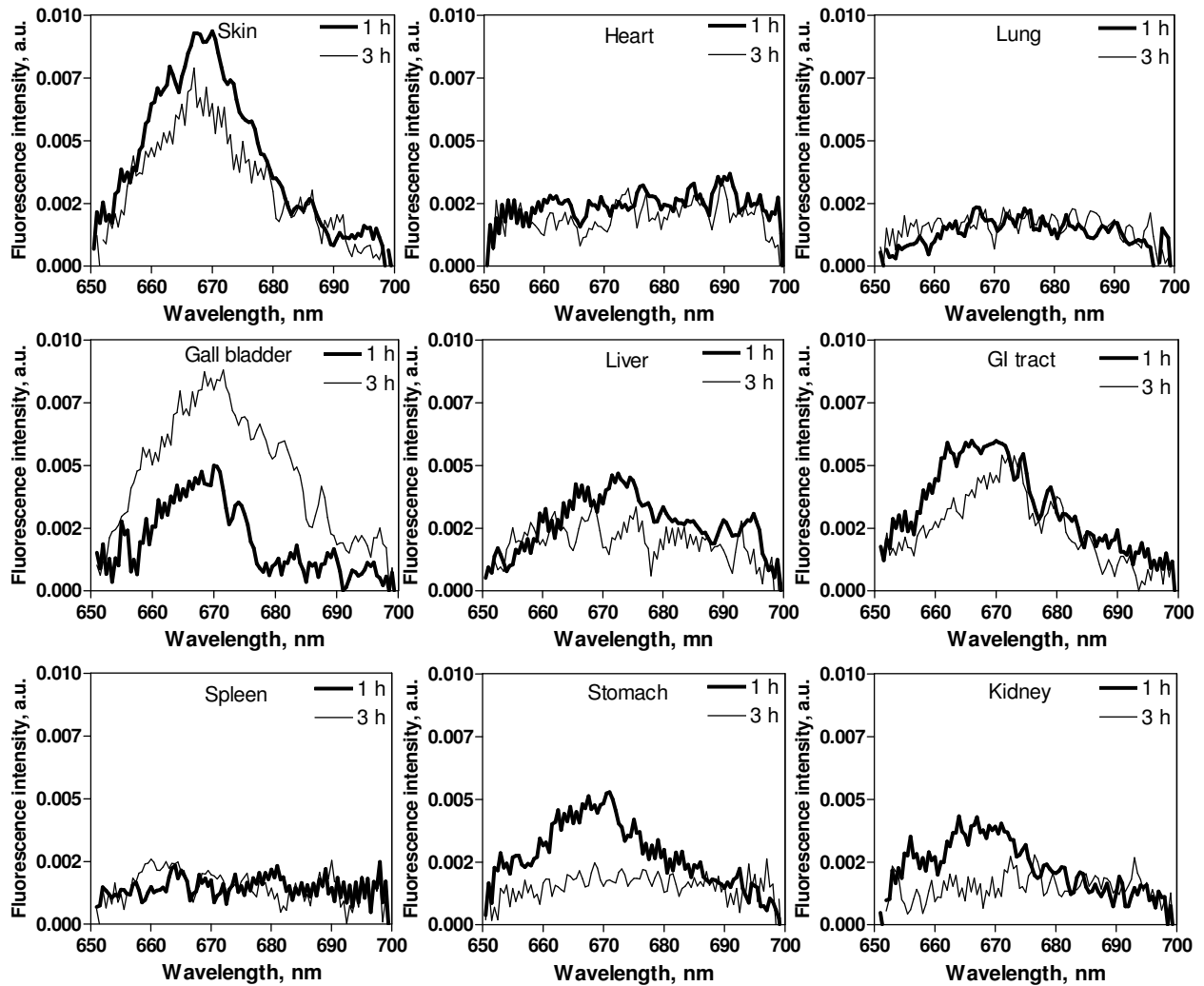


Figure 2.9 Comparison of emission spectra in the 650 – 700 nm region using 400 nm excitation in various normal organs at 1 and 3 h post Ce6-PVP administration. Except for skin and gall bladder, it is evident that the emission spectra of normal organs were lower compared to the emission spectra of tumor.

Fluorescence emission spectra of skin, heart, lung, gall bladder, liver, spleen, kidney and gastrointestinal tract are shown in Figure 2.9. Except for the gall bladder, all other organs showed a decreased of fluorescence emission of Ce6-PVP at 3 h compared to 1 h post drug administration. Essentially, fluorescence images that showed greater red fluorescence intensity had visibly higher spectral

peak, thus suggesting that that the macroscopic fluorescence imaging were reproducible. The key issue in fluorescence imaging is that the emitted fluorescence intensity measured from a tissue surface is not necessarily proportional to the fluorophore concentration because the light is altered by the tissue's intrinsic absorption and scattering properties. Hence the utility of spectrometric point fluorescence detection was employed as a complimentary technique. Spectra measurements were carried out at 1 and 3 h post drug administration to correlate the tumor intensity ratios obtained with fluorescence imaging to the tumor fluorescence spectral signal of the tissue. All the macroscopic fluorescence images correlated well to the spectra measurement. The Ce6-PVP induced spectra emission after normalization demonstrated a good separation to differentiate malignant tumors from normal tissues. Besides measuring physical parameters such as concentration of photosensitizer and tissue properties, this method can potentially improve the assessment of cancer location and its extent within the local-regional area. While fluorescence point spectroscopy studies are promising, it has several drawbacks as a screening tool as it can only interrogate a small volume of tissue (typically, 0.5 – 1 mm³) directly beneath the probe tip. Point measurements inevitably involve a degree of random sampling, which may not allow identification of early stage disease [86]. Hence, the combination techniques of fluorescence imaging and spectroscopy have been proven in good agreement with the actual tumor boundary found by histopathological mapping and early stage of disease [87, 88].

2.4.6 Quantitative assessment of Ce6-PVP accumulation in human nasopharyngeal tumor (CNE2) xenograft

Maximum fluorescence was observed in CNE2 tumor tissue at 30 min and 1 h post drug administration (Figure 2.10). At 3 h post drug administration the fluorescence decreased by 50% of the initial 1 h uptake. The overall

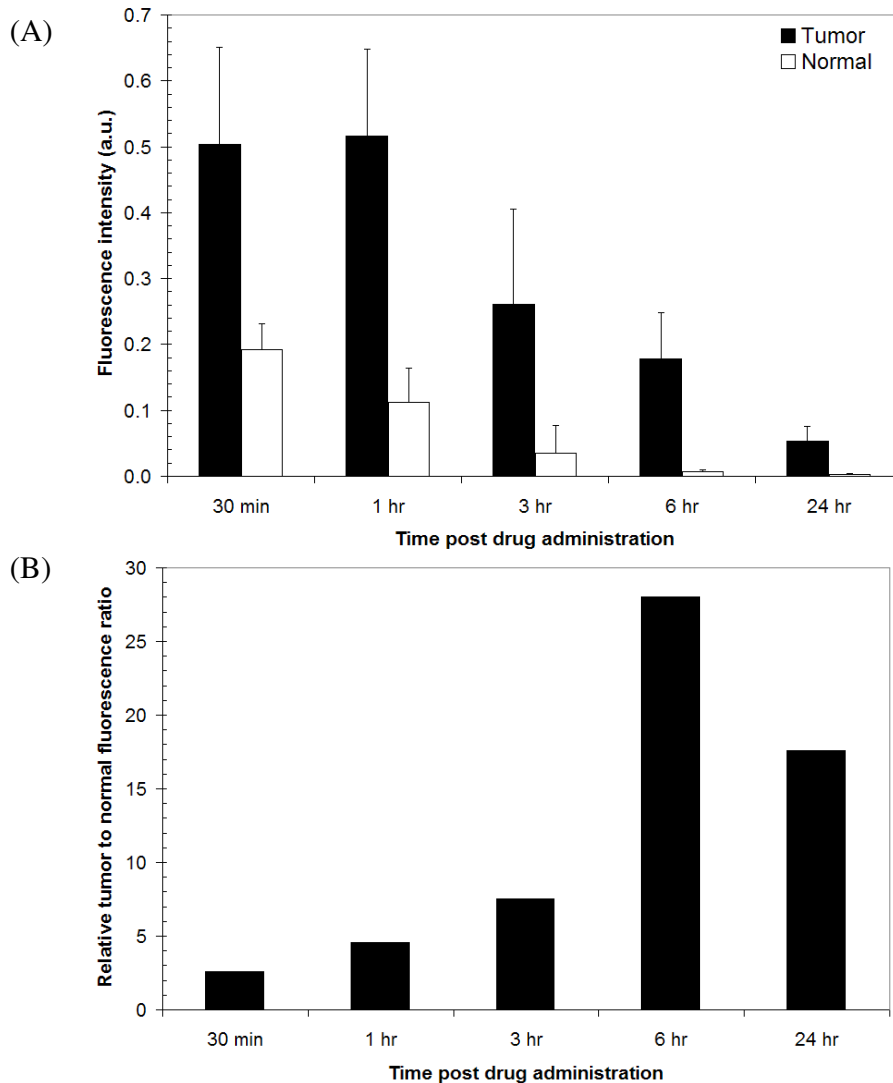


Figure 2.10 (A) Quantification of Ce6-PVP fluorescence intensity in tumor and normal tissue in CNE2 tumor model as a function of time as determined by fluorescence imaging technique. Each time point represents a mean of at least 3 animals \pm SE. (B) The selectivity of Ce6-PVP was determined by tabulating the relative tumor to normal fluorescence ratio.

and 90% at 6 h and 24 h respectively. At all time points, the difference between the level of fluorescence between tumor and normal tissue were statistically significant ($p < 0.05$). Selectivity of Ce6-PVP was evaluated by determining the ratio of drug fluorescence in CNE2 tumor versus normal tissue at the following time points – 30 min, 1 h, 3 h, 6 h and 24 h. The tumor to normal tissue ratio was 2.6 at 30 min. The ratio increased gradually from 4.6 to 7.6 at 1 h and 3 h time points respectively. The tumor to normal tissue selectivity ratio was highest at 6 h with a value of 28.1. Ce6-PVP microscopic fluorescence was also observed in the CNE2 tumor tissues as early as 30 min post drug administration (Figure 2.11). Overall microscopic fluorescence peaked at 3 h, correlating to the fluorescence of the macroscopic images. Fluorescence thereafter gradually started to decline, and only mild microscopic fluorescence was observed in the tumor tissues at the 6 h time point.

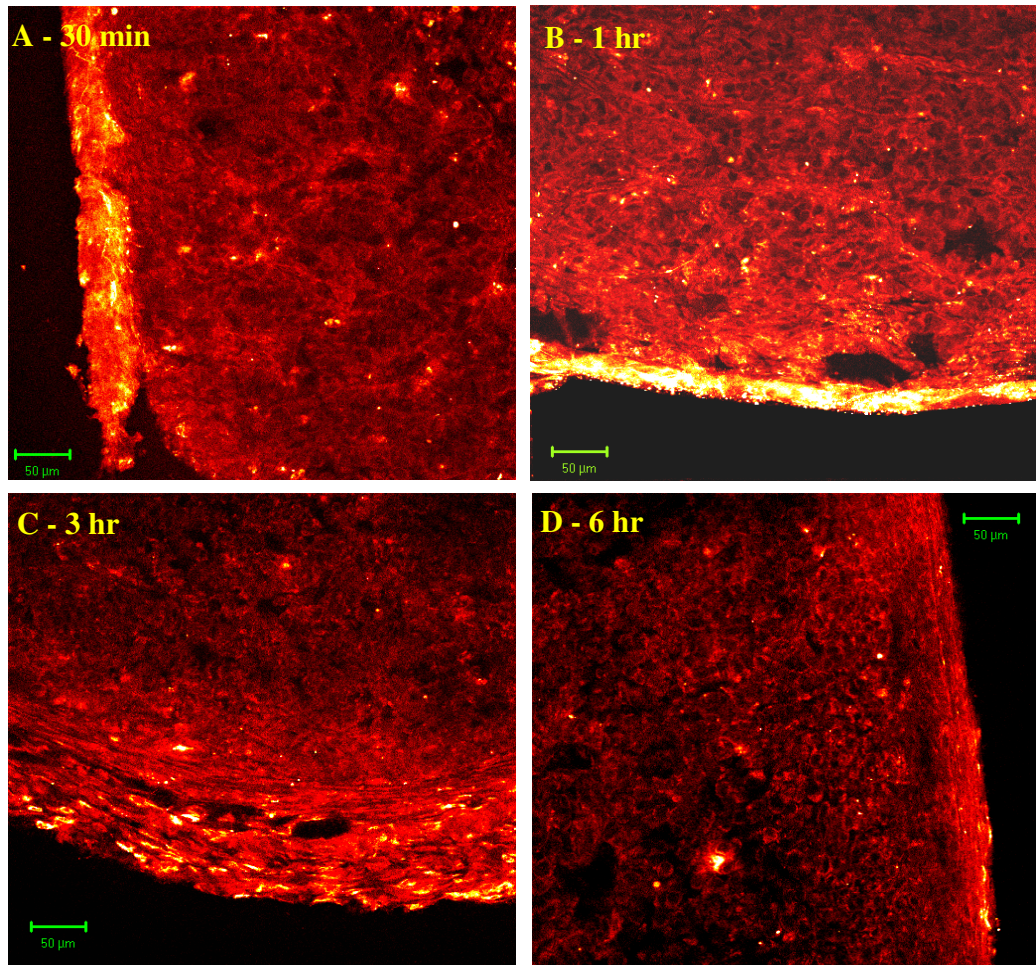


Figure 2.11 Fluorescence confocal microscopy of Ce6-PVP localization in tumors at various time points.

The main advantage of the fluorescence imaging technique lies in its ability to precisely label neoplasm by means of preferential uptake of photosensitizer by the target cells. Our studies showed that Ce6-PVP selectively localized in NPC tumors whereby fluorescence peaked rapidly within 30 min to 1 h post drug administration. The accumulation of Ce6-PVP in CNE2 tumor tissue was almost twice as much compared to normal tissue at the 3 h time point. The drug started to clear from the tumor tissue at about 6 h, thus making it a promising agent for systemic application for PDD. In the macroscopic images, at 30 min post drug administration, the tumor to normal ratio was lower, since the normal tissue also exhibited high fluorescence. However, at the later time points from 3 h to 6 h the fluorescence in the normal regions started to clear and the fluorescence selectively accumulated in the tumor thus increasing the tumor to normal ratio. This is in agreement with a study performed by Kikuchi et. al. where the authors noticed that the mean Ce6 fluorescence intensity calculated from the fluorescent images was significantly higher in tumors than normal mucosa at the 6 h time point [89].

2.4.7 A comparison of Ce6-PVP induced fluorescence quantification using image processing and tissue extraction method in human bladder tumor (MGH) xenografts

xenografts

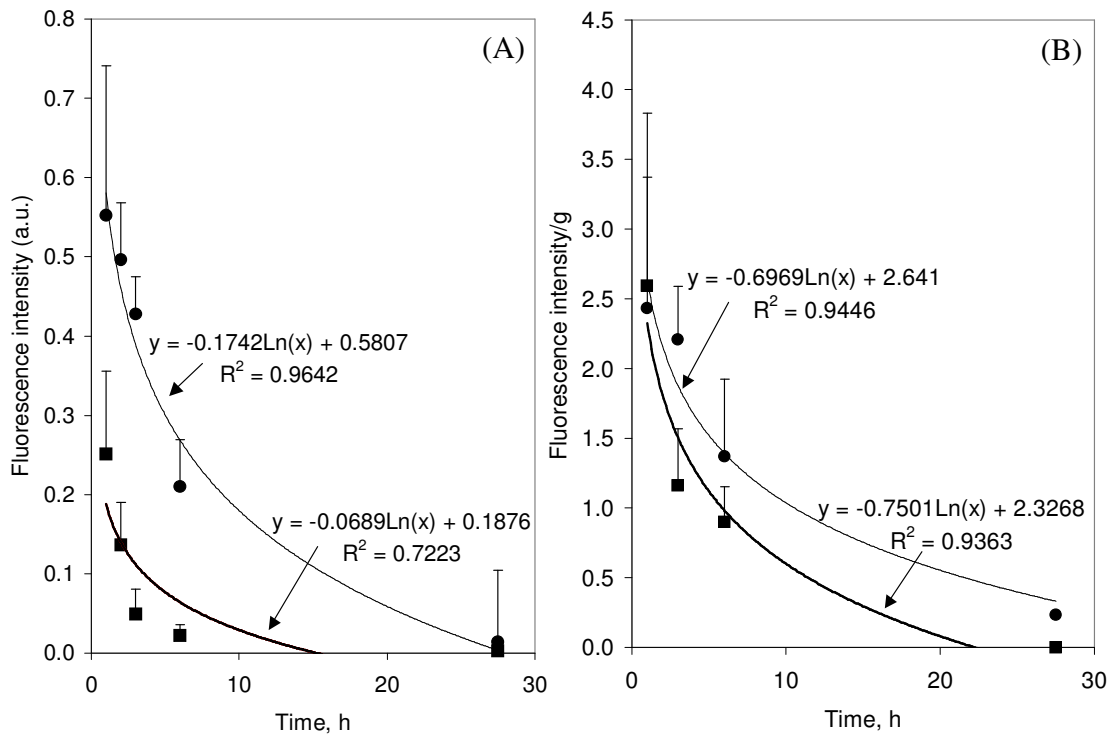


Figure 2.12 A comparison of fluorescence quantification using image processing and tissue extraction method. (A) Fluorescence intensity tabulated as the ratio of red to blue pixel intensity in normal (■) and tumor (●) tissue at various time points post drug administration using the fluorescence image processing technique. (B) Fluorescence intensities expressed as per gram of tissue using the tissue extraction technique. The best-fit logarithmic trend line were plotted in order to compare the correlation coefficient value between two methods of quantification. Each time point represents a mean of at least 3 animals \pm SE.

Fluorescence distributions of the photosensitizer in MGH tumor and normal tissue were assessed at various time points post intravenous administration of Ce6-PVP using the fluorescence imaging technique (Figure 2.12 A), thereafter these results were compared to those using tissue extraction technique (Figure 2.12 B). Both methods showed similar trends in fluorescence kinetics with higher fluorescence intensity observed in the tumor compared to normal tissue.

Logarithmic trendlines showed a higher correlation coefficient values (R^2) for MGH tumor than normal tissue. When both trendlines were compared, the image processing technique and the tissue extraction method displayed very similar results. However, the fluorescence imaging data underestimated the concentration of the photosensitizer in tumor and normal tissue. The present work also confirmed that direct fluorescence imaging on the surface of the subcutaneous bladder tumor xenograft gives consistent results for relative concentrations of the photosensitizer when compared to results derived from the tissue extraction method. In order to be compatible with the tissue extraction data, direct fluorescence readings from the fluorescence endoscope system have to be multiplied by factors in the range 4 - 5. Due to differing pigmentations and structures of various tissues, light absorption and scattering make direct fluorescence measurements unsuited for quantitative comparisons of photosensitizer levels in tissues [90]. Nevertheless, cautious interpretation of the data of in vivo fluorescence imaging could allow real-time estimation of relative drug concentration in normal as well as in tumor tissue.

2.4.8 Comparison of fluorescence distribution of Ce6-PVP versus Ce6 only in MGH tumor and normal tissue

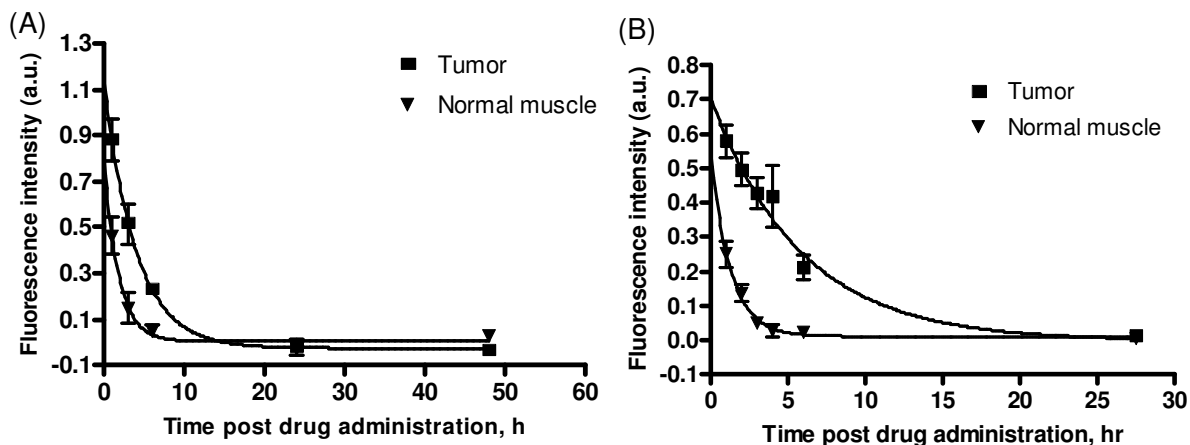


Figure 2.13 The kinetics of fluorescence intensity of Ce6-PVP (A) and Ce6 (B) in normal tissue of femoral muscle and tumor tissue at various time points post drug administration based on fluorescence image analysis. Each time point represents a mean of 5 animals \pm SE.

The fluorescence distribution profiles of Ce6-PVP and Ce6 in MGH tumor and surrounding normal muscle exhibited very similar kinetics (Figure 2.13). Tumor fluorescence of both compounds peaked at 1 h post drug administration with Ce6 having a higher fluorescence intensity compared with that of Ce6-PVP. The fluorescence in normal tissue was low compared to fluorescence in tumor tissue at all time intervals. Minimal fluorescence in both tumor and normal muscle were observed at 27.5 h, as 98 % of its maximum detected was cleared. The calculated $t_{1/2}$ values of fluorescence in tumor and normal muscle were 4.0 h (95 % CI 2.6 – 8.9) and 0.9 h (95 % CI 0.5 – 2.4) respectively for Ce6-PVP whereas for Ce6, the calculated $t_{1/2}$ values were 2.7 h (95 % CI 1.9 – 4.7) and 1.3 h (95 % CI 0.7 – 5.6) for tumor and normal muscle, respectively. This inferred that Ce6-PVP resided longer in tumor tissue and eliminated faster from normal tissue compared to Ce6.

Table 2.1 In order to study the in vivo selectivity of the photosensitizers in MGH tumor, the ratio of drug fluorescence in tumor over normal tissue were tabulated. Each time point represents a mean of 5 animals for Ce6-PVP and 4 animals for Ce6.

Time points	1 h	3 h	6 h
Ce6-PVP	2.2	8.7	9.3
Ce6	1.9	3.5	4.5

At 1 h post drug administration, the tumor to normal tissue selectivity ratio of both photosensitizer was low, since normal muscle also exhibited high levels of fluorescence (Table 2.1). However, from 3 to 6 h, the fluorescence in normal muscle started to clear and fluorescence selectively accumulated in the tumor tissue, thus increasing the tumor to normal tissue selectivity ratio. Overall, Ce6-PVP exhibited higher selectivity compared to Ce6.

2.4.9 Fluorescence monitoring in skin

The fluorescence distribution of the photosensitizer in skin was assessed at various time points post intravenous administration of Ce6-PVP (Figure 2.14). Regardless of the drug doses administered, the fluorescence kinetics exhibited similar trends in the skin. It was observed that peak photosensitization occurred at 1 h post drug administration. However, the fluorescence intensity decreased from 6 h post administration onwards. The calculated $t_{1/2}$ values for 2.5, 3.5 and 5 mg/kg of the photosensitizer in skin were 0.7 h (95 % CI 0.4 – 1.8), 0.8 h (95 % CI 0.5 – 1.3) and 0.8 h (95 % CI 0.6 – 1.5) respectively. Irrespective of the photosensitizer concentration administered, fluorescence of the skin was not detected at 42 h post drug administration. It was observed that peak photosensitization of the skin occurred at 1 h post drug administration of the Ce6-PVP. However, the fluorescence intensity decreased from 6 h post administration onwards. By 24 to 42 h, no Ce6-PVP fluorescence was detected. For Ce6 alone, similar trends of distribution and clearance were observed. When data for Ce6-PVP and Ce6 alone of skin were compared, Ce6-PVP had a faster clearance rate with $t_{1/2}$ values of 0.8 h (95 % CI 0.6 to 1.5) compared to $t_{1/2}$ values of 2.7 h (95 % CI 1.9 to 4.4) for Ce6 alone. In contrast, the fluorescence level of the skin after the administration of 5 mg/kg Photofrin showed an increasing trend and still detected up to 72 h post administration.

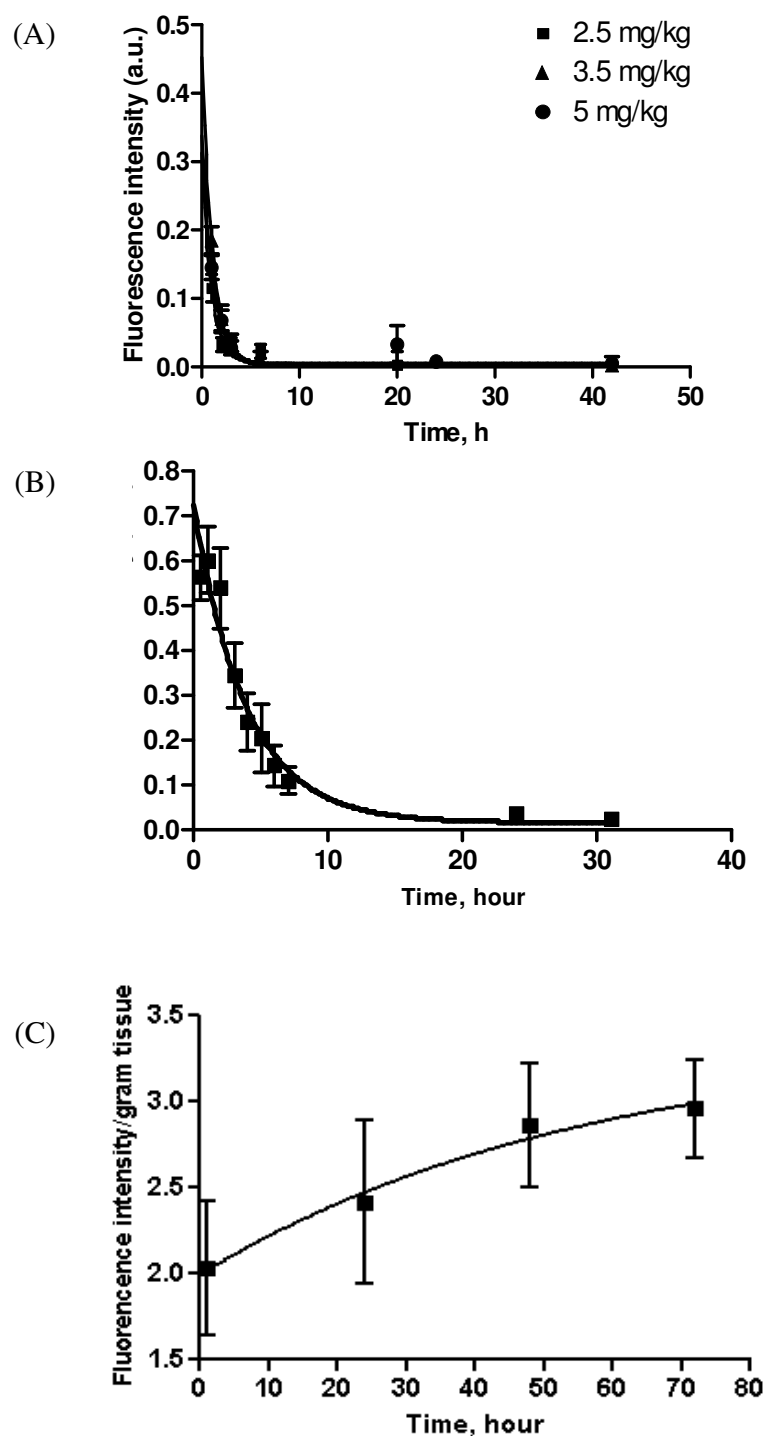


Figure 2.14 Fluorescence intensities of (A) Ce6-PVP, (B) Ce6 alone and (C) Photofrin measured over time in skin of Balb/c nude mice. For Ce6-PVP and Photofrin, mice were given a dose of 2.5, 3.5 and 5 mg/kg whereas for Ce6, mice were given 5 mg/kg only. Each plot represents a mean of at least 8 animals. Bars = standard deviation.

It is important to realize that following the administration of chemicals such as a photosensitizer, the skin is susceptible to photosensitivity and photoallergy [91]. Photosensitizers alone may have no toxic side effects, but when present in significant levels in the skin, they are known to exert severe cutaneous phototoxicity such as erythema or edema in the presence of light. Thus, photosensitizers with fast elimination rate from the skin are desirable in order to avoid prolonged photosensitivity in patients. Compared to Ce6 alone or Photofrin, the new formulation of Ce6-PVP uses its PVP component to alter its pharmacokinetics, thereby giving a faster clearance rate from the skin. It was documented that Photofrin induces cutaneous photosensitivity for up to 4-6 weeks during which time patients have to protect themselves from bright light, especially sunlight. In a comparative study to quantify the concentrations of 9 different photosensitizers in a C3H mammary carcinoma model, Qian et al. found that Ce6 had lower skin to tumor concentration ratios than Photofrin II [92]. Gomer et al. then compared another chlorine e6 derivative, NPe6 to Photofrin II, and the results showed significantly less skin damage using NPe6 with the same light and drug doses [93]. Following this, several studies have shown that NPe6 has good efficacy against superficial malignancies with temporary generalized skin photosensitivity that usually resolves within 1 or 2 weeks of dosing [94-96]. Similarly, our studies showed that Ce6-PVP exhibit even faster clearance from normal tissue and skin compared to Ce6 as detected by fluorescence imaging. In comparison to other photosensitizers such as Photofrin, 5-aminolevulinic acid, Foscan and Hypericin that are already in clinical use, the clearance rate of Ce6-PVP is faster, thus could potentially avoid the problem of prolonged skin photosensitization.

2.4.10 Tumor response post PDT

Using cross section from the center of the treatment field of the tumor, the volume of overall tumor necrosis was compared between control and PDT-treated animals using different combination of drug-light intervals (DLI), drug and light doses. Generally, tumor necrosis was enhanced with the increase in dosage of the photosensitizer and light. The region of necrosis in the tumor decreased with increasing DLI. Greater necrosis was observed for the 1 h DLI at all three drug doses compared to DLI between 3 and 6 h (Figure 2.15, Table 2.2). When the drug doses were increased to 3.5 and 5 mg/kg, and the light dose was increased to 150 J/cm², the percentage of necrosis was found to increase significantly ($p < 0.05$) compared to tumors treated at the drug dose of 2.5 mg/kg at 100 J/cm². At 200 J/cm², complete necrosis was observed at 2.5, 3.5 and 5 mg/kg ($p < 0.05$). However, drug toxicity to animals was observed when mice were administered more than 3.5 mg/kg at irradiations of 150 and 200 J/cm². When tumors were treated at 3 h DLI, significant tumor necrosis was observed with higher light doses of 150 and 200 J/cm² when compared to tumors treated with 100 J/cm² at a drug dose of 2.5, 3.5 and 5 mg/kg, respectively (Figure 2.16, Table 2.2). At 3 h DLI, lower drug and light doses did not seem to be as effective as 1 h DLI in inducing tumor necrosis. At 6 h DLI, no tumor necrosis was observed when the animals were treated with 5 mg/kg of Ce6-PVP at 50 J/cm² and less than 32 % of tumor necrosis was observed when the light dose was increased to 300 J/cm².

Vascular mediated PDT: 1 hr drug-light interval

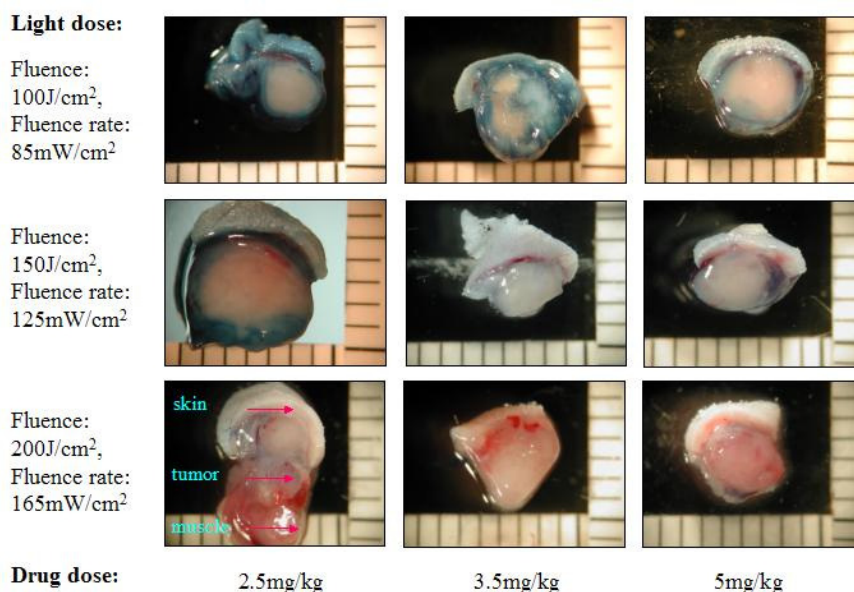


Figure 2.15 Cross-section of tumors xenografted on mice stained with Evans Blue dye at 48 h post PDT after treatment with various drug and light dose at 1 h drug-light interval. Blue region indicated viable tissue while white region indicated tumor necrosis.

Cellular mediated PDT: 3 hr drug-light interval

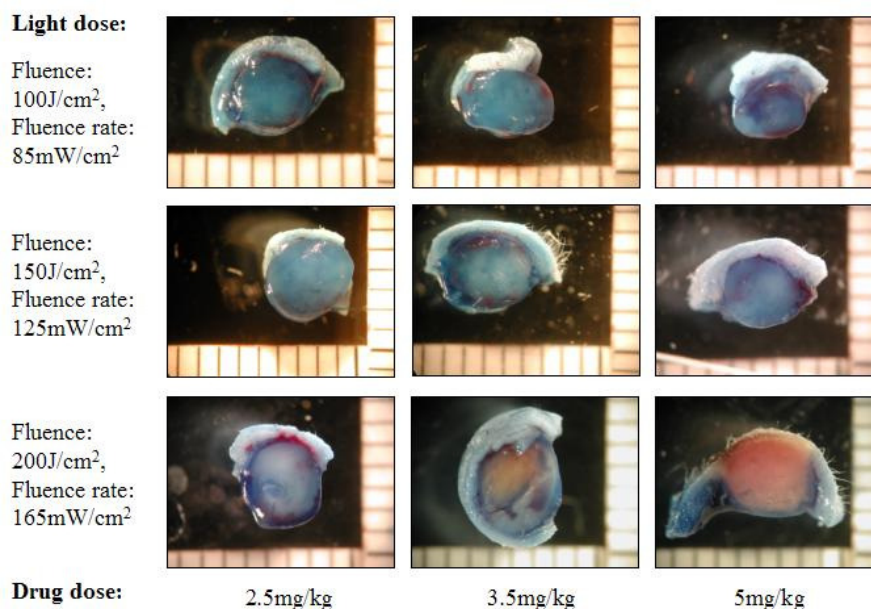


Figure 2.16 Cross-section of tumors xenografted on mice stained with Evans Blue dye at 48 h post PDT after treatment with various drug and light dose at 3 h drug-light interval. Blue region indicated viable tissue while white region indicated tumor necrosis.

Table 2.2 Percentage of tumor necrosis evaluated at 48 h post PDT after treatment with Ce6-PVP using various parameters.

Drug-light interval, h	Fluence, J/cm ²	Fluence rate, mW/cm ²	Ce6-PVP dose, mg/kg	Percentage of necrosis, %
1	50	41.5	5.0	74.8 ± 7.1
1	100	85	2.5	55 ± 31.7
1	100	85	3.5	62.5 ± 15.7
1	100	85	5.0	79.6 ± 10.8
1	150	125	2.5	70.4 ± 6.5
1	150	125	3.5	85.6 ± 14.0
1	150	125	5.0	95.1 ± 5.6
1	200	165	2.5	100
1	200	165	3.5	100
1	200	165	5.0	100
3	100	85	2.5	0
3	100	85	3.5	0
3	100	85	5.0	37.1 ± 32.6
3	150	125	2.5	46.1 ± 26.9
3	150	125	3.5	55.3 ± 30.6
3	150	125	5.0	71.6 ± 12.8
3	200	165	2.5	86.3 ± 7.3
3	200	165	3.5	89.8 ± 2.7
3	200	165	5.0	87.6 ± 10.5
6	50	41.5	5.0	0
6	300	165	5.0	31.5 ± 10.3

Table 2.3 Percentage of tumor necrosis evaluated at 48 h post PDT after treatment with Ce6 using various parameters.

Drug-light interval, h	Fluence, J/cm ²	Fluence rate, mW/cm ²	Ce6 dose, mg/kg	Percentage of necrosis, %
1	50	41.5	2.5	62 ± 15.1
3	50	41.5	2.5	25.5 ± 13.1
6	50	41.5	2.0	43.2 ± 10.0
6	100	85	2.5	67.9 ± 4.9

Tumor responses were also assessed after irradiation with Ce6 only (Table 2.3). Mice administered with more than 2.5 mg/kg of Ce6 and irradiated with light dose of more than 50 J/cm² at 1 and 3 h DLI did not survive up to 48 h post treatment due to phototoxicity. Only data from surviving mice is presented in Table 2.3. At the dose of 2.5 mg/kg at 1 h DLI, Ce6 mediated PDT was able to induce 62 % of tumor necrosis without causing any mortalities. At the same drug dose, the percentage of necrosis dropped to an average of 25.5 % when tumors were irradiated at 3 h DLI. However, when irradiation was performed at 6 h DLI with only 2 mg/kg, the percentage of necrosis increased to 43.2 %.

PDT requires an optimum dual dosimetry of drug and light dose to ensure tissue response. In order to achieve irreversible tumor necrosis it is necessary to surpass a certain threshold of light absorption. The light dose applied to the surface of the tumor must be sufficient to allow penetration to the deepest part of the tumor. In this chapter, it was demonstrated the dependence of fluence and fluence rate in determining the extent of necrosis in tumor using Ce6-PVP. Depending on the drug-light intervals, low light intensities could result in an

inefficient activation of the photosensitizer leading to poor tumor response whereas high light intensity could result in a better treatment outcome. In this experiment, for every drug-light interval where irradiation of the tumors was performed, the percentage of tumor necrosis increased with total fluence, but for longer drug-light intervals (3 or 6 h), high total fluences failed to produce a significant delay in tumor regrowth. This is in line with other literatures documenting well-known reciprocity between drug-light interval and light dose, which has been demonstrated in various experimental tumors [97]. Long drug-light interval However, high light intensity also causes the deoxygenation of tissue and possible hyperthermia which impede the subsequent biological processes [98]. Furthermore, a high light dose can also cause systemic toxicity, as has been demonstrated in this study. In addition, when a high light dose was administered, serious damage to normal tissue as well as internal organs beyond the irradiation area was observed.

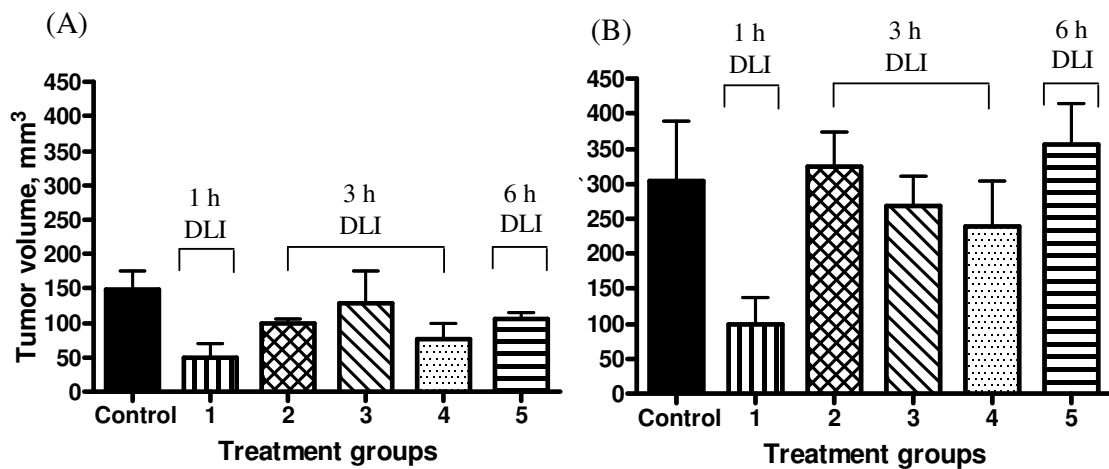


Figure 2.17 Short term evaluation of MGH tumor growth post PDT using various drug and light dosimetry. Mice were treated with the following parameters: Group 1 = 100 J/cm²; 85 mW/cm² at 1 h DLI, Group 2 = 150 J/cm²; 125 mW/cm² at 3 h DLI, Group 3 = 200 J/cm²; 165 mW/cm² at 3 h DLI, Group 4 = 300 J/cm²; 167 mW/cm² at 3 h DLI and Group 5 = 300 J/cm²; 167 mW/cm² at 6 h DLI. (A) Tumor volumes at 7 days post PDT and (B) tumor volumes at 14 days post PDT, with each point represent the mean of 4 animals. Bars = SE.

Based on the tumor necrosis study, selected parameters were chosen for the tumor growth delay studies. Tumors in all treatment groups exhibited growth inhibition at 7 days post PDT compared to the control group (Figure 2.17 A). However, after 14 days post PDT, only tumors treated at 1 h DLI at the light dose exhibited significant tumor growth inhibition ($p < 0.05$) compared to the control group (Figure 2.17 B). At the light dose of 300 J/cm², treatment at the 3 h DLI gave a better response when compared to the 6 h DLI. However, no significant growth inhibition of tumor was observed when treated at 3 and 6 h DLI compared to the control.

2.4.11 Toxicity effects

Mice were evaluated for survival after treatment with various parameters using Ce6 and Ce6-PVP. It was found that Ce6 alone was highly toxic at light doses exceeding 50 J/cm² at 1 and 3 h drug-light interval (Table 2.4). Even at 6 h drug-light interval, survival after treatment with 2.5 mg/kg of Ce6 and light dose of 100 J/cm² was 83%. On the contrary, Ce6-PVP was only toxic during the 1 h drug-light interval irradiation (Table 2.5). Ce6-PVP phototoxicity was mainly attributed to the combination of high light (200 J/cm²) and high drug doses (5 mg/kg) during which high bioavailability of the photosensitizer in serum as well as in normal tissue was detected at 1 h. There was a positive correlation between increasing doses of light and drug and toxicity, at the 1 h drug-light interval irradiation. When both photosensitizers were compared at the same drug-light interval, Ce6 was found to be more toxic than Ce6-PVP.

Table 2.4 The survival of mice was expressed as the number of mice that recovered from treatment 24 h post treatment with Ce6 alone.

Drug-light interval, h	Fluence, J/cm ²	Fluence rate, mW/cm ²	Ce6 dose, mg/kg	Survival.%
1	50	41.5	2.5	100 (3/3)
1	100	85	5	0 (0/3)
1	150	125	2.5	0 (0/3)
1	150	125	3.5	0 (0/3)
3	50	41.5	2.5	100 (4/4)
3	100	85	2.5	0 (0/4)
3	300	165	5	0 (0/4)
6	100	85	2.5	83 (5/6)

Mice were subjected to various parameters such as differing drug-light intervals, fluences, fluence rates and drug doses.

Table 2.5 The survival of mice was expressed as the number of mice which recovered from treatment 24 h post treatment with Ce6-PVP.

Drug-light interval, h	Fluence, J/cm²	Fluence rate, mW/cm²	Ce6-PVP dose, mg/kg	Survival, %
1	50	41.5	5.0	100 (3/3)
1	100	85	2.5	100 (3/3)
1	100	85	3.5	100 (3/3)
1	100	85	5.0	100 (3/3)
1	150	125	2.5	100 (3/3)
1	150	125	3.5	86 (6/7)
1	150	125	5.0	43 (3/7)
1	200	165	2.5	0 (0/3)
1	200	165	3.5	0 (0/3)
1	200	165	5.0	0 (0/3)
3	50	41.5	2.5	100 (3/3)
3	100	85	2.5	100 (3/3)
3	100	85	3.5	100 (3/3)
3	100	85	5.0	100 (3/3)
3	150	125	2.5	100 (3/3)
3	150	125	3.5	100 (3/3)
3	150	125	5.0	100 (3/3)
3	200	165	2.5	100 (3/3)
3	200	165	3.5	100 (3/3)
3	200	165	5.0	100 (3/3)
6	50	41.5	5.0	100 (3/3)
6	300	165	5.0	100 (3/3)

Mice were subjected to various parameters such as differing drug-light intervals, fluences, fluence rates and drug doses.

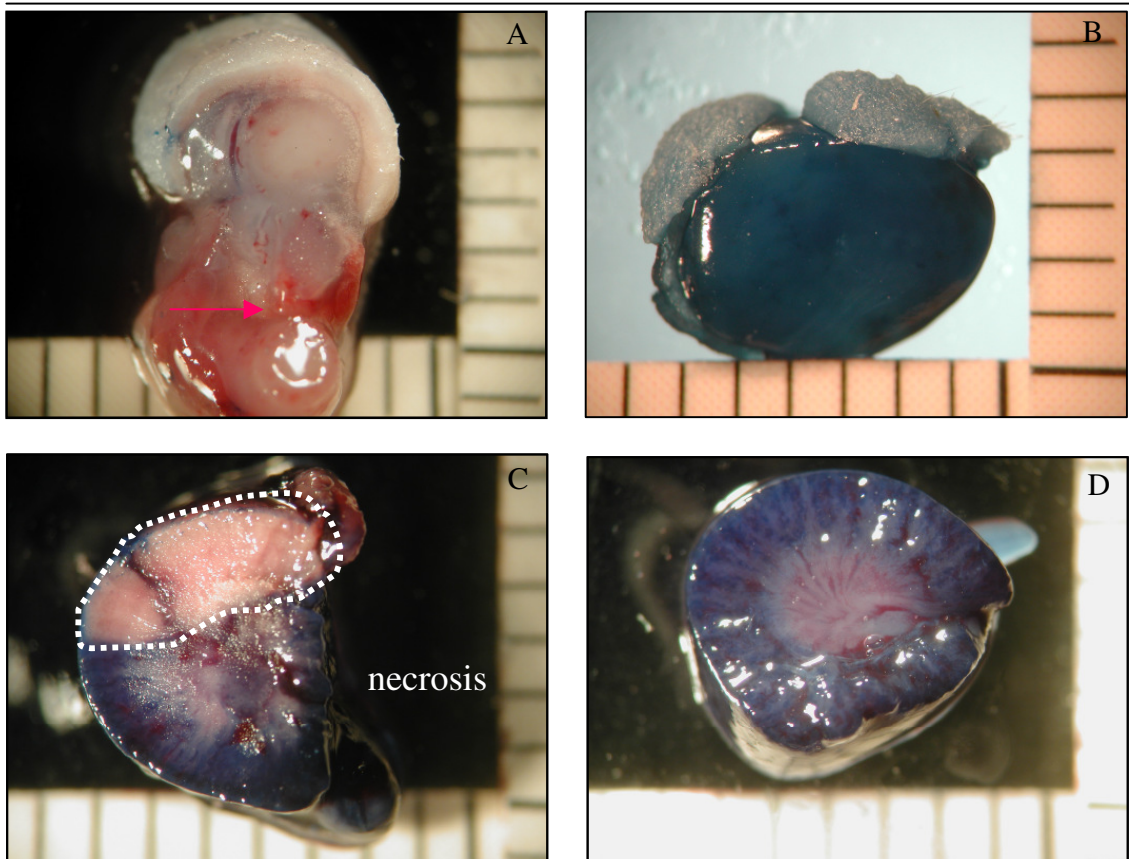


Figure 2.18 Cross section images of tumor and kidneys stained with Evan's Blue dye using a camera mounted on a stereomicroscope. The white area represents necrotic tissue whereas the blue area represents viable tissue. (A) The depth of necrosis in tumor was found to be around 8 mm. (B) Control tumor was administered with photosensitizer but not irradiated with light. (C) The kidney located underneath the irradiated side of the flank, showed necrosis (white line) after PDT, indicating that the depth of necrosis could reach more than 1 cm. (D) The kidney located on the opposite site of irradiation did not show any necrosis effect at post PDT. Bar = 1 mm.



Figure 2.19 Ce6-PVP induced depth of necrosis on the rat tumor model. Drug-light interval: 3 h; drug dose: 2.5 mg/kg for Rat 1 and 5 mg/kg for Rat 2; light dose: 200 J/cm² and 165 mW/cm²

In this experiment, mortality after PDT was mainly attributed to deeper penetration of necrosis beyond the tumors and into normal tissue. When post mortem was performed in mice treated at 1 h drug-light interval with high drug and light dose using Ce6-PVP, necrosis was observed to penetrate into the kidney (Figure 2.18). Total depth of necrosis was estimated to be around 1 - 1.2 cm. Preliminary experiments were conducted on two SD rats tumor model in order to confirm the depth of necrosis induced by Ce6-PVP mediated PDT (Figure 2.19). When a dose of 2.5 mg/kg Ce6-PVP was administered for rat 1 with a tumor height of 7.50 mm, complete tumor necrosis was found with a depth of 7.50 mm. When a higher dose of 5 mg/kg Ce6-PVP administered for rat 2, with a tumor height of 12.6 mm, the depth of tumor necrosis was found to be approximately 12 mm. Therefore, high-dose PDT at early time points using Ce6-PVP require stringent precautions due to its phototoxic effects.

A recent study had reported that PDT induced damage to other parts of organs besides the irradiated tumor [99]. Even death was reported in patients who underwent PDT treatment as a direct result of dose related toxicity [100].

Therefore, determining the correct drug and light dosimetry plays a crucial role in PDT to avoid unnecessary damage to normal tissue and to secure survival post PDT. Incorporating Ce6 with PVP has resulted in a potent, water-soluble photosensitizer preparation with less toxicity. A study has shown a reduced toxicity of a drug when conjugated to PVP when compared to its parent compound [62]. Furthermore, it was suggested that by coupling PVP to potentially immunogenic drugs, enzymes and hormones, it may be possible to diminish allergic hazards and drug inactivation due to specific antibodies in prolonged treatments [101]. Therefore, it was hypothesized that PVP may be used to improve the pharmacological activity and to reduce phototoxic effects of a photosensitizer such as Ce6.

2.4.12 Correlation of Ce6-PVP uptake in serum and percentage of tumor necrosis at post PDT

It was demonstrated that the intensity ratio of Ce6-PVP in tumor to healthy tissue of femoral muscle was higher compared to that of Ce6. This shows that Ce6 achieved higher specificity in the PVP formulation compared with that of Ce6 only. However, this higher specificity was not due to a higher permeability of the tumor tissue towards Ce6-PVP formulation. Rather, higher specificity was achieved through enhanced accumulation in tumor and rapid elimination of Ce6-PVP in normal tissue compared with that of Ce6.

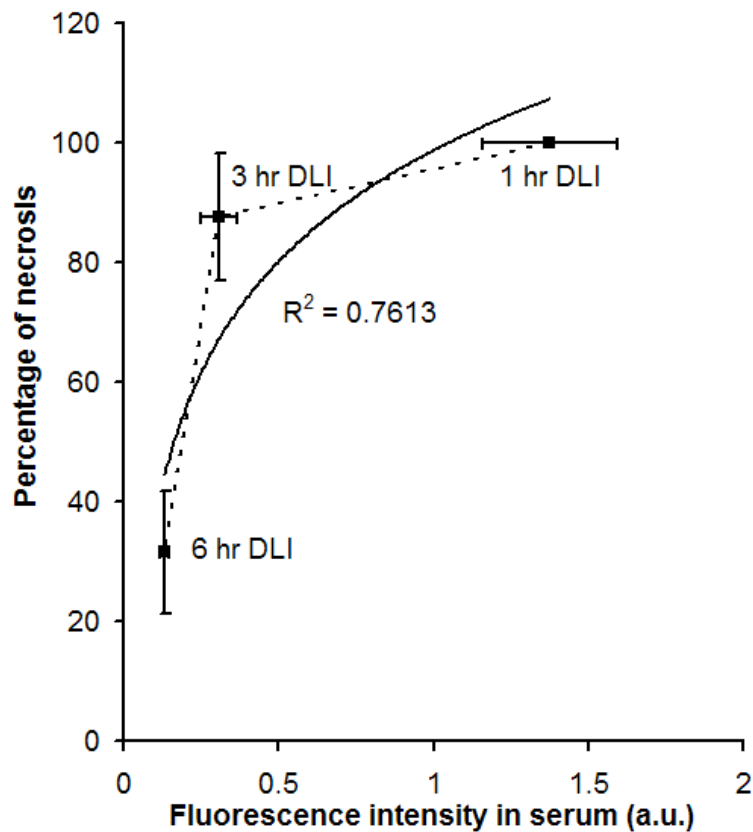


Figure 2.20 Correlation of percentage of necrosis post Ce6-PVP mediated PDT and level of Ce6-PVP in serum. The fluorescence intensity measured spectrometrically determined the level of Ce6-PVP in serum. Drug dose: 5.0 mg/kg, light dose of 200 J/cm² at 165 mW/cm². Each bar represents a mean of 3 animals. Bars = SE.

Even though a high tumor to normal tissue selectivity ratio of the Ce6-PVP was observed at 3 – 6 h DLI, tumor regression study performed in this chapter did not show an improved tumor response after 2 weeks post PDT (Figure 2.17). It was hypothesized that by the time a high selectivity was achieved (3 – 6 h post drug administration), the threshold concentration of the photosensitizer to produce reactive cytotoxins (i.e. free radicals and singlet oxygen) was probably not sufficient to induce a complete PDT response, thus the poor tumor response. This led us to believe that the tumor response for Ce6-PVP mediated PDT was strongly dependent on the drug-light interval.

A correlation between the percentage of tumor necrosis at post Ce6-PVP mediated PDT and the level of Ce6-PVP in serum was derived (Figure 2.20). The efficacy of Ce6-PVP mediated PDT was significantly more effective when irradiation was performed at 1 h DLI using high drug and light doses in which the drug level in the plasma was at its peak. The degree of relationship between the mean area of tumor necrosis after PDT and the mean fluorescence intensity of Ce6-PVP in serum was found to have a R^2 value of 0.7613. This observation further suggests that the mechanism of action of Ce6-PVP was much dependent on the drug accumulation in the vasculature rather than in the tumor tissue. This is in accordance with other studies of another form of water soluble Ce6, NPe6, where its efficacy was reported to be attributed mainly to the destruction of tumor vasculature by PDT. Maximal tumor response was achieved when light irradiation started within 2 h post intravenous administration of NPe6 and this effectiveness decreased when light treatments were initiated after 6 h [102]. In another investigation by Saito et al., NPe6 was found primarily in the plasma

during the first 2 h [103]. Their results ascertained that the NPe6 efficacy is dependent on its levels in the plasma rather than in the tumor tissue. The efficacy of NPe6 could be improved by increasing the drug dose, but this had to be done at the expense of tissue selectivity [94]. However, it has been contended that the necrosis of a margin of normal tissue surrounding the tumor is deemed necessary to achieve tumor cure [104]. Interestingly, our studies showed that Ce6-PVP concentration in plasma correlated well with fluorescence intensity in the tumor tissue. It is known that photosensitizers with hydrophilic properties are primarily transported by serum albumin and localize in the vasculature of the tumor, whereas hydrophobic photosensitizers tend to bind to lipoproteins and are internalized by cells through receptor-mediated endocytosis [80]. Cunderlikova et al. have reported that a decrease in the pH increased Ce6 binding to lipoproteins thereby implying that protonation could change the target of the photosensitizer's localization [105]. Ce6-PVP, being a hydrophilic compound, would tend to circulate in the blood and could be protonated in the proximity of a low pH environment of the tumor tissue and internalized by cells. This could explain the high level of fluorescence in blood as well as in the tumor tissue (Figure 2.10 and Figure 2.12).

2.5 Conclusion

Of late, constant efforts are being made to produce an ideal photosensitizer that is (i) a single compound; (ii) has increased absorbance in the red region of visible light; (iii) gives a high quantum yield of triplet formation; (iv) has good cytotoxic oxygen species generation; (v) shows increased selectivity for malignant tissue over normal tissue; (vi) and exhibits no dark toxicity. To date, Ce6-PVP seems to fulfill these requirements as an ideal photosensitizer. Polyvinylpyrrolidone in the

final formulation of Ce6-PVP ensures a higher relative bioavailability in healthy and tumor tissue compared to suspended chlorin, based on the same parenteral route of administration. This leads to several advantageous effects in the tumor tissues such as (a) high specific activity (the photosensitizing effect and the subsequent necrosis is higher than with chlorin alone) (b) selective accumulation in the tumor tissue, which is 2 to 4.8 times higher than with chlorin. It was demonstrated that Ce6-PVP accumulated selectively in a human bladder and nasopharyngeal tumor xenograft indicating the clinical potential in the detection of these cancer using fluorescence endoscopy. Fluorescence imaging modality may be able to identify the progression and margin of cancer in real-time, thereby providing a more sensitive and specific detection tool for bladder cancer. The preclinical evaluation of Ce6-PVP presented in this study has shown to have many desirable properties of an ideal photosensitizer and displays great potential to be an effective therapeutic agent. It was demonstrated that Ce6-PVP mediated PDT was most efficient when greatly localized in the circulating serum tumor as well as in the tumor tissue. The effectiveness of PDT also depends on the optimization of factors such as fluence (total light dose) and fluence rate. The frequency of complete tumor necrosis that can be achieved is considerably higher than those of chlorin (according to depth and frequency of complete tumor necrosis, inhibition of tumor growth) and Ce6-PVP has reduced systemic toxicity compared to Ce6 only at post PDT.

CHAPTER 3

New formulation of chlorin e6 – polyvinylpyrrolidone shows improved selectivity and specificity for fluorescence diagnostic imaging and photodynamic therapy of cancer

3.1 Summary

The focus of this chapter is to compare both the temporal and spatial kinetics of fluorescence intensities and PDT efficacy of an improved formulation of Ce6-PVP compared to Ce6 delivered using dimethylsulfoxide (DMSO) or 0.9 % sodium chloride. The Ce6-PVP used in this chapter had a purity of > 92%. Fluorescence data at 1, 3 and 6 h post drug administration were fitted into nonlinear regression analysis and receiver operating curves. In vitro and in vivo photodynamic efficiency were also studied using peripheral mononuclear cells, K562 leukemic cells and MGH poorly differentiated human bladder carcinoma cells. Temporal and spatial fluorescence results showed that Ce6-PVP had the higher tumor to normal tissue ratio compared to the other formulations. The sensitivity and specificity derived from the area under the receiver operating characteristic curve shows that the formulations are able to discriminate tumor from peritumoral muscle in the following order: Ce6-PVP > Ce6 > Ce6-DMSO. The present study also evaluated the potential use of Ce6-PVP for fluorescence detection and PDT on NSCLC and SCLC xenografts. Human NSCLC (NCI-H460) and SCLC (NCI-H526) tumor cell lines were used to establish tumor xenografts in the chick chorioallantoic membrane (CAM) model as well as in the Balb/c nude mice. In the CAM model, Ce6-PVP was applied topically (1.0 mg/kg) and fluorescence intensity was charted at various time points. Tumor-bearing mice were given

intravenous administration of Ce6-PVP (2.0 mg/kg) and laser irradiation at 665 nm (fluence of 150 J/cm² and fluence rate of 125 mW/cm²). Fluorescence studies in CAM tumor xenografts showed that Ce6-PVP had a selective localization and a good accuracy in demarcating NSCLC compared to SCLC from normal surrounding CAM after 3 h post drug administration. Irradiation at 3 h drug-light interval showed greater tumor necrosis against human NSCLC xenografts in nude mice. SCLC xenografts were observed to express resistance to photosensitization with Ce6-PVP. In vitro PDT results proved that Ce6-PVP was found to induce selective phototoxicity in leukemic cells compared to peripheral mononuclear blood cells. In addition, light irradiation at 1 h was found to induce greater tumor necrosis without causing animal toxicity. In conclusion, PVP significantly enhanced the Ce6 concentration in tumors compared with Ce6 alone and increased the therapeutic index of phototreatment without any side effects. This findings highlight the importance of optimising formulations as a way to improve photosensitizer accumulation in tumor tissue.

3.2 Introduction

Among the problems that are not yet adequately solved in the area of photosensitizer delivery are the difficulties in preparing pharmaceutical formulations that enable parenteral administration of the photosensitizer, poor tumoral selectivity, and a possible prolonged cutaneous photosensitivity due to slow elimination of the photosensitizer. Chlorins are promising photosensitizers with respect to their high phototoxic potential and relatively strong absorption in the red region of the visible spectrum leading to destruction of diseased tissue in deeper tissue layers. Although promising, chlorins are in general very lipophilic, making its administration *in vivo* relatively complicated. Water-soluble chlorin derivatives have been known to be prepared through stabilization and chemical transformation of lipophilic chlorophylls into a freely water-soluble sodium salt mixture. However, aqueous formulations or emulsions may not be suitable for tetra- or polypyrrole-based structures such as chlorins as these photosensitizers have an inherent tendency to aggregate by molecular stacking, which can severely curtail subsequent photosensitization processes [106, 107]. Therefore, multiple means of delivering chlorin-based photosensitizers have been explored ranging from liposomal formulation, glycoconjugation, microspheres, entrapment in biodegradable nanoparticles, to the use of excipients such as dimethylsulfoxide (DMSO). Due the amphiphilic nature of DMSO, it is used frequently to dissolve chemicals with poor water solubility. But the toxicological consequence of its interaction with a photosensitizer still remains unclear. Biocompatible block copolymers are also used increasingly in the pharmaceutical industry to enhance drug solubility and bioavailability [108]. Polymer-photosensitizer conjugation or encapsulation of the photosensitizer in colloidal carriers such as oil-dispersions, liposomes and polymeric particles has been

investigated [109, 110]. Polymers currently being used with chlorin derivatives are polyethyleneglycol and N - (2-hydroxypropyl) methacrylamide (HPMA) [56, 58, 111].

In the pursuit for strategies to optimize the photosensitizer Ce6 for improved fluorescence diagnosis and photodynamic therapy of cancer, formulation of Ce6 with PVP was investigated. Ce6 has improved efficacy and has decreased side effects compared to first generation photosensitizers from hematoporphyrin derivatives. PVP is nontoxic, biocompatible, generally recognized as safe, and is a widely used soluble additive in the pharmaceutical area. PVP is known to form water-soluble complexes with a number of pharmacological substances and investigations into the formation of PVP – complexes with drugs have been described [65, 112].

In the previous chapters, the purity of Ce6 in the PVP formulation used in the experiments contained not less than 75% with the remaining composition consisting of purpurins [113]. In this chapter, the uptake and photodynamic activity of the newly improved formulation of Ce6-PVP was investigated. The weight ratio of the sodium salt of Ce6 and PVP remained at 1:1 and the purity level of Ce6 was optimized to 92 – 99 %.

3.3 Materials and methodology

3.3.1 Photosensitizers and chemicals

The earlier Ce6-PVP used in Chapter 2; hereafter designated as 75% Ce6-PVP. The new formulation of Ce6-PVP was manufactured by ORPEGEN Pharma GmbH, Heidelberg, Germany, the external collaborator for this research project. The new Ce6-PVP was relatively free of impurities and the purity of the drug is around 92 – 99 %. Reversed phased HPLC chromatograms were provided by ORPEGEN Pharma. The detection wavelength used in the spectrophotometric detector was set at 400 nm. Instrument settings were optimized to obtain fragmentation spectra of chlorin e6 as follows: gradient: 50 –100%, column: Lichrospher RP-18e 250 × 4.6 mm (Merck, Germany) and elution temperature: 25°C. In both cases it was a co-lyophilisate of Ce6 sodium salt and PVP (pharmaceutical grade polymer, molecular mass ≈ 12,000 g/mol) in a 1:1 mass ratio. Ce6 sodium salt lyophilized without further addition of PVP and is readily soluble in aqueous solution. An alternate source of Ce6 in the acetic acid form was obtained from Frontier Scientific (Logan, Utah). It was dissolved in dimethylsulfoxide (DMSO), (Sigma, USA) to give a 1 mM stock solution; and diluted further with 0.9% sodium chloride (NaCl) to constitute a 10% DMSO concentration in the final preparation immediately before intravenous administration.

3.3.2 *In vitro* photosensitizing efficacy

To distinguish between necrotic and apoptotic cells following PDT, Annexin V binding and propidium iodide (PI) uptake were assessed by flow cytometry using a commercially available kit according to the instructions by the manufacturer. Peripheral mononuclear blood (PMN) cells obtained from healthy volunteers and

a K562 leukemic cell line were used for this experiment. Cells were incubated with 10 μ M of either Ce6 or Ce6-PVP for 30 min before exposure to a light dose of 1 J/cm². Cells were harvested and resuspended in binding buffer provided in the kit. Designated concentration of the Annexin V stock solution and PI stock solution were added to the cell suspension. After incubation for 10 min in the dark, the cells were immediately analyzed with a FACScan flow cytometer (Becton Dickinson) equipped with an excitation laser line at 488 nm. The FITC – Annexin V (green fluorescence) and the PI (orange fluorescence) were collected in log scale through 530 \pm 20 nm and 575 \pm 15 nm band pass filter respectively.

3.3.3 Bladder tumor model

Male Balb/c athymic nude mice, 6–8 weeks of age, weighing an average of 24 g were obtained from the Animal Resource Centre, Western Australia. The cells were cultured as a monolayer in RPMI-1640 medium supplemented with 10% fetal bovine serum, 1% non-essential amino acids (Gibco, USA), 1% sodium pyruvate (Gibco, USA), 100 units mL⁻¹ penicillin–streptomycin (Gibco, USA) and incubated at 37°C, 95% humidity and 5% CO₂. Before inoculation, the cell layer was washed with phosphate-buffered saline (PBS), trypsinized, and counted using a hemocytometer. Approximately 3.0 \times 10⁶ MGH cells in 150 μ L of Hanks' Balanced Salt Solution (Gibco, USA) were injected subcutaneously into the lower flanks of the mice. The animals were used for experiments when the tumors measured around 5 – 10 mm in diameter. All procedures were approved by the Institutional Animal Care and Use Committee, SingHealth, Singapore, in accordance with international standards.

3.3.4 Cell culture

MGH, a poorly differentiated human bladder carcinoma cells were grown as subcutaneous tumor xenografts. The NCI-H460 cell line originates from human carcinoma of the large cell lung cancer. NCI-H526 cell lines originate from human carcinoma of the lung from the variant small cell lung cancer were obtained from the American Type Culture Collection, USA. NCI-H460 cells were cultured as a monolayer whereas NCI-H526 cells were cultured in suspension in RPMI-1640 medium supplemented with 10 % fetal bovine serum, 1% non-essential amino acids (Gibco, USA), 1 % sodium pyruvate (Gibco, USA), 100 units/mL penicillin/streptomycin (Gibco, USA) and incubated at 37°C, 95 % humidity and 5 % CO₂. Before inoculation, the monolayer cells were washed with phosphate-buffered saline, trypsinized, and counted using a haemocytometer. Suspension cells were directly counted using a haemocytometer without trypsinization.

3.3.5 Chick chorioallantoic membrane (CAM) tumor xenograft

Fertilized chicken eggs were incubated at 37°C in a humidified atmosphere inside a hatching incubator equipped with an automatic rotator (Octagon 20, Brinsea, Somerset, UK). At embryo age (EA) 7, a window of about 1.5 cm was opened in the eggshell to detach the shell membrane from the developing CAM. Then, the window was sealed with sterilized parafilm to avoid contamination and the eggs were returned to the static incubator for further incubation until the day of experiments. On EA 9, approximately 5×10^6 NCI-H460 and NCI-H526 cells were inoculated on the CAM. The window of the eggs were resealed with sterile parafilm and returned to the static incubator. Grafted cells were allowed to grow on the CAM for up to 5 days. On EA 14, Ce6-PVP was dissolved in 0.9% sodium chloride to constitute a stock solution of 1 mg/mL. The stock solution was further

diluted to obtain a volume of 80 μL containing a dose of 1 mg/kg body weight of the chick's embryo. The photosensitizer was applied on the entire surface of the CAM and left to incubate for 30 min. The window was resealed to avoid evaporation of the drug solution from the CAM. After 30 min incubation, imaging was performed at 0.5, 1, 2, 3, 4, 5, 6, and 24 h post drug administration. All procedures involving preparation and administration of the photosensitizer were conducted under low ambient lighting.

3.3.6 Fluorescence imaging and image analysis

Mice were randomly assigned to receive a dose of 2.5 mg/kg of the Ce6-PVP, Ce6 or Ce6-DMSO via tail vein injection. At 0, 1, 3 and 6 h post drug administration, mice were sacrificed and the skin overlaying the tumor was carefully removed to expose the tumor and normal peritumoral muscle for fluorescence imaging. A commercially available fluorescence endoscopic system (Karl Storz, Tuttlingen, Germany) was used to perform the macroscopic fluorescence digital imaging. A modified xenon short arc lamp (D – Light system in blue light mode, Karl Storz) filtered by a band pass filter (375 – 480 nm) was used for excitation of the photosensitizer in tissue. Fluorescence was captured via a sensitive CCD camera (Tricam SL PAL, Karl Storz) attached to an endoscope integrated with a long pass filter (cut-off wavelength 560 nm). The red channel registered the photosensitizer fluorescence and the blue channel captured the diffusely back-scattered excitation light. The distance between tissue surface and probe lens was standardized before imaging. This was done to minimize variations due to geometrical factors such as fluorescence excitation and collection angles. In addition, a short exposure of the surface of tumor and peritumoral muscle to the excitation light (10 s) was performed to avoid

excessive photobleaching effects. The intensities of the red (IR) and blue channels (IB) of the fluorescence images were extracted using the software MicroImage (Olympus Optical Co. (Europa) GmbH, Germany) according to the following equation:

$$IR_N = [IR_t/IB_t] - [IR_{t_0}/IB_{t_0}] / (\text{equimolar dose of Ce6 administered})$$

with IR_N = normalized relative fluorescence intensity of tumor or peritumoral muscle at time, t , after drug administration; IR = intensity of red channel; IB = intensity of blue channel; t = time in hours after drug administration; t_0 = time before photosensitizer administration. The red-to-blue intensity ratio algorithm is independent of the observation geometry, the distance between the endoscope tip and the observed tissue as well as the fluctuation of the excitation irradiance [26].

3.3.7 Nonlinear regression and statistical analysis of fluorescence intensity

The normalized relative fluorescence intensities (after subtraction of background signal of fluorescence intensities) versus time obtained from equations (1) were analyzed by means of nonlinear regression method (Graph-Pad Prism™ Version 4.03) by fitting a three parameter monoexponential decay curve to fit the K , decay rate constant (in hours^{-1}). Bi-exponential decay curves fit the data more poorly than the mono-exponential ones and were therefore not considered for the analysis. The validity of K in the mono-exponential model was verified with the test of runs in each case. For all of the fits, the test of runs did not detect any deviation from the model of monoexponential decay. To compare the fits of the Ce6 formulations to each data set, the K was compared using extra sum-of-

squares F test by comparing a global fit (one shared best-fit K value for all the data sets) to individual fits (a different best-fit K value for each data set). For all the formulations, the F tests showed that the individual fits for tumor, peritumoral muscle and skin was determined as the preferred fit in the analysis. These ratios for tumor and peritumoral muscle from 1 to 6 h post drug administration were then analyzed for sensitivity and specificity in demarcating tumor from peritumoral muscle by fitting the data into the receiver operating characteristic (ROC) curve (Graph-Pad Prism™ Version 4.03). The ROC curve illustrates the tradeoff between sensitivity and specificity by plotting the tumor fluorescence against the peritumoral fluorescence for the different possible probability thresholds of a fluorescence diagnostic test of the various Ce6 formulations. White light imaging was used to confirm the presence of tumor and peritumoral muscle.

3.3.8 Statistical analysis of fluorescence image

To statistically evaluate the temporal fluorescence of Ce6-PVP, logistic regression and receiver operating characteristics (ROC) curve [115] was determined using the GraphPad software for Windows (GraphPad, San Diego, CA). The elimination rate constant of Ce6-PVP was calculated by a method fitting the data to a one-phase exponential decay equation. The validity of fitted curve was verified with the test of runs (F test) in each case. Area under the curve (AUC), P value, and cut-off point were obtained from the ROC curve. The area under the ROC curve measures accuracy of the fluorescence images. The accuracy of the ROC curve analysis is based on how well the fluorescence images discriminates the tumor region from the normal CAM, as defined by white light imaging. The closer the curve follows the left border and then the top border

of the ROC space, the more accurate the test. The closer the curve comes to the 45-degree diagonal of the ROC space, the less accurate the test. In addition, likelihood ratios (where the likelihood ratio is defined as the ratio of the probability of the fluorescence signal for tumor to the probability of the fluorescence signal for normal region) were calculated to help determine the 'best' cut-off point to compare sensitivity and specificity between NSCLC and SCLC.

3.3.9 Chemical extraction and spectrofluorimetry analysis

After imaging at 1, 3 and 6 h, the following tissues were removed and rinsed with PBS: tumor, muscle, skin, liver, spleen, kidney, brain, heart, lung, large intestine and small intestine. The organs were then blotted dry on tissue paper, weighed and frozen at $-80\text{ }^{\circ}\text{C}$ until extraction. Samples of each tissue (15 – 35 mg) were mixed with 1 – 2 mL of SolvableTM (Packard Instrument, USA) and incubated at $50\text{ }^{\circ}\text{C}$ for 16 h in the dark as described previously by Bellnier et al [116].

SolvableTM contains 3% N,N-dimethyl lauryl amine oxide, 3% alkyloxypolyethyleneoxyethanol and 2% sodium hydroxide in water. It was confirmed that this method did not affect the fluorescence property of Ce6 (unpublished data). The fluorescence ($\lambda_{em} = 665\text{ nm}$) of the solubilized samples was measured by a spectrofluorophotometer (model RF-5301 PC, Shimadzu; $\lambda_{ex} = 400\text{ nm}$). The level of fluorescence intensity of the tissue samples is proportional to the tissue concentration of Ce6. The background fluorescence before drug administration was also subtracted and was normalized to the weight of organs. Dunn's multiple comparison test were performed on the various groups. Statistical significance was accepted at $p < 0.05$

3.3.10 PDT treatment on murine xenograft model

Male Balb/c athymic (nu+/nu+) mice were used for tumor xenografting at the age of 8–10 weeks. Approximately 3.0×10^6 NCI-H460 and NCI-H526 cells suspended in 150 μ L of Hank's buffered saline solution were injected subcutaneously into both lower flanks of the mice. The animals were used for experiments when the tumors measured around 5-10 mm. For the bladder tumor model, a dose of 5 mg/kg of the photosensitizer was administered intravenously through the tail vein. For the lung tumor model, a dose of 2.0 mg/kg of the photosensitizer was administered intravenously. The mice were anaesthetized with 50 μ L cocktail of ketamine hydrochloride (50 mg/mL, Trittau, Germany) and valium (1:1 vol/vol) through intraperitoneal injection. A portable diode laser (Ceralas PDT 665, Biolitec) emitting at a wavelength of 665 ± 3 nm was used for irradiation. The peak power output was calibrated to 1.65 W at the fiber tip before commencement of irradiation. The laser energy with a total fluence of 100 J/cm² and a fluence rate of 83 mW/cm² was delivered to the surface of the bladder tumor via a silica fiber frontal light distributor (FD model, Medlight, Switzerland). For the lung tumor, a total fluence of 150 J/cm² and a fluence rate of 125 mW/cm² was delivered. The fiber was positioned to produce a 1.0 cm² circular spot of light irradiation. Fluence rate was measured using a power meter (LaserCheck, Coherent, USA). PDT treatment was performed after a drug-light interval (DLI) of either 1, 3 or 6 h on one tumor while the contralateral tumor that was not irradiated served as controls. All procedures were approved by the national experimental animal welfare institution (Institutional Animal Care and Use Committee, SingHealth, Singapore), in accordance with international standards.

3.3.11 Assessment of tumor response post PDT

The evaluation of tumor necrosis was performed using Evans Blue (EB) (Merck, Germany) vital staining. At 48 h post PDT, 1% EB in PBS was injected intraperitoneally at a volume of 0.4 mL. Six hours later, mice were sacrificed and the tumors were excised. Gross images of the whole tumor were first taken for fractal analysis of blood vessel. Fractal analysis has been shown to be an effective technique for measuring the complexity of blood vascular networks (Kirchner et al., 1996). This kind of analysis can be summed up as simply a measure for space-filling. Rectangular region of interests which maximally covered the tumors were selected from the captured images. These images were inverted and skeletonized with a fixed thresholding. The fractal dimensions of the 2-D binary images were then computed using the box-counting method [117]. The computed fractal dimension, D_f , gives us a statistical measure of the space filled by the blood vessels. Then, around 2 – 3 mm thick cross-section slices were cut and imaged under a stereoscopic microscope (Stemi 2000C, Zeiss, Germany). The unstained area was attributed to tissue necrosis, whereas the stained area indicated viable tissue. Digital images were saved in JPEG format, and all analyses were carried out using NIH ImageJ 1.37v software. Each image captured had the same calibration values to allow uniformity in the processing of the images. The tumor was outlined using the freehand drawing tool to measure the total tumor area. Similarly the necrotic area of the tumor was measured. The percentage of necrosis was calculated as the necrotic area divided by the total tumor area multiplied by 100. Statistical analysis (Student t test) was used for multiple comparisons. The criterion for statistical significance was set at the 0.05 level.

3.4 Results and discussions

3.4.1 HPLC chromatogram of two formulations of Ce6-PVP and Ce6

A representative chromatogram of the new Ce6-PVP with higher purity in normal phase conditions is shown in Figure 3.1. It was concluded that the new Ce6-PVP was relatively free of impurities and the purity of the drug was more than 92 %.

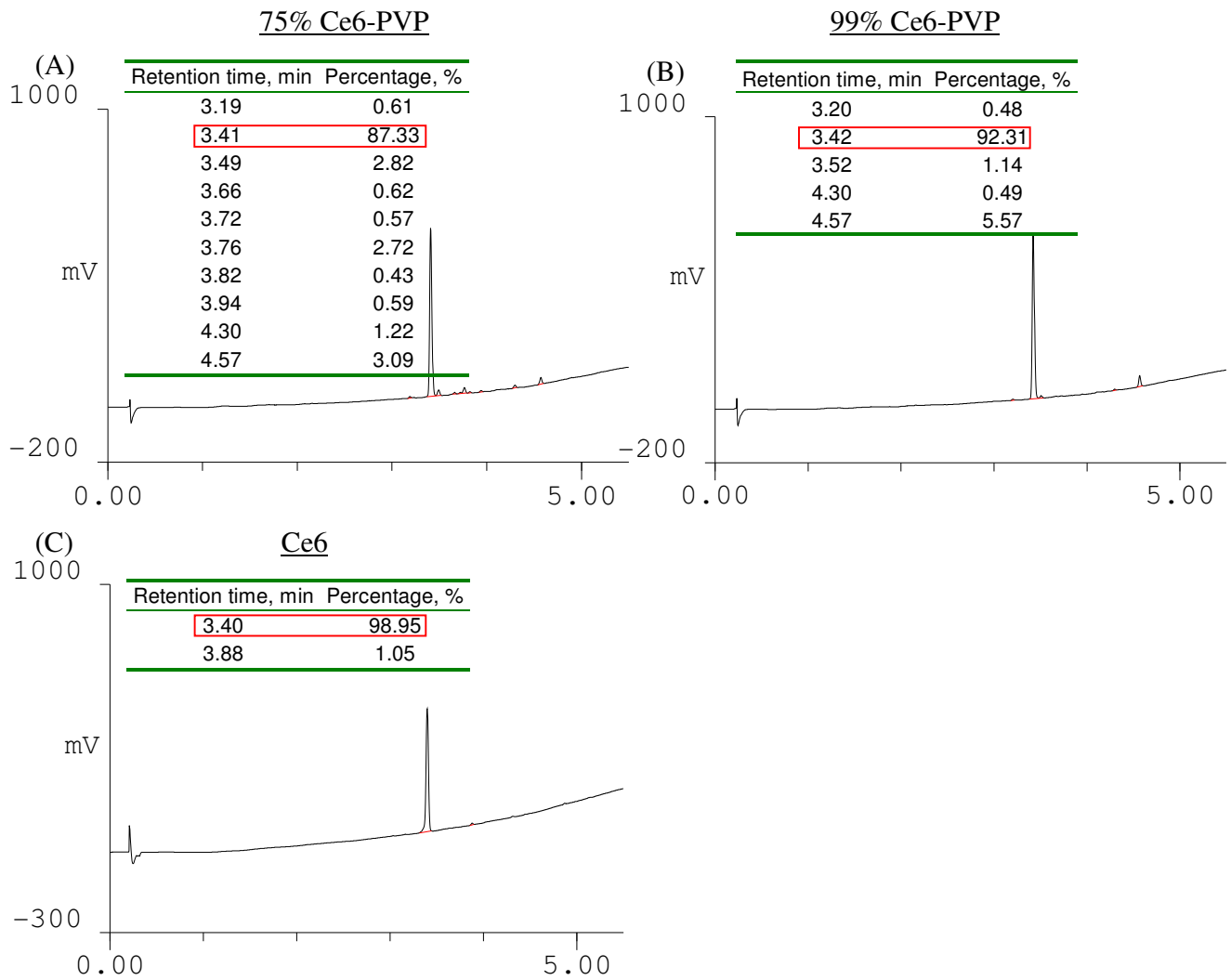


Figure 3.1 HPLC chromatogram describing the chemical purity of 75% Ce6-PVP and 99% Ce6-PVP and Ce6.

3.4.2 *In vitro* photosensitizing efficacy

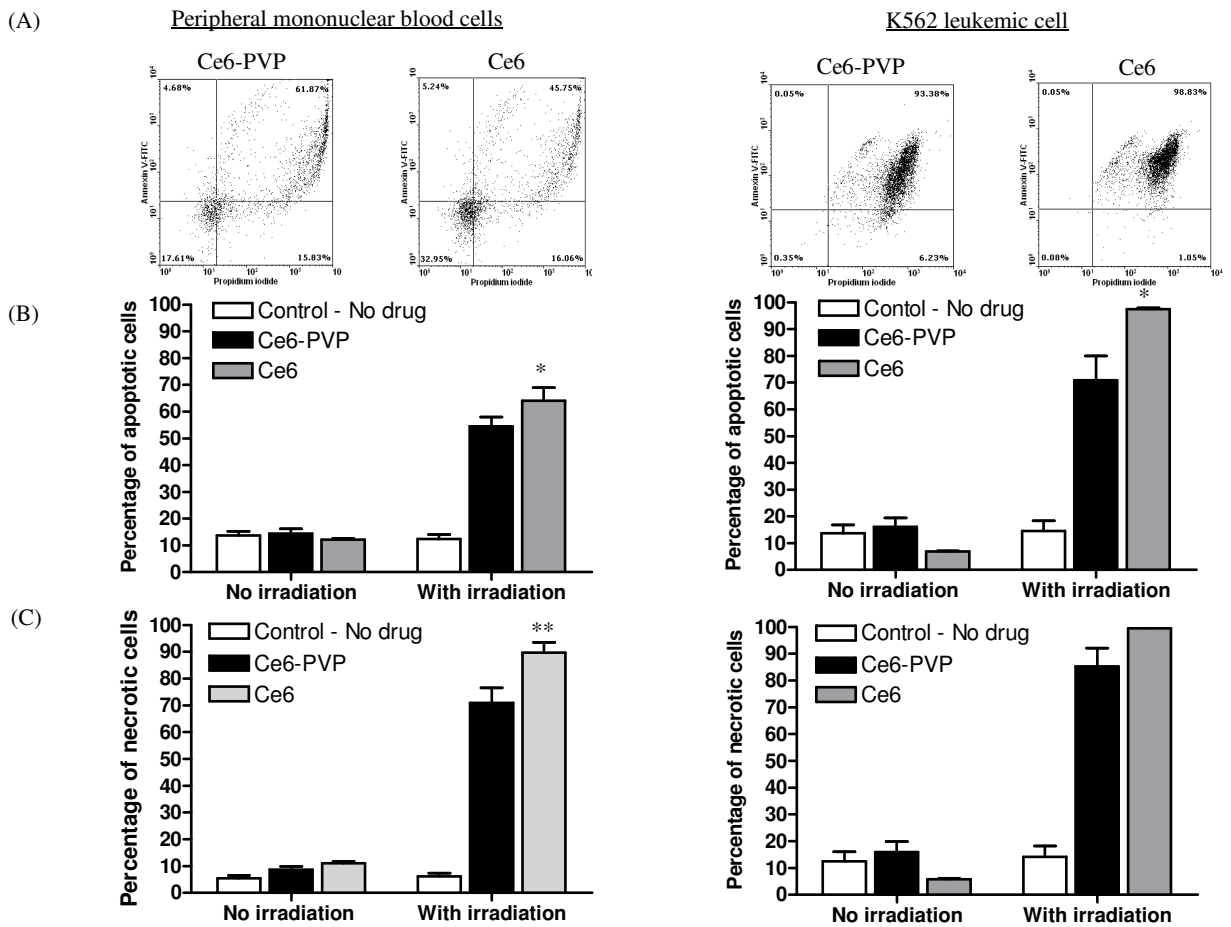


Figure 3.2 (A) Representative of flow cytometry analysis of PDT induced apoptosis and necrosis for PMN blood (normal) cells (left panel) and K562 leukemic cells (right panel) after treated with Ce6 and Ce6-PVP. Apoptosis and necrosis was detected through the accumulation of Annexin – V and propidium iodide (PI) stained cells respectively. Cells were incubated with a concentration of 10 μM of either Ce6 or Ce6-PVP for 30 min before light irradiation of 1 J/cm^2 . Three main subpopulations, corresponding to viable cells (lower left quadrant), apoptotic cells stained with Annexin – V (upper right quadrant), and dead/necrotic PI-stained cells (lower right quadrant), can be readily differentiated. (B) In terms of apoptosis, both Ce6 and Ce6-PVP demonstrated lower percentage of apoptotic cell death in PMN cells compared to K562 leukemic cells. However, Ce6 displayed higher photocytotoxicity in both PMN and K562 cells compared to Ce6-PVP, indicating the potency of Ce6. (C) When the total percentage of cell death (apoptosis and necrosis) was tabulated, Ce6 was found to induce significant cell death in PMN cells compared to Ce6-PVP, indicating toxicity to normal cells, while for K562 cells photocytotoxicity was comparable between the Ce6 and Ce6-PVP. For K562 cells, data for Ce6-PVP represent a mean value of 6 replicates while data for Ce6 represents a mean value of 3 replicates. For PMN cells, data for Ce6-PVP represent a mean value of 15 replicates taken from 5 volunteers while data for Ce6 represents a mean value of 6 replicates taken from 2 volunteers. Bars = SD. * $p < 0.05$ and ** $p < 0.01$ with respect to Ce6-PVP).

Ce6-PVP and Ce6 were evaluated for their photocytotoxicity against K562 leukemic cell line and peripheral mononuclear cells (Figure 3.2). Necrotic cells were identified through PI staining and apoptotic cells were identified through Annexin V staining, detected by flow cytometry after PDT. Cells illuminated without the photosensitizers and cells kept in the dark in the presence of the photosensitizers did not present any significant loss of viability. For the K562 cell line, total dead cells were estimated to be around 90% and 100% for Ce6-PVP and Ce6 respectively. On the contrary, under the same treatment condition, the peripheral mononuclear blood cells treated with Ce6-PVP exhibited relatively lower percentage of total dead cells (70%, $p < 0.01$) compared to Ce6 (90%). Often, photosensitizers are administered in relatively high doses, which lead to nonspecific toxicity in normal cells. Thus it is of interest to evaluate the intrinsic sensitivity of normal (PMN cells) and cancerous (K562 cells) leukemia cells to PDT using Ce6 formulated with or without PVP using *in vitro* phototoxicity experiment that strictly controlled for light and photosensitizer exposure. *In vitro* Ce6-PVP mediated PDT studies demonstrated that leukemic cells were considerably more affected than PMN cells, supporting the hypothesis that Ce6-PVP accumulated preferentially in tumor cells compared to normal cells. This is extremely important for the application of PDT in cancer, since Ce6-PVP is administered intravenously and is supposed to localize and kill only the malignant cells after light irradiation. A recent *in vitro* investigation on cervical and esophageal cancer cell lines determined that the mechanism of Ce6-PVP induced cell death involves the induction of ROS via a type I mechanism which resulted in the rapid increase in lactate dehydrogenase that suggested characteristics of necrotic cell death pathway [118]. In our experiment, more apoptotic cells were observed and this contrary results may be due to differences

in drug dosage, formulation, light dose/source and cell lines since work carried out by us and other groups has shown the proportion of PDT-induced apoptosis and necrosis is dependent on the treatment parameters used.

3.4.3 Biodistribution of Ce6 formulations

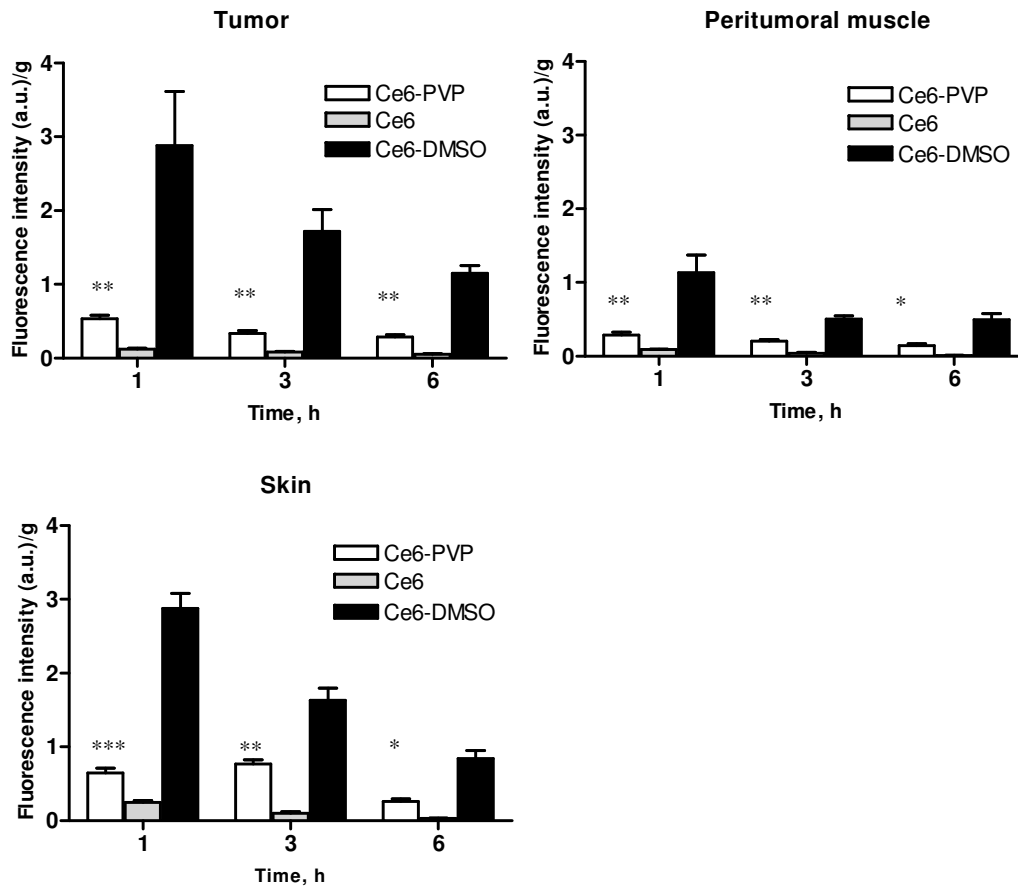


Figure 3.3 Comparison of biodistribution of Ce6-PVP, Ce6 and Ce6-DMSO in tumor, muscle and skin at 1, 3 and 6 h post drug administration respectively using chemical extraction method. For all data points, $n = 4 \pm SD$. Statistical significance was calculated by two-way ANOVA with Bonferroni post hoc test (* $p < 0.05$; ** $p < 0.01$, *** $p < 0.001$ with respect to Ce6). All Ce6-DMSO data points were statistically significant with respect to Ce6.

The amount of photosensitizers from tumor, peritumoral muscle and skin were quantified using the chemical fluorescence extraction technique and cuvette-based spectrofluorimetry (Figure 3.3). The amount of Ce6-PVP accumulation was significantly higher in the tumor, muscle and skin compared to Ce6 at all time points. Ce6-DMSO tumor accumulation was observed to increase 24 fold compared to Ce6 at 1 h. Similarly, Ce6-DMSO accumulation was higher in muscle and skin at 3 and 6 h post administration in compared to Ce6. The tumor

to normal peritumoral muscle ratio for Ce6-PVP was higher compared to Ce6 (Table 3.1) suggesting that Ce6-PVP has a good tumor tissues accumulation ratio, with no significant accumulation in other normal tissue. Although Ce6-DMSO showed the highest tumor to normal peritumoral muscle ratio, it also resulted in higher accumulation in other normal organs. Figure 3.3 shows comparative biodistribution of Ce6-PVP, Ce6 and Ce6-DMSO in eight organs using chemical extraction method. The data demonstrates that the amount of drug was comparable in all the organs between Ce6 and Ce6-PVP. In contrast, the amount of the Ce6-DMSO accumulation was significantly 10-fold higher in the liver, spleen, kidney, brain, heart and lung. The most significant amount of photosensitizer detected from all of the tested formulations was concentrated in the small and large intestines with relatively similar concentrations. The accumulation of Ce6-PVP in tumor significantly exceeded liver, spleen, kidney, brain, and heart tissues compared to Ce6.

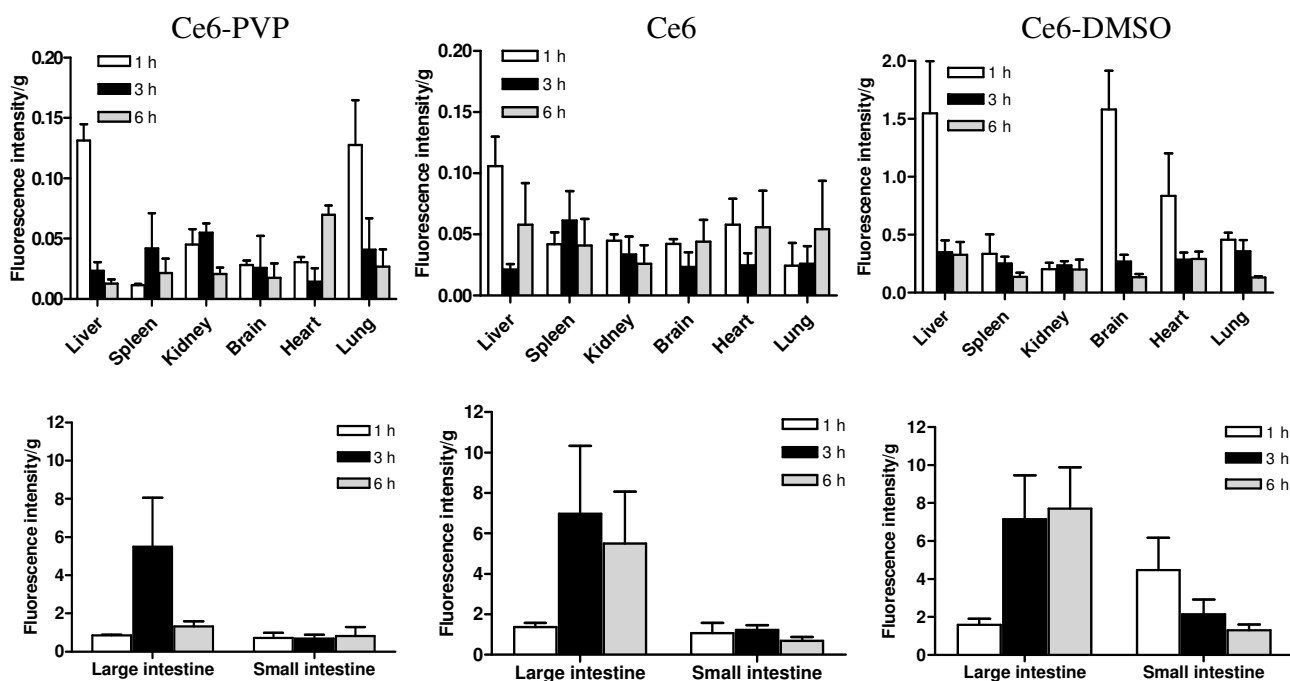


Figure 3.4 Comparison of biodistribution of Ce6-PVP, Ce6 and Ce6-DMSO in normal tissue of various organs in mice using chemical extraction method. Each data point represents a mean of 3 animals \pm SD.

Table 3.1 Comparison of tumor to normal tissue ratio in various organs after intravenous administration of 5 mg/kg Ce6-PVP, Ce6 or Ce6-DMSO.

	Muscle	Skin	Liver	Spleen	Kidney	Brain	Heart	Lung
Ce6-PVP	1.8	1.5	2.0	23.5	10.1	16.6	15.5	2.9
Ce6	1.0	0.4	1.2	2.9	3.0	3.9	3.1	4.3
Ce6-DMSO	2.6	1.0	1.2	8.5	15.6	0.9	3.1	5.9

Ratio was calculated by dividing the fluorescence intensity span of tumor to the fluorescence intensity span of the various tissues from 1 to 6 h post drug administration. The span was tabulated using nonlinear regression analysis.

In vivo biodistribution data indicated that the tumor uptake of Ce6 in the PVP formulation was enhanced compared to Ce6 alone. At the same time, Ce6-PVP accumulation in the skin was also higher than Ce6 suggesting that Ce6-PVP has

the potential for skin photosensitivity in mice due to their relatively thin skin. However, this may not be a significant problem for human skin since human skin is considerably thicker than mice skin [119]. It was further confirmed that Ce6-PVP had preferential tumor accumulation in comparison with all normal tissues, with tumor to normal tissue ratio ranging from 1.5 to 23.5 (Table 3.1). The excretion of organic photosensitizer normally starts from the liver into the bile via the gall bladder. The bile is routed into the duodenum where it was possible for unchanged Ce6 to be absorbed into the circulation a second time from the small intestine as well as being excreted via fecal elimination. Hence, high photosensitizer level was observed in the small and large intestines. Not surprisingly, Ce6 delivered using DMSO showed 6-fold enhancement of Ce6 accumulation in tumor, muscle and skin compared to Ce6 alone or Ce6-PVP. This was mainly due to the membrane penetrant-carrier properties of DMSO. However, the decay rate constant of Ce6-DMSO was found to be greater than the decay rate constant of Ce6 and Ce6-PVP in tumor. This resulted in rapid elimination Ce6-DMSO from the tumor tissues that could limit its therapeutic effect. Furthermore, it was an indication that the penetration effect provided by DMSO was irreversible in tumor and even in normal cells. Moreover, the enhanced uptake was indiscriminate and also accumulating in normal organs. This effect was clearly seen in our in vivo study.

3.4.4 Sensitivity and specificity of Ce6 formulations

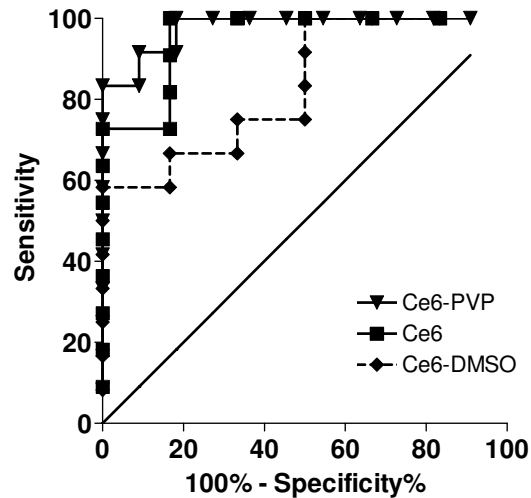


Figure 3.4 ROC curves comparing fluorescence intensities of Ce6-PVP, Ce6 and Ce6-DMSO for classifying tumor from peritumoral muscle. The areas under the curve (AUC) were then compared in order to make a fair judgment of the effectiveness of Ce6 formulations without being constricted to single values of sensitivity and specificity, which largely depend on the cut-off fluorescence intensity value chosen to distinguish normal from malignant tissue. The closer the curve comes to the 45-degree diagonal solid line, the less accurate the fluorescence diagnostic. The following is a rough guide for classifying the accuracy of fluorescence intensities based on the AUC: 1 – 0.9 = excellent; 0.9 – 0.8 = good; 0.8 – 0.7 = fair; 0.7 – 0.6 = poor; and 0.6 – 0.5 = fail. The AUC for Ce6-PVP, Ce6 and Ce6-DMSO were 0.98 ± 0.02 , 0.95 ± 0.05 and 0.83 ± 0.1 respectively. The ROC curves also potentially demonstrate how the fluorescence diagnostic scheme can be adjusted to obtain the desired degree of sensitivity at the cost of specificity. Ce6-PVP induced fluorescence showed the highest sensitivity and specificity in detecting tumor from peritumoral muscle.

Figure 3.4 displays a ROC curve that illustrates the ability of Ce6, Ce6-PVP and Ce6-DMSO induced fluorescence to discriminate between tumors and peritumoral muscle. Area under the ROC curve was used to compare the sensitivity and specificity of the temporal fluorescence of the three formulations. A non-discriminative fluorescence has an area of 0.5. A perfect discriminative fluorescence has an area of 1.00. The area under the ROC curve was 0.98 ± 0.02 for Ce6-PVP ($p = 0.0001$), 0.95 ± 0.05 for Ce6 ($p = 0.003$) and 0.83 ± 0.1 ($p = 0.0246$) for Ce6-DMSO. The optimal cut-off level of fluorescence intensity that

maximizes 100% sensitivity for Ce6-PVP yielded 83% specificity, but a lower specificity of 73% and 58% for Ce6 and Ce6-DMSO respectively. Thus, based on this results, Ce6-PVP induced fluorescence was found to yield high sensitivity and specificity in demarcating tumor from normal peritumoral muscle of the xenograft model compared to Ce6 alone and Ce6-DMSO. This data signifies that fluorescence imaging using Ce6-PVP could be clinically relevant for determining the location of invisible cancerous lesions/tissue. To further evaluate the effect of PVP on the retention rate of Ce6 fluorescence in comparison to Ce6 alone or Ce6 delivered using DMSO, the decay rate constant (K) of the photosensitizer fluorescence in tumor tissues have been estimated from 1 to 6 h post drug administration. Fluorescence intensity of Ce6-PVP ($K = 0.1386 \pm 0.04 \text{ hour}^{-1}$) was retained longer in tumor compared to Ce6 ($0.1755 \pm 0.04 \text{ hour}^{-1}$) and Ce6-DMSO ($0.2007 \pm 0.08 \text{ hour}^{-1}$). As such, the half-life was calculated to be 5.0, 3.9 and 3.4 h for Ce6, Ce6-PVP and Ce6-DMSO respectively.

The decrease in the constant decay rate of Ce6-PVP in tumor and muscle compared to Ce6 and Ce6-DMSO could also reflect the possibility that PVP may have a retention effect on the uptake of Ce6. At the moment, it was hypothesized that the major therapeutic effect of Ce6-PVP observed in this study was likely to have been the result of the traditional role of PVP as a plasma expander [120]. As with any effective plasma volume expander, PVP decreases the viscosity of blood by hemodilution and thus may dilute the active Ce6 in the circulation. Interestingly, PVP has also been reported to localize in malignant tumors [121] and remained mainly in blood with no specific normal tissue distribution [122]. Furthermore, the administration of PVP was found to cause significant decreases in the plasma concentrations of total cholesterol, phospholipid and triglyceride

concentrations in normal rats and hyperlipidemic human subjects [123, 124].

Therefore, another hypothesis that PVP has a biological effect on the *in vivo* transport of Ce6 seems to be an appealing one.

3.4.5 *In vivo* photodynamic therapy on tumor xenografts

The extent of tumor necrosis in the MGH bladder tumor model was identified using vital staining with EB at 48 h post PDT (Figure 3.5). The results of these experiments are presented in Table 3.2. Complete tumor necrosis was achieved when irradiation was performed at 1 h drug-light interval using Ce6-PVP. At 3 h drug-light interval, Ce6-PVP treated tumors exhibited 40 ± 9.8 % necrosis. No adverse side effects were observed in any animal at post PDT after administration of Ce6-PVP. At the same drug and light dose, complete tumor necrosis was observed for only 67% of Ce6 treated animals at 3 h drug-light interval. Severe side effects were observed for animals treated at 1 h drug-light interval post Ce6 administration and animals treated at 1 and 3 h post Ce6-DMSO administration.

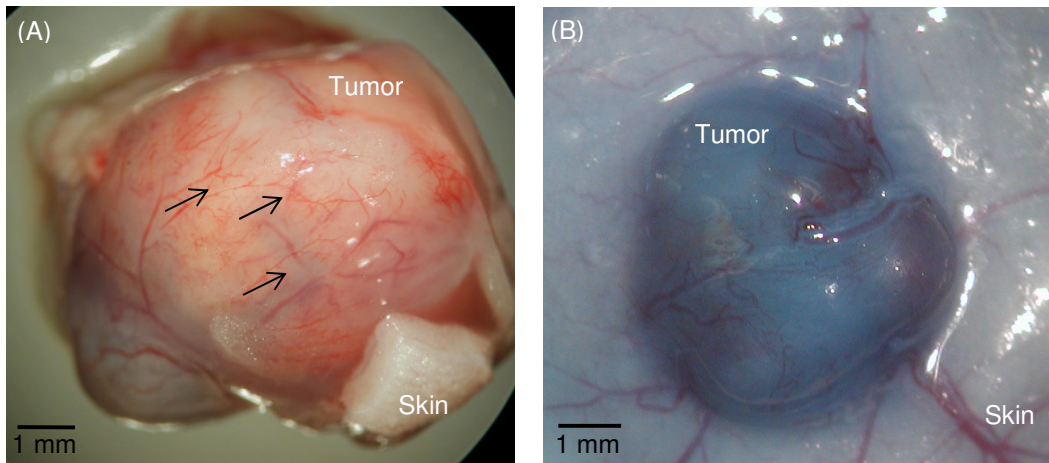


Figure 3.5 A representative macroscopic view of whole MGH tumor xenograft stained with Evans Blue dye at 48 h post PDT after treatment at 1 h drug-light interval mediated PDT with Ce6-PVP (A) and control tumor (with Ce6-PVP, no light irradiation) (B). Necrotic tumor tissue appeared white and was almost devoid of vital staining. Shrinkage of tumor blood vessels was observed on the surface of tumor (arrow).

Table 3.2 A comparison of the percentage of necrotic tumor and survival of mice evaluated at 48 h post PDT after administration of 5 mg/kg Ce6-PVP, Ce6 or Ce6-DMSO with irradiation at a fluence and fluence rate of 100 J/cm² and 85 mW/cm² respectively. Each data point represents a mean of 3 – 5 animals.

Photosensitizer	Percentage of necrotic tumor tissue, %		Survival ^a , %	
	Drug-light interval, h		Drug-light interval, h	
	1	3	1	3
Ce6	NA ^b	100 ^c	0	67
Ce6-PVP	100	40 ± 9.8	100	100
Ce6-DMSO	NA ^b	NA ^b	0	0

^a The survival of mice was expressed as the number of mice which recovered from treatment at 24 h post treatment.

^b Tumor necrosis could not be evaluated in animals that died due to treatment toxicity.

^c Necrotic tissue was evaluated from the 67% animals that survived PDT.

Fractal dimension analysis of tumor vasculature at post PDT were studied to draw some general preliminary conclusions on the effect of Ce6- PDT on tumor vasculature (Figure 3.6). The fractal dimension score indicates the amount of space-filled by blood vessels (Figure 3.7). Vessel fractal dimension was spatially heterogeneous. In the tumor treated with Ce6 at 3 h drug-light interval, fractal dimension was lower compared to tumor treated at 1 h drug-light interval and control, showing evidence of vascular occlusion. In Ce6-PVP treated tumors, however, fractal dimension did not differ from controls.

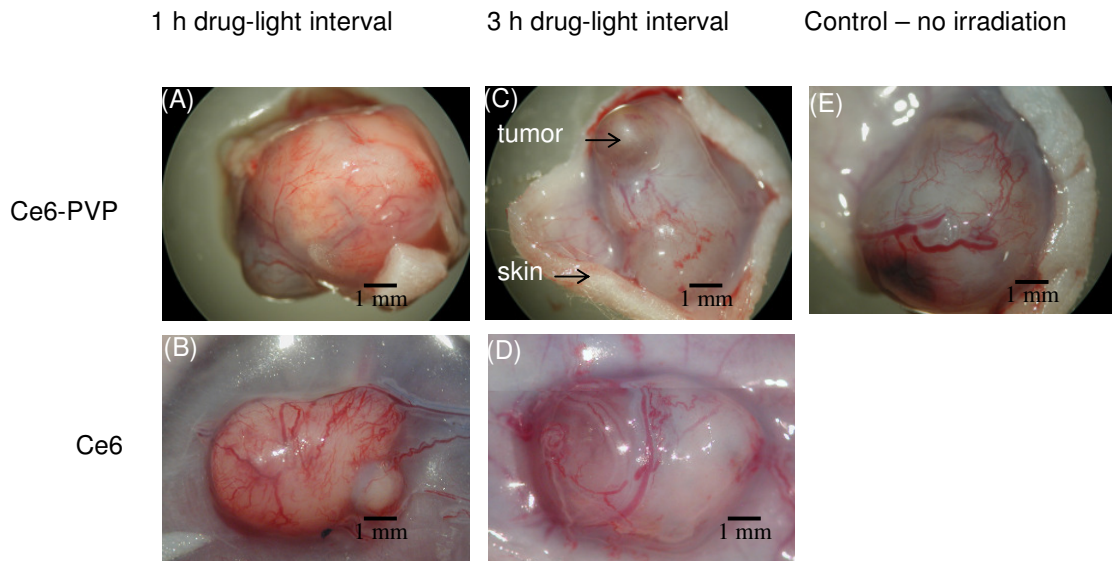


Figure 3.6 Extent of tumor vascular destruction following treatment with PDT post injection of Ce6 and Ce6-PVP at 1 (A, B) and 3 h (C, D) drug-light interval. The fractal dimension analysis was performed to evaluate the damage of tumor blood vessels post PDT. Shrinkage of tumor blood vessels was observed at post PDT. Control tumor with no light irradiation (E).

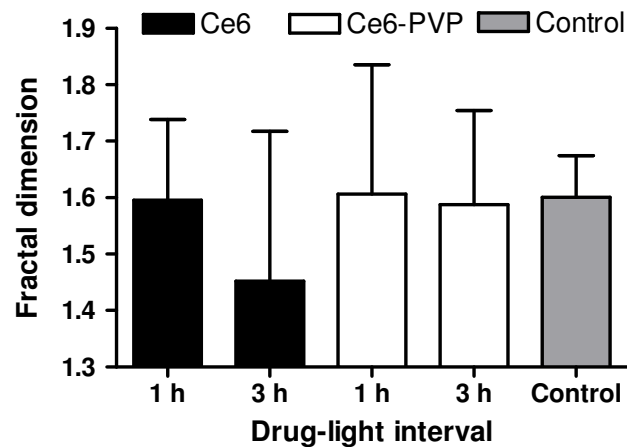


Figure 3.7 Preliminary analysis of tumor blood vessel fractal dimension on PDT treated tumor xenografts. Columns indicates the amount of space-filled by blood vessels; bars, standard deviation. Data analysis was only based on 1 animal for each treatment group.

The phototoxicity of Ce6, Ce6-PVP and Ce6-DMSO was examined in vivo using human bladder tumor-bearing mice. Ce6-PVP was found to cause greater tumor necrosis at 1 h compared to 3 h drug-light interval after exposure to 100 J/cm² delivered at 85 mW/cm² as a single fraction without causing any side effects to the mice at post treatment. However, administration of Ce6 alone or Ce6-DMSO mediated PDT resulted in severe side effects (paralysis and death) at post PDT. This phenomenon of acute toxicity in animals with other modes of PDT has been reported previously [125]. Adverse side effects are mainly due to PDT induced damage to normal organs [99]. This could be due to the increased solubility of Ce6 by DMSO and thus the increased uptake of Ce6-DMSO in normal tissue which resulted in acute toxicity due to irradiation to the surrounding normal tissue [126]. Furthermore, many studies have reported adverse results with respect to DMSO effects on metabolism and toxicity of other xenobiotics. It is known that DMSO is not a biologically inert compound and combinations of DMSO with other toxic agents could constitute its greatest toxic potential [127]. Therefore, the interaction of DMSO with Ce6 suggests a serious toxicological implication that needs to be taken into consideration when giving parenteral administration. Post PDT toxicity observed for Ce6 alone can be attributed to the fact the chlorins is extremely potent photosensitizer. One known chlorin-based photosensitizer that was reported to have acute PDT toxicity effect is m-tetrahydroxyphenylchlorin [128]. In Chapter 2, it was demonstrated that using a formulation with PVP, a significant reduction in the post PDT systemic toxicity of Ce6 could be achieved. Because of this reduced toxicity, higher doses of Ce6-PVP than that of the parent drug can be used in PDT, allowing the treatment to be potentially repeated many times to improve efficacy without any adverse effects. However, it is important to note that PDT performed to date only used a single dose of Ce6 (e.g., 5 mg/kg).

A smaller dose of Ce6 may preclude PDT related toxicity in the animals, and this warrants further studies.

3.4.6 Ce6-PVP induced fluorescence on human lung carcinoma

Little is known about the comparative efficacy of PDT in treating non-small cell lung carcinoma (NSCLC) and small cell lung carcinoma (SCLC), despite ongoing clinical trials treating lung cancers. Lung cancer became one of the first cancers to be considered for PDT which has been used as an adjuvant treatment over the last 27 years [129]. Currently, PDT is used either to treat microinvasive endobronchial NSCLC or to palliate patients with completely or partially obstructing endobronchial NSCLC [130]. Despite the generally refractory nature of these type of tumors, central type of tumors with identifiable endobronchial lesions which could be easily accessed bronchoscopically for illumination have been successfully treated with PDT [131]. PDT can preserve lung function, limiting surgical trauma and postoperative pain as well as used in combination with other therapeutic modalities such as chemotherapy [130]. Photosensitizer-induced fluorescence detection aimed at enhancing optical contrast to improve tumor visibility has been extensively investigated to develop 'tumor selective' imaging methods [132, 133]. The lack of tumor selectivity, complex pharmacokinetics and the fact that some photosensitizers may cause prolonged skin photosensitivity, make the clinical application of fluorescence detection and PDT more complex [134, 135]. These limitations have led to the development of second-generation photosensitizers, which usually produce shorter periods of photosensitivity, longer activation wavelengths, higher tumor-to-normal tissue concentration, excellent antitumor effect and higher quantum yields of $^1\text{O}_2$ [136]. Studies showed that derivatives from chlorophylls are potent photosensitizers

[137, 138], of which mono-L-aspartyl chlorin e6 (NPe6, Laserphyrin) is undergoing clinical trials in Japan for the treatment of endobronchial lung cancer [139]. Fluorescence bronchoscopy has been reported to enhance the diagnostic accuracy and definition of the intra-epithelial cancer within the bronchi [140]. This technique has become more attractive for clinical use since more effective 2nd generations of photosensitizers have been clinically implemented and tested. Newer formulations of photosensitizers were intended to reduce common side effects such as skin photosensitivity, nausea, vomiting and transiently raised liver transaminase levels. Following the above rationale, the use of PVP in combination with Ce6 was therefore investigated in preclinical lung cancer models.

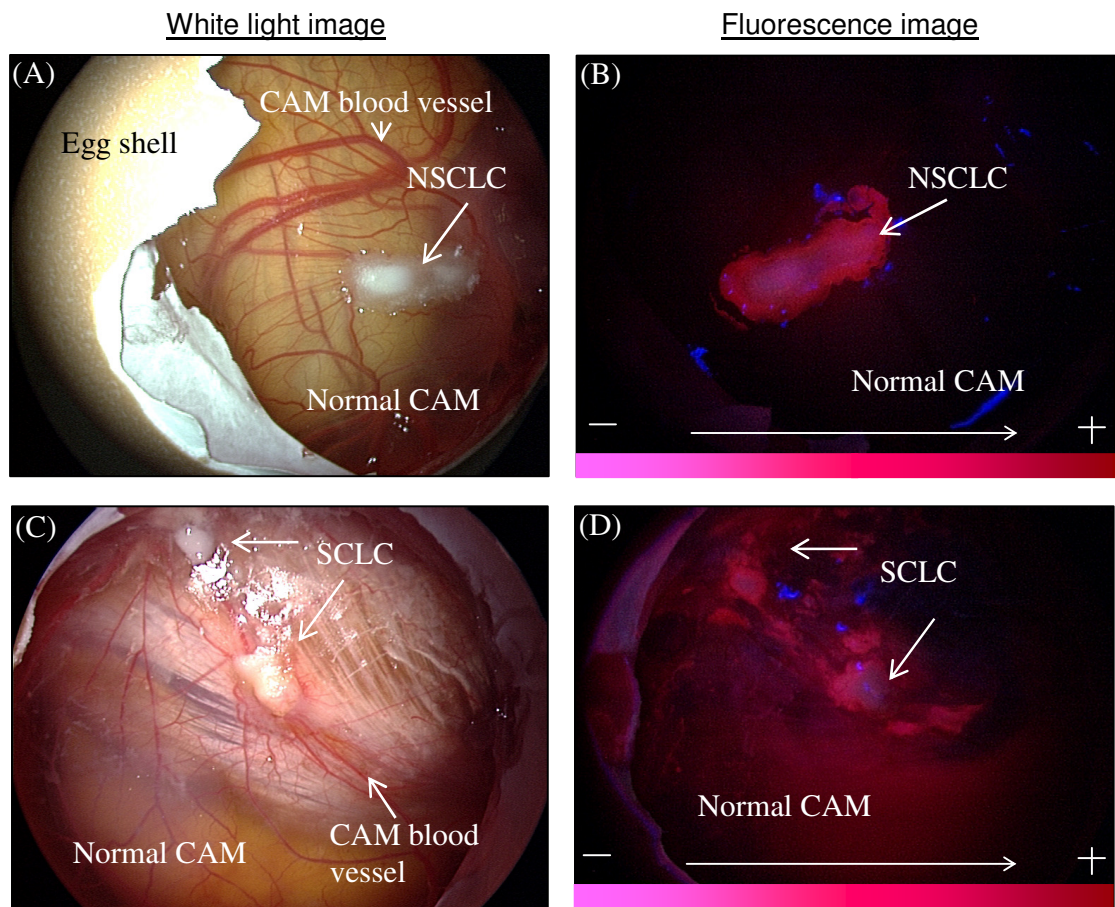


Figure 3.8 Fluorescence imaging of lung cancers xenografted on the CAM model. Representative of white light images of NSCLC and SCLC grafted on CAM before administration of photosensitizer (A, C). Before incubation of Ce6-PVP, the CAM tumor xenografts were imaged under blue light illumination, to confirm that there was no autofluorescence. Tumor fluorescence images at 3 h post-topical administration of 1 mg/kg of Ce6-PVP under blue light illumination (B, D).

As it was important to establish if cellular localization of Ce6-PVP was also exhibited in human lung tumor, the CAM tumor xenograft was employed here. It was demonstrated that this method of examining fluorescence uptake and retention in tissue explants on the CAM model provided a reliable means for direct, comparative visualization *in situ* of human tumors [141]. Inoculation of human NSCLC (NCI-H460) and SCLC (NCI-H526) into highly vascularized CAM led to the disseminated tumor growth on the surface of the CAM (Figure 3.8 A, C). Typical fluorescence intensity image of NSCLC and SCLC are illustrated in Figure 3.8 B and D, respectively. Intense red fluorescence was macroscopically visible in the tumor cells under blue light, as compared to non-malignant epithelium of the CAM after 30 minutes post incubation with Ce6-PVP. The fluorescence retention by the lung tumor xenografts after topical administration was quantitatively evaluated using image-processing techniques and charted as a function of time (Figure 3.9). High differential fluorescence intensity was observed between NSCLC xenografts and its surrounding normal CAM tissue compared to SCLC xenografts. The average intensity of the red-to-blue intensity ratio of NSCLC xenograft was higher than that of SCLC xenograft. The fluorescence intensity elimination rate constant for NSCLC, SCLC and normal CAM was calculated to be 0.13, 0.25, and 0.38 min⁻¹ respectively, suggesting that Ce6-PVP is being retained longer in NSCLC than SCLC. Normal CAM had a faster elimination rate of Ce6-PVP.

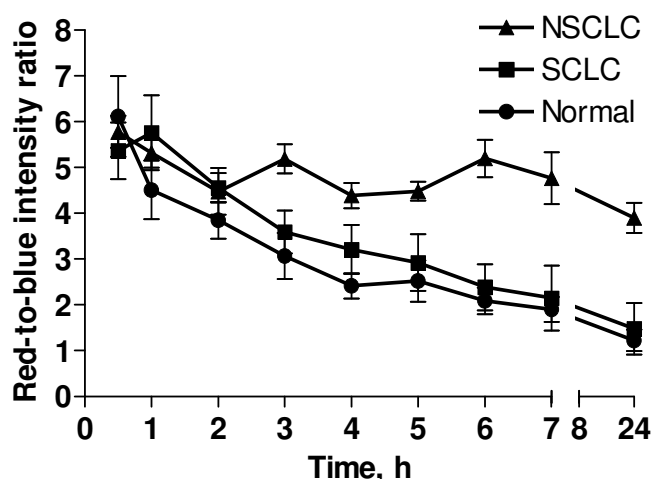


Figure 3.9 Fluorescence kinetics of Ce6-PVP on NSCLC (▲) and SCLC (■) xenografted on CAM examined up to 24 h post topical drug administration. Values are expressed as red-to-blue intensity ratio of fluorescence images post administration of drug normalized with images before drug administration. For tumor, each point represents a mean of 5 eggs whereas for normal (●), each point represents a mean of 10 eggs. Bars = standard error of the mean. Non-linear regression analysis demonstrated that all the curves were statistically different with each other. The elimination rate constant for NSCLC, SCLC and normal CAM was in the following order: NSCLC < SCLC < normal CAM.

ROC curve analysis was applied from 0.5 to 5 h post administration of Ce6-PVP to validate the ability of the photosensitizer to discriminate NSCLC and SCLC from normal CAM membrane. The area under the curve (AUC) were then compared in order to make a fair judgment of the effectiveness of Ce6-PVP without being constricted to single values of sensitivity and specificity, which largely depend on the cut-off fluorescence intensity value chosen to distinguish normal from malignant region (Table 3.3). The following is a rough guide for classifying the accuracy of Ce6-PVP based on the AUC: 1 – 0.9 = excellent; 0.9 – 0.8 = good; 0.8 – 0.7 = fair; 0.7 – 0.6 = poor; and 0.6 – 0.5 = fail. The AUC for NSCLC were 0.52, 0.68, and 0.66, at 0.5 h, 1 h and 2 h respectively (P values were not statistically significant) indicating that shorter exposure times resulted in lower accuracy. The greatest AUC was observed from 3 h post drug

administration onwards: *i.e.* 0.88, 0.94 and 0.90 at 3 h, 4 h and 5 h respectively (all P values were statistically significant). For SCLC, the AUC were 0.52, 0.70, 0.68, 0.70, 0.74, and 0.58 at 0.5 h, 1 h, 2 h, 3 h, 4 h and 5 h respectively (P values were not statistically significant). This result showed no improvement in fluorescence accuracy in demarcating SCLC from the normal surrounding CAM.

Table 3.3 A comparison of areas under the ROC curves between NSCLC and SCLC at various time post drug administration.

Time post Ce6 - PVP administration, h	NSCLC		SCLC	
	Area under the ROC curve	P value	Area under the ROC curve	P value
0.5	0.52	0.9024	0.52	0.9025
1	0.68	0.2704	0.70	0.2207
2	0.66	0.3272	0.68	0.2704
3	0.88	0.0200*	0.70	0.2207
4	0.94	0.0071*	0.74	0.1417
5	0.90	0.0143*	0.58	0.6242

An area of 1 represents a perfect discrimination of tumor from normal tissue; an area of 0.5 represents no discrimination between normal and abnormal. The P value indicates whether the area under the ROC is significantly different from 0.5. *If the P value is < 0.05, the area under the ROC curve is significantly different (see description of statistical analysis). For tumors, each point represents a mean of 5 eggs whereas for normal, each point represents a mean of 10 eggs.

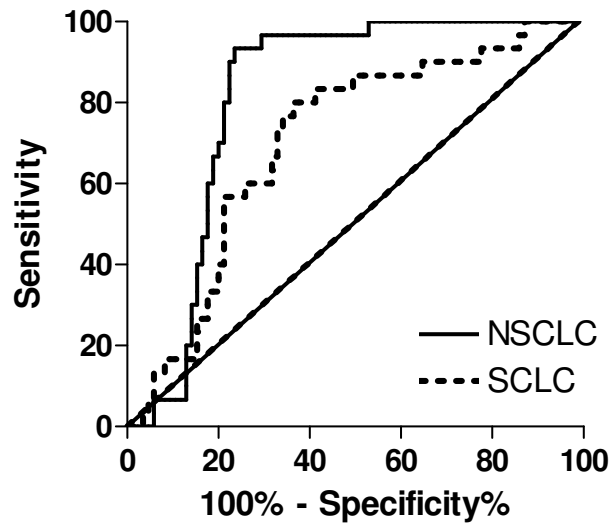


Figure 3.10 Receiver operating characteristic curves illustrating the ability of Ce6-PVP to separate NSCLC (solid line) and SCLC (dotted line) from normal chorioallantoic membrane in the CAM model. The ROC curve of two indistinguishable populations (i.e. abnormal versus normal region), represented by the 45-degree line (area under the ROC curve = 0.5), is included for comparison. Area under the ROC curve was 0.82 ± 0.04 ($p < 0.0001$) and 0.70 ± 0.05 ($p = 0.0009118$) for NSCLC and SCLC respectively.

To evaluate the overall quality of fluorescence intensity discrimination between NSCLC and SCLC, a combined ROC was generated from 0.5 to 5 h post drug administration. The sensitivity and the specificity were calculated using different threshold (cut-off) values to distinguish healthy from malignant tissue (Figure 3.10). For NSCLC, the highest combined sensitivity and specificity were 90% and 78% (cut-off value > 4.0 ; likelihood ratio = 4.03), whereas for SCLC it was 57% and 79% respectively (cut-off value > 4.1 ; likelihood ratio = 2.68), implying that fluorescence mediated Ce6-PVP has distinctly higher rate of sensitivity for the detection of disseminated lesions of NSCLC than with SCLC.

3.4.7 Ce6-PVP induced PDT on human lung carcinoma

To determine the efficacy of Ce6-PVP mediated PDT, nude mice bearing NSCLC and SCLC tumors were administered with 2.0 mg/kg of the photosensitizer. PDT was performed on using light generated by a diode laser system ($\lambda = 665 \text{ nm}$) at the light dose of 150 J/cm^2 and fluence rate of 125 mW/cm^2 . The area of tumor necrosis was measured by Evan's blue dye staining at 48 h post PDT. Strong heterogeneous staining was observed in the untreated controls (Figure 3.11 A, B) indicating occurrence of spontaneous, albeit limited necrosis, whereas in the PDT treated tumor, tissue damage was clearly evident as an unstained area (Fig 3.11 C – F). NSCLC tumors irradiated at 3 and 6 h drug-light interval exhibited extent of tumor necrosis of $84 \pm 7\%$ and $50 \pm 4\%$ respectively. When PDT treatment was performed on SCLC models using the same parameter, it was observed that irradiation at 3 h drug-light interval resulted in $50 \pm 9\%$ of tumor necrosis while irradiation at 6 h drug-light interval resulted in $26 \pm 8\%$ tumor necrosis. Thus, we conclude that SCLC was only moderately sensitive to Ce6-PVP mediated PDT.

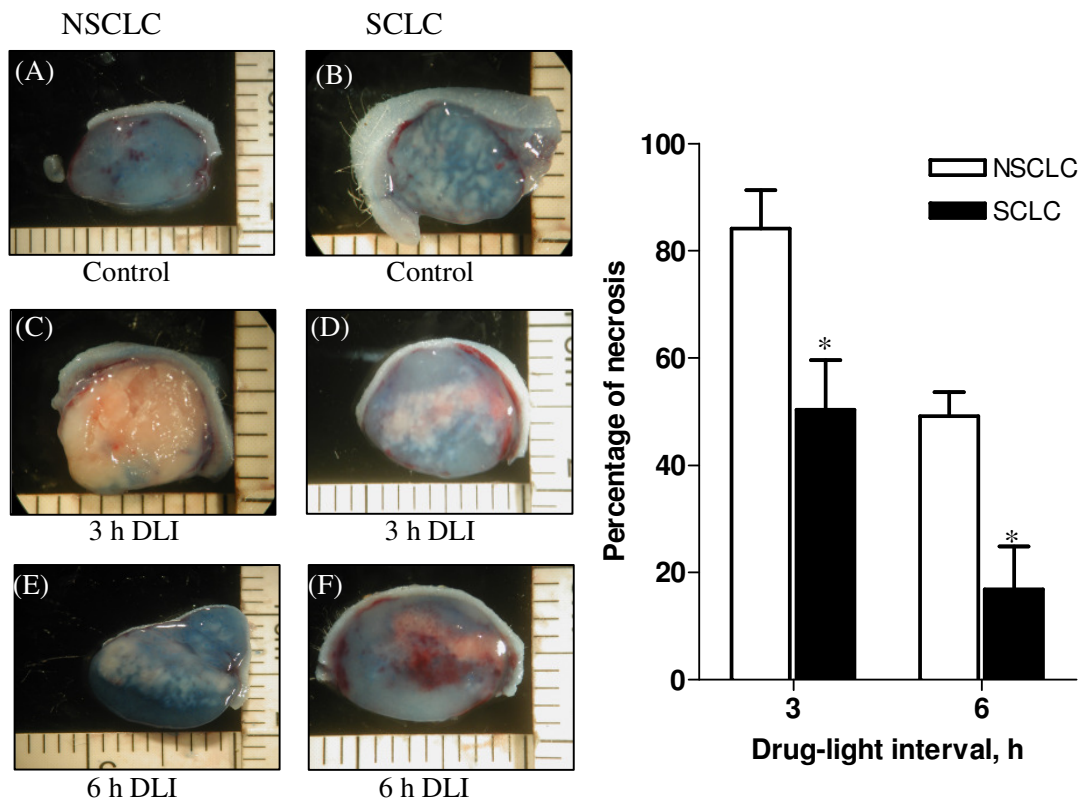


Figure 3.11 A morphologic study of NSCLC and SCLC tumor damage efficiency using the method of vital staining with Evans blue at 48 h post Ce6-PVP mediated PDT. Strong homogeneous staining was observed in the untreated controls (A, B), whereas in the treated tumor at 3 h drug-light interval (DLI) (C, D) and at 6 h DLI (E, F), tissues damage was clearly distinguishable as an unstained area in the tumor. Drug dose: 2.0 mg/kg; light dose: 150 J/cm²; 125 mW/cm². Each data point is an average of at least 5 animals, Bars = standard error of the mean. *The mean difference is significant at the 0.05 level compared to the NSCLC group.

Almost all PDT studies were concerned with NSCLC due to the referral patterns in the clinics [131]. Although PDT has also been shown to be effective in the clinical treatment of SCLC [142], little preclinical data exist comparing the efficacy or tendency for resistance toward photosensitization between these two tumor histologies. In this study, a certain degree of resistance to PDT in SCLC xenografts observed. There are already a variety of molecular markers that have been implicated in the pathogenesis of SCLC [143] thus making it difficult to hypothesize the molecular basis of acquired resistance towards photosensitization in this experiments. Generally, in lung cancer four types of multidrug resistance have been identified, i.e., classical multidrug resistance (MDR), non-P-glycoprotein MDR (also called MRP), atypical MDR (mediated through altered expression of topoisomerases II) and lung resistance-related protein [144]. Previous evidence indicates that SCLC cell lines and tumors express multidrug resistance-associated protein i.e., MRP1, ATP binding cassette [ABC]C1 [145] and ABCG2 (ATP-binding cassette protein for breast cancer resistance protein) [146]. Hence, one plausible reason to explain the lack of activity of Ce6-PVP in SCLC is the possible existence of ABC transporters of chlorin-based photosensitizers in this tumor histology. It was reported that cancer cell lines that expresses ABCG2 was found to efflux some of the chlorophyll based photosensitizers and thus may confer resistance to this treatment modality [147, 148]. It has been suggested that by inhibiting ABCG2 transport using tyrosine kinase inhibitors (e.g. Gleevec), it is likely to be a more successful approach to enhancing clinical PDT [149].

3.5 Conclusion

In conclusion, the studies demonstrated that the new formulation of Ce6-PVP has a higher sensitivity and specificity for tumors and is able to induce cell death in tumor following PDT without acute toxicity in mice compared to Ce6 alone or Ce6-DMSO. Photosensitization with Ce6-PVP for 3 hours of exposure time appeared to be most effective in detecting NSCLC in CAM model. Furthermore, PDT at 3 h drug-light interval resulted in a better tumor necrosis in NSCLC xenograft model. SCLC xenografts were found to manifest a certain degree of resistance to photosensitization with Ce6-PVP. Despite the limited activity of Ce6-PVP in the SCLC xenografts, it is conceivable that the combined modality of fluorescence imaging and targeted photodynamic therapy using Ce6-PVP may still have a potential role in SCLC. This warrants for additional studies on the molecular mechanisms of photosensitization resistance in SCLC to overcome this important clinical problem.

CHAPTER 4

Membrane transport enhancement of chlorin e6 - polyvinylpyrrolidone and its photodynamic efficacy on the chick chorioallantoic model

4.1 Summary

The aim of this chapter is to investigate the use of Ce6–PVP for the detection of human bladder cancer cells (MGH) implanted on the chick chorioallantoic membrane (CAM) model. The CAM was used to model tumor spheroids that resemble small residual bladder tumors prior to vascularization. Uptake kinetics studies were determined for both systemic and topical administrations of Ce6–PVP to the normal CAM as well as the MGH human bladder tumor implanted on CAM using fluorescence imaging technique. Rapid elimination of Ce6–PVP was observed following topical application compared to systemic administration in the normal CAM system. Ce6–PVP was found to localize selectively in the xenografted bladder tumor in contrast to the CAM tissue. Neither dark toxicity nor irritancy was observed on the CAM tissue at the dose of 2 mg/kg Ce6–PVP. Macroscopic fluorescence imaging showed that Ce6-PVP induced fluorescence had a higher sensitivity and specificity for delineating tumor from the surrounding normal CAM compared to Ce6 alone. The uptake ratio of Ce6-PVP to that of Ce6 was found to have a 2-fold increase across the CAM, indicating that PVP was able to facilitate diffusion of Ce6 across membrane. Confocal laser scanning microscopy further confirmed the Ce6-PVP has better penetration in the CAM compared to Ce6. In conclusion, the Ce6–PVP formulation appeared to have the potential as a fluorescent marker for fluorescence diagnosis of human bladder cancer.

4.2 Introduction

Bladder cancer is a prevalent disease and is the sixth most common form of malignancy worldwide [37]. According to The Singapore Urological Association, it is the ninth most common cancer for males but much less frequent in females in Singapore. Mortality rates are very high due to the invasive nature of bladder cancer. Therefore, the best approach for management of bladder cancer aims at early detection as this allows for early treatment that gives more favorable prognosis and thereby reduces mortality rates. Regular white light cystoscopies with cold cup biopsies are the current methods used in the surveillance of high-risk patients for recurrent bladder cancer. However, these methods are insufficient to detect all urothelial neoplasia especially flat lesions such as carcinoma *in situ*. Therefore, superior methods of detecting flat urothelial neoplasia with the use of specific fluorescent dyes are constantly being sought after.

In recent years, enhanced visualization of bladder cancer with various photosensitizers has been reported [32-35]. However, only two photosensitizers, porfimer sodium (Photofrin[®]) and 5-aminolevulinic acid hexyl ester (Hexvix[®]), were approved for photodynamic therapy (PDT) and photodynamic diagnosis (PDD) of bladder cancer [33]. It was previously reported the use of 5-aminolevulinic acid and hypericin in bladder cancer, concluding that the sensitivity of the fluorescence cystoscopy was greater than that of conventional cystoscopy [13, 36]. However, one setback is the formulation of lipophilic photosensitizers for the instillation into bladder cavities or systemic administration. With current formulations, the procedures are time consuming and demanding on the patients. Typically, bladder instillation take around 1 to 3 h

incubation to allow for selective accumulation of the photosensitizer in the tumor [37]. In the case of hypericin, human serum albumin (HSA) was used as solubilizing agent for the preparation of bladder instillation fluid. Hypericin was incubated in the bladder for 2 h before the PDD procedure [38]. Moreover, hypericin is also known to bind tightly to HSA due to which the bioavailability of the photosensitizer might be compromised. Recently, a water-soluble hypericin derivative (Hyp-S) using polyvinylpyrrolidone (PVP) as a carrier was reported to have shown improved water solubility as well as high affinity for cellular membranes [39]. In addition, N-methyl-pyrrolidone (NMP) was also proposed as a penetration enhancer for hypericin formulation that allowed faster response time [40].

Studies have shown that therapeutic outcome of topical photosensitizer-based PDT is in part influenced by pharmaceutical and physicochemical considerations, such as tissue-penetration characteristics [150]. The delivery control of the photosensitizing agent into the cancer cells is one of the major factors, which directly affect the therapeutic efficiency of PDT. Ce6 is an asymmetric molecule bearing three ionizable carboxylic acid groups. It has been shown that Ce6 is a promising cancer phototherapeutic agent [78]. The conjugation of a trisodium salt of Ce6 to PVP, a water-soluble polymer, has been reported to improve its clinical efficacy [151]. In addition, Ce6-PVP has also been used in photodynamic inactivation against bacteria isolated from periodontal diseases, surgical site infections and diabetes foot infections [152, 153]. Previous reports from our laboratory have shown that the formulation of Ce6 with PVP is an effective photosensitizer for the application in photodynamic therapy and fluorescence diagnosis of cancer [126, 154, 155].

The potential to improve biological activity of topically administered drugs by co-precipitation with PVP has been extensively investigated. PVP is a biocompatible water-soluble polymer with a fast dissolution rate. Numerous studies have shown enhanced dissolution rates of drugs in PVP. A maximum enhancement of drug dissolution is found when the ratio of drug to polymer in these systems is low. It has been proposed that the increased drug dissolution rate is a result of its presence as a high energy form, possibly in a non-crystalline state [156]. PVP is also often used to obtain an amorphous formulation and it has been shown that it is able to interact with weak carboxylic acids via hydrogen bonding.

The chick chorioallantoic membrane (CAM) model is a convenient model for the study of early *in vivo* cancer research and drug delivery [157]. The use of CAM model for photosensitizer transport studies across membrane has been established [40]. For PDT of urological cancers, the application mode of photosensitizers is mostly by intravesical instillation. This environment can be simulated by topically applying the photosensitizers in the CAM [158], thereby providing a good correlation to the clinical environment of PDT. In the previous chapters, extensive *in vivo* studies on murine model using Ce6-PVP suggested that PVP has a biological effect on the *in vivo* transport of Ce6. In this chapter, it was demonstrated that selective and enhanced visualization of human bladder cancer on the CAM tumor model was achieved through topical administration of Ce6-PVP. The diffusion and penetration effect of Ce6 and Ce6-PVP on the CAM was also compared. The efficacy of Ce6-PVP as a topical photosensitizer for PDT was investigated using a range of light doses intended for irradiation in the bladder.

4.2.1 Theory: Fick's Law of diffusion

The diffusion of the photosensitizer over a membrane barrier was based on the theoretical principle of Fick's Law (Figure 4.1) [150]. With appropriate measurement and characterization of the CAM, the diffusion coefficient of various formulations of photosensitizer can be calculated using the Fick's first law of diffusion, which describes the passive diffusion of photosensitizer across the trans-membrane of CAM mathematically:

$$\frac{dm}{dt} = \frac{D \cdot A \cdot (K_1 \cdot C_g - K_2 \cdot C_b)}{h} \quad (1)$$

dm/dt is the rate of appearance of drug at the site of absorption,

D is the effective diffusion coefficient of the drug in the CAM,

A is the surface area of the CAM available for absorption by passive diffusion (which is assumed to be circular and flat),

K_1 is the partition coefficient of drug between CAM and the fluid outside the CAM,

C_g is the concentration of drug in solution in fluid at the site of absorption,

K_2 is the partition coefficient of drug between the CAM and the fluid inside the CAM,

C_b is the concentration of drug inside the CAM at the site of absorption,

h is the thickness of the CAM.

Hence, $K_1 \cdot C_g$ and $K_2 \cdot C_b$ represent the concentrations of drug inside the CAM membrane at the fluid outside CAM/membrane interface and membrane/fluid inside CAM interface, respectively. The expression:

$$\frac{(K_1 \cdot C_g - K_2 \cdot C_b)}{h} \quad (2)$$

h , thickness of CAM

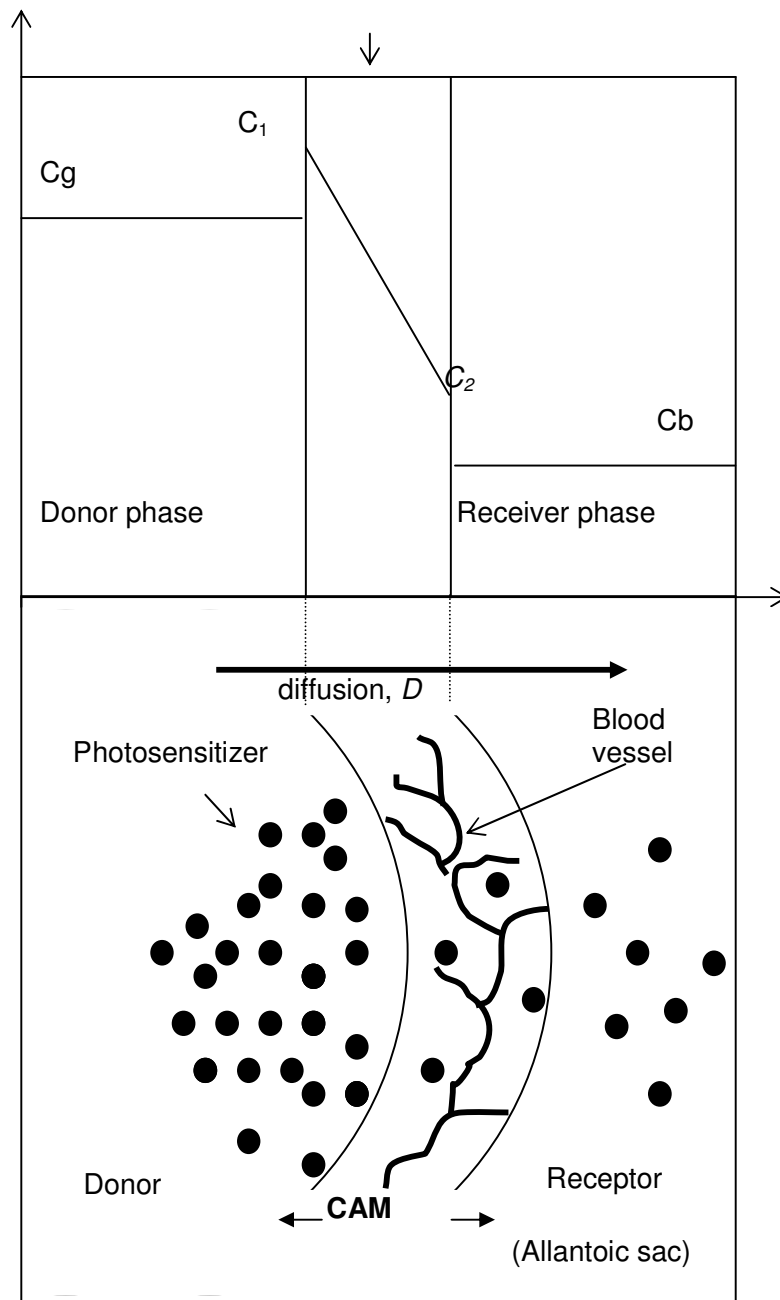


Figure 4.1 A diagrammatic representation of a photosensitizer transport model using CAM. The concentrations across the cells are represented in the top part of the figure. The concentration gradient across the membrane of thickness h is shown at steady state. C_g is not expected to equal C_1 unless the partition coefficient of the drug into the membrane from the donor phase is unity.

represents the concentration gradient of drug across the 'membrane'. The fluid inside the CAM acts as a 'sink' for absorbed drug and ensures that the concentration of drug inside the CAM at the site of absorption is low in relation to the concentration of drug in solution in the fluids outside the CAM at the site of absorption, i.e. $C_g \gg C_b$. The passive absorption process is driven solely by the concentration gradient of the diffusible species of the drug, which exists across the CAM/fluid barrier. Under such conditions that $K_1 \cdot C_g \gg K_2 \cdot C_b$ and thus $(K_1 \cdot C_g - K_2 \cdot C_b)$ approximates to $K_1 \cdot C_g$, the equation (1) may be written in the form:

$$\frac{dm}{dt} = \frac{D \cdot A \cdot (K_1 \cdot C_g)}{h} \quad (3)$$

Therefore, this equation allows the comparison of diffusion coefficients of different formulations.

4.3 Material and methodology

4.3.1 Photosensitizer preparation

Ce6–PVP was dissolved in 0.9% sodium chloride to constitute a stock solution of 1 mg/mL. On the day of treatment, the stock solution was diluted with 0.9% of sodium chloride (NaCl) to obtain a volume of 100 mL containing a dose of 2 mg/kg body weight of the chick’s embryo. For transport study, Ce6-PVP and Ce6 from ORPEGEN Pharma GmbH, Heidelberg, Germany was used. UV-VIS absorption spectra of the photosensitizers were recorded on a Shidmadzu UV-VIS spectrophotometer. Fluorescence emissions spectra were recorded on a RF-5301 PC Shidmadzu spectrofluorimeter. Emission spectra were obtained in the $\lambda_{em} = 500 - 750$ nm range, with excitation at $\lambda_{ex} = 400$ nm.

4.3.2 Preparation of chick chorioallantoic membrane (CAM) tumor model

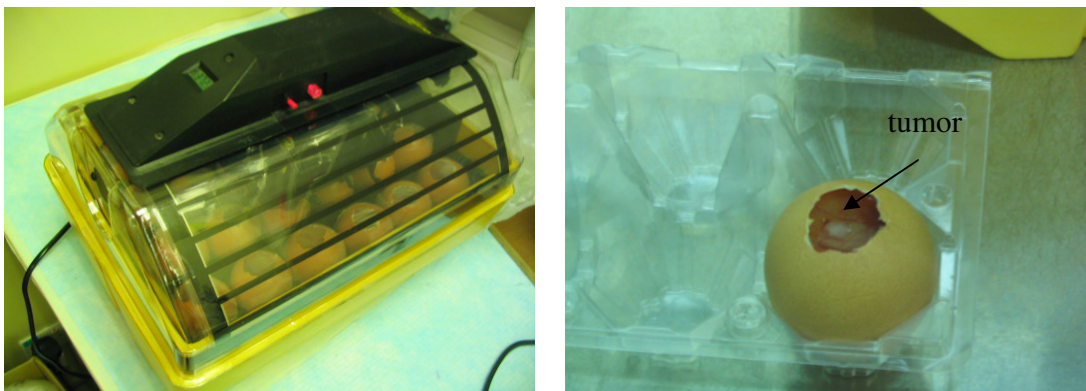


Figure 4.2 (A) Egg incubator and (B) Xenograft tumor on the CAM.

Ce6-PVP was dissolved in 0.9 % sodium chloride to constitute a stock solution of 1 mg/mL. On the day of treatment, the stock solution was diluted with 0.9 % of sodium chloride (NaCl) to obtain a volume of 100 μ L containing a dose of 2 mg/kg body weight of the chick’s embryo. Fertilized chicken eggs were obtained

from the specific pathogen free facility of Agri-food and Veterinary Authority of Singapore. The eggs were cleaned with 70 % warm ethanol before placing them on trays with blunt ends upwards. Eggs were incubated at 37°C in a humidified atmosphere inside a hatching incubator equipped with an automatic rotator (Octagon 20, Brinsea, Somerset, UK) (Figure 4.2). On embryo age (EA) 7, a window of about 1.5-2 cm was opened in the eggshell to detach the shell membrane from the developing CAM using sterilized forceps. Then, the window was sealed with sterilized parafilm to avoid contamination and the eggs were returned to the static incubator for further incubation until the day of experiments. For xenograft experiments, the CAM was prepared as mentioned earlier. Then on EA 9, approximately 3×10^6 MGH cells were harvested using routine cell culture techniques. Cells were collected by centrifugation at 1,200 rpm for 5 min and the supernatant was discarded. Cells were drawn up into a sterile pipette and layered onto the CAM, avoiding contact between the CAM and the pipette. The window of the eggs were resealed with sterile parafilm and returned to the static incubator. Grafted cells were allowed to grow on the CAM for up to 5 days. Experimentations were only performed on eggs of EA 14 to EA 15 during which the eggs were mature, in order to minimize biological variations [159]. All experiments were performed in the tissue culture hood.

4.3.3 Administration of photosensitizer.

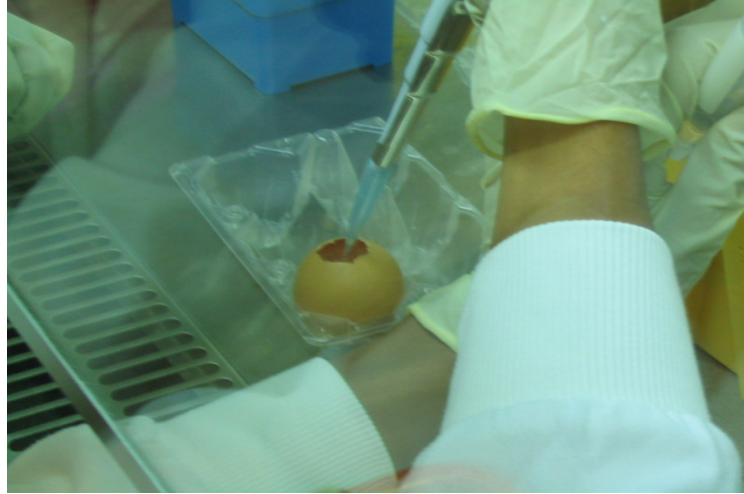


Figure 4.3 Topical administration of photosensitizer on CAM

On EA 14, eggs were randomly placed in three groups; the first group received topical Ce6–PVP administration, the second group received systemic administration of Ce6–PVP, and the third group received topical administration of 0.9% NaCl as control. For topical administration, 100 μ L of the photosensitizer was applied on the entire surface of the CAM and left to incubate for 30 min (Figure 4.3). The windows were resealed to avoid evaporation of the drug solution from the CAM. Prior to imaging, the CAM area was washed thrice with 1 mL of 0.9% NaCl saline to remove excess photosensitizer on the CAM tissue. For systemic administration, 100 μ L of the photosensitizer was injected directly into the yolk sac using a 26-gauge needle syringe. After 30 min incubation, imaging was performed at various time points until 24 h post drug administration. During the interval between each imaging sessions, the eggs were sealed with fresh parafilms and returned to the static incubator to ensure viability of the embryo throughout the experiments. All procedures were conducted under low

ambient lighting. Fluorescence imaging was then performed using the Karl Storz fluorescence endoscopy system (Karl Storz, Tuttlingen, Germany) to compare fluorescence images between the two modes of photosensitizer administration.

4.3.4 Fluorescence intensity imaging on CAM tumor model

Fertilized chicken eggs were incubated at 37°C in a humidified atmosphere inside a hatching incubator equipped with an automatic rotator (Octagon 20, Brinsea, Somerset, UK). On embryo age (EA) 7, a window of about 1.5 cm was opened in the eggshell to detach the shell membrane from the developing CAM. Then, the window was sealed with sterilized parafilm to avoid contamination and the eggs were returned to the static incubator for further incubation until the day of experiments. On EA 9, approximately 10×10^6 MGH cells were harvested using routine cell culture techniques. Cells were collected by centrifugation at 1200 rpm for 5 min and the supernatant was discarded. Cells were drawn up into a sterile pipette and layered onto the CAM, avoiding contact between the CAM and the pipette. The window of the eggs were resealed with sterile parafilm and returned to the static incubator. Grafted cells were allowed to grow on the CAM for up to 5 days. On EA 14, the eggs received a topical administration of 0.0625, 0.0313 and 0.0156 mg/mL Ce6 or Ce6-PVP constituted in 0.9% sodium chloride. A volume of 500 μ L of the photosensitizer was applied on the entire surface of the CAM and left to incubate for 30 min. The window was resealed to avoid evaporation of the drug solution from the CAM. After 30 min incubation, imaging was performed at 0.5, 1, 2, 3, 4, 5, and 6 h post drug administration. All procedures were conducted under low ambient lighting. Fluorescence images were attained using the Karl Storz fluorescence endoscopy system (Karl Storz, Tuttlingen, Germany). The intensities of the red and blue channels of the

fluorescence images were quantified using the software MicroImage (Olympus Optical Co. (Europa), Germany). The red channel registered the photosensitizer's fluorescence and the blue channel captured the diffusely back-scattered excitation light. By applying the red-to-blue intensity ratio as a diagnostic algorithm, the intensities of the red fluorescence of Ce6-PVP are determined as a function of time. Such algorithm is independent of the geometries of excitation/collection of signals and the power of excitation during the fluorescence imaging process.

4.3.5 Statistical analysis of fluorescence image

To statistically evaluate the fluorescence of Ce6-PVP, logistic regression and receiver operating characteristics (ROC) curve was determined using the GraphPad software (GraphPad, San Diego, USA). The elimination rate constant and fluorescence half-life ($t_{1/2}$) values of Ce6 and Ce6-PVP were calculated by a method fitting the data to a one-phase exponential decay equation. The validity of the fitted curve was verified with the test of runs in each case. Area under the curve (AUC), P value, and cut-off point were obtained from the ROC curve. The area under the ROC curve measures accuracy of the fluorescence images. The accuracy of the ROC curve analysis is based on how well the fluorescence intensity discriminates the tumor region from the normal CAM. The closer the curve follows the left border and then the top border of the ROC space, the more accurate the fluorescence. The closer the curve comes to the 45-degree diagonal of the ROC space, the less accurate the fluorescence.

4.3.6 Transport of photosensitizer across CAM

One mL of 0.0625 mg/mL Ce6 or Ce6-PVP solution was instilled to cover the whole surface area of the CAM. The window was covered with parafilm to prevent evaporation of the solution and incubated for 30 min in the dark. After incubation, the remaining drug was removed from the CAM surfaces by using micropipettes. Each surface was washed once with 1 mL 0.9% w/v NaCl solutions to remove excess photosensitizer. Then 1 mL of solution in the receptor compartment of the egg was syringed out followed by harvesting the chick embryo for photosensitizer quantification. These samples were immediately frozen and kept at - 20°C for further analyses. The contact area of each CAM was assumed to be circular and the diameter of the CAM was measured thrice diagonally across the egg at approximately 60° from each other to cover the circumferential perimeter of the CAM when the egg was sitting upright. For extraction of photosensitizers, 200 µL of the sample from the receptor compartment was dissolved in 800 µL of Solvable™ where as the chick embryo was dissolved in 4 mL of Solvable™. These samples were then incubated at 50 °C overnight followed by centrifugation at 1200 rpm. The emission intensity of Ce6 or Ce6-PVP in the resulting supernatant was determined spectrophotometrically ($\lambda_{\text{ex}} = 400 \text{ nm}$, $\lambda_{\text{em}} = 665 \text{ nm}$) and assumed as the amount of uptake after correcting for weight of the chick embryo.

4.3.7 Laser confocal fluorescence microscopy

After an incubation period of 2 min with Ce6 or Ce6-PVP, the CAM was harvested and fixed immediately in 4% paraformaldehyde. The CAM was then embedded with optimal cutting compound (OCT) on the cryostat. Cryo-sections of 20 µm thickness were obtained and mounted on the microscope slides for

confocal fluorescence imaging (Carl Zeiss, LSM 510, Germany). A 488 nm argon laser was used to excite the tissue. Fluorescence emissions in the wavelength range of 665 – 670 nm was split by a dichroic filter and detected through a band pass filter. Voltage gain, PMT voltage and sensitivity (contrast, brightness, and filters) were fixed for all fields and slides imaged. The images were analysed using an image analysis software package. Whole images were analysed to determine relative fluorescence intensities after correction for background autofluorescence. Digital quantification was carried out using contour superimposition where the contour of the region of interest was outlined and the pixel intensities per unit area determined.

4.3.8 Photodynamic therapy of CAM model

A portable diode laser (Ceralas PDT 665, Biolitec) emitting at a wavelength of 665 ± 3 nm was used for irradiation on the CAM model. The peak power output was calibrated to 1.65 – 1.75 W at the bulb-shaped diffusing fiber tip (Medlight, Lausanne, Switzerland) before commencement of irradiation. Fluence rate was measured using a power meter (LaserCheck, Coherent). PDT treatment were designed to study the effect of increasing light doses: 1 J/cm² delivered at 1 mW/cm², 10 J/cm² delivered at 10 mW/cm², 15 J/cm² delivered at 15 mW/cm² and 20 J/cm² delivered at 20 mW/cm²) and the fluence rate. All experimentation was performed under dim lighting.

4.3.9 Flow cytometry analysis

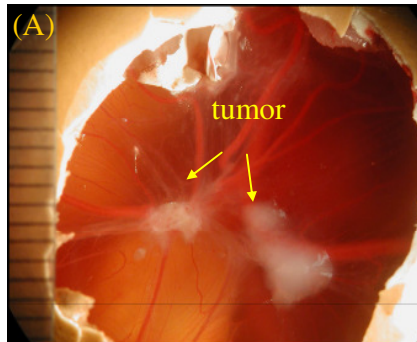
After 1 – 2 h post PDT treatment on the CAM, tumors and adjacent tissues were harvested. The tissues were meshed and put through a 70 µm cell strainer (Becton Dickinson, USA) to obtain single cell suspension. According to the

manufacturer's protocol, all cells were washed with cold PBS and stained with the dual dyes, namely YO-PRO-1 and Propidium Iodide (PI) nucleic acid stains (Vybrant Apoptosis Assay Kit #4, Molecular Probes, USA). After 30 mins incubation on ice, cells were washed in 1 mL of PBS. Erythrocytes were lysed using 500 µl of FACSLysing Solution (1:10 dilution) and cells were analysed using the flow cytometer (FACS Calibur; Becton Dickinson, USA) at excitation wavelength of 488nm. Viable cells do not take up any of the dyes and showed low fluorescence. Cells undergoing early apoptosis will be more permeable to YO-PRO-1 dye while cells that are in the late apoptosis and secondary necrosis will uptake both YO-PRO-1 and PI dye. The uptake proportion of fluorescence dyes was quantified using CellQuest software (Becton Dickson).

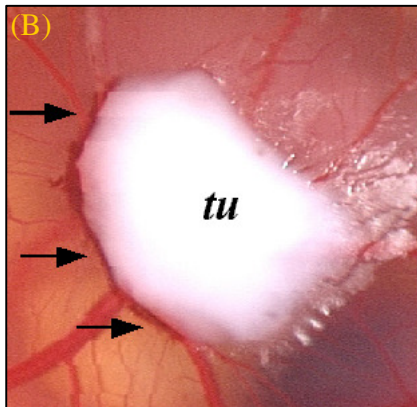
4.4 Results and discussion

4.4.1 Multicellular spheroids on the CAM model

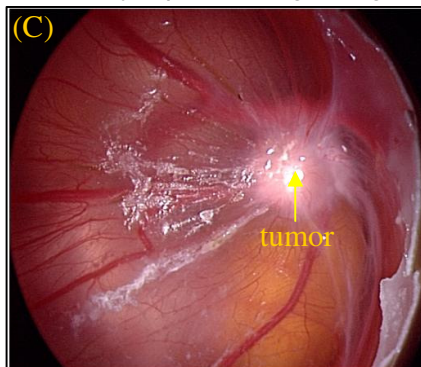
The CAM model serves as a convenient model for the study of PDD effects [141]. This model has several advantages including its simplicity, rapidity, sensitivity, ease of performance and its relatively lower cost, thus suitable for large-scale screening. Here, we have demonstrated that the CAM can be used as a three dimensional short-term cell culture system to culture poorly differentiated human bladder cancer cells (Figure 4.4). After 2 days of cell inoculation, there were visible opaque areas on the CAM membranes and a formation of fine capillaries in the tumor seeding area, indicating tumor growth [141]. The well vascularized CAM is a suitable system for *in vivo* induction of tumor for cancer research. This model was used to achieve highly reliable growth of established human prostate cancer cell lines [160], endometrium tissue [161] and human larynx carcinoma cells [162] as to name just a few. The extra-embryonic membrane acts as an excellent host to grow human cells since developing eggs are not yet immunocompetent, thereby enabling the grafting of the foreign cells. In contrast to conventional *in-vitro* cell cultures, 3-dimensional cultures using the CAM model may preserve specific biochemical and morphological features similar to the corresponding tissues *in vivo*. A major advantage of establishing 3-dimensional, spherical aggregate from permanent cell line on the CAM is that basic mechanisms of cell growth, proliferation, and differentiation can be studied in a reproducible format. Multicellular spheroids have been used as surrogates of tiny tumors for studying distribution and efficacy of chemotherapeutic agents. These spheroids resemble small residual tumors prior to vascularization.



Low magnification view of the tumor cell implanted on the CAM



High magnification view of the tumor cell at day 2 post xenografting



Formation of tumor spheroids of the MGH tumor cell implant after 5-6 days post xenografting

Figure 4.4 Xenografting of tumor spheroids on the CAM model. (A) MGH tumor (*tu*) was xenografted on the CAM. (B) Formation of neovasculature (arrow) surrounding the implanted cells after 2 days of xenografting. (C). Formation of spheroid like structure of the tumor on the CAM.

4.4.2 Fluorescence imaging of Ce6-PVP in normal CAM

Following systemic administration of Ce6-PVP, non selective red fluorescence on the CAM was observed upon excitation of the blue light at 0.5, 4 and 24 h post administration (Figure 4.5). However when Ce6-PVP was applied topically, non selective red fluorescence was only observed at 0.5 h post administration. Minimal fluorescence was observed at 4 h post administration and by 24 h, no fluorescence was observed on the CAM. Ce6-PVP seemed to localize in the vasculature of the CAM as well at 24 h for systemic administration and at 0.5 h for topical administration. In the context of this report, the CAM model closely simulates a PDT clinical environment of human bladder cancer in terms of (a) formation of superficial tumors, (b) mode of photosensitizer application by topical administration via intravesical instillation, and (c) the extraembryonic membrane mimic of the bladder mucosa. After 30 min of topical or systemic administration of the photosensitizer, non selective red fluorescence on the normal CAM was observed upon excitation of the blue light. The photosensitizer seemed to localize in the vasculature of the CAM as well. The fluorescence kinetics were tabulated using red to blue ratiometric analysis and the data was fitted with a logarithmic regression trendline (Figure 4.6). Overall, fluorescence on the CAM showed a time dependent decrease for both topical and systemic applications. For topical application, fluorescence peaked soon after 30 min of drug incubation. Fluorescence remained high up to 1 h post administration and then started to decrease thereafter. When the data was fitted with the logarithmic trendline, the correlation coefficient for topical and systemic administrations were found to be 0.89 and 0.36 respectively, indicating that the decreasing rate of fluorescence from the normal CAM after topical administration was faster compared to the systemic administration of the drug.

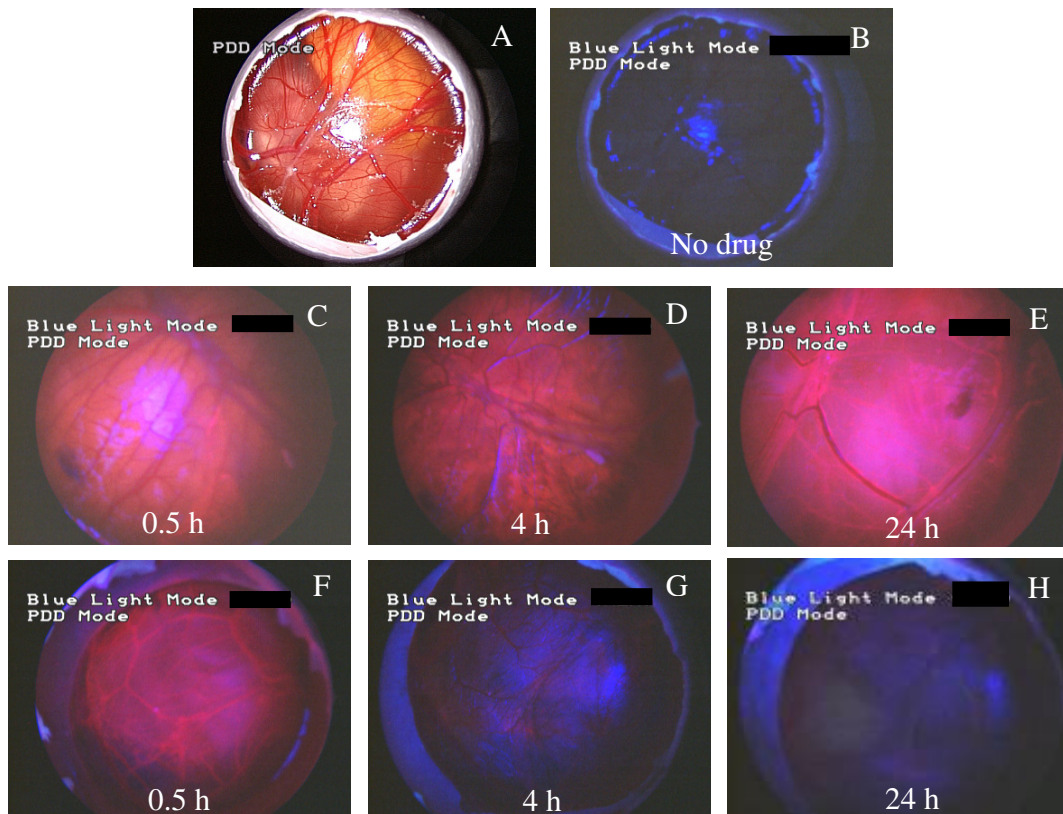


Figure 4.5 Representative images of normal CAM before and after administration of the Ce6-PVP. CAM before administration of the photosensitizer under white light and blue light mode (A-B). CAM fluorescence at 0.5, 4 and 24 h after systemic (C-E) and topical (F-H) administration of the photosensitizer.

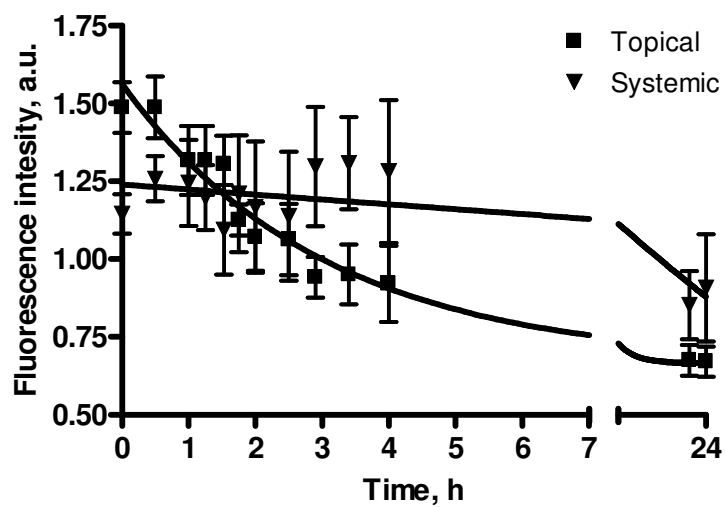


Figure 4.6 The Ce6-PVP fluorescence kinetics on normal CAM examined up to 24 h post drug systemic administration (■) and topical administration (▼). Values are expressed as fluorescence intensities after normalization with CAM before drug administration. Each point represents a mean of 5-measurements/6 eggs/time point. Bars = SE.

4.4.3 Fluorescence imaging of Ce6-PVP in CAM tumor xenografts

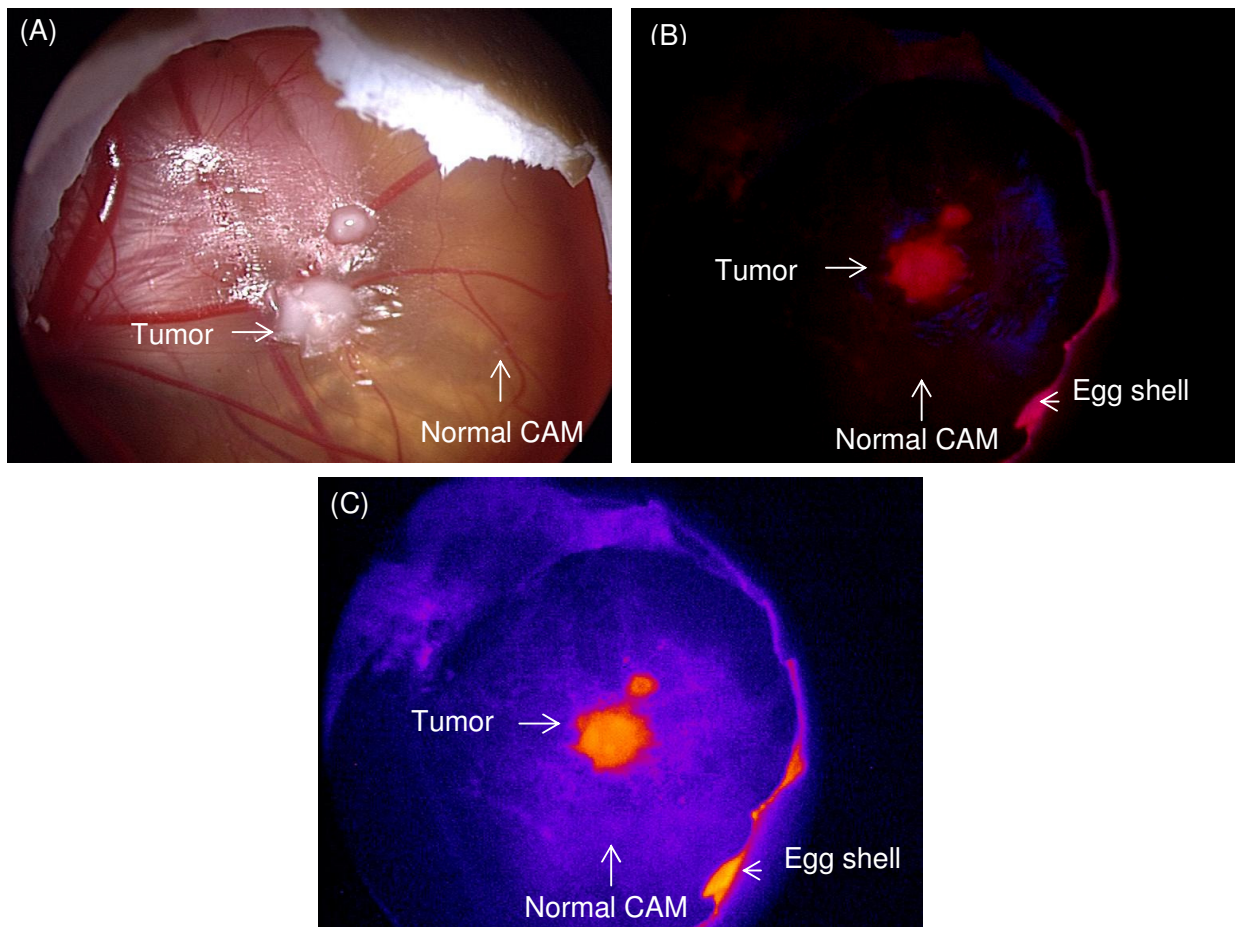


Figure 4.7 Fluorescence imaging of MGH human bladder tumor xenografted on the CAM model. (A) White light image of the tumor before drug administration, (B) Ce6-PVP induced red fluorescence in tumor imaged under blue light illumination at 3 h post drug administration. Minimal fluorescence was observed in the adjacent normal CAM suggesting a faster clearance rate from normal tissue of the CAM. (C) By displaying the fluorescent image in a pseudo color using simple image processing technique, a clear discrimination of the tumor border can be visualized.

Having determined the clearance rates from the two modes of drug administration, the topically administered mode was used to study the photosensitizer on the CAM tumor model. The fluorescence retention of Ce6 and Ce6-PVP by the MGH bladder tumor xenografts was assessed using image-processing techniques (Figure 4.7). Before incubation of the photosensitizers, the CAM tumor xenografts were imaged under blue light illumination, to ensure that there was no autofluorescence. After topical administration of Ce6-PVP, an intense red fluorescence in the bladder tumor xenografts was observed, suggesting uptake and localization in the malignant cells on the CAM. Fluorescence in the normal CAM tissue was lower compared to fluorescence in the tumor tissue, suggesting a faster clearance rate from normal tissue of the CAM. When the time-dependent evolution of the fluorescence was plotted and fitted with non-linear regression analysis, a higher mean retention profile of Ce6-PVP was observed compared to Ce6. The fluorescence intensity elimination rate constant for tumor and normal CAM after Ce6 administration was calculated to be 0.19 and 0.21 min^{-1} respectively. For Ce6-PVP, elimination rate constant for tumor and normal was calculated to be 0.02 and 0.18 min^{-1} for respectively. Half-life of Ce6-PVP in tumor was approximately 9 times longer than Ce6, suggesting that Ce6-PVP is being retained longer in the tumor. No difference in half-life of both photosensitizers was observed in the normal CAM.

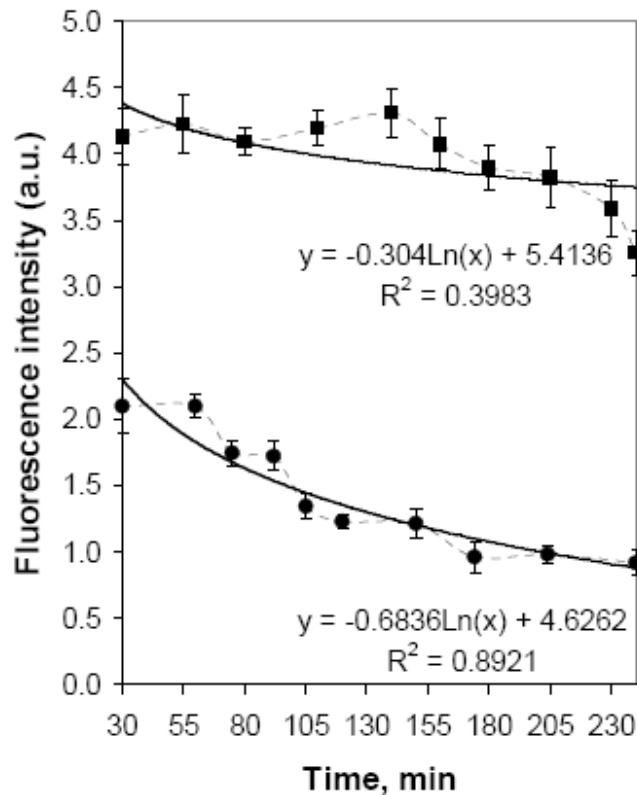


Figure 4.8 The Ce6–PVP fluorescence kinetics on normal CAM (●) and bladder tumor cell xenografts on CAM (■) plotted against time. The CAM was topically incubated with the drug for 30 min prior to the fluorescence measurement. A logarithmic trendline (solid line) was used to best fit a curve to the data. Higher fluorescence intensity was observed in the tumor xenografts compared to the normal CAM tissue. Each point represents a mean of 7 eggs. Bars = SE.

Fluorescence kinetics on normal and tumor CAM were charted as a function of time (Figure 4.8). High differential fluorescence intensity was observed between tumor and normal CAM tissue, indicating preferential localization of Ce6-PVP in the bladder tumor. It was also observed that fluorescence in the tumor remained high in the first 2 h post drug administration. Subsequently, fluorescence started to decrease but still displayed sustained fluorescence for up to 4 h compared to normal. This suggested that fluorescence diagnosis may be delayed as tumor fluorescence will still be adequate for 4 h after topical administration of drug.

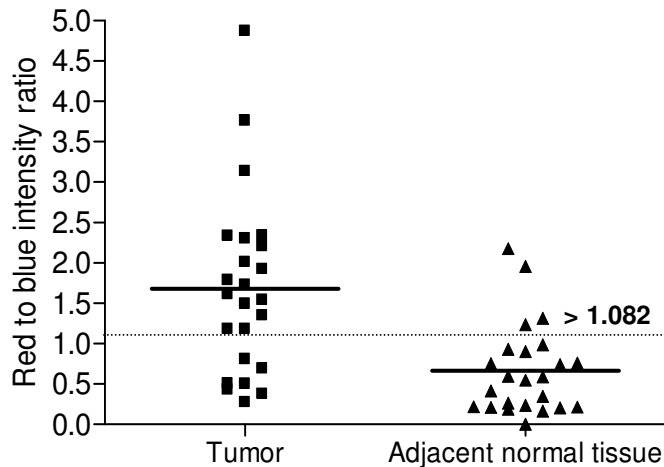


Figure 4.9 A scatter plot comparing the fluorescence intensity in tumor and the adjacent normal CAM tissue was compiled from 1 – 5 h post topical drug administration. The points on the scatter plot are normalized individual measurements from 24 eggs. The dotted line is the cut-off fluorescence intensity threshold derived from the ROC curve to classify tumor from normal tissue with a sensitivity and specificity of 70.8% (95% CI 48.9% to 87.4%) and 83.3% (95% CI 62.6% to 95.3%) respectively.

The fluorescence retention from 1 to 5 h post topical administration of Ce6-PVP in bladder tumor xenografts on CAM was tabulated using the red to blue ratio algorithm and fitted into a ROC curve to validate the ability of Ce6-PVP to discriminate tumor from adjacent normal CAM membrane. By applying a cut-off value to these ratios as a diagnostic criterion, it allowed the generation of sensitivity and specificity values to distinguish tumor from healthy CAM. A cut-off red to blue ratio of > 1.08 gave the highest combined sensitivity and specificity of 70.8% (95% CI 48.9% to 87.4%) and 83.3% (95% CI 62.6% to 95.3%) respectively (Figure 4.9). Raising the value to > 1.33 gave the sensitivity and specificity values of 62.5% (95% CI 40.59% to 81.20%) and 91.2% (95% CI 73.0% to 99.0%) respectively.

In PDT of the bladder, the favored method for administration of photosensitizer is through intravesical instillation because of the non-existence of substantial side effects or systemic photosensitivity [163]. In this context, this report has demonstrated that Ce6-PVP may be used as a topical formulation as it allows for fast tumor accumulation and rapid clearance. In the clinical setting, this is a major advantage as it enables shorter drug application time while retaining tumor selectivity for reasonable time window without the associated prolonged photosensitivity. This in turn improve patient compliance for fluorescence diagnosis procedures., The fluorescence kinetics of the photosensitizer was charted by applying post digital image processing. Although the data presented here is semi-quantitative, the ability to non-invasively measure the fluorescence of the photosensitizer represents a straightforward method to correlate drug dynamics in the tissue. Furthermore, the Ce6 fluorescence was excited by a xenon-arc lamp fluorescence designed for the excitation of ALA-induced PPIX fluorescence. This indicates that Ce6 can be used as an alternative fluorescent marker with the existing Karl Storz fluorescence endoscope system without modification.

A combined ROC curve analysis was performed from 0.5 to 5 h post administration of Ce6 and Ce6-PVP to validate the ability of the photosensitizers to discriminate tumor from normal CAM membrane (Table 4.1). The area under the curve (AUC) were then compared in order to make a fair judgment of the effectiveness of the photo-sensitizers without being constricted to single values of sensitivity and specificity, which largely depend on the cut-off fluorescence intensity value chosen to distinguish normal from malignant region. The AUC for Ce6 and Ce6-PVP were 0.83 ± 0.06 and 0.99 ± 0.01 respectively ($p < 0.001$)

indicating that Ce6-PVP has better accuracy. The sensitivity and the specificity were calculated using different threshold (cut-off) values to distinguish healthy CAM from tumor. For Ce6, the highest combined specificity and sensitivity were 79.2% and 79.2% (cut-off value > 4.0), whereas for Ce6-PVP it was 81.8% and 98.0% respectively (cut-off value > 4.1), implying that fluorescence mediated Ce6-PVP has distinctly higher rate of sensitivity for the detection of MGH tumor. In order to correlate drug dose to the selectivity and sensitivity of Ce6-PVP induced fluorescence on tumor, ROC curves were generated for 3 serial dilution of Ce6-PVP dose. Selectivity and sensitivity was observed to be drug dose dependent (Figure 4.10). Area under the ROC curve was 0.83 ± 0.02 , 0.78 ± 0.02 and 0.79 ± 0.03 for 0.0625 and 0.0313 and 0.016 mg/mL respectively.

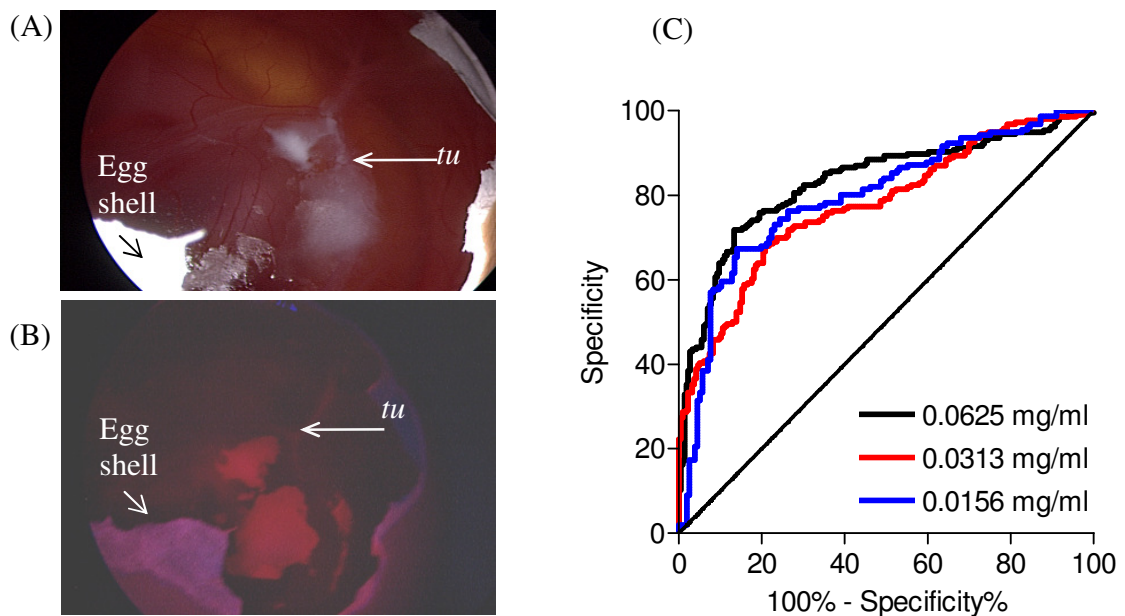


Figure 4.10 (A) Representative images of MGH tumor (tu) xenografted on the CAM under white light. (B) Selective red fluorescence was observed on the MGH tumor at 3 h post topical administration of Ce6-PVP while no fluorescence was observed on the normal CAM tissue. (C) Receiver operating characteristic (ROC) curves illustrating the ability of various drug dose of Ce6-PVP to separate MGH tumor from adjacent normal chorioallantoic membrane ($p < 0.0001$). The ROC curve of two indistinguishable populations (i.e. tumor versus normal region), represented by the 45-degree line (area under the ROC curve = 0.5), is included for comparison. Area under the ROC curve was 0.83 ± 0.02 , 0.78 ± 0.02 and 0.79 ± 0.03 for 0.0625 and 0.0313 and 0.016 mg/mL respectively. The y axis represents the specificity of the Ce6-PVP induced fluorescence and the x axis represents the sensitivity of the Ce6-PVP induced fluorescence.

Table 4.1 A comparison of half-life, specificity and sensitivity of Ce6 and Ce6-PVP in tumor and normal tissue on the CAM model.

Best-fit values	Ce6		Ce6-PVP	
	Tumor	Normal	Tumor	Normal
K	0.19 ± 0.04	0.21 ± 0.08	0.02 ± 0.01	0.18 ± 0.03
Half life, h	3.7	3.4	34.5	3.8
Area under the ROC curve	0.8316 ± 0.06*		0.9909 ± 0.01*	
Specificity, %	79.2 (CI 57.9 to 92.9)		81.8 (CI 70.4 to 90.2)	
Sensitivity, %	79.2 (CI 57.9 to 92.9)		98.0 (CI 89.4 to 99.9)	

Non-linear regression of time-dependent changes in fluorescence was used to estimate the decay rate constant (K) and half-life from 1 to 5 h post topical administration of Ce6 and Ce6-PVP in MGH tumor and normal CAM. Half-life = 0.69/K; CI = confidence interval; *p < 0.0001

4.4.4 Membrane transport study

This experiment aimed to study the effect of PVP on the uptake of Ce6 across membrane using CAM as a drug transport model. Four parameters were extracted from the experimental eggs to determine the effectiveness of PVP for transporting Ce6 into the membrane after topical application. The thickness of the CAM was determined using OCT imaging (Figure 4.11). The average thickness was determined to be $100 \pm 1.9 \mu\text{m}$. Equal volume and concentration of Ce6 or Ce6-PVP was applied topically for 30 min on the CAM. A comparison between the uptake of Ce6-PVP transported across the CAM in the receptor compartment was approximately double compared to Ce6 (0.055 ± 0.0135 and 0.030 ± 0.003 a.u., respectively, $p = 0.0464$) (Figure 4.12 A). Since the experimental conditions were similar, the difference in the amount of photosensitizer transported can be inferred as due to differences in membrane permeability. The diffusion coefficient tabulated using Ficks's law (Eq. (1)), for Ce6-PVP was found to be 1.4 fold higher compared to Ce6 indicating a higher diffusivity (Figure 4.12 B). However, the diffusion coefficient was not statistically significant. Chick embryos were excised and the photosensitizer were extracted and analysed for fluorescence intensities per gram of tissue (Figure 4.12 C). The uptake of Ce6-PVP by the chick embryos was roughly two fold lower when compared with that of the Ce6 (0.012 ± 0.002 and 0.009 ± 0.002 intensity/g, respectively, $p = 0.0274$).

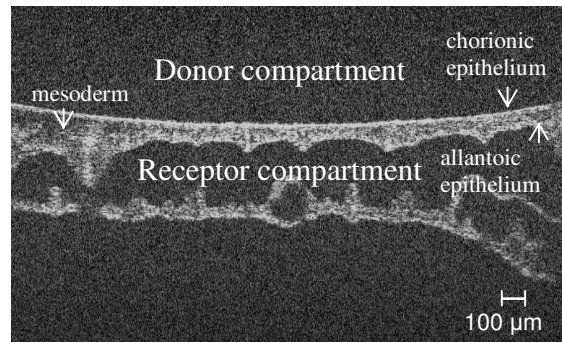


Figure 4.11 Optical coherence tomography (OCT) imaging of the CAM. OCT is a high-resolution noninvasive imaging technique based on laser interferometry, used to assess CAM thickness. The chorionic epithelium, mesoderm and allantoic epithelium layers can be visualized in the OCT structural image. The thickness of the CAM was estimated to be around $100 \pm 1.9 \mu\text{m}$.

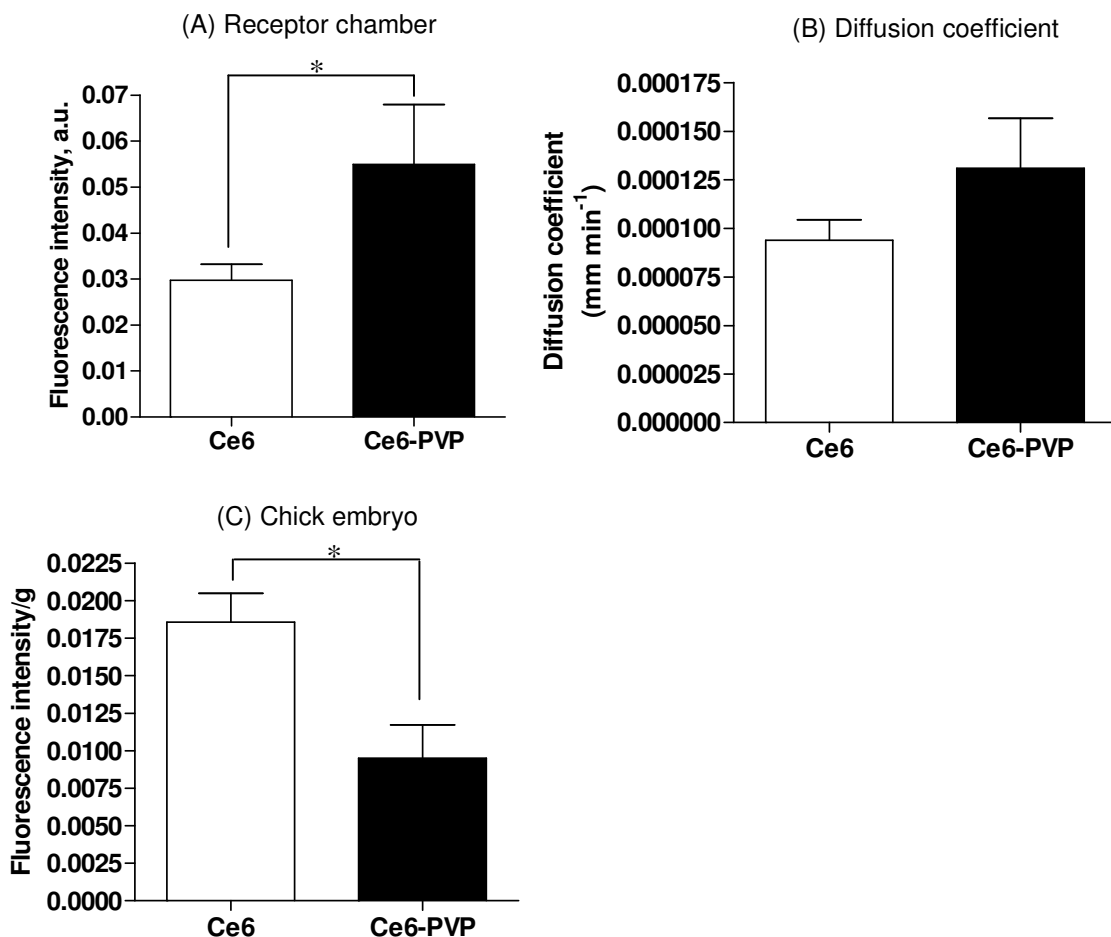


Figure 4.12 Drug transport study comparing Ce6 and Ce6-PVP in the CAM model. (A) Uptake studies of Ce6 and Ce6-PVP in the receptor chamber, (B) comparison of diffusion coefficient of Ce6 and Ce6-PVP across the CAM. * $p < 0.05$ and (C) uptake studies of Ce6 and Ce6-PVP in the chick embryo .

Many drug formulations that include the use of polymers to affect the rate of drug delivery have been extensively studied. PVP has been utilized to increase the solubility of the drug and modulates the delivery of the drug from the composition and through the target tissue. Likewise, many investigations in the area of photobiology have focused on ways to develop formulation of photosensitizer to improve drug selectivity in tumor tissue in order to enhance PDT efficacy. It has been found that topical application of photosensitizer is effective for photodynamic therapy in superficial bladder cancer [152]. Although the bladder is an easily accessible organ for topical treatment, a glycosaminoglycan layer on the bladder mucosa can prevent the sufficient uptake and integration of many intravesically applied therapeutic compounds [153]. Therefore, the use of PVP photosensitizer is expected to overcome this problem. To address the important question of whether PVP enhances the transport of Ce6 across membrane, transport experiments were designed using the CAM model to assess uptake and diffusion coefficient of the photosensitizers using the assumption that diffusion was the dominant process for Ce6-PVP distribution. No other published data from experimental studies has reported on the effect of PVP on the transport of Ce6. PVP was found to increase the transport of Ce6 and acted as a co-enhancer for transmembrane delivery. In addition, under the experimental conditions employed in this study, enhanced diffusion coefficient was calculated for Ce6-PVP compared to Ce6, indicating the improved amphiphilicity characteristic of Ce6-PVP and its diffusivity through a lipophilic matrix. This was further confirmed in the in vitro experiment where intracellular accumulation of Ce6-PVP in bladder cancer cells was much higher compared to Ce6 alone. Interestingly, Ce6-PVP accumulated to a much lesser extent in the chick embryo, which further confirms the lack of apparent Ce6-PVP uptake and retention in normal tissue.

4.4.5 Fluorescence confocal microscopy imaging

In order to determine if Ce6-PVP had higher diffusivity compared to Ce6 through membrane at the microscopic level, the CAM was harvested and prepared for microscopic sections. The fluorescence intensities of both photosensitizer after topical application for 2 min were captured by confocal microscopy. This enabled the measurement of relative concentrations of fluorescent molecules inside the CAM tissue, as the fluorescence intensity is proportional to the concentration of the photo-sensitizer. The images were then analysed using image quantification software to calculate fluorescence intensity. Ce6-PVP was found to be significantly higher in the CAM compared to Ce6 (Figure 4.13).

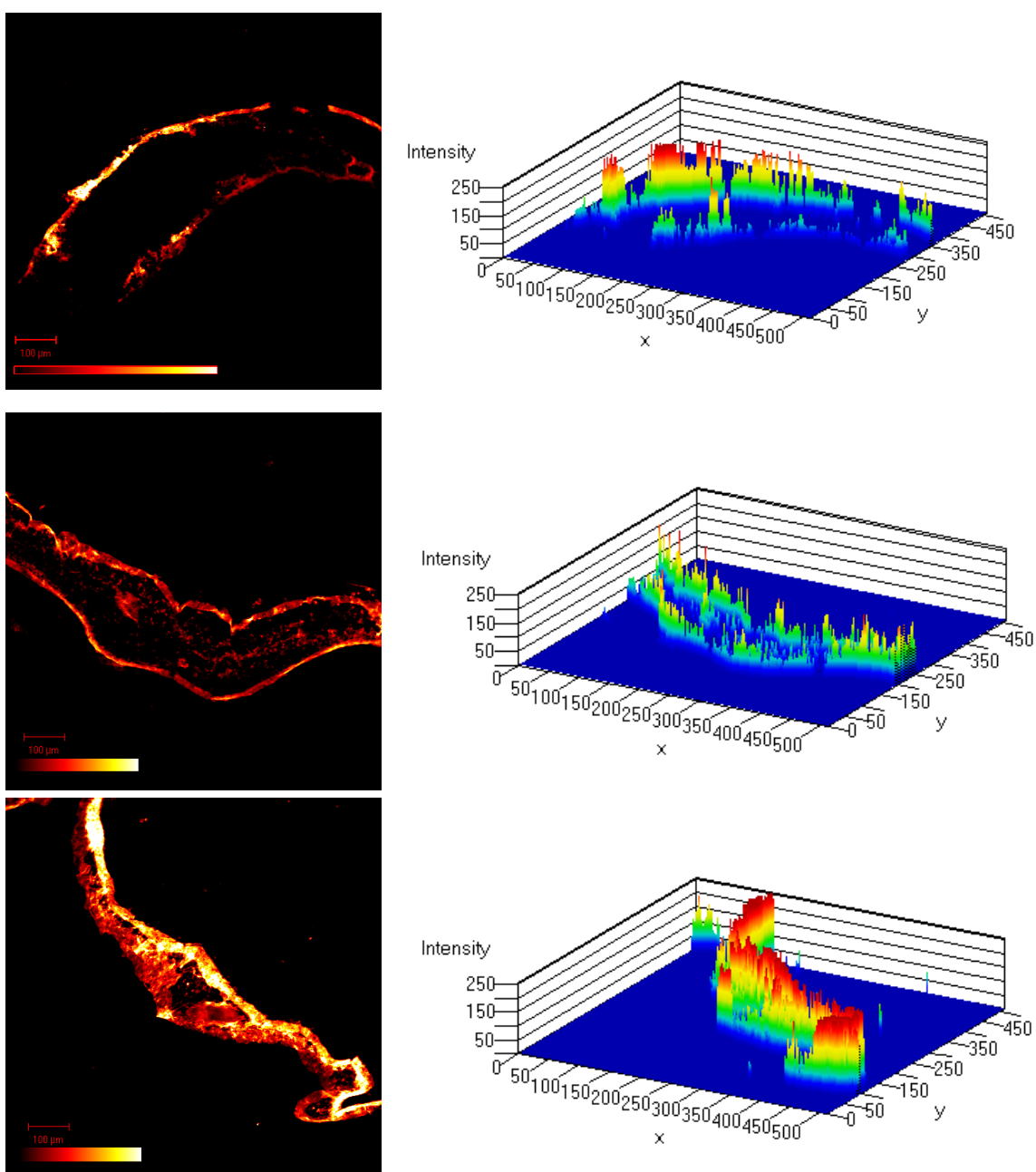


Figure 4.13 Fluorescence confocal microscopy imaging in the CAM. Different increase in fluorescence on CAM treated with Ce6 or Ce6-PVP captured by confocal microscopy and its corresponding topographical contouring image. Confocal images of (A) CAM with no photosensitizer showed some autofluorescence; (B) CAM incubated with Ce6 for 2 mins showed a minimal fluorescence; and (C) CAM incubated with Ce6-PVP for 2 mins showed a 14-fold fluorescence increase after correction for background autofluorescences. Scale bar, 100 μm .

4.4.6 Photodynamic therapy efficacy of Ce6-PVP

All CAM models were sensitized with Ce6-PVP at the dose of 0.0625 mg/mL and received various light dose and fluence rate (Figure 4.14). One to two hours after PDT, the tumor and its surrounding normal area were harvested from the CAM and flow cytometry analysis were performed to assess for total cell death. In general, the percentage of cell death of normal CAM area was lower than tumor when PDT was performed with the same fluence and fluence rate. There were no statistical significance on the percentage of cell death in tumor and normal CAM tissue at 24 h following irradiation at the light dose of 1 J/cm², 15 J/cm², 20 J/cm² delivered at 1 mW/cm², 15 mW/cm² and 20 mW/cm² respectively. Only irradiation at 10 J/cm² delivered at a fluence rate of 10 mW/cm² resulted in statistically significant percentage of cell death in tumor. PDT induced cell death in normal CAM irradiated at 10 J/cm² and 10 mW/cm² was not significant compared to other light doses.

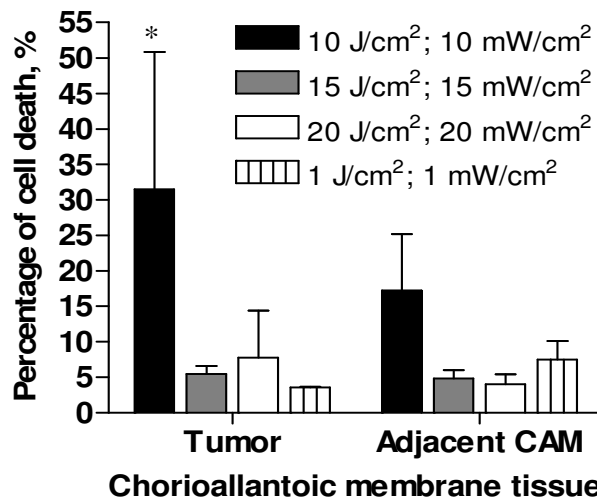


Figure 4.14 CAM with bladder tumor xenografts after topical administration of Ce6-PVP (0.625 mg/mL) and exposed to increasing light doses (1, 10, 15 and 20 J/cm²) at 665 nm. The efficacy of Ce6-PVP mediated PDT for eradication of bladder tumor in the CAM model seems to be inversely proportional to the light dose used. *p < 0.05 compared to 1, 15 and 20 J/cm².

Diffuse superficial transitional cell carcinoma refractory to standard therapies poses a clinical dilemma and PDT appears to be a promising treatment and palliative modality. A successful PDT of epithelial cancer requires a specific photosensitization of malignant tissue. Through fluorescence imaging on the CAM tumor model, we have shown that specific localization of Ce6-PVP in the bladder tumor can be attained longer compared to Ce6 alone. This suggests that *in situ* application of Ce6-PVP in the bladder is capable of exhibiting selective retention in the tumor and thus highly selective photodynamic destruction of the tumor tissue can be achieved. However, the complexity of determining light dosimetry for irradiation in the bladder makes the clinical application of new photosensitizer rather a challenging undertaking. Because it is difficult to optimize many parameters in a clinical context for each new photosensitizer, an animal model such as the CAM model provides preclinical data of high interest for the clinical use of PDT. The rationale for the PDT response study on the CAM model was to simulate light dosimetry that is commonly used in PDT of the bladder, so as to establish the basis for clinical treatment of the efficacy of the new Ce6-PVP formulation. The level of PDT response of tumor tissue analyzed using flow cytometry shows a strong dependence on the light dose at the applied conditions in the CAM. Higher percentage of cell death was observed at 10 J/cm² compared to 15 J/cm² and 20 J/cm². No significant tumor cell death observed after irradiation at 1 J/cm². This suggests that there is a threshold for a photodynamic reaction to cause cell death using Ce6-PVP. However, as addressed by many researchers, experimentation on different animal tumor models, and the interdependence of photosensitizer concentration, route of administration, and incubation time determines the irradiance and radiant exposure to cause PDT-induced tissue damages [164-166]. As such,

extrapolation of PDT parameters obtained from preclinical study to clinical application warrants further studies.

4.5 Conclusion

Based on the CAM tumor model, Ce6-PVP has been shown to be a good photosensitizer, capable of inducing highly selective fluorescence in cancerous cells. Thus, it could become a promising diagnostic tool to enhance visualization of surgical margin of the tumor cells as well as allowing for easy visualization for targeted biopsy using fluorescence endoscopy. This in turn, can help diagnose and treat bladder cancers at their earlier stages. PVP has been successfully proven to enhance membrane permeation of Ce6, via the CAM transport model. Nonlinear regression analyses have shown that the new formulation of Ce6-PVP has a longer half-life in the tumor than Ce6. Ce6-PVP displayed higher selectivity and sensitivity towards tumor xenografts. It is proposed that the use of Ce6-PVP, combined with low irradiance, could improve the efficiency of topical Ce6-PVP-mediated PDT.

CHAPTER 5

Effect of polyvinylpyrrolidone on the interaction of chlorin e6 with plasma proteins and its subcellular localization

5.1 Summary

A photophysical study on the binding interaction of chlorin e6 and the polymer polyvinylpyrrolidone with bovine serum albumin (BSA) and human plasma proteins such as very low density lipoprotein (VLDL), high density lipoprotein (HDL) and low density lipoprotein (LDL) was performed using a steady-state fluorescence technique. Ce6-PVP has good photostability at 3 different temperatures (4 °C, 21 °C and 37 °C) when dissolved in aqueous solution containing 5% and 10% serum. In the partition coefficient determination, Ce6-PVP was relatively more hydrophilic when compared to Ce6. The emission profile of Ce6-PVP underwent a marked increased and bathochromic shift upon addition of the proteins, indicating that the proteins introduced motional restriction on the Ce6 molecule. These results also suggested that the association energy of Ce6-PVP with VLDL might be slightly greater than that with other lipoproteins when compared to Ce6 alone. Colocalization of Ce6 and PVP in cells was also assessed using confocal microscopy. PVP was found to localize within the cytoplasmic compartment of cells and the association of Ce6 with PVP led to an enhanced cellular uptake of Ce6 by the cells. The present study supported the hypothesis that PVP improves the permeation of Ce6 through biological membranes in cells.

5.2 Introduction

The use of the photosensitizer Ce6 and its derivatives for selective and effective photodynamic destruction of human malignant tumors has become increasingly apparent [137]. To date, many formulations of Ce6 have been developed and, have significant tumor localizing capacity. This present chapter investigated the efficacy of Ce6 formulated using PVP. PVP is a water-soluble polymer of pharmaceutical grade, known to form water-soluble complexes with a number of pharmacological substances and many investigations into the formation of PVP – complexes with drugs have been described [65, 112]. The chemically and biologically inert PVP has been initially use as a plasma substitute, although this has now been discontinued due to accumulation of large molecular weight fractions in the body [167]. As the molecular weight of PVP decreases, the rate of polymer dissolution, oral absorption and excretion increases. Therefore, lower molecular weight PVP is typically preferred for parenteral applications. PVP is now a well used pharmaceutical binder although more novel uses include the polymer as a controlled release and transdermal penetration enhancer [168]. Ce6-PVP was developed with the rationale to provide a novel photosensitizer formulation of a high chemical and photochemical stability, good solubility both in water and in biological fluids, high affinity to tumor tissue, low phototoxicity as well as to provide a method of preparation of such photosensitizer [113, 169]. In this context, Ce6-PVP is a promising formulation for the photochemotherapy of tumors. Many postulations have been proposed for the preferential accumulation of a photosensitizer in neoplastic tissue. Among them are (a) greater proliferative rates of neoplastic cells thus higher uptake, (b) poorer lymphatic drainage, (c) leaky tumor vasculature, (d) specific interaction between the photosensitizer and marker molecules on neoplastic cells, and (e) specific low-density lipoprotein

(LDL) receptor-photosensitizer interaction leading to increased photosensitizer concentrations in neoplastic tissue. Injected photosensitizers bind mostly to serum proteins, but the binding protein differs according to the chemical characteristics of the photosensitizer. Various pharmacokinetic investigations have led to the general agreement that hydrophobic dyes are associated with lipoproteins, while their hydrophilic counterparts bind preferentially to other serum proteins, such as albumin [170]. Photosensitizer redistribution between plasma proteins defines photosensitizer interaction with cells, its intracellular localization and kinetics of accumulation in the tumor and photodynamic efficacy *in vivo* [171]. For that reason, plasma proteins binding affinity to photosensitizers play an essential role in drug distribution. The objective of this chapter was to investigate the interactions of plasma proteins with Ce6 in the presence or absence of PVP by examining changes in both the bathochromic and hyperchromic shifts of Ce6 using spectrophotometry. The rate and extent of binding Ce6 and Ce6-PVP to HDL, LDL and VLDL was calculated. Examination of the subcellular localization PVP, Ce6 and Ce6-PVP using confocal microscopy were carried out. Since no experimental evidence of Ce6–PVP interactions have ever been published, it is hope that this study will offer a new insight into the understanding of the mechanism of PVP interaction with Ce6.

5.3 Materials and methodology

5.3.1 Photosensitizer and serum proteins

Ce6-PVP was obtained from ORPEGEN Pharma GmbH, Heidelberg, Germany as a co-lyophilisate of Ce6 sodium salt and PVP (molecular mass \approx 12,000 kDa) in a 1:1 mass ratio. Ce6 was also obtained from ORPEGEN Pharma and lyophilized without further addition of PVP. Human LDL (6.1 mg/mL; molecular weight, 3500 kDa), HDL (16.4 mg/mL; molecular weight, 175–500 kDa) and VLDL (2.37 mg/mL, molecular weight, 6000 – 27000 kDa) were purchased from Sigma Chemical Co. (St. Louis, MO, USA).

5.3.2 Determination of photosensitizer stability using fluorescence spectrometry

20 μ M of Ce6 or Ce6-PVP was dissolved in 1 mL of the following solutions: PBS, water, and fetal calf serum (5%, and 10%). Solution stability was assessed as a function of time for 27 days at 3 different temperatures (4 $^{\circ}$ C, room temperature (RT) and 37 $^{\circ}$ C) by measuring the fluorescence emission spectrum using the spectrofluorophotometer RF-5301 PC (Shimadzu, Kyoto, Japan). Fluorescence emission was measured from 620 to 630 nm upon excitation at 400 nm. Non-linear regression fitting using one phase exponential decay was used to determine the half-life using Graph-Pad Prism™ version 2.0 package (Intuitive Software for Science, San Diego, USA).

5.3.3 Preparation of photosensitizer–protein complex and measurement.

The emission properties of Ce6 and Ce6-PVP at a concentration of 0.01 mg/mL in 0.9% physiological saline were investigated..Protein solutions were prepared in nine different concentrations; 0%, 0.005%, 0.01%, 0.015%, 0.02%, 0.05%, and 0.1%. A total of 80 μ L of the photosensitizer was added into 720 μ L of each

concentration of the protein solutions. The solutions were mixed well and incubated for 1 h on ice in order to examine only photosensitizer–substrate interaction in the absence of active lipolysis, and to exclude the possible effects of the changing of the size and composition of lipoprotein particles on the binding to photosensitizers. Emission was measured using a HITACHI U-3010 spectrophotometer. The scan range was from 500 to 800 nm using a WI (VIS) lamp. Curves were fitted using GraphPad Prism software. Derived Vmax and Km values with standard errors are listed in Table I.

5.3.4 Determination of partition coefficient.

Log P (logarithm of the partition coefficient in water/1-octanol system) determinations were performed using equilibration techniques. Partitioning was carried out in centrifuge bottles. Partition coefficients of Ce6 were evaluated in a system of 1-octanol–PBS at four different pH values, 5.0, 6.0, 7.0 and 8.0. Fifty μ L of 0.01 mg/mL Ce6 and Ce6-PVP in 0.9 % NaCl was added to 5 mL of 1-octanol followed by the addition of an equal volume of PBS at a specified pH (3 mL). After each phase was presaturated with the other, the tubes were vortexed for 2 min at room temperature (21 °C). Tubes were centrifuged for 2 min at 3000 rpm to separate the octanol and water phases. After centrifugation, the solutes in both phases were analyzed. 1.8 mL of the buffer phase was pretreated with 0.2 mL of 10% Triton X-100 to ensure deaggregation of the drug. Absorption was measured with a UV-Vis absorption spectrometer. The partition coefficients (P) were calculated as:

$$P = C_{\text{oct}} / C_{\text{PBS}} = \text{abs}_{\text{oct}} / \text{abs}_{\text{PBS}}$$

where C_{oct} and C_{PBS} represent the photosensitizer concentrations in the organic and the aqueous phase, respectively, abs_{oct} the absorbance of the compound measured in the octanol and abs_{PBS} the absorbance in the PBS solution.

5.3.5 Labelling of PVP with fluorescein fluorescein isothiocyanate (FITC)

PVP (1.25 g) and KOH (1.25 g) were dissolved in 50 mL water. The solution was transferred in to a 100 mL pressure bottle. The pressure bottle was closed with a teflon screw cap, then placed on a heating mantle and heated to a surface temperature of 135 °C for 15 h. The assembly was then cooled, the bottle opened and the solution was filtered. The pH of the remaining solution was adjusted to pH 7 using HCl. The solution was then transferred to a dialysis bag (MWCO = 3000Da, Spectrapore) and dialyzed against milliQ water (4L x 6) for three days. The contents of the dialysis bag were then transferred to a 250 mL round bottomed flask and lyophilized to obtain a pure opened ring PVP (PVPRO) (1g). Potentiometric titration showed that, the percentage of ring opening is 3.5 ($\pm 0.3\%$). ¹H-NMR (D₂O): d 0.9-1.4 (br., endgroups), 1.4-1.5 (br. s), 1.5-1.8 (br. s), 1.8-2.1 (br. s), 2.1-2.35 (br. s), 3.0-3.4 (br. s), 3.4-3.6 (br. s), 3.6-3.9 (br. s). 20 mg of PVPRO was dissolved in 20 mL 0.1 M sodium carbonate buffer and 2 mL of FITC (1 mg/mL) was added at room temperature and stirred gently with a magnetic stir bar. After 2 h, the solution was transferred to a dialysis bag (MWCO = 3000Da, Spectrapore) and dialyzed against deionized water for 3 days. The content of the dialysis bag was then transferred to a 100 mL round bottomed flask and lyophilized to produce PVP-FITC (16.8 mg). This was dissolved into 16.8 mL PBS. 10 μM of PVP-FITC was then prepared in RPMI medium and used for cell culture studies.

5.3.6 Intracellular localization by confocal laser scanning microscopy.

MGH cells were maintained in RPMI medium containing 10% fetal calf serum (FCS), sodium pyruvate (110 mg/mL), penicillin (100 U/mL) and streptomycin (100 mg/mL) under 5% CO₂. The cells were seeded at 1 x 10⁵ per well of the 8-well Labtek chamber slide (Nunc, Naperville, CT) in 0.5 mL of RPMI medium. After a 24 h attachment and growth period at 37°C, the cells were incubated with Ce6, Ce6-PVP and PVP-FITC for (10 μM) for 30 min. Cells were then washed and fixation was performed in 3.7% formaldehyde and 0.05% Triton X-100 in PBS for 5 min. The cells were then stained with DAPI ($\lambda_{\text{ex}} = 378$ nm, emission filter = BP 400 - 440 nm) rhodamine-phalloidin ($\lambda_{\text{ex}} = 543$ nm, emission filter = LP 590 nm) using the procedure adapted from the experimental protocol (Subcellular Structure Localization Kit, Chemicon). The coverslips were then mounted on a slide, using antifade mounting medium (Vectashield, Vector), before imaging using a confocal laser-scanning microscope (CLSM). Confocal parameters are listed as follows: 40x/0.55 objective lens; 488 nm exciting wavelengths for Ce6/Ce6-PVP and FITC; 488/568 nm beam-splitter for FITC; 660 - 670 nm band-pass barrier filter for Ce6/Ce6-PVP fluorescence detection.

5.4 Results and discussions

5.4.1 Partition coefficient

One of the challenges in formulating photosensitizers is the optimization of their amphiphilic properties so that they are hydrophilic enough to be administered as aqueous solutions and be eliminated rapidly from the body after photodynamic therapy. At the same time, the photosensitizers must be lipophilic enough to be retained by, and preferentially localized in tumor tissue. The lipophilicity of photosensitizers is thought to be an important parameter in controlling penetration through the cellular membrane and cellular uptake of photosensitizers. In this context, this study reported the influence of pH on the lipophilicity of Ce6 or Ce6-PVP. One of the traditional ways of evaluating the amphiphilicity of medicinal compounds is to determine their partition coefficients between 1-octanol and PBS. It is a simplistic way of calculating the manner by

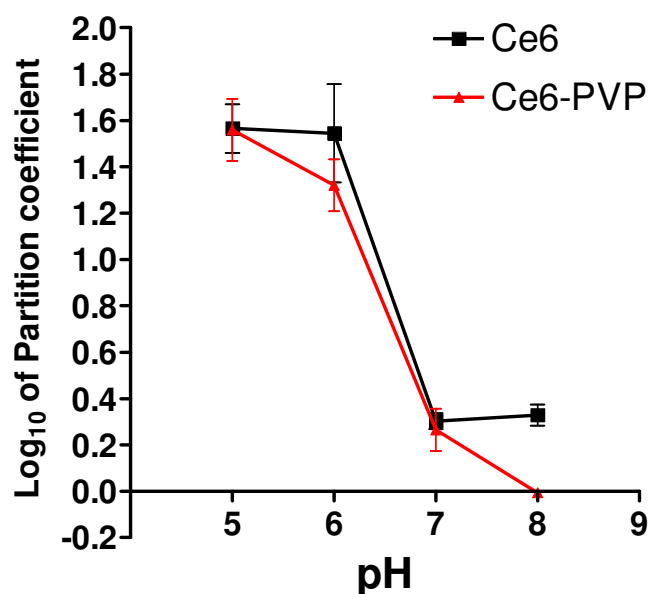


Figure 5.1 Partition coefficients of the Ce6 and Ce6-PVP between 1-octanol and PBS at various pH values.

which an organic compound is distributed in the body. It is termed a "two compartment or two-phase" system: aqueous (water) and organic (lipid) layers.

Figure 5.1 shows the partition coefficients of the Ce6 and Ce6-PVP at various pH values. Comparison of the partition coefficients of Ce6 with Ce6-PVP showed that the expected effect of PVP, i.e. to decrease the hydrophobicity of Ce6 at pH 6 and 8. As the pH of the aqueous buffer was lowered from pH 7, the partition coefficient was found to increase. The results suggested that a larger fraction of Ce6-PVP was incorporated into the 1-octanol phase under more acidic conditions. It was documented that the pH 7.4 of blood may cause protonation of the photosensitizer. In a previous study, it was shown that the Ce6 fraction bound to lipid membranes and low density lipoproteins (LDL) increased whereas the one bound to HSA decreased when the pH changed from 7.4 to 6.5 [172]. Ce6 existed in the amphiphilic form in pH 7.4, thus some Ce6 may be lost because the hydrophilic part of the Ce6 may interact with other serum proteins. Thus, the results here implied that passive diffusion of Ce6 or Ce6-PVP into tumor cells might be enhanced due to the slightly acidic extracellular pH of tumor tissue.

5.4.2 Fluorescence properties of Ce6-PVP in various biological media

Qualitative and quantitative changes in emission spectra resulting from a change of reaction medium can provide information about interaction between the excited states and the environment. Such information can be of great importance in explaining the photoreactivity of a photosensitizer in a certain formulation. The stability of Ce6-PVP deteriorated drastically when dissolved in water (Figure 5.3 A). By day 27, the emission intensity of Ce6-PVP had reduced by 98%, 72% and 100% when dissolved in water at a temperature of 37°C, room temperature (21°C) and 4°C, respectively.

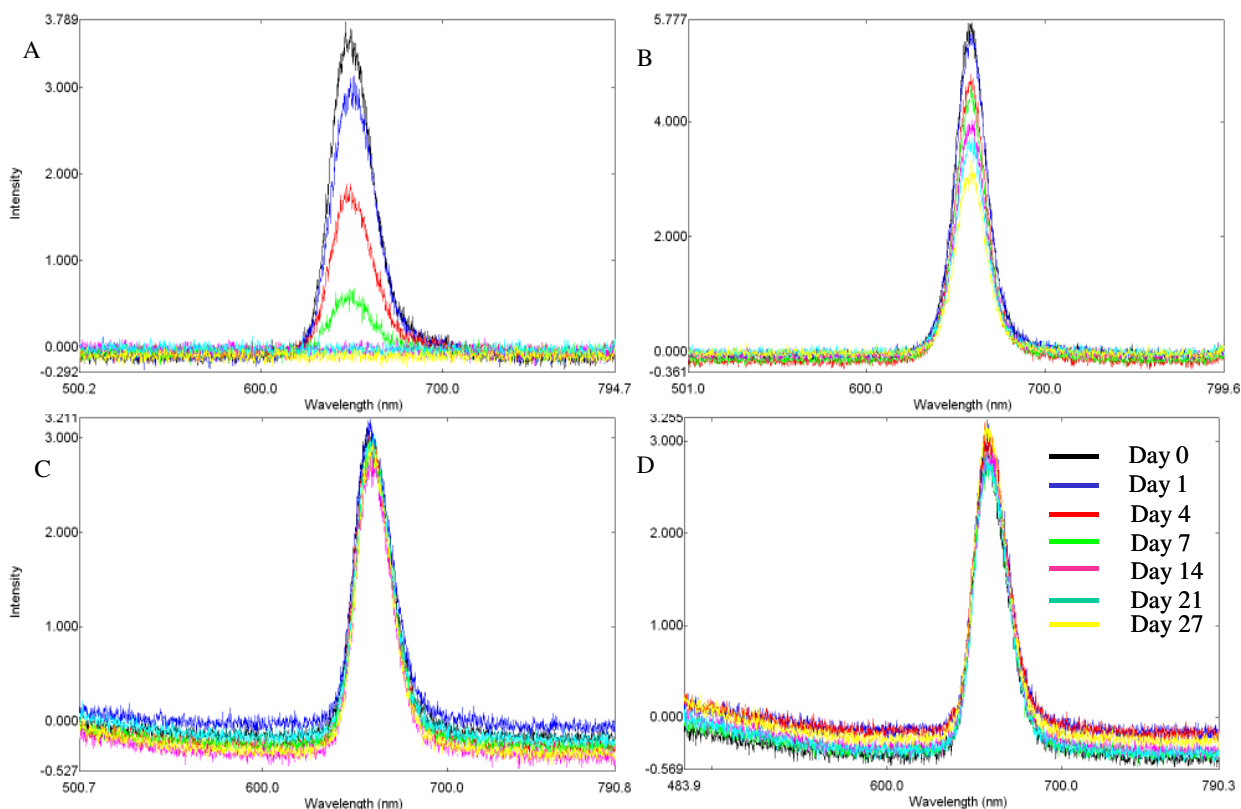


Figure 5.2 Graphs showing representative emission spectra of Ce6-PVP in (A) water, (B) PBS (C) 5% fetal calf serum (D) 10% fetal calf serum at room temperature assessed as a function of time (from 0 to 27 days).

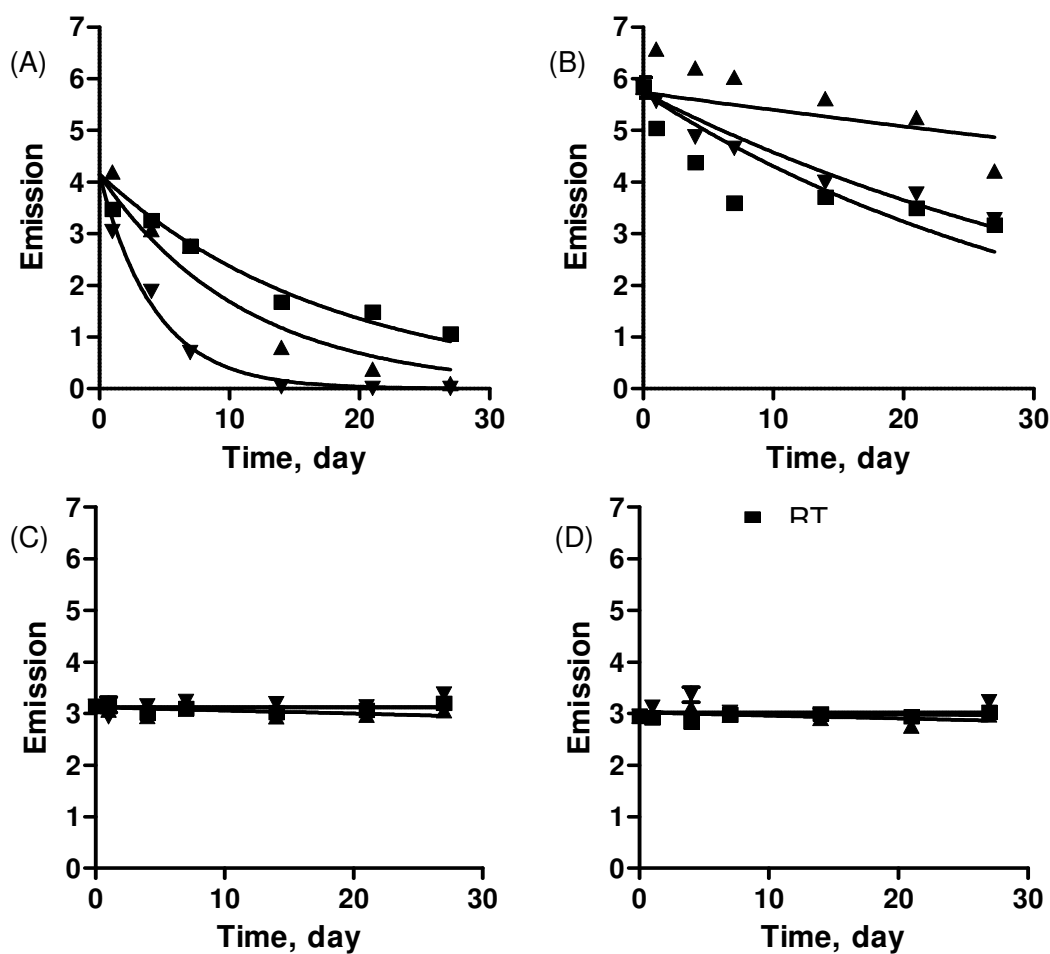


Figure 5.3 The effect of (A) water, (B) phosphate buffered saline (PBS), (C) 5% fetal calf serum (FCS) and (D) 10% fetal calf serum (FCS) on the emission intensity of Ce6-PVP (0.5 mg/mL) at room temperature (RT 21 °C) (■), 37 °C (▲) and 4 °C (▼) for a period of up to 27 days. Each data point represents the average of 3 measurements. Experiments were repeated twice and showed similar trends.

On the other hand, when Ce6-PVP was dissolved in PBS, the emission intensity of Ce6-PVP had reduced by 27% at a temperature of 37 °C by day 27 (Figure 5.3 B). During the same time period, the emission intensity of Ce6-PVP had reduced by 45% and 44% when dissolved in PBS at room temperature (21 °C) and 4 °C, respectively. Ce6-PVP dissolved in 5% and 10% FCS was found to be very stable (Figure 5.3 C and D). In both concentrations of FCS solutions, the fluorescence emission intensities remained stable throughout the 27 day period

at all the three temperatures. When the fluorescence emission data of Ce6-PVP dissolved in water, was fitted to non-linear regression equation using one phase exponential decay, the half-life of the fluorescence intensity was found to be 12 day (95% CI 10.8 to 14.3) at RT, 7.7 days (95% CI 6.8 to 8.9) at 37°C and 3.0 days (95% CI 2.5 to 3.5) at 4°C. The half-life of the Ce6-PVP dissolved in PBS was found to be 24.2 days (95% CI 20.3 to 30.0) at RT, 114 days (95% 71.4 to 285.0) at 37°C, and 30.7 days (95% CI 25.2 to 39.3) at 4°C. Ce6-PVP appeared to remain stable in the presence of 5% and 10% FCS throughout the 27 days survey period. The nature of degradation of Ce6-PVP is not really well understood mechanism of photodegradation and has not often been determined as this is a new compound. Degradation mechanisms at higher temperature could be due to molecules of Ce6-PVP were energized that could either have led to hydrolysis, oxidation-reduction, racemization, decarboxylation, ring cleavage or photolysis reactions. This would have given rise to a by-product that was not fluorescing at 665 nm. It was interesting to observe that at lower temperature of 4°C, in the absence of 5% and 10% FCS, the fluorescence emission of Ce6-PVP was lower than in RT and 37°C. This could be due to the increase of molecular aggregation at low temperature and thus could have led to a reduction in the fluorescence yield. This effect had been observed for other photosensitizers where aggregated species are more easily quenched to than the monomeric ones. Further study is warranted to elucidate the mechanism of degradation of Ce6-PVP.

Serum is a very complex supplement with serum albumin being the most abundant protein. Its concentration is 10 times more the total concentration of all lipoproteins. It serves as a carrier for both hydrophilic and amphiphilic

photosensitizers. Despite being the most abundant protein in the circulatory system, albumin is known to have very limited binding sites for tetrapyrrolic photosensitizers [173, 174]. However in this experiment, the high stability of Ce6-PVP in FCS has led to the hypothesis that Ce6-PVP is a vascular targeting photosensitizer whose efficacy is augmented by high plasma protein binding that may also contribute to minimal skin photosensitization.

5.4.3 Effect of different plasma lipoproteins on spectral properties of Ce6 and Ce6-PVP

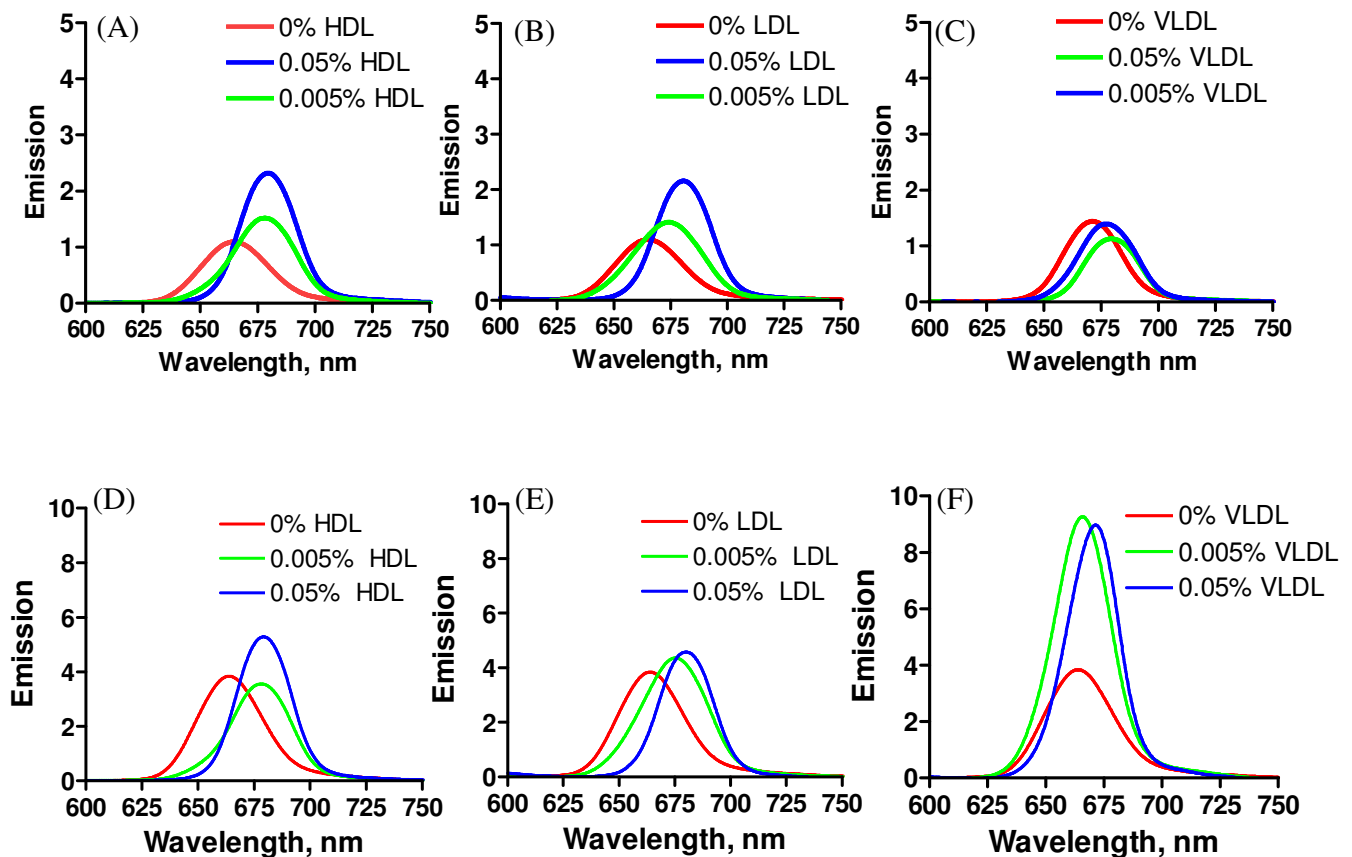


Figure 5.4 The fluorescence emission spectra of Ce6 dissolved in saline with (A) HDL, (B) LDL and (C) VLDL at concentrations of 0% (red), 0.005% (green) and 0.05% (blue). The fluorescence emission spectra of Ce6-PVP dissolved in saline with (D) HDL, (E) LDL and (F) VLDL at concentrations of 0% (red), 0.005% (green) and 0.05% (blue).

Lipoproteins are complex particles that consist of spherical hydrophobic cores of triglycerides or cholesteryl esters surrounded by amphipathic (polar and non-polar) mono-layers of phospholipids, cholesterol, and apolipoproteins. Lipoproteins are usually classified by their size and density as 'very low-density lipoprotein' (VLDL), 'low-density lipoprotein' (LDL) and 'high-density lipoprotein' (HDL). Their main function is to transport endogenous and dietary fats in the blood and lymphatic vessels. Lipoproteins are also the key components that regulate the transport of photosensitizers in the body's circulatory system. The association of photosensitizers to lipoproteins is dependant on the non-polar moieties of the photosensitizers and lipids, aggregation properties, polarity, pH effects and the chemical nature of side-groups in the photosensitizer. In this study it was observed that the peak of the spectral wavelength of both Ce6 and Ce6-PVP increased with the increase in concentration of LDL (Figure 5.4). The emission spectra of Ce6 with different concentrations of LDL exhibited a major shift in wavelength peaks. For example, Ce6 with 0% LDL showed a peak at 664.8 nm. Ce6 with 0.005% LDL showed a peak at 674.4 nm, producing a shift of 9.4 nm in the spectral wavelength. Ce6 with 0.05% LDL showed a peak at 680.8 nm, producing a total shift of 16 nm from Ce6 with 0% LDL.

Ce6-PVP with LDL showed equivalent wavelength shifts in comparison to Ce6 with LDL. Ce6-PVP with 0% LDL exhibited a peak at 664.2 nm wavelength. Ce6-PVP with 0.005% LDL showed a peak at 675.4 nm, producing a shift of 11.2 nm. Ce6-PVP with 0.05% LDL exhibited a peak at 680.2 nm, producing a total shift of 16 nm from Ce6-PVP with 0% LDL. A similar observation was noted in which both Ce6 and Ce6-PVP emissions increased with increasing concentration of

LDL. Ce6-PVP combined with LDL produced double the emission intensity to that of Ce6 with LDL at the same wavelength.

The emission spectra of Ce6 with different concentrations of HDL exhibited major shifts in wavelength peaks. Ce6 with 0% HDL exhibited a peak at 664.8 nm. Ce6 with 0.005% HDL had a peak at 678.2 nm, producing a shift of 13.4 nm. Ce6 with 0.05% HDL had a peak at 679.8 nm, giving a total shift of 15 nm. Overall, Ce6-PVP exhibited a slightly higher wavelength shift in comparison to that of Ce6 in general. Ce6-PVP with 0% HDL showed a peak at 664.2 nm. Ce6-PVP with 0.005% HDL had a peak at 678.4 nm, giving a shift of 14.2 nm. However, Ce6-PVP with 0.005% HDL exhibited a slight decrease of fluorescence emission. Ce6-PVP with 0.05% HDL had a peak at 679.4 nm, giving a total wavelength shift of 15.2 nm. Here, the emission intensity for Ce6-PVP was twice as high as that of Ce6.

The emission spectra of Ce6-PVP with different concentrations of VLDL exhibited a slight shift in wavelength peaks. Ce6-PVP 0% VLDL showed a peak at 664.2 nm. Ce6-PVP with 0.005% VLDL had a peak at 666 nm, giving a shift of 1.8 nm. Ce6-PVP with 0.05% VLDL had a peak at 671.4 nm, giving a total shift of 7.2 nm. The Ce6-PVP with 0%, 0.005% and 0.05% VLDL produced an almost threefold increase in emission intensity.

It was documented that the bathochromic shift of the porphyrin Soret band indicates a π - π interaction between the porphyrin and binding protein [175]. The induction of a bathochromic shift from the formation of a porphyrin–protein complex is well documented [176]. There are two possible factors that can lead

to bathochromic shifts. The first possibility is related to the increased p electron orbitals at the periphery of the porphyrin when the tetrapyrrolic macrocycle associates with adjacent aromatic ligands in serum proteins via ionic binding and van der Waals forces [177]. Ce6 and Ce6-PVP may both form complexes via p-p interaction between the aromatic ligands of the lipoprotein and the tetrapyrrolic macrocycle of Ce6. Another possible factor leading to bathochromic shift is the monomerization from dimers or aggregated states. Porphyrinic compounds that has an amphiphilic structure such as Ce6 tend to self-associate in aqueous solution that depends on factors such as the nature of the polar side chains, the pH of the surrounding medium, and the stereochemistry of the porphyrin molecule [178]. It is possible that the addition of lipoprotein might induce monomerization and thus lead to bathochromic shift. Hence, the lipoprotein may actually function as an endogenous drug carrier for Ce6 via receptor mechanisms in photodynamic therapy of tumors [179].

5.4.4 Association binding measurement

Upon systemic administration, most photosensitizers bind to various serum proteins, including HDL, LDL and albumins for their transport and distribution. Hence, the presence of these serum proteins in the blood may improve PDT to target tumors by enhancing the intracellular accumulation of the photosensitizer.

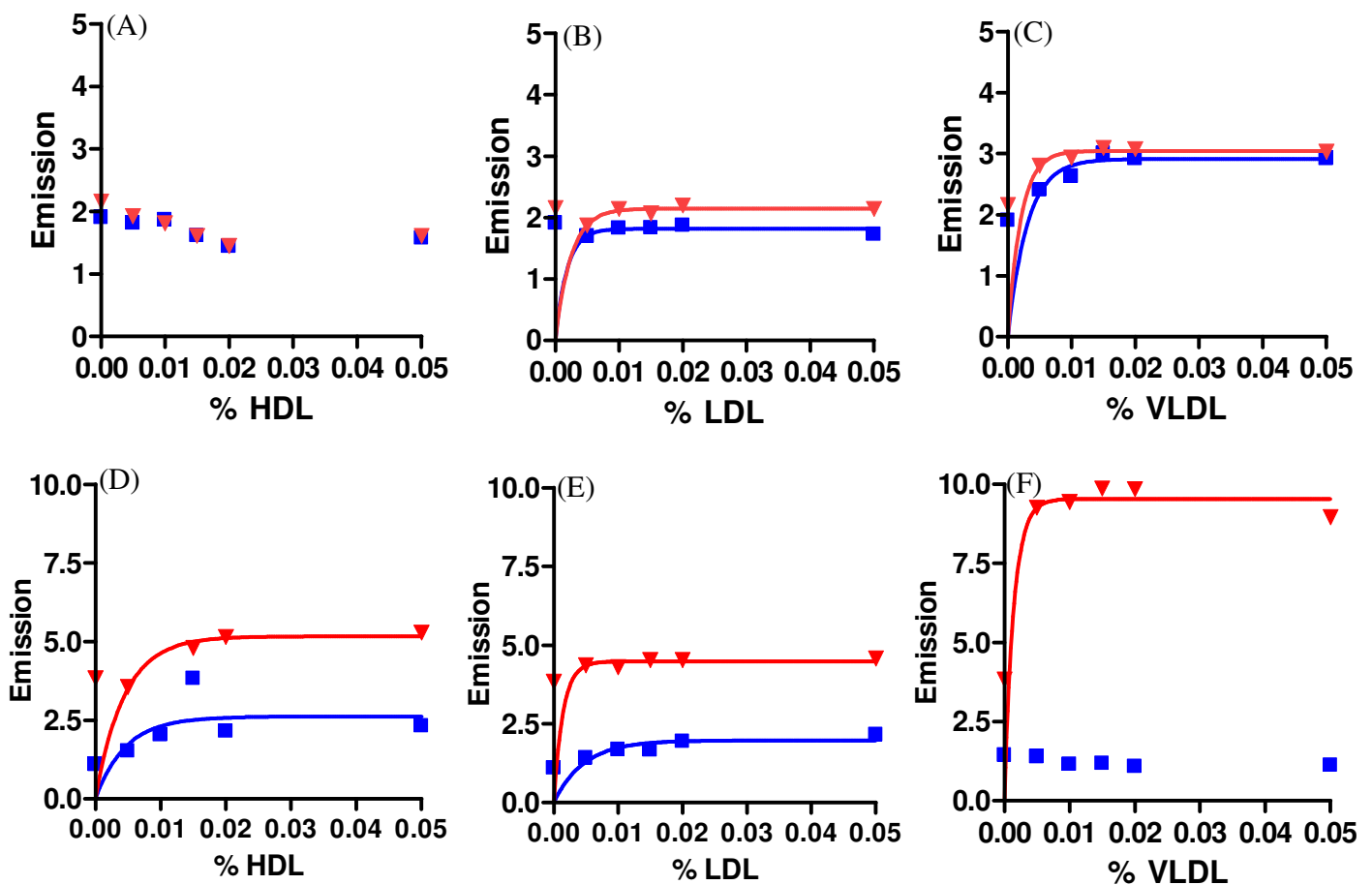


Figure 5.5 The equilibrium titration of Ce6 (■) and Ce6-PVP (▼) in various lipoprotein buffer solutions at pH 7.0. Low concentration (0.01 mg/mL) of the photosensitizers combined with (A) HDL, (B), LDL and (C) VLDL and high concentration (0.06 mg/mL) of the photosensitizers combined with (D) HDL, (E), LDL and (F) VLDL. Curves were fitted and constants derived from one site binding equation and are presented in the main text. Y axis units are relative fluorescent units per mL of the solution. On graphs (A) and (F) trendlines were not presented for some of the data sets because the data did not fit in the binding equation.

via receptor-mediated endocytosis [180]. Using a spectrophotometry method, the binding of lipoprotein with Ce6 and Ce6-PVP has been studied to understand the influence of PVP on the distribution of Ce6 with various lipoproteins. Non-specific binding was measured by incubating Ce6 and Ce6-PVP with various concentration of human lipoproteins. The affinity association of Ce6 and Ce6-PVP is analyzed by plotting the emission peaks against increasing concentrations of HDL, LDL and VLDL (Figure 5.5). Data analysis was performed using one site binding equation:

$$Y = \frac{B_{\max} * X}{(K_d + X)}$$

This equation describes the binding of a photosensitizer to a lipoprotein receptor following the law of mass action. 'Y' in the above equation is the fluorescence intensity of the photosensitizer, which is assumed to be linearly proportional to the concentration of the photosensitizer, 'B_{max}' is the maximal binding (binding capacity). 'X' is the concentration of the lipoprotein, and 'K_d' is the concentration of photosensitizer required to reach half-maximal binding (binding affinity). The absorbance level of Ce6 was measured to confirm that all the photosensitizer concentrations used for this experiment were consistent with one another. A preliminary binding affinity of different lipoproteins to both Ce6 and Ce6-PVP were calculated and presented in Table 5.1. In general, when the concentration of the lipoproteins increased, the fluorescence intensity of both Ce6 and Ce6-PVP increased until a plateau was reached (Figure 5.5). The plateau occurred because the free binding sites of the lipoproteins were no longer free to interact with Ce6. It was observed that the B_{max} of all three lipoproteins binding with Ce6-PVP was slightly higher compared to that of Ce6, at the photosensitizer concentration of 0.01mg/mL. When the binding capacity for various lipoproteins

was measured in the presence of high Ce6 concentration (i.e. 0.06 mg/mL), the B_{max} of the HDL increased by 1.7 fold, the B_{max} of the LDL increased by 1.2 fold and the B_{max} of VLDL decreased by 2.6 fold in comparison to the values obtained for the low Ce6 concentration. For the high concentration of Ce6-PVP, the B_{max} of HDL, LDL and VLDL increased by 3.3, 2.1 and 3.0 fold, respectively compared to the values obtained for the low concentration of Ce6-PVP. If these preliminary results could be further confirmed, it may have important indication that the binding capacity of Ce6 to the lipoproteins is influenced by PVP as well as by the concentration levels of the photosensitizer.

Table 5.1 The influence of different concentrations of three lipoproteins on the protein binding affinity (B_{max}) of Ce6 and Ce6-PVP. The value of B_{max} is expressed in terms of percentage.

Photosensitizer	Ce6			Ce6-PVP		
	HDL	LDL	VLDL	HDL	LDL	VLDL
Low concentration (0.01 mg/mL)	1.66	1.84	3.10	1.68	2.23	3.13
High concentration (0.06 mg/mL)	2.74	2.23	1.19	5.71	4.58	9.53

It is well established that porphyrins have a high affinity for human serum proteins, albumin, HDL, LDL, and VLDL. However, this selective mechanism is yet to be elucidated [173]. It is possible that an over expression of LDL receptors on the tumor cell surface or on neovascular endothelial cells may result in the enhanced uptake of LDL-bound photosensitizer by receptor-mediated endocytosis [181]. Since LDL is the main component of lipoprotein in the blood, it is the most likely lipoprotein to interact with photosensitizer. It has been shown

that lipophilic photosensitizers have a high affinity for LDL and VLDL whereas amphiphilic photosensitizers have a higher affinity for HDL. In contrast, a very hydrophilic photosensitizer has been reported to have a high affinity for albumin [175]. However, in this experiment, it was observed that low concentrations (i.e. 0.01 mg/mL) of Ce6 and Ce6-PVP had high binding affinities for LDL and VLDL, while only a low binding affinity was observed with HDL. This suggests that the LDL and VLDL are the principal carriers for Ce6, which supports the existing literatures demonstrating the role of LDL receptors as carrier molecules to Ce6 and thereby improving the photodynamic therapy [182]. Thus, hydrophilic Ce6-PVP bound to LDL may preferentially accumulate in proliferating endothelial cells through the LDL receptor-mediated endocytosis pathway.

A significant increase in fluorescence yield was observed when low concentration of Ce6-PVP was bound with VLDL. The fluorescence yield increased even higher at high concentration of Ce6-PVP. However, no association of VLDL was observed for high concentration of Ce6 alone (Figure 5.5). This suggests that Ce6 could be aggregated at high concentrations thereby blocking it from binding to the lipoproteins. The tissue distribution of VLDL receptor (VLDLR) has been studied in adult humans and in various animals. Expression of VLDLR was found in several tissues, including heart, skeletal muscle, adipose tissue, kidney, placenta, and brain (Montel et al., 2007). The presence of VLDLR was also demonstrated in gastric adenocarcinoma cells [183] and breast carcinomas [184]. This inevitably suggests a possible uptake of Ce6-PVP in cancer cells via VLDLR.

Published literature has shown that by increasing the lipophilicity of Ce6 its binding affinity to LDL also increased, thus potentially enhancing its tumor-localizing ability [105]. In one study using the murine model, it was demonstrated that a relatively hydrophilic compound N-aspartyl chlorin e6 (NPe6) was bound predominantly to albumin and HDL, while only 1% to 2% of the compound was bound to LDL [185]. The generalization that hydrophobic compounds are transported in vivo via lipoproteins appears to be true for the photosensitizer family of benzoporphyrin derivatives (BPDs). Preclinical studies of benzoporphyrin derivative monoacid ring A (BPD-MA) biodistribution showed that the majority of the BPD-MA is associated with LDL [186]. It is possible that this factor may not be a problem for cellular uptake of Ce6 by the tumor tissues, as the photosensitizers in serum are probably in a dynamic state as they are transferred between various protein fractions within the same serum.

5.4.5 Subcellular localization

In vitro experiments were conducted to compare the cellular uptake of Ce6 and Ce6-PVP. MGH human bladder cancer cells were incubated with 10 μ M Ce6 or Ce6-PVP for 30 min and subsequently observed the fluorescence by confocal laser scan microscopy equipped with a 63x, numerical aperture 1.3 oil immersion objective (Figure 5.6). The fluorescence images were displayed in pseudo colors for organelle markers and photosensitizer, respectively. Cellular uptake of Ce6-PVP was significantly higher compared to Ce6 (0.182 ± 0.065 and 0.043 ± 0.008 intensity (a.u.)/area, respectively, $p = 0.0015$) (Figure 5.7). The colocalization study indicated that intracellular deposition of both Ce6 and Ce6-PVP was localized in cytoplasm and nucleus. The precise step involving the transfer of Ce6 from PVP carriers to cellular membranes is still unknown. Therefore, PVP was labeled with FITC to study the uptake dynamics of PVP into cells. Fluorescence of PVP-FITC was observed in the cytoplasmic area of the cells

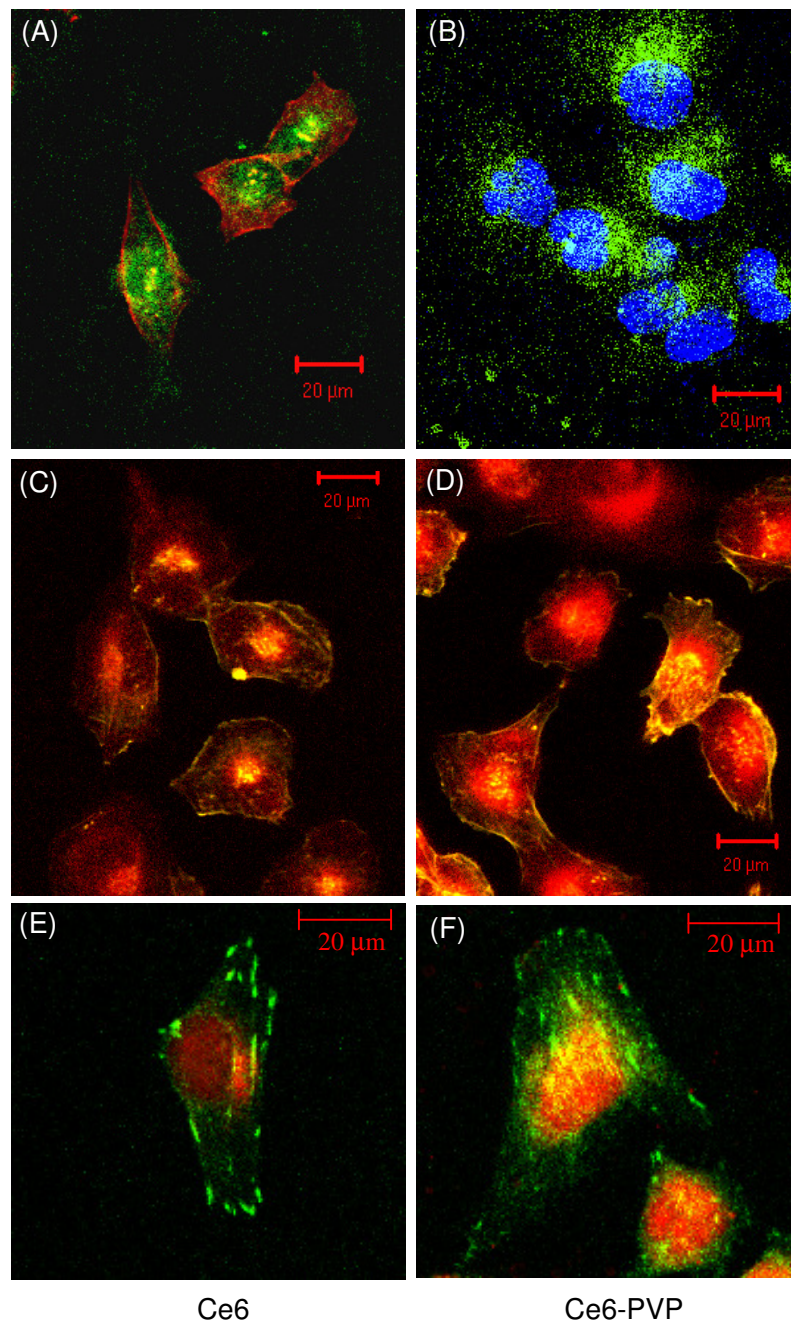


Figure 5.6 MGH cells were incubated with PVP-FITC (green) for 30 min and co-stained (A) rhodamine-phalloidin (red) and, (B) DAPI (blue). Cells were also incubated with (C) Ce6 (red) and (D) Ce6-PVP (red) for 30 min and co-stained with rhodamine-phalloidin (yellow).

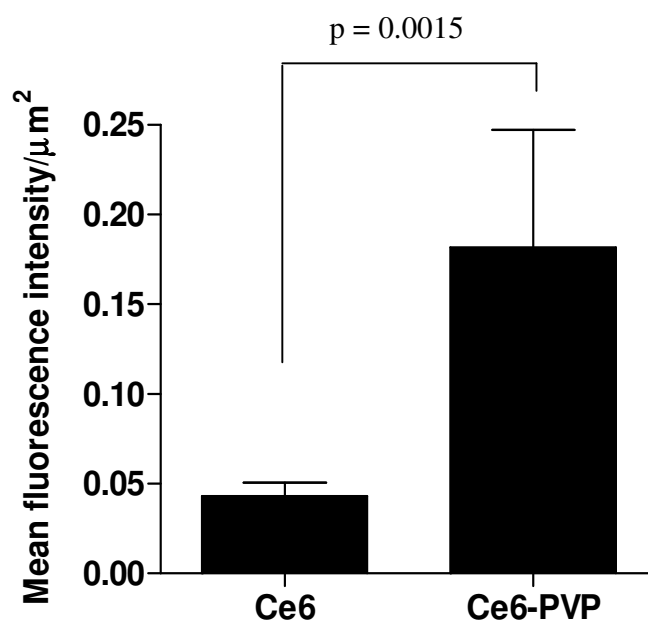


Figure 5.7 Determination of Ce6 and Ce6-PVP fluorescence intensities distribution in MGH cells by image analysis. Each bar represents average intensities of 10 cells divided by the area of the cell. Error bars represent the standard error of the mean.

with no nuclear colocalization, indicating the transport of PVP across cellular membrane. This result is in good agreement with the intracellular transport of ^{125}I -labeled PVP in isolated rat hepatocytes 187 (England et al., 1986). Another study also demonstrated drug co-precipitate with PVP were transported across membrane in high energy amorphous phase (Corrigan et al., 1980). Another hypothesis proposed that lipophilic photosensitizer (i.e. hypericin) is bound to the hydrophilic PVP carrier with weak hydrogen bonds and that the photosensitizer is able to cross the cellular membranes after being released from the PVP carrier molecule [83]. Hence, in the current study, the cellular uptake of Ce6-PVP in MGH cells was observed to be higher compared to that of Ce6. This implies that PVP may increase the rate of membrane transport of Ce6 in the cells. We also hypothesize that because of the presence of numerous lipoprotein receptors on the tumor cells, Ce6-PVP may aggregate s more efficiently within the tumor cells

than in non tumor cells. As a whole, the data presented here indicate that the critical determinant of differences in phototoxicity between Ce6 and Ce6-PVP was that the presence of PVP enhanced the rate of cellular accumulation as well as solubility in aqueous media.

5.7 Conclusion

Ce6-PVP was found to be stable in a protein environment. A decrease in pH from 7 to 6 caused the partition coefficient of both Ce6 and Ce6-PVP to become more lipophilic. However, Ce6-PVP was slightly less lipophilic than Ce6. The cellular internalization of Ce6-PVP was higher than Ce6, and fluorescence microscopy revealed the penetration of PVP into the intracellular compartment of the cells. This supported the hypothesis that PVP improves the permeation and solubility of Ce6 through biological membranes in cells. The fluorescence intensity of Ce6-PVP, when bound with HDL, LDL and VLDL, was significantly higher compared to Ce6 alone. This indicated that PVP affects the level of association of Ce6 with lipoproteins, which would also be expected to influence the intracellular distribution of Ce6. This further supports the hypothesis that the externally added macromolecule PVP improves the uptake of Ce6 in cells. In particular, Ce6-PVP was found to interact more with VLDL, suggesting a role for the VLDL-receptor pathway with regard to Ce6-PVP biodistribution.

CHAPTER 6

Evaluation of clinical response of chlorin e6 – polyvinylpyrrolidone mediated fluorescence diagnosis and photodynamic therapy

6.1 Summary

Photodynamic therapy (PDT) using a chlorin e6 – polyvinylpyrrolidone (Ce6-PVP) was investigated as a treatment for refractory superficial bladder cancer that had failed the usual treatment options. Two patients with biopsy proven carcinoma of the bladder were treated with intravenous or intravesical instillation of Ce6-PVP. Five hours after intravenous administration and 3.5 h after intravesical administration of Ce6-PVP, both patients were exposed to a laser light at 665 nm. Patients were followed for 6 months for safety, efficacy, recurrence, and palliative response. Serum and urine samples at various intervals were collected for spectrometric quantification of photosensitizer level. The levels of inflammatory cytokines before and after post PDT were also determined. After PDT with Ce6-PVP, complete response was observed in both patients, with no evidence of recurrence at any treated site at the 1-month follow-up. However, urinary bladder smooth muscle contraction was observed for patient that received intravenous Ce6-PVP mediated PDT. Patient that received intravesical PDT was disease-free 6 months after PDT. Intravesical treatment of Ce6-PVP mediated PDT seemed to be safe and effective for the clinical treatment of bladder cancer. Expressions of IL-1a, IL-1 β , IL-8, IL-10, IL-12, IFN- γ and TNF- α were not observed in patient given intravesical Ce6-PVP – PDT at 24 h post treatment. However, there was decreased expression of the cytokines from its baseline level in patient treated with intravenous Ce6-PVP – PDT. IL-6

was observed to be upregulated in both patients at post PDT.. Upregulation of IL-6 suggested that a systemic immunologic response might have occurred following PDT. This finding however requires further study to confirm this hypothesis. In a different cohort of patients, fluorescence imaging was performed on 3 patients with histologically confirmed angiosarcoma and 6 bladder cancer patients were instilled with Ce6-PVP. A dose of 2 – 4 mg/kg of Ce6-PVP was administered intravenously for the angiosarcoma patients while a dose of 0.0625 mg/mL were topically instilled to the bladder cancer patients. The resultant macroscopic and microscopic fluorescence intensities were imaged and quantified to explore possible mechanisms of penetration and distribution of the photosensitizer. It was noted that Ce6-PVP enhanced the image contrast between the diseased lesion and surrounding normal tissue in the fluorescence image. In clinical biopsies of bladder tumors, fluorescence intensity increased with the stage of disease indicating its potential use as a diagnostic fluorescent marker. The depth of topical penetration into bladder tumor tissue was found to range from 100 – 200 μm . The findings in this chapter highlighted the distinct advantage of Ce6-PVP as a diagnostic and therapeutic agent for photodynamic therapy of bladder cancer and as a fluorophore for fluorescence imaging of angiosarcoma.

6.2 Introduction

Transitional cell carcinoma (TCC) accounts for 90% of all bladder tumors, of which 70% are low or medium grade and superficial. Carcinoma in situ (CIS) is an aggressive form with a variable and often unpredictable natural history that is frequently associated with disease progression. In the USA, the incidence of bladder cancer is three-times higher in men than in women and it is the fourth most common cancer in men after prostate, lung and colorectal cancer [189]. In Singapore, bladder carcinoma is the tenth most common cancer affecting men and the disease-free survival after radical cystectomies was 64%, 35% and 32% at 1, 3 and 5 years, respectively [190]. Recent development of new diagnostic and therapeutic photodynamic applications in combination with optical delivery and imaging systems holds promise as an alternative, minimally invasive and potentially curative treatment for bladder cancer [191, 192]. Photodynamic therapy (PDT) is primarily suggested for the therapy of papillary transitional cell carcinoma (TCC) and refractory CIS, and prophylaxis of recurrent superficial TCC in those patients who have failed intravesical chemotherapy or immunotherapy [193]. Additional approaches, such as PDT with different photosensitizers and thermotherapy in combination with intravesical chemotherapy, have been evaluated in Phase III clinical studies [194]. This chapter compares 2 cases of study to evaluate the safety and effectiveness of Ce6-PVP administered intravenously versus intravesically in the treatment of refractory bladder carcinoma. This study also examines the fluorescence distribution of Ce6–PVP in angiosarcoma lesions and normal skin in patients.

6.3 Materials and methodology

6.3.1 Angiosarcoma patients

The clinical study was approved by the Clinical Ethics Committee, National Cancer Centre Singapore. Fluorescence imaging was performed on patients with histologically confirmed angiosarcoma that underwent PDT. All were male with a median age of 61 years. Patients were administered intravenously with 2 – 4 mg/kg of 75% Ce6-PVP prepared in 0.9% NaCl by a clinician from the National Cancer Centre of Singapore. The solution was injected intravenously over 10 minutes by infusion. Fluorescence imaging was performed on various parts of the lesion and normal skin from 1 – 3 h post drug administration (before PDT) and 5, 6 and 48 h post drug administration (post PDT). Fluorescence intensity was tabulated as follows:

$$IN_t = IR_t / IB_t$$

with IN_t = normalized fluorescence intensity after time, t ; IR_t = intensity of red channel at time t ; IB_t = intensity of blue channel at time t ; t = time in hours after drug administration. The spectral measurement was also performed on the lesion and normal skin at 1 and 3 h post Ce6-PVP administration using a fiber optics-based fluorescence spectrometer (Spex SkinSkan, JY Inc., Edison, NJ, USA) (described in 2.3.5). All patients had to remain under minimum ambient light conditions for 48 h.

6.3.2 Bladder cancer patients

Patients with rapidly recurring, multi-focal, BCG-refractory superficial bladder transitional cell carcinoma (pTcis, pTa, pT1) would be selected. Patients who had undergone exhausted conventional therapies and were candidates for either

radical cystectomy or radiotherapy were suitable for this study. Study exclusion criteria included porphyria, gravidity, breast feeding, psychotic disease, invasive stage pT2 or greater bladder cancer or metastatic disease, non-urothelial bladder tumors, ASA (American Society of Anaesthesiologist) score 4 or greater, major renal or liver failure, leukopenia with less than 3500 white blood cells per 10⁹ μL and thrombocytopenia with fewer than 100,000 platelets per 10⁹ μL. Patients with prior intravesical chemotherapy or immunotherapy were not be excluded.

6.3.2.1 Clinical history for patient received intravenous administration of Ce6-PVP

The first patient is a 78-year-old Chinese lady who had a medical history of rectal prolapse treated with a rectopexy and uterine fibroids treated with a total hysterectomy with bilateral salpingo-oophrectomy. She was first seen in 1997 for lower urinary tract symptoms especially urge incontinence. Urodynamic studies showed detrusor instability. She was treated with oral medications, showed good response and discharged subsequently. Her lower urinary tract symptoms recurred in August 2001. A flexible cystoscopy was performed to further investigate her condition, and it showed cystitis on the posterior wall and bilateral walls of the bladder. Urine cytology was taken and it showed high-grade urothelial carcinoma. In view of such findings, she underwent a rigid cystoscopy and bilateral retrograde pyelogram. Biopsy of the 'cystitis' area showed carcinoma-in-situ, and she received 6 doses of intravesical BCG. She was put on regular follow-up to monitor her disease progress. Repeated cystoscopy did not show any recurrence till December 2003. In December 2003, rigid cystoscopy and biopsy showed carcinoma-in-situ. As patient was not keen for surgical intervention, she received another 6 doses of intravesical BCG. CT scan of the abdomen and pelvis, did not detect any bladder wall thickening, extravesical

extension of tumor, enlarged regional lymph nodes or intra-abdominal metastases. She was well till October 2004, when a repeat cystoscopy showed suspicious lesions on the posterior and left lateral wall of the bladder. Biopsy of these areas showed recurrence of carcinoma-in-situ. As this is the third recurrence of carcinoma-in-situ after 2 cycles of intravesical BCG previously, the option of intravenous administration of Ce6-PVP mediated photodynamic therapy (PDT) was offered to the patient. Ce6-PVP was dissolved with 0.9% NaCl. Patient weight was 45 kg at the time of treatment. 100 mL of Ce6-PVP solution that constituted a dose of 2.5 mg/kg body weight was syringed out into the infusion bag and protected from light. A sterile drip infusion i.v. set was also provided. 100 mL of Ce6-PVP solution (0.9% NaCl) that constituted a dose of 2.5 mg/kg body weight was syringed out into a sterile drip infusion i.v. set and protected from light was also provided. The solution was injected intravenously over 10 minutes of infusion. Drug administration was performed in a dim environment and patient's eye and skin were protected from intense light using eye goggle and blanket.

6.3.2.2 Clinical history for patient received intravesical administration of Ce6-PVP

The second patient is a 78 Chinese year old woman who has multiple co-morbidities including hypertension, diabetes mellitus on diet control, previous cerebrovascular accident with good functional recovery, bilateral cataracts, glaucoma of the right eye, Meniere's disease, previous total thyroidectomy for multinodular goiter and Hashimoto's thyroiditis and total hysterectomy and bilateral salpingo-oophorectomy (THBSO). She first presented with asymptomatic microscopic haematuria to the Department of Urology, Singapore General Hospital. This was not associated with any weight loss or loss of

appetite. She had earlier been investigated at Changi General Hospital, Singapore for the same problem with an intravenous urography which was normal and a urine cytology which showed atypical urothelial cells suspicious for malignancy. A bedside ultrasound done showed possible bladder lesions which was confirmed on flexible cystoscopy. A flexible cystoscopy on 23rd Feb 2007 showed a 1cm solid lesion at the right trigone. She underwent a TURBT and excision of umbilical nodule on 9th March 2007. Intraoperative findings revealed a solid 1.5 cm tumor at the right side of the trigone not involving both the ureteric orifices. Bladder capacity at that time was measured at 400 mL. Histology of the tumor revealed a lymphoepithelioma-like high grade undifferentiated carcinoma which was noted to be different from the CIS and high grade papillary urothelial carcinoma previously. This was noted to be invading the lamina propria, while muscularis propria involvement cannot be absolutely excluded. Her case was discussed at the Uropathological Conference and she was recommended for intravesical administration of Ce6-PVP mediated photodynamic therapy (PDT). After discussion with the patient regarding her options and alternative treatment such as radical cystectomy, she was agreeable for PDT.

6.3.4 Light source and fiber positioning

A medical-grade Biolitec Ceralas PDT laser was used to deliver light at 665 nm. The laser light was delivered via a spherical light diffuser fiber (model: SD) obtained from Medlight S.A, Switzerland. The fiber was sterilized using gas plasma sterilization method. Trans-abdominal ultrasonography was used to position the fiber in the central region of the bladder through a constant flow cystoscope using a 5 Fr ureteral catheter marked at cm intervals with the help of ultrasound imaging. The ureteral catheter was inserted through the

catheterisation slide and the tip was placed against the bladder wall farthest from the entry point. The bulb-shaped fibre tip was then placed halfway along the catheter. Anteroposterior and lateral positioning of the fibre tip was controlled by endoscopy. The cystoscope was fixed to a mounting device. Continuous irrigation with isotonic saline solution was maintained during the entire irradiation.

6.3.5 Light irradiation

Light dose was simulated and calculated ex-vivo before the actual irradiation. Once the simulation once confirmed, a schematic diagram was prepared (Figure 6.1) for the clinician. All light irradiation, drug administration and other clinical procedures were performed by a clinician from the Department of Urology at the Singapore General Hospital.

6.3.5.1 Intravenous drug administration

Light irradiation of the bladder was performed 5 h post drug administration. The bladder was distended with saline until the bladder reached a diameter of 7 cm to smooth mucosal folds. This corresponded with a bladder volume of approximately 180 cm³, which was maintained constant throughout the procedure. Irradiation was delivered in 3 fractions with each irradiation lasting for 20 minutes followed by dark intervals of 5 minutes. A total light dose of 24 J/cm² was delivered to the bladder wall at a fluence rate of 6.7 mW/cm² (Table 6.1).

6.3.5.2 Intravesical drug administration

A total volume of 40 mL of Ce6-PVP with a concentration of 0.0625 mg/mL was prepared in PBS. The solution was filtered with 0.22 µm acetate filter and administered intravesically to the patients. Light irradiation of the bladder was

performed 3.5 h after the completion of intravesical instillation. The bladder was distended with saline until the bladder reached a diameter of 6.6 cm to smooth mucosal folds. This corresponded with a bladder volume of approximately 150 cm³, which was maintained constant throughout the procedure. Irradiation was delivered in 3 fractions with each irradiation lasting for 5 minutes followed by dark intervals of 5 minutes. A total light dose of 10 J/cm² was delivered to the bladder wall at a fluence rate of 11 mW/cm² (Table 6.1). PDT was done using laser 665 nm for 15 minutes and a total of 10 Joules was delivered. Bladder volume was kept constant at 150 mL by transabdominal sonography.

Table 6.1 A summary of PDT treatment parameters were administered to the patients.

Delivery mode	DLI	Bladder volume (cm³)	Equivalent radius (cm)	Light fluence rate (mW/cm²)	Light dose (J/cm²)	Light fractionation
Intravenous	5 h	180	3.5	6.7	24	20 min light x 3 sessions, (5 min dark intervals in between)
Intravesical	3.5 h	150	3.3	11.0	10	5 min light x 3 sessions, (5 min dark intervals in between)

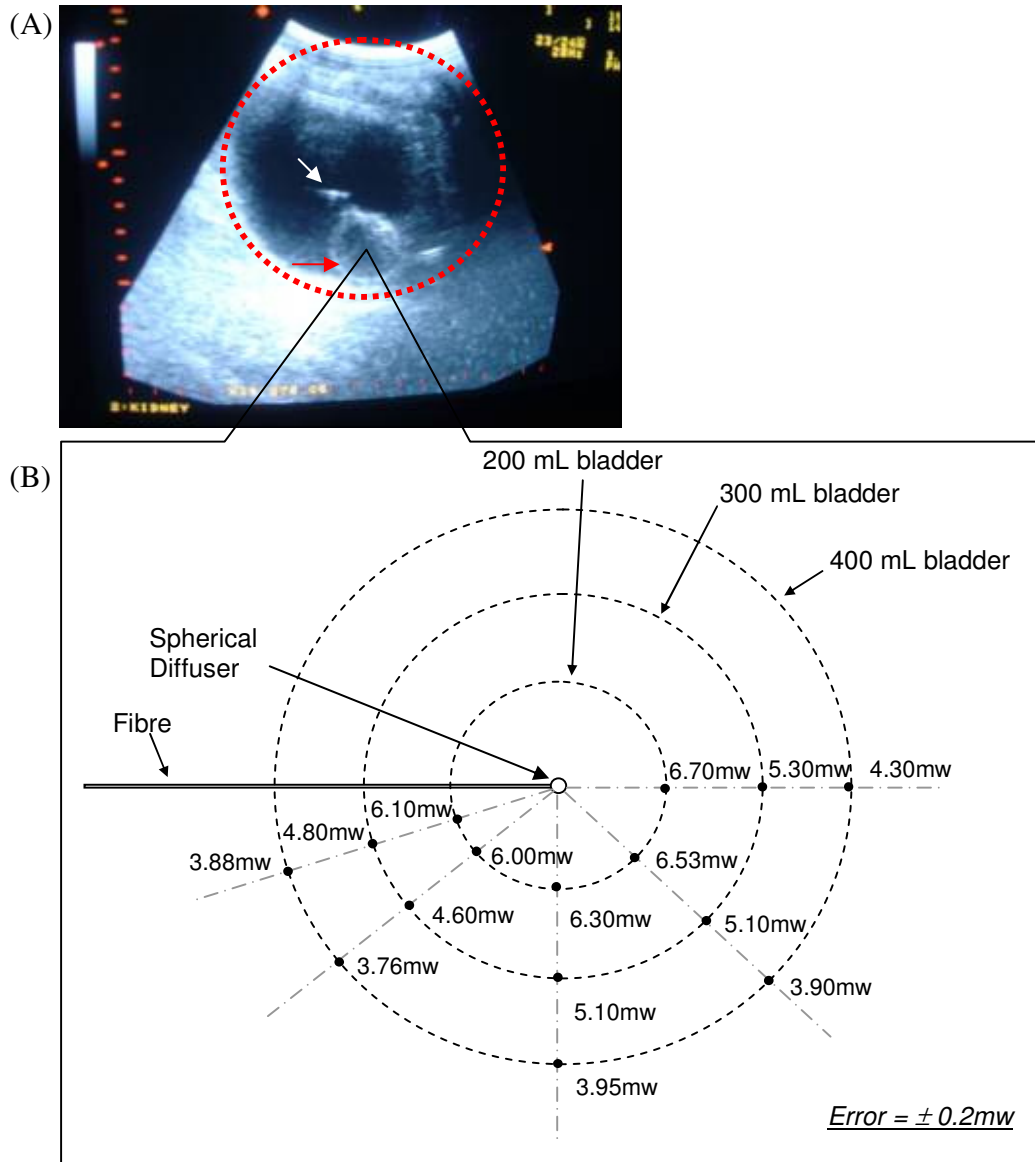


Figure 6.1 (A) Ultrasound image of the position of the fiber tip (white arrow) and balloon (red arrow) in the bladder (red circle). (B) Schematic diagram of the intensity output of the fiber for various bladder volumes was prepared for the clinician.

6.3.6 Laser confocal fluorescence microscopy studies

A total of 6 patients with recurrent bladder cancers were selected for this study. The patients were administered intravesically with a volume of 40 mL of 0.0625 mg/mL of Ce6-PVP prepared in PBS. Approximately 1 – 2 h of incubation, the bladder was inspected carefully by a urologist. Multiple biopsies were taken so that they could be assessed for routine pathology examination. Each tissue was sectioned and examined under the laser confocal scanning fluorescence microscope and documented before obtaining the pathology report for correlation. A 5 – 10 µm thick sections were stained for haemotoxylin and eosin while the 15 – 20 µm thick sections were prepared for confocal fluorescence imaging. A 488 nm Argon laser was used to excite Ce6-PVP. Fluorescence emissions in the wavelength range of 665-670 nm was split by a dichroic filter and detected through a band pass filter. Voltage gain, PMT voltage and sensitivity (contrast, brightness, and filters) were fixed for all fields and slides imaged.

6.3.7 Analysis of serum and urine uptake

For analysis of serum and urine, the patient was administered intravenously with 2.5 mg/kg of Ce6-PVP. The solution was injected intravenously over 10 minutes of infusion. Photosensitizer levels in serum and urine were assayed using fluorescence spectrofluorimetry. Urine samples were collected at 1, 2, 24 and 48 h post drug administration. Samples were then centrifuged and the supernatant were assayed immediately. Blood samples were collected at 1, 3, 4, 6.5, 24 and 48 h post drug administration. Serum was isolated from blood by centrifugation, and samples were kept at -70 °C until assayed. Serum concentrations of Ce6-PVP were determined by admixture with Solvable™ (Packard Bioscience) and

heating at 50 °C for 12 h followed by analysis of fluorescence emission spectra. Fluorescence emission was measured from 665 to 670 nm upon excitation at 400 nm using a spectrofluorophotometer RF-5301 PC (Shidmadzu). All samples were protected from exposure to surrounding light.

6.3.8 ELISA detection of human inflammatory cytokines

Human inflammatory cytokines analysis (IL-1a, IL-1b, IL-6, IL-8, IL-10, IL-12, IFN- γ and TNF- α) was performed using the commercial enzyme-linked immunosorbent assay (ELISA) kit purchased from SuperArray, USA (Cat. No. MEH-002A). Serum samples were thawed to room temperature, and assayed in duplicates with a standardised laboratory technique according to the manufacturer's protocol. Absorbance was read in an ELISA plate at 450 nm with corrections at 570 nm.

6.4 Results and discussions

6.4.1 Fluorescence imaging of angiosarcoma lesions in patients

Patients with angiosarcoma were given 2 – 4 mg/kg of Ce6-PVP through intravenous administration. The accumulation of Ce6-PVP in the angiosarcoma lesion was visualized through its typical red fluorescence after blue light excitation (Figure 6.2 B). Clear demarcation of the lesion was observed in the fluorescence image indicating excellent selectivity of the Ce6-PVP. Fluorescence in the lesion was more intense compared to the fluorescence in the normal skin. No observable variations were found for the intensity of the fluorescence between lesions.

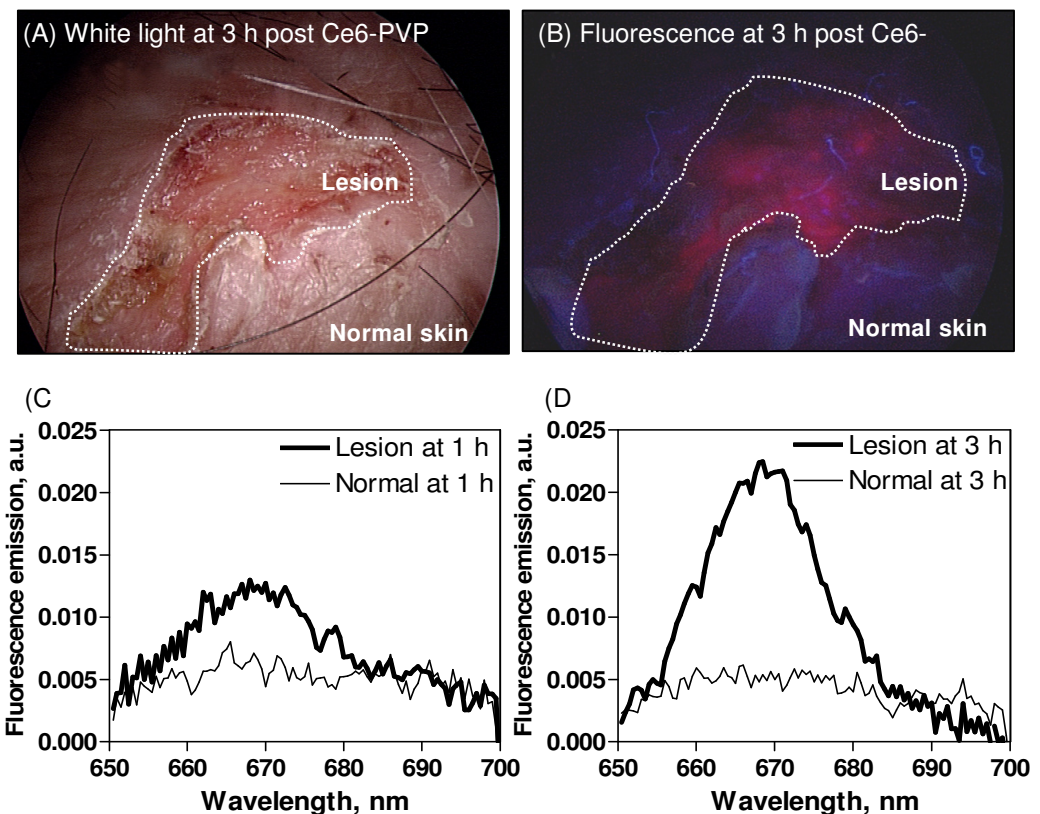


Figure 6.2 White light image (A) and its corresponding fluorescence image (B) of angiosarcoma lesion and the surrounding normal skin at 3 h post intravenous administration of Ce6-PVP. Spectra kinetic of Ce6-PVP intensity at 1 hr (C) and 3 hr (D) in normal skin and angiosarcoma lesions from patient. The fluorescence spectra from the cancerous lesion were found to be higher than the surrounding normal skin.

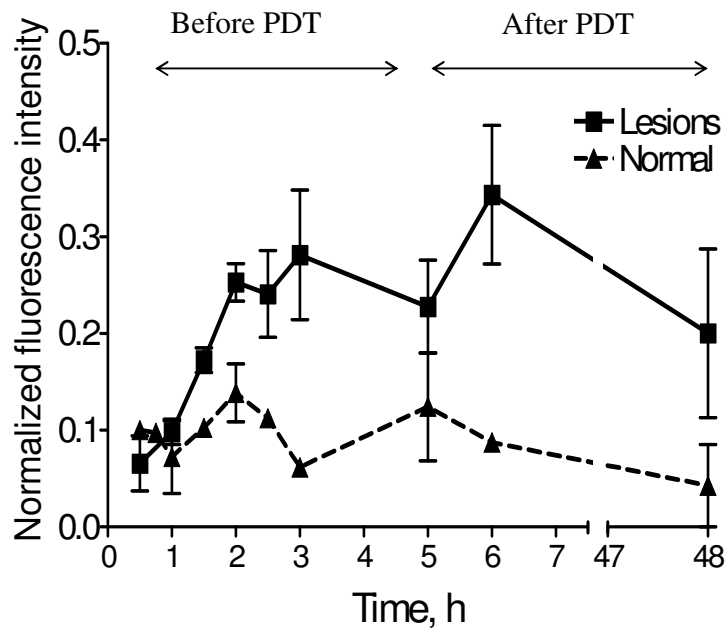


Figure 6.3 Scatter plot of red-to-blue intensities in normal skin and angiosarcoma lesions plotted against time from 3 patients after intravenous administration of Ce6–PVP. Red fluorescence from the cancerous lesion was found to be higher than the surrounding normal skin.

Spectra measurement from the cancerous lesion areas showed a distinct Ce6-PVP induced fluorescence spectrum that discriminate between the cancerous lesion and normal skin, with the lesion showing higher fluorescence emission intensity compared to normal tissue (Figure 6.2 C, D). These results confirmed that fluorescence imaging clearly captured the fluorescence in angiosarcoma and good correlation was found between fluorescence imaging and spectral measurement in the patient. This is in agreement with other reports, that fluorescence ratio imaging in combination with relative spectral measurement of the photosensitizer might be a viable method for the optical diagnosis of cancer [200]. Furthermore, in vivo and real-time determination of the time course of photosensitizer's fluorescence could potentially be a crucial pre-irradiation screening tool to determine the exact location and extent of the tumor before

photodynamic therapy. The appreciable red fluorescence emission of Ce6-PVP captured using a CCD camera system together with digital imaging, could be utilized either for a directed biopsy or for preoperative planning to demarcate tumor margins. The routine employment of such systems is being assessed in studies with other photosensitizers in various oncologic and non-oncologic applications of the skin [195].

When the measurement of red-to-blue intensities were plotted against time, the intensities in the lesions increased rapidly over the first 3 h (Figure 6.3).

Fluorescence intensities were always lower in the normal skin compared to the lesions. The loss of fluorescence at 5 h could be attributed to the photobleaching effect of Ce6-PVP immediately after PDT. Interestingly, the red fluorescence recovered at 6 h post drug administration, suggesting that the circulating Ce6-PVP in the serum seemed to be redistributed into the lesions after PDT. At 48 h post injection, the fluorescence was lower but still sustained in the lesions..

However, PDT efficacy at 48 h drug-light interval might not be good due to an overall decrease in the photosensitizer level in the lesions, which may cause a decrease in tumor response due to the photosensitizer threshold that is needed for a good response. It was reported that PDT performed at 3 h drug-light interval was effective in achieving local control of the angiosarcoma lesions for up to 14 months [196]. This is in agreement with other clinical PDT protocols using another hydrophilic Ce6 derivative (Npe6), where light irradiation was performed around 3 – 8 h post drug administration with minimal systemic photosensitization [94, 95]. This study also further confirms that Ce6-PVP has a faster elimination rate in the normal human skin compared to other porphyrin-based

photosensitizers [197], indicating that Ce6-PVP may not cause prolonged substantial skin photosensitization in human.

6.4.2 Ce6-PVP mediated PDT response for refractory bladder carcinoma patients

Soon after intravenous mediated PDT was completed, patient had nausea and vomited. Patient also experienced pain after the treatment and needed to be administered with morphine. Haematuria was observed in the urine 24 h post treatment (Figure 6.4). Patient was evaluated about 2 months after PDT. A rigid cystoscopy and bilateral retrograde pyelogram were performed and it showed a small fibrotic bladder (130cc) with mucosal sloughing and bilateral hydroureter secondary to reflux. Bladder biopsy showed necrotic tissue with no viable tumor and urine cytology did not show any malignant cell. Similarly, patients given intravenous administration of Photofrin, an FDA approved photosensitizer for the treatment of bladder cancer was also reported experienced bladder contracture [201].

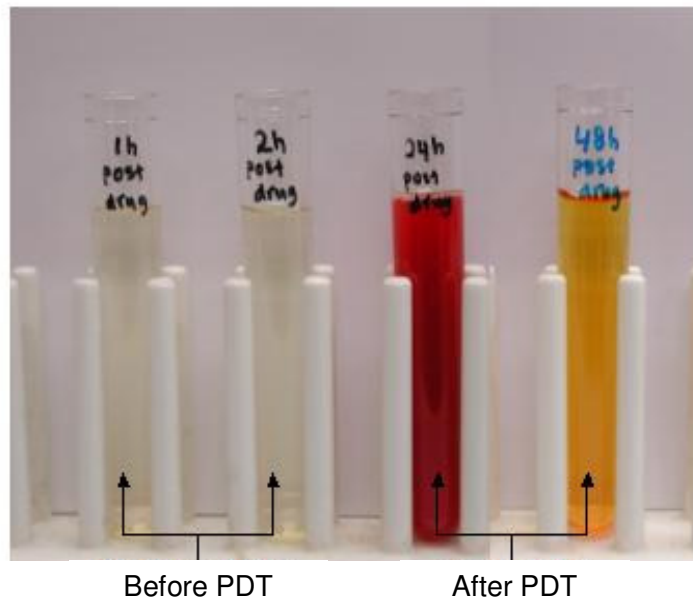


Figure 6.4 Urine sample collected before and after PDT from patient given intravenous administration of Ce6-PVP. Blood was observed after 24 h post treatment. There was no blood detected at 48 h post treatment

Intravesical instillation of 50 mL of Ce6-PVP was performed for 1 h. Rigid cystoscopy and biopsy was performed under fluorescence imaging. No gross tumor was noted and the bladder capacity was noted to be 600 mL. The patient tolerated the procedure well and was discharged on the 2nd post operative day. A rigid cystoscopy and biopsy was done on 4 month post PDT. Bladder capacity was noted to be 630 mL. Histology of the biopsies from the right lateral wall, left lateral wall, dome and posterior wall did not reveal any malignancy. Urine cytology was reported as atypical cells, which were probably reactive. A subsequent flexible cystoscopy performed on 7 month post PDT did not reveal any recurrences. Bladder capacity was noted to be more than 500 mL and a uroflow performed at that time showed a Qmax of 17.1 with a voided volume of

494 mL. Recent preclinical study using orthotopic rat model has demonstrated that intravesical was better than intravenous aminolaevulinic acid (ALA)-induced protoporphyrin IX as a photosensitizer in eradicating bladder carcinoma with PDT [202]. Likewise, in clinical studies, intravesical PDT of the bladder was shown to be more effective with lesser side effects [203].

6.4.3 Analysis of serum and urine uptake of Ce6-PVP

The kinetics of Ce6-PVP in serum for both patients was analyzed using cuvette based spectrophotometric method. Figure 6.5 shows the detectable concentration of Ce6-PVP in serum for patient given intravenous administration of the photosensitizer. Intravesical administration did not show any detectable Ce6-PVP in patient's serum. Figure 6.6 shows the injected dose of 2.5 mg/kg as a function of time after injection in serum and urine. The pharmacokinetic parameters obtained using non-linear regression analyses of one phase exponential decay are summarized in Table 6.2. Plasma concentration declined rapidly in the first 24 h. The photosensitizer concentration continued to decrease to a level near baseline at 48 h post injection. The $t_{1/2}$ of Ce6-PVP in serum was calculated to be 9.9 h. This is in accordance with Kessel's $t_{1/2}$ measurement of NPe6 in serum of cancer patients [204]. In clinical practice, it would take just over 4.7 times the half-life for a drug's serum concentration to reach steady state after regular dosing. Effectively, this meant that administration of Ce6-PVP could be repeated as soon as 50 h after the initial dosing for repeated PDT treatment. Rapid elimination of Ce6 was also observed from the urine of patients after intravenous administration of Ce6-PVP and $t_{1/2}$ was calculated to be 24.6 h, which is 2.5 times longer compared to the $t_{1/2}$ in serum. The longer $t_{1/2}$ was

expected in the urine because of the water-soluble nature of the Ce6-PVP, suggesting that one of the elimination routes was through the kidneys.

Table 6.2 Comparison of span, rate constant decay (K) and half-life ($t_{1/2}$) of Ce6-PVP in serum and urine sample from clinical patients.

Best-fit values	Serum	Urine
Span	12.02 ± 0.19	1.36 ± 0.13
95% CI for Span	11.63 to 12.42	1.09 to 1.63
K	0.07 ± 0.003	0.03 ± 0.01
95% CI for K	0.06 to 0.08	0.01 to 0.05
$t_{1/2}$ (hours)	9.9 h	24.6 h
95% CI for $t_{1/2}$	9.04 to 11.0 h	14.9 to 69.6 h
Goodness of fit, R ²	0.9924	0.5824

The Plateau was fixed to 0.0, and non-linear regression was performed to fit only the span and K. Values are denoted ± standard error of the mean. R² is the goodness of fit; CI is the confidence interval.

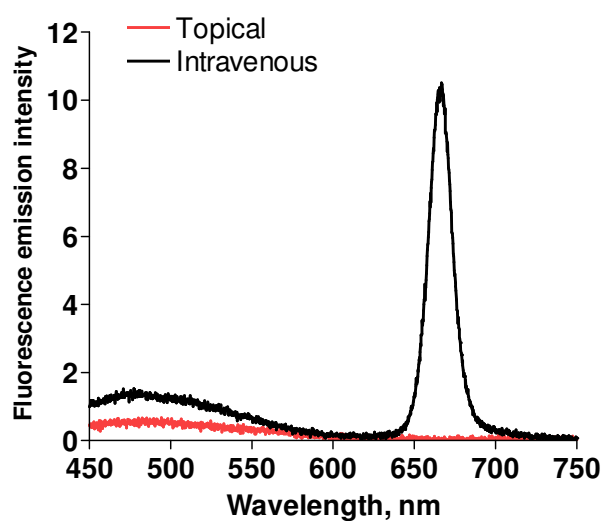


Figure 6.5 Emission spectra of Ce6-PVP in serum at 1 h post drug administration, recorded with a spectrophotometer after excitation at 400 nm. Ce6-PVP was not detected in the serum of patient that received intravesical administration (red line), indicating that no systemic absorption of the photosensitizer was observed.

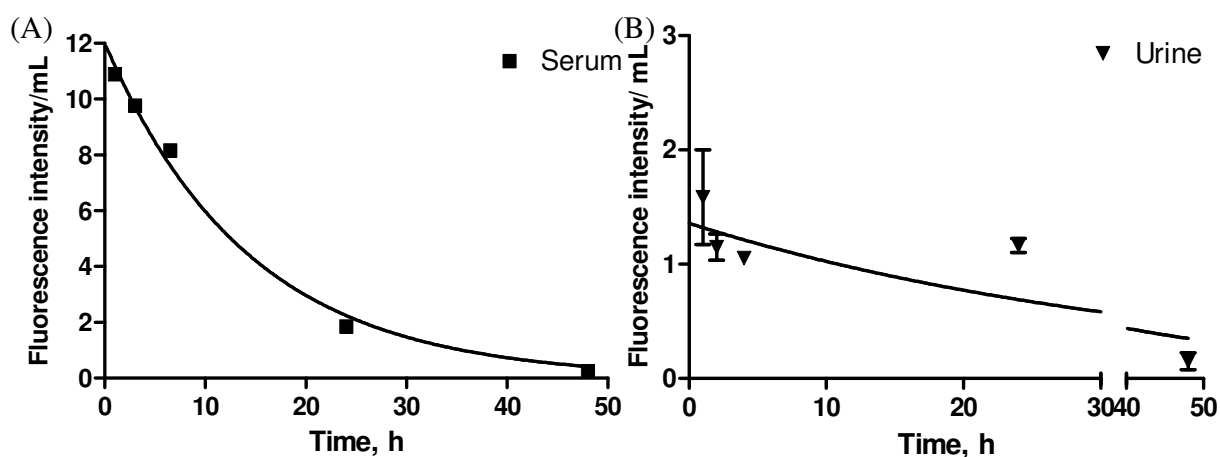


Figure 6.6 Uptake kinetic of Ce6-PVP in serum (A) and urine (B) from patient after intravenous administration as determined using spectrofluorimetry. Fluorescence emission was measured from 665 nm – 670 nm ($\lambda_{ex} = 400$ nm). For urine, triplicates sample/time point was analysed for each data point while for serum, 4 replicates/time point for each data point were analysed.

6.4.4 Fluorescence imaging and laser confocal microscopy study of refractory bladder carcinoma patients

Ce6-PVP mediated fluorescence cystoscopy was well tolerated by the patients and no adverse effects were noted. The preliminary result presented here showed that Ce6-PVP mediated fluorescence cystoscopy enabled the visualization of tumors and suspicious areas in the bladder urothelium that could not be clearly seen by white light cystoscopy (Figure 6.7). To date several photosensitizers have been used in the diagnosis of bladder cancer. Various studies have reported on 5-aminolevulinic acid (ALA) and its derivative hexyl-ALA induced porphyrin mediated fluorescence detection of bladder cancer with a sensitivity ranging from 89% to 96% [37, 205, 206]. However, current formulations of ALA are unstable and require preparation immediately before use [85]. Besides, the systemic use of porphyrins is normally associated with prolonged skin photosensitivity and bladder damage [207]. Recently, hypericin with PVP was proposed as light stable photosensitizer with tumor selective properties and sensitivity similar to those of ALA and derivatives [208]. Hence, the results here demonstrated that the formulation of Ce6-PVP might similarly be effective in the fluorescence diagnosis of other malignancies in hollow organs.

Confocal microscopy examination revealed that there was an increased in Ce6-PVP induced fluorescence with the stages of the disease (Figure 6.8). The degree of fluorescence intensity as revealed by confocal laser microscopy was in the following order: acute and chronic inflammation < low grade papillary urothelial carcinoma < high grade papillary transitional cell carcinoma. For this reason the degree of Ce6-PVP induced fluorescence could be used as an indicator for determining the invasiveness of bladder malignancies. This

increased in the selective uptake of Ce6-PVP in higher grade tumor cells compared to lower grade tumor cells could be ascribed to the fast metabolic activity of higher grade cells compared to the lower grade tumor cells. Furthermore, it was suggested that modifications in the adhesion properties of neoplastic cells, by alteration of expression of transmembrane glycoproteins that mediate the cell-to-cell and the cell-to-extracellular matrix adhesion, such as catherins and integrins, may play a pivotal role in the development and progression of bladder cancer that are responsible for the selective penetration and uptake of the photosensitizer hypericin in these lesions [35, 209].

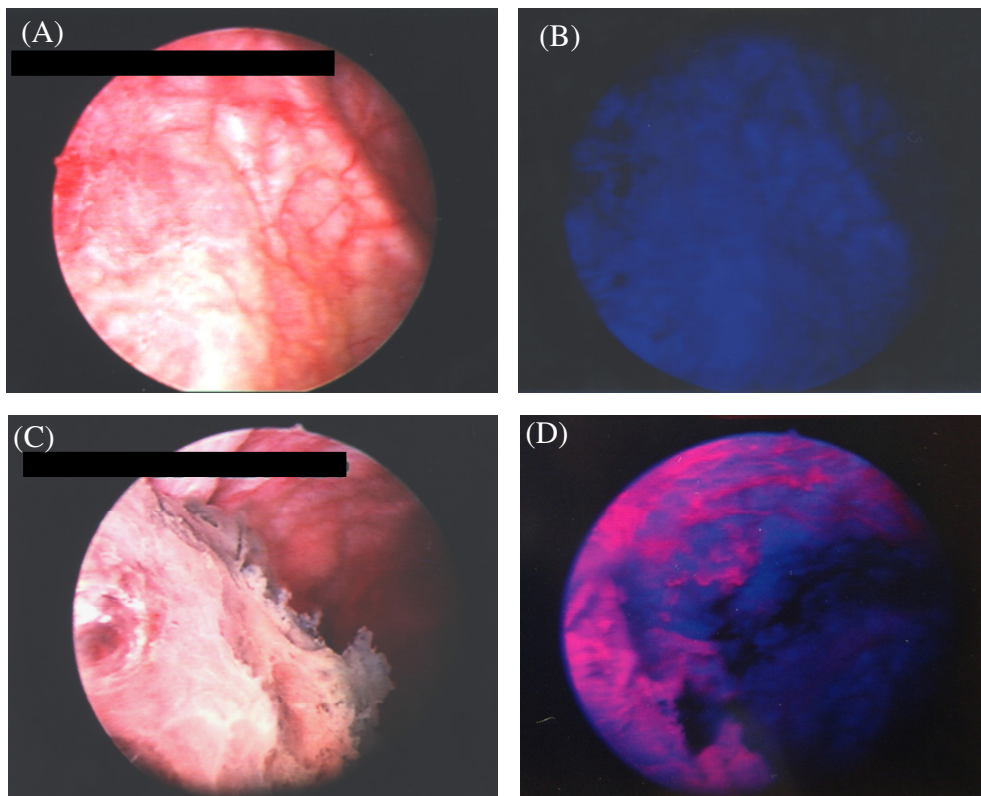


Figure 6.7 Representative images of optical detection of human bladder carcinoma using Ce6-PVP as a fluorescent marker. (A) Normal bladder under white light illumination and (B) its corresponding image taken using blue light excitation. (C) Carcinoma of the bladder under while light illumination and (D) its corresponding image using HAL fluorescence cystoscopy (B). Lesion was clearly visualized under blue light.

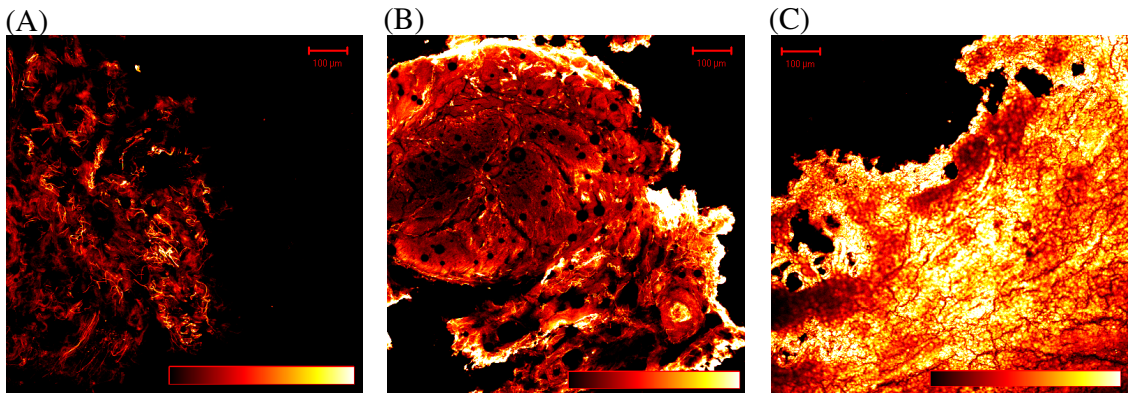


Figure 6.8 Laser confocal microscopy and histopathology of cross section of biopsy sample of bladder wall. Laser confocal microscopy of cryo-section of bladder biopsy; images show Ce6 fluorescence for acute and chronic inflammation (A), low grade papillary urothelial carcinoma (B) and high grade papillary transitional cell carcinoma (C). Bar = 100 µm.

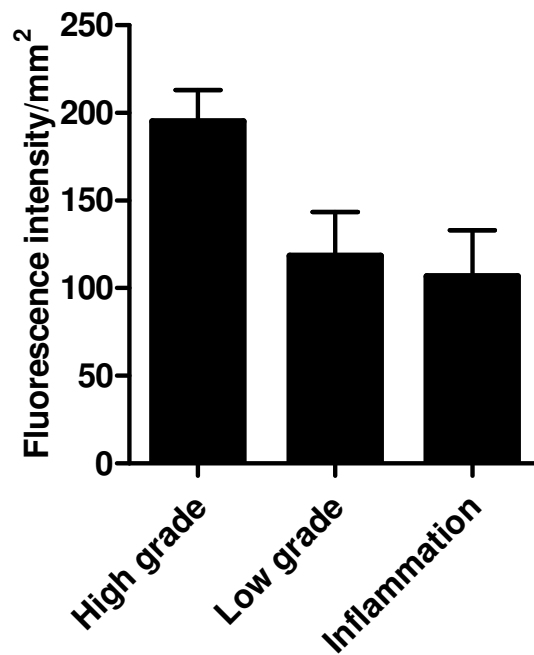


Figure 6.9 Measurement of fluorescence kinetics of different histopathological grades of bladder biopsies. Error bars represent the standard error of the mean of 6 patients.

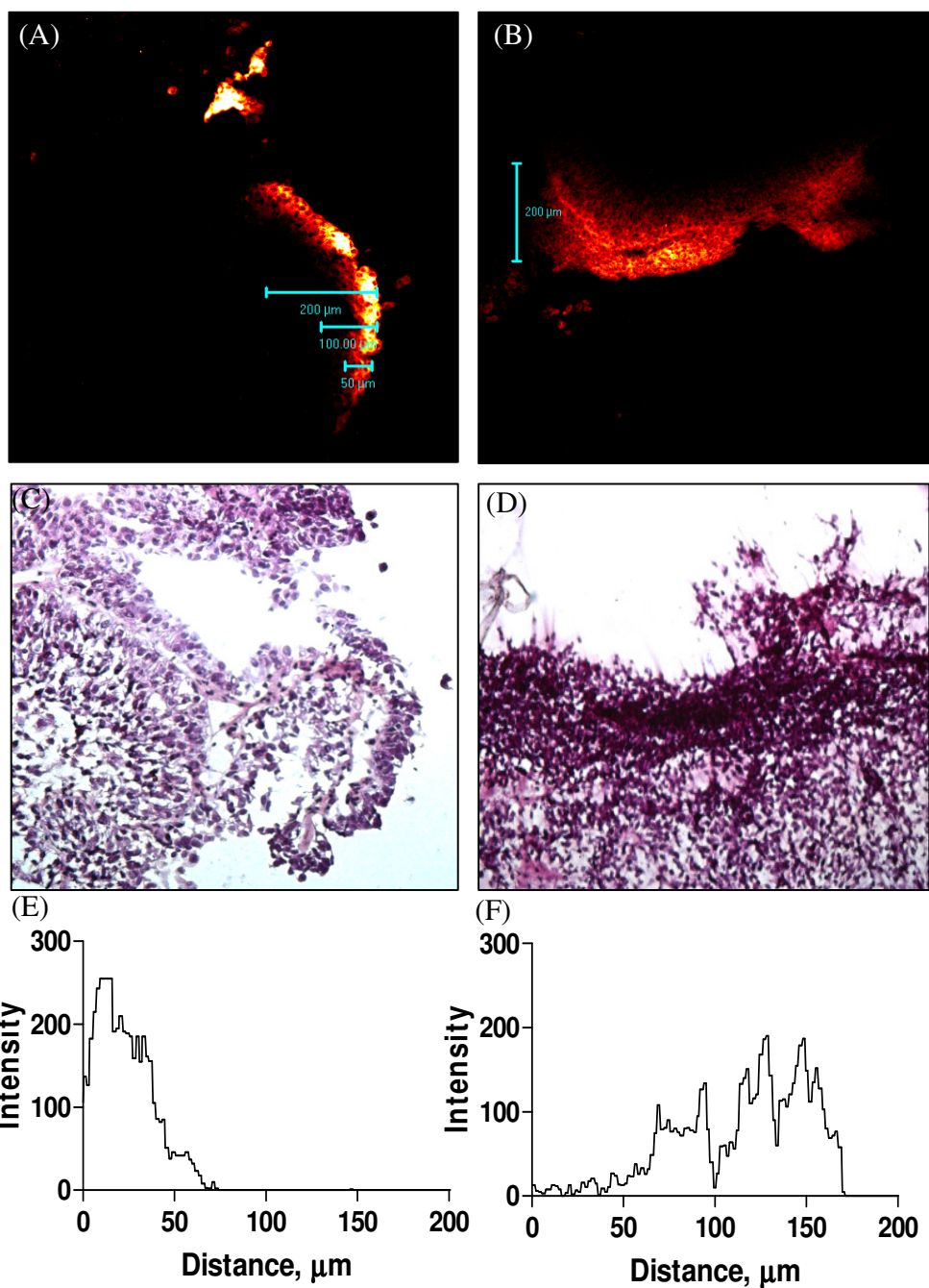


Figure 6.10 Cross section of fluorescence image (A, B) and corresponding hematoxylin–eosin-stained image (C, D) and measurement of fluorescence intensity and depth of penetration of Ce6-PVP (E, F) in bladder tumor biopsy tissue at 2 h after oral administration of Ce6-PVP.

In Figure 6.10, the penetration of Ce6-PVP after intravesical administration is seen in the urothelium of the bladder. The depth of topical penetration of Ce6-PVP into bladder tumor tissue was found to range from 80 – 180 μm . Because the penetration of 665 nm light at treatment power can approach up to 5 mm in certain tissue, it is of utmost importance that the photosensitizer does not penetrate deeper into the muscle layer of the bladder because whole bladder PDT could potentially cause severe bladder contraction. This result demonstrated that topical application of Ce6-PVP was a convenient and safe method of specifically directing Ce6-PVP to bladder tumors, avoiding the widespread distribution in the muscle layers that would have occurred following intravenous administration.

6.4.5 Analysis of cytokines at post PDT

The cytokines investigated in this study were divided into 3 categories: (1) IL-12 and IFN- γ which are generally secreted by lymphocytes and macrophages involved in the proinflammatory, neutrophil activating, granulomatous response; (2) IL-10 associated with a humoral immune response that may inhibit proinflammatory cytokines; and (3) TNF- α , IL-6, and IL-8, which are released by macrophages and monocytes and primarily activate other cells, including T lymphocytes and neutrophils. The results of inflammatory cytokine released into the serum before and after intravenous mediated PDT are shown in Figures 6.11. The patient given intravenous administration of Ce6-PVP had significantly higher baseline levels IL-1b, IL-6, IL-8, IL-10, IL-12, IFN- γ and TNF- α whereas patient given intravesical instillation of Ce6-PVP did not have quantifiable cytokines in serum. There was decreased expression of IL-1a, IL-1b, IL-8, IL-10, IL-12, IFN- γ and TNF- α from its baseline level in patient treated with intravenous Ce6-PVP –

PDT. The expression of these cytokines also could not be detected in patient given intravesical Ce6-PVP – PDT at 24 h post treatment. Only IL-6 was observed to be upregulated in both patients at post PDT (Figure 6.11). As the measurement of cytokine at post PDT was only performed with 2 patients, it wasn't clear as to why these cytokines were downregulated in the bladder cancer patient given intravenous administration of Ce6-PVP-PDT. However, the hypothesis that PDT light and drug dose might have an immune modulatory effect remains to be further investigated. Recently, photodynamic therapy - activated immune response against distant untreated tumors in recurrent angiosarcoma was reported [196]. High dose PDT carried out at a high fluence rate resulted in local control of the disease for up to a year; however, the disease recurred and PDT had to be repeated [199]. Other studies have shown that the secretion of a large array of proinflammatory cytokines in the serum of treated patients following mycobacterial stimulation suggesting the involvement of systemic immune responses of the antitumor effect [210, 211]. Another preliminary study showed that quantifiable concentrations of interleukin 1-beta, interleukin 2, and TNF-alpha were detected in urine samples from the PDT patients with the highest light energies, while no urinary cytokines were found in the PDT patient who received the lowest light energy nor in any of the control subjects, suggesting that a local immunologic response may occur following PDT for bladder cancer [212]. The results further suggest that the increased expression of IL-6 serum after PDT might have a possible correlation to systemic immunological responses. Cytokines, such as IL-6, produced by the tumor cells could attract immunocompetent cells such as macrophages and lymphocytes to the tumor sites and stimulate them [213]. Although it has not been demonstrated whether secreted cytokines can inhibit or stimulate the growth of bladder cancer

cells, patients with invasive bladder cancer that expressed variant IL-6 was associated with improved 5-year overall and disease-specific survival [214].

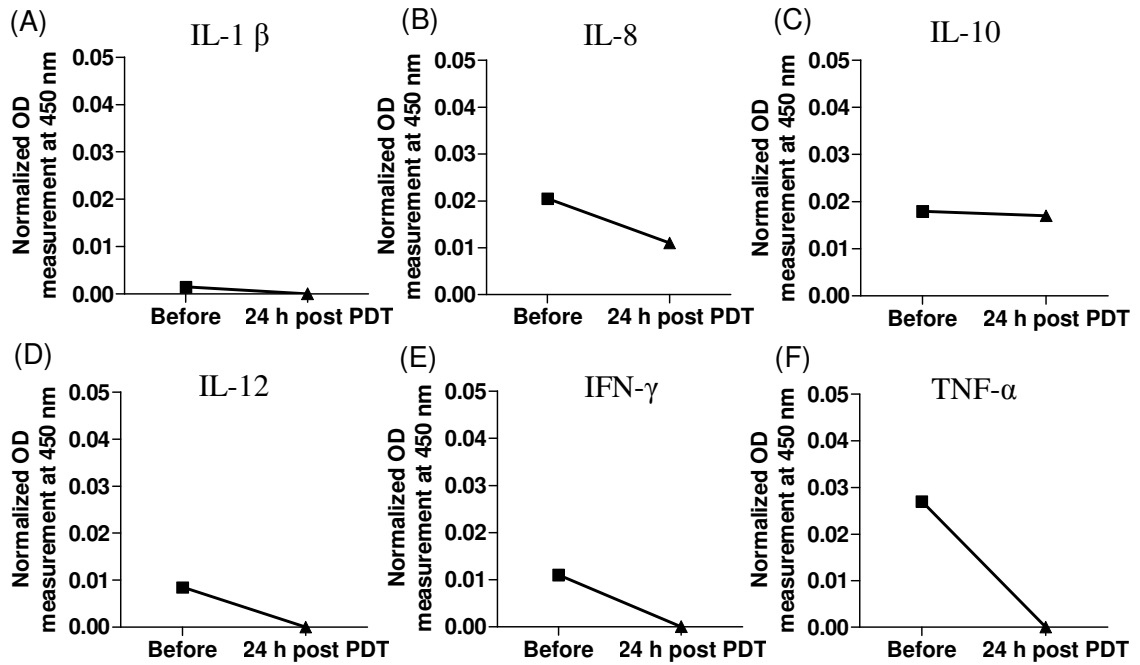


Figure 6.11 Serum cytokines (IL-1 β , IL-8, IL-10, IL-12, IFN- γ and TNF- α) levels after PDT. Serum samples were obtained before PDT and 24 h post PDT for patient treated with intravenous mediated PDT (A – F). Results are presented as average of duplicate experiments.

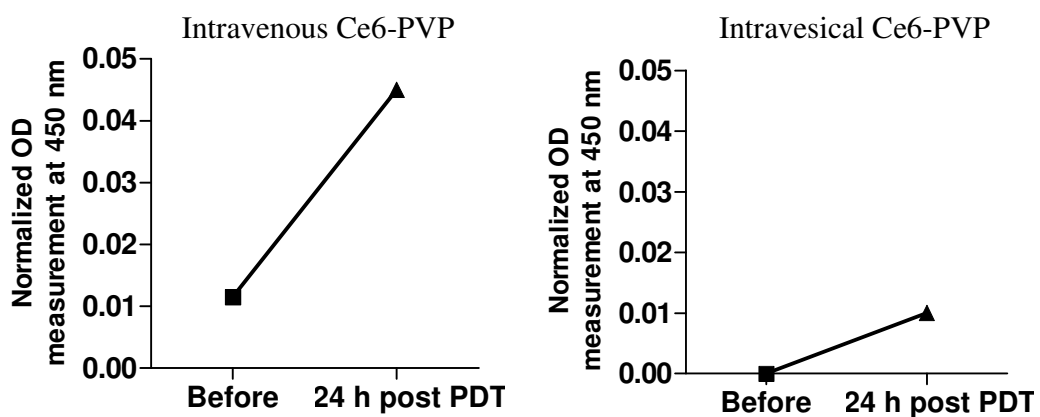


Figure 6.12 Comparison of IL-6 for patient treated with intravenous or intravesical Ce6-PVP mediated PDT. Results are presented as average of duplicate experiments.

6.5 Conclusion

Review of the above cases suggested that intravesical mediated PDT with Ce6-PVP was a safe and well-tolerated procedure that could be an effective therapy for the refractory bladder carcinoma. The selective responses seen in the patient given intravesical administration of Ce6-PVP indicated that photosensitizer exhibited the same preferential retention within tumor tissues as seen in other porphyrin or ALA compounds. It was suggested that with further refinement in the methodology, intravesical mediated PDT may be feasible as an outpatient treatment for superficial bladder TCC under local anaesthetic [215]. It should be cautioned that the finding of a negative association between major inflammatory cytokines (i.e. IL-1a, IL-1b, IL-8, IL-10, IL-12, IFN- γ and TNF- α) and the upregulation of IL-6 at post Ce6-PVP – PDT treatment is based on a relatively short period of follow-up. Long-term follow-up will be needed to validate these findings. The use of PVP had led to a high solubility of an injectable aqueous formulation of Ce6 that is safe for use in patients and have observed selective uptake in angiosarcoma lesions compared to normal skin. Further studies involving larger numbers of patients are required to confirm the efficacy of Ce6-PVP mediated PDT in the management of refractory bladder carcinoma and fluorescence diagnosis of angiosarcoma.

CHAPTER 7

Conclusion and future perspective

7.1 Conclusion

The overall aim of this work was to study the photophysical, photochemical and pharmacokinetic properties of the photosensitizer Ce6 formulated with PVP so as to gain a better understanding of the efficacy and mechanisms of Ce6-PVP induced fluorescence imaging and photodynamic therapy of cancer. The chlorophyll derivative, Ce6 was obtained by a chemical treatment of a chlorin-containing substance extracted from the biomass of *Spirulina* algae. The polyvinylpyrrolidone used for the preparation of Ce6-PVP was a water-soluble grade polymer. PVP in the final formulation ensured a higher bioavailability of Ce6 in tumor tissue compared to suspended chlorin. This thesis has contributed to the optimization and expansion of PDT field and is described in the following paragraphs:

In chapter 2, pharmacokinetic studies were performed in animal implanted with human nasopharyngeal (CNE2) and bladder tumor (MGH) by means of light-induced fluorescence ratiometric imaging, fiber optics-based fluorescence spectrometric measurement, chemical extraction and confocal fluorescence microscopy after intravenous administration of Ce6-PVP. Good red fluorescence image and emission signal with a peak at about 665 nm was recorded in the malignant tissue, indicating highly selective accumulation compared to the surrounding normal tissue. Selective accumulation in the tumor tissue, which was approximately 2 to 5-fold higher than with Ce6 only, was observed in the model of CNE2 and MGH tumor xenografts. Its bioavailability peaked shortly after

parenteral administration (up to 2 hours) in the blood compartment and the tissue it targeted, consistent with the critical time window within which PDT was effective. Biodistribution data exhibited fast clearance rate of Ce6-PVP from normal tissue with no significant prolonged accumulation in normal skin. Compared to porphyrins, Ce6-PVP was eliminated from the body very quickly, within 10 – 12 h after parenteral administration. After 24 h, less than 4 – 6% of the administered Ce6-PVP was detected in the body tissues and serum of mice. This improves the risk to benefit ratio in favour of Ce6-PVP as there was no prolonged skin accumulation of the photosensitizer. The photosensitizing effect of Ce6-PVP and the subsequent necrosis was higher than Ce6 itself. The frequency of complete tumor necrosis could be achieved with Ce6-PVP. Ce6-PVP was found to have less acute toxicity compared to Ce6 only in tumor-bearing nude mice. After illumination at 665 nm, Ce6-PVP elicited no acute phototoxicity for at 3 h drug-light interval at drug dose of 2.5 – 5 mg/kg and light dose of 50 – 300 J/cm². On the other hand, Ce6 elicited acute toxicity at the light dose of 100 J/cm² at 1 h drug-light interval which resulted in normal tissue damage. These results indicated that Ce6-PVP was a safe PDT agent, exhibiting negligible effects in normal tissue.

In chapter 3, a highly purified version of Ce6-PVP was synthesized and it was demonstrated that this new formulation showed improved selectivity and specificity for fluorescence diagnostic imaging and PDT of human cancer compared to Ce6 or Ce6 delivered using DMSO.

In chapter 4, Ce6-PVP preferential uptake by tumor versus normal tissue was confirmed in the CAM model, demonstrating the feasibility of this formulation to

visualize and demarcate cancer. The effect of PVP on the transport of Ce6 across live membrane was evaluated on the CAM model. The highly purified Ce6-PVP was transported across the membrane twice as much compared to Ce6 alone. Thus, PVP was proven to enhance membrane permeability of Ce6. The sensitivity and specificity Ce6-PVP for tumor detection was also increased compared to the formulation with a lower purity level of Ce6-PVP. Using irradiation at a low light dose of 10 J/cm^2 , apoptotic cell deaths were detected in tumor cells implanted on the CAM after treated with Ce6-PVP.

In chapter 5, the interactions of Ce6 and Ce6-PVP with lipoproteins were investigated using steady-state fluorescence measurements. Upon increasing Ce6-PVP concentration, the fluorescence increased drastically, suggesting that PVP effectively prevent the agglomeration of Ce6, which could have important implications for the successful outcome of fluorescence diagnosis and PDT. It is concluded that Ce6-PVP at high concentration bound considerably with VLDL indicating that VLDL was its principal carriers. In vitro studies have shown that PVP localized in the cell cytoplasm and Ce6-PVP was internalized more efficiently compared to Ce6 only.

In chapter 6, preliminary results on the clinical study of refractory bladder cancer and angiosarcoma patients treated with Ce6-PVP mediated fluorescence imaging and PDT were presented. Fluorescence imaging and spectroscopy data showed a significant accumulation of Ce6-PVP in angiosarcoma lesions, showing that Ce6-PVP could provide a useful tool for demarcation of tumor lesions. There was a significant reduction of tumor after intravesical administration Ce6-PVP at post PDT for refractory bladder cancer patients. However, patient given

intravenous Ce6-PVP experienced severe side effect while patient given intravesical administration of Ce6-PV exhibited no adverse reactions. In bladder cancer biopsies, microscopic fluorescence intensity was found to increase with higher grades of cancer. These preliminary results suggested that intravesically administered Ce6-PVP mediated PDT was of value in the management of refractory bladder cancer.

In conclusion, this thesis has presented evidence that the Ce6-PVP formulation had improved bioavailability, selectivity and photosensitizing properties towards malignant tissue. This formulation was found to have several advantageous effects such as providing a novel photosensitizer of a high chemical and photochemical stability, good solubility both in water and in biological fluids, high affinity to the target region or the surface of the body or a tissue, large depth of necrosis, efficient generation of the active species that cause destruction of the pathologically changed tissue, low phototoxicity as well as to provide a method of preparation of such photosensitizer. Ce6-PVP has a high stability in proteinous environment, without losing efficacy of Ce6 as a photosensitizer. The association ensures also a deep penetration of irradiation into biological tissues, a high degree of pathological tissues necrosis and strong inhibition of neoplasm growth at post PDT. These findings were of important relevance for future development use in clinical photodynamic therapy.

7.2 Future perspective

As the work progressed, both here and elsewhere in the field of photobiology, the role of PVP in the photosensitizer formulation has been questioned. The results presented in this thesis specifically indicated that PVP enhanced pharmacokinetic enrichment of Ce6 in the final PVP-containing formulation, exhibiting a more pronounced antitumor activity with respect to the extent of tumor necrosis, the inhibition of tumor proliferation and the prolongation of survival time at post Ce6-PVP mediated PDT. Ce6-PVP was formulated in the form of a lyophilized composition for easy reconstitution prior to use in a liquid aqueous carrier for injections. The work performed here had laid a promising foundation for the use of Ce6-PVP formulation in photodynamic therapy and fluorescence diagnosis. Several avenues for future work could be directed towards developing the composition in the form of a preparation for external use, for instance in the form of a solution or a lotion in appropriate solvent, or an ointment, gel or cream in a typical vehicle, to be applied on the skin or mucosal tissue such as in the oral or bladder cavity. It is also possible to prepare the invention in a semisolid pharmaceutical formulation for the topical application is desirable specifically for local efficacy. The clinical study suggested that topically applied Ce6-PVP could be efficacious for bladder cancer and perhaps other dermal malignancies, such as basal cell carcinoma, as well as non-malignant conditions of the skin, such as psoriasis. Ce6-PVP had shown a good efficacy on skin making it possible to treat skin diseases (i.e. angiosarcoma), as a preventive measure or as a therapy.

BIBLIOGRAPHY

1. McCaughan JS, Jr.: Photodynamic therapy: a review. *Drugs Aging* 1999, 15:49-68.
2. Huang Z: A review of progress in clinical photodynamic therapy. *Technol Cancer Res Treat* 2005, 4:283-293.
3. Moan J, Peng Q: An outline of the hundred-year history of PDT. *Anticancer Res* 2003, 23:3591-3600.
4. van den Bergh H: Photodynamic therapy of age-related macular degeneration: History and principles. *Semin Ophthalmol* 2001, 16:181-200.
5. Wilson BC: Photodynamic therapy for cancer: principles. *Can J Gastroenterol* 2002, 16:393-396.
6. Dolmans DE, Fukumura D, Jain RK: Photodynamic therapy for cancer. *Nat Rev Cancer* 2003, 3:380-387.
7. Olivo M, Chin W: Perylenequinones in Photodynamic Therapy: Cellular versus Vascular Response. *J Environ Pathol Toxicol Oncol* 2006, 25:223-238.
8. Pervaiz S, Olivo M: Art and science of photodynamic therapy. *Clin Exp Pharmacol Physiol* 2006, 33:551-556.
9. Sibata CH, Colussi VC, Oleinick NL, Kinsella TJ: Photodynamic therapy in oncology. *Expert Opin Pharmacother* 2001, 2:917-927.
10. Olivo M, Soo KC: Photodynamic Therapy Comes of Age. *SGH Proceedings* 2001, 9:197-201.
11. van den Bergh H: On the evolution of some endoscopic light delivery systems for photodynamic therapy. *Endoscopy* 1998, 30:392-407.
12. Juzeniene A, Peng Q, Moan J: Milestones in the development of photodynamic therapy and fluorescence diagnosis. *Photochem Photobiol Sci* 2007, 6:1234-1245.
13. Sim HG, Lau WK, Olivo M, Tan PH, Cheng CW: Is photodynamic diagnosis using hypericin better than white-light cystoscopy for detecting superficial bladder carcinoma? *BJU Int* 2005, 95:1215-1218.
14. Brown SB, Brown EA, Walker I: The present and future role of photodynamic therapy in cancer treatment. *Lancet Oncol* 2004, 5:497-508.
15. Vicente MG: Porphyrin-based sensitizers in the detection and treatment of cancer: recent progress. *Curr Med Chem Anti-Canc Agents* 2001, 1:175-194.
16. DaCosta RS, Wilson BC, Marcon NE: Fluorescence and spectral imaging. *ScientificWorldJournal* 2007, 7:2046-2071.
17. Wong Kee Song LM, Marcon NE: Fluorescence and Raman spectroscopy. *Gastrointest Endosc Clin N Am* 2003, 13:279-296.
18. Perelman LT: Optical diagnostic technology based on light scattering spectroscopy for early cancer detection. *Expert Rev Med Devices* 2006, 3:787-803.
19. Schultz CP: The potential role of Fourier transform infrared spectroscopy and imaging in cancer diagnosis incorporating complex mathematical methods. *Technol Cancer Res Treat* 2002, 1:95-104.
20. Ell C: Improving endoscopic resolution and sampling: fluorescence techniques. *Gut* 2003, 52 Suppl 4:iv30-33.
21. Kherlopian AR, Song T, Duan Q, Neimark MA, Po MJ, Gohagan JK, Laine AF: A review of imaging techniques for systems biology. *BMC Syst Biol* 2008, 2:74.

-
22. Chen Y, Gryshuk A, Achilefu S, Ohulchansky T, Potter W, Zhong T, Morgan J, Chance B, Prasad PN, Henderson BW, et al: A novel approach to a bifunctional photosensitizer for tumor imaging and phototherapy. *Bioconjug Chem* 2005, 16:1264-1274.
 23. Thong PS, Olivo M, Kho KW, Zheng W, Mancer K, Harris M, Soo KC: Laser confocal endomicroscopy as a novel technique for fluorescence diagnostic imaging of the oral cavity. *J Biomed Opt* 2007, 12:014007.
 24. Andersson-Engels S, Klinteberg C, Svanberg K, Svanberg S: In vivo fluorescence imaging for tissue diagnostics. *Phys Med Biol* 1997, 42:815-824.
 25. Zaak D, Hofstetter A: The current diagnosis of superficial bladder cancer must be reconsidered. *Urol Int* 2002, 69:85-90.
 26. Zheng W, Olivo M, Soo KC: The use of digitized endoscopic imaging of 5-ALA-induced PPIX fluorescence to detect and diagnose oral premalignant and malignant lesions in vivo. *Int J Cancer* 2004, 110:295-300.
 27. Vrouenraets MB, Visser GW, Snow GB, van Dongen GA: Basic principles, applications in oncology and improved selectivity of photodynamic therapy. *Anticancer Res* 2003, 23:505-522.
 28. Wilson BC, Patterson MS: The physics, biophysics and technology of photodynamic therapy. *Phys Med Biol* 2008, 53:R61-109.
 29. Juarranz A, Jaen P, Sanz-Rodriguez F, Cuevas J, Gonzalez S: Photodynamic therapy of cancer. Basic principles and applications. *Clin Transl Oncol* 2008, 10:148-154.
 30. Awan MA, Tarin SA: Review of photodynamic therapy. *Surgeon* 2006, 4:231-236.
 31. Kessel D: Delivery of photosensitizing agents. *Adv Drug Deliv Rev* 2004, 56:7-8.
 32. Ramaswamy B, Manivasager V, Chin WW, Soo KC, Olivo M: Photodynamic diagnosis of a human nasopharyngeal carcinoma xenograft model using the novel Chlorin e6 photosensitizer Fotonol. *Int J Oncol* 2005, 26:1501-1506.
 33. Berg K, Selbo PK, Weyergang A, Dietze A, Prasmickaite L, Bonsted A, Engesaeter BO, Angell-Petersen E, Warloe T, Frandsen N, Hogset A: Porphyrin-related photosensitizers for cancer imaging and therapeutic applications. *J Microsc* 2005, 218:133-147.
 34. Chin W, Lau W, Cheng C, Olivo M: Evaluation of Hypocrellin B in a human bladder tumor model in experimental photodynamic therapy: Biodistribution, light dose and drug-light interval effects. *Int J Oncol* 2004, 25:623-629.
 35. Kamuhabwa A, Agostinis P, Ahmed B, Landuyt W, Van Cleynenbreugel B, Van Poppel H, De Witte P: Hypericin as a potential phototherapeutic agent in superficial transitional cell carcinoma of the bladder. *Photochem Photobiol Sci* 2004, 3:772-780.
 36. Cheng CW, Lau WK, Tan PH, Olivo M: Cystoscopic diagnosis of bladder cancer by intravesical instillation of 5-aminolevulinic acid induced porphyrin fluorescence--the Singapore experience. *Ann Acad Med Singapore* 2000, 29:153-158.
 37. Zaak D, Karl A, Knuchel R, Stepp H, Hartmann A, Reich O, Bachmann A, Siebels M, Popken G, Stief C: Diagnosis of urothelial carcinoma of the bladder using fluorescence endoscopy. *BJU Int* 2005, 96:217-222.
 38. Olivo M, Lau W, Manivasager V, Tan PH, Soo KC, Cheng C: Macro-microscopic fluorescence of human bladder cancer using hypericin fluorescence cystoscopy and laser confocal microscopy. *Int J Oncol* 2003, 23:983-990.
 39. Uzdensky AB, Bragin DE, Kolosov MS, Kubin A, Loew HG, Moan J: Photodynamic effect of hypericin and a water-soluble derivative on isolated

-
- crayfish neuron and surrounding glial cells. *J Photochem Photobiol B* 2003, 72:27-33.
40. Saw CL, Olivo M, Chin WW, Soo KC, Heng PW: Transport of hypericin across chick chorioallantoic membrane and photodynamic therapy vasculature assessment. *Biol Pharm Bull* 2005, 28:1054-1060.
 41. Leunig A, Mehlmann M, Betz C, Stepp H, Arbogast S, Grevers G, Baumgartner R: Fluorescence staining of oral cancer using a topical application of 5-aminolevulinic acid: fluorescence microscopic studies. *J Photochem Photobiol B* 2001, 60:44-49.
 42. Fan KF, Hopper C, Speight PM, Buonaccorsi G, MacRobert AJ, Bown SG: Photodynamic therapy using 5-aminolevulinic acid for premalignant and malignant lesions of the oral cavity. *Cancer* 1996, 78:1374-1383.
 43. Pegaz B, Van Den Bergh H, Konan YN, Debefve E, Borle F, Ballini JP, Wagieres G, Spaniol S, Albrecht V, Scheglmann D, Nifantiev NE: Pre-clinical evaluation of a novel water-soluble chlorin e6 derivative (BLC 1010) as photosensitizer for the closure of the neovessels. *Photochem Photobiol* 2005, 81(6):1505-10
 44. Morlet L, Vonarx V, Foultier MT, Gouyette A, Stewart C, Lenz P, Patrice T: In vitro and in vivo spectrofluorometry of a water-soluble meta-(tetrahydroxyphenyl)chlorin (m-THPC) derivative. *J Photochem Photobiol B* 1997, 39:249-257.
 45. Kostenich GA, Zhuravkin IN, Furmanchuk AV, Zhavrid EA: Photodynamic therapy with chlorin e6. A morphologic study of tumor damage efficiency in experiment. *J Photochem Photobiol B* 1991, 11:307-318.
 46. Spikes JD: Chlorins as photosensitizers in biology and medicine. *J Photochem Photobiol B* 1990, 6:259-274.
 47. Cunderlikova B, Gangeskar L, Moan J: Acid-base properties of chlorin e6: relation to cellular uptake. *J Photochem Photobiol B* 1999, 53:81-90.
 48. Colasanti A, Kisslinger A, Kusch D, Liuzzi R, Mastrocinque M, Montforts FP, Quarto M, Riccio P, Roberti G, Villani F: In vitro photo-activation of newly synthesized chlorin derivatives with red-light-emitting diodes. *J Photochem Photobiol B* 1997, 38:54-60.
 49. Bachor R, Shea CR, Gillies R, Hasan T: Photosensitized destruction of human bladder carcinoma cells treated with chlorin e6-conjugated microspheres. *Proc Natl Acad Sci U S A* 1991, 88:1580-1584.
 50. Schmidt-Erfurth U, Diddens H, Birngruber R, Hasan T: Photodynamic targeting of human retinoblastoma cells using covalent low-density lipoprotein conjugates. *Br J Cancer* 1997, 75:54-61.
 51. Bisland SK, Singh D, Garipey J: Potentiation of chlorin e6 photodynamic activity in vitro with peptide-based intracellular vehicles. *Bioconjug Chem* 1999, 10:982-992.
 52. Gijssens A, Missiaen L, Merlevede W, de Witte P: Epidermal growth factor-mediated targeting of chlorin e6 selectively potentiates its photodynamic activity. *Cancer Res* 2000, 60:2197-2202.
 53. Pegaz B, Debefve E, Borle F, Ballini JP, Wagnieres G, Spaniol S, Albrecht V, Scheglmann D, Nifantiev NE, van den Bergh H, Konan YN: Preclinical evaluation of a novel water-soluble chlorin E6 derivative (BLC 1010) as photosensitizer for the closure of the neovessels. *Photochem Photobiol* 2005, 81:1505-1510.
 54. Namiki Y, Namiki T, Date M, Yanagihara K, Yashiro M, Takahashi H: Enhanced photodynamic antitumor effect on gastric cancer by a novel photosensitive stealth liposome. *Pharmacol Res* 2004, 50:65-76.

-
55. Kopecek J, Kopeckova P, Minko T, Lu ZR, Peterson CM: Water soluble polymers in tumor targeted delivery. *J Control Release* 2001, 74:147-158.
 56. Hamblin MR, Miller JL, Rizvi I, Ortel B, Maytin EV, Hasan T: Pegylation of a chlorin(e6) polymer conjugate increases tumor targeting of photosensitizer. *Cancer Res* 2001, 61:7155-7162.
 57. Hamblin MR, Miller JL, Rizvi I, Loew HG, Hasan T, Ortel B, Maytin EV: Pegylation of charged polymer-photosensitizer conjugates: effects on photodynamic efficacy. *Br J Cancer* 2003, 89:937-943.
 58. Shiah JG, Sun Y, Peterson CM, Straight RC, Kopecek J: Antitumor activity of N-(2-hydroxypropyl) methacrylamide copolymer-Mesochlorine e6 and adriamycin conjugates in combination treatments. *Clin Cancer Res* 2000, 6:1008-1015.
 59. Seventeenth Report of the Joint FAO/WHO Expert Committee on Food Additives, Wld Hlth Org. techn. Rep. Ser., 1974, No. 539; FAO Nutrition Meetings Report Series, 1974, No. 53.
 60. Rudowski WJ: Evaluation of modern plasma expanders and blood substitutes. *Br J Hosp Med* 1980, 23:389-399.
 61. Kishida A: A site-specific polymeric drug carrier for renal disease treatment. *Trends Pharmacol Sci* 2003, 24:611-613.
 62. Le Garrec D, Gori S, Luo L, Lessard D, Smith DC, Yessine MA, Ranger M, Leroux JC: Poly(N-vinylpyrrolidone)-block-poly(D,L-lactide) as a new polymeric solubilizer for hydrophobic anticancer drugs: in vitro and in vivo evaluation. *J Control Release* 2004, 99:83-101.
 63. Duncan R: The dawning era of polymer therapeutics. *Nat Rev Drug Discov* 2003, 2:347-360.
 64. Yoshioka Y, Tsutsumi Y, Mukai Y, Shibata H, Okamoto T, Kaneda Y, Tsunoda S, Kamada H, Koizumi K, Yamamoto Y, et al: Effective accumulation of poly(vinylpyrrolidone-co-vinyl laurate) into the spleen. *J Biomed Mater Res A* 2004, 70:219-223.
 65. Kaneda Y, Tsutsumi Y, Yoshioka Y, Kamada H, Yamamoto Y, Kodaira H, Tsunoda S, Okamoto T, Mukai Y, Shibata H, et al: The use of PVP as a polymeric carrier to improve the plasma half-life of drugs. *Biomaterials* 2004, 25:3259-3266.
 66. Maeda H, Sawa T, Konno T: Mechanism of tumor-targeted delivery of macromolecular drugs, including the EPR effect in solid tumor and clinical overview of the prototype polymeric drug SMANCS. *J Control Release* 2001, 74:47-61.
 67. Taylor LS, Zografi G: Spectroscopic characterization of interactions between PVP and indomethacin in amorphous molecular dispersions. *Pharm Res* 1997, 14:1691-1698.
 68. Isakau HA, Parkhats MV, Knyukshto VN, Dzhagarov BM, Petrov EP, Petrov PT: Toward understanding the high PDT efficacy of chlorin e6-polyvinylpyrrolidone formulations: Photophysical and molecular aspects of photosensitizer-polymer interaction in vitro. *J Photochem Photobiol B* 2008, 92:165-174.
 69. Dougherty TJ: An update on photodynamic therapy applications. *J Clin Laser Med Surg* 2002, 20:3-7.
 70. Chatterjee DK, Fong LS, Zhang Y: Nanoparticles in photodynamic therapy: An emerging paradigm. *Adv Drug Deliv Rev* 2008.
 71. Milgrom LR: Towards recombinant antibody-fragment targeted photodynamic therapy. *Sci Prog* 2008, 91:241-263.
 72. Derycke AS, de Witte PA: Liposomes for photodynamic therapy. *Adv Drug Deliv Rev* 2004, 56:17-30.

-
73. Bechet D, Couleaud P, Frochot C, Viriot ML, Guillemin F, Barberi-Heyob M: Nanoparticles as vehicles for delivery of photodynamic therapy agents. *Trends Biotechnol* 2008, 26:612-621.
 74. Castano AP, Demidova TN, Hamblin MR: Mechanisms in photodynamic therapy: Part three--Photosensitizer pharmacokinetics, biodistribution, tumor localization and modes of tumor destruction. *Photodiagnosis and Photodynamic Therapy* 2005, 2:91-106.
 75. Rück A, Steiner R: Basic reaction mechanisms of hydrophilic and lipophilic photosensitizers in photodynamic tumor treatment. *Minimally Invasive Therapy and Allied Technologies* 1998, 7:503 - 509.
 76. Kessel D, Woodburn K: Biodistribution of photosensitizing agents. *Int J Biochem* 1993, 25:1377-1383.
 77. Josefsen LB, Boyle RW: Photodynamic therapy: novel third-generation photosensitizers one step closer? *Br J Pharmacol* 2008, 154:1-3.
 78. Kostenich GA, Zhuravkin IN, Zhavrid EA: Experimental grounds for using chlorin e6 in the photodynamic therapy of malignant tumors. *J Photochem Photobiol B* 1994, 22:211-217.
 79. Parkhots MV, Knyukshto VN, Isakov GA, Petrov PT, Lepeshkevich SV, Khairullina AY, Dzhagarova BA: Spectral-luminescent studies of the "Photolon" photosensitizer in model media and in blood of oncological patients. *J of Applied Spectroscopy* 2003, 70:921-926.
 80. Chowdhary RK, Sharif I, Chansarkar N, Dolphin D, Ratkay L, Delaney S, Meadows H: Correlation of photosensitizer delivery to lipoproteins and efficacy in tumor and arthritis mouse models; comparison of lipid-based and Pluronic P123 formulations. *J Pharm Pharm Sci* 2003, 6:198-204.
 81. Ferrario A, Gomer CJ: Systemic toxicity in mice induced by localized porphyrin photodynamic therapy. *Cancer Res* 1990, 50:539-543.
 82. Kodaira H, Tsutsumi Y, Yoshioka Y, Kamada H, Kaneda Y, Yamamoto Y, Tsunoda S, Okamoto T, Mukai Y, Shibata H, et al: The targeting of anionized polyvinylpyrrolidone to the renal system. *Biomaterials* 2004, 25:4309-4315.
 83. Das K, Smirnov AV, Wen J, Miskovsky P, Petrich JW: Photophysics of hypericin and hypocrellin A in complex with subcellular components: interactions with human serum albumin. *Photochem Photobiol* 1999, 69:633-645.
 84. Brindle K: New approaches for imaging tumor responses to treatment. *Nat Rev Cancer* 2008, 8:94-107.
 85. Jain S, Kockelbergh RC: The role of photodynamic diagnosis in the contemporary management of superficial bladder cancer. *BJU Int* 2005, 96:17-21.
 86. Stringer M, Moghissi K: Photodiagnosis and fluorescence imaging in clinical practice. *Photodiagnosis and Photodynamic Therapy* 2004, 1:9-12.
 87. Wagnieres GA, Star WM, Wilson BC: In vivo fluorescence spectroscopy and imaging for oncological applications. *Photochem Photobiol* 1998, 68:603-632.
 88. Mang T, Kost J, Sullivan M, Wilson BC: Autofluorescence and Photofrin-induced fluorescence imaging and spectroscopy in an animal model of oral cancer. *Photodiagnosis and Photodynamic Therapy* 2006, 3:168-176.
 89. Kikuchi T, Asakura T, Aihara H, Shiraki M, Takagi S, Kinouchi Y, Aizawa K, Shimosegawa T: Photodynamic therapy of intestinal tumors with mono-L-aspartyl chlorin e6 (NPe6): a basic study. *Anticancer Res* 2003, 23:4897-4900.
 90. Moan J, Ma LW, Juzeniene A, Iani V, Juzenas P, Apricena F, Peng Q: Pharmacology of protoporphyrin IX in nude mice after application of ALA and ALA esters. *Int J Cancer* 2003, 103:132-135.

-
91. Lankerani L, Baron ED: Photosensitivity to Exogenous Agents. *J Cutan Med Surg* 2005.
 92. Qian P, Evensen JF, Rimington C, Moan J: A comparison of different photosensitizing dyes with respect to uptake C3H-tumors and tissues of mice. *Cancer Lett* 1987, 36:1-10.
 93. Gomer CJ, Ferrario A: Tissue distribution and photosensitizing properties of mono-L-aspartyl chlorin e6 in a mouse tumor model. *Cancer Res* 1990, 50:3985-3990.
 94. Taber SW, Fingar VH, Coots CT, Wieman TJ: Photodynamic therapy using mono-L-aspartyl chlorin e6 (Npe6) for the treatment of cutaneous disease: a Phase I clinical study. *Clin Cancer Res* 1998, 4:2741-2746.
 95. Chan AL, Juarez M, Allen R, Volz W, Albertson T: Pharmacokinetics and clinical effects of mono-L-aspartyl chlorin e6 (NPe6) photodynamic therapy in adult patients with primary or secondary cancer of the skin and mucosal surfaces. *Photodermatol Photoimmunol Photomed* 2005, 21:72-78.
 96. Kato H, Furukawa K, Sato M, Okunaka T, Kusunoki Y, Kawahara M, Fukuoka M, Miyazawa T, Yana T, Matsui K, et al: Phase II clinical study of photodynamic therapy using mono-L-aspartyl chlorin e6 and diode laser for early superficial squamous cell carcinoma of the lung. *Lung Cancer* 2003, 42:103-111.
 97. Zhou X, Pogue BW, Chen B, Demidenko E, Joshi R, Hoopes J, Hasan T: Pretreatment photosensitizer dosimetry reduces variation in tumor response. *Int J Radiat Oncol Biol Phys* 2006, 64:1211-1220.
 98. Beyer W: Systems for light application and dosimetry in photodynamic therapy. *J Photochem Photobiol B* 1996, 36:153-156.
 99. van Duijnhoven FH, Rovers JP, Engelmann K, Krajina Z, Purkiss SF, Zoetmulder FA, Vogl TJ, Terpstra OT: Photodynamic Therapy With 5,10,15,20-Tetrakis(m-Hydroxyphenyl) Bacteriochlorin for Colorectal Liver Metastases Is Safe and Feasible: Results From a Phase I Study. *Ann Surg Oncol* 2005, 12(10):808-16.
 100. Schouwink H, Rutgers ET, van der Sijp J, Oppelaar H, van Zandwijk N, van Veen R, Burgers S, Stewart FA, Zoetmulder F, Baas P: Intraoperative photodynamic therapy after pleuropneumectomy in patients with malignant pleural mesothelioma: dose finding and toxicity results. *Chest* 2001, 120:1167-1174.
 101. Von Specht BU, Milgrom L, Segal S: Induction of a stable hapten-specific immunosuppression by a hapten conjugated to poly(N-vinylpyrrolidone) (PVP). *Clin Exp Immunol* 1978, 33:292-297.
 102. Ferrario A, Kessel D, Gomer CJ: Metabolic properties and photosensitizing responsiveness of mono-L-aspartyl chlorin e6 in a mouse tumor model. *Cancer Res* 1992, 52:2890-2893.
 103. Saito K, Mikuniya N, Aizawa K: Effects of photodynamic therapy using mono-L-aspartyl chlorin e6 on vessels and its contribution to the antitumor effect. *Jpn J Cancer Res* 2000, 91:560-565.
 104. Maugain E, Sasnouski S, Zorin V, Merlin JL, Guillemin F, Bezdetnaya L: Foscan-based photodynamic treatment in vivo: correlation between efficacy and Foscan accumulation in tumor, plasma and leukocytes. *Oncol Rep* 2004, 12:639-645.
 105. Cunderlikova B, Kongshaug M, Gangeskar L, Moan J: Increased binding of chlorin e(6) to lipoproteins at low pH values. *Int J Biochem Cell Biol* 2000, 32:759-768.
 106. Komagoe K, Tamagake K, Katsu T: The influence of aggregation of porphyrins on the efficiency of photogeneration of hydrogen peroxide in aqueous solution. *Chem Pharm Bull (Tokyo)* 2006, 54:1004-1009.

-
107. Tanielian C, Schweitzer C, Mechin R, Wolff C: Quantum yield of singlet oxygen production by monomeric and aggregated forms of hematoporphyrin derivative. *Free Radic Biol Med* 2001, 30:208-212.
 108. Adams ML, Lavasanifar A, Kwon GS: Amphiphilic block copolymers for drug delivery. *J Pharm Sci* 2003, 92:1343-1355.
 109. Konan YN, Gurny R, Allemann E: State of the art in the delivery of photosensitizers for photodynamic therapy. *J Photochem Photobiol B* 2002, 66:89-106.
 110. van Nostrum CF: Polymeric micelles to deliver photosensitizers for photodynamic therapy. *Adv Drug Deliv Rev* 2004, 56:9-16.
 111. Westerman P, Glanzmann T, Andrejevic S, Braichotte DR, Forrer M, Wagnieres GA, Monnier P, van den Bergh H, Mach JP, Folli S: Long circulating half-life and high tumor selectivity of the photosensitizer meta-tetrahydroxyphenylchlorin conjugated to polyethylene glycol in nude mice grafted with a human colon carcinoma. *Int J Cancer* 1998, 76:842-850.
 112. Lukyanov AN, Torchilin VP: Micelles from lipid derivatives of water-soluble polymers as delivery systems for poorly soluble drugs. *Adv Drug Deliv Rev* 2004, 56:1273-1289.
 113. Isakau HA, Trukhacheva TV, Petrov PT: Isolation and identification of impurities in chlorin e6. *J Pharm Biomed Anal* 2007, 45(1):20-9.
 114. Isakau HA, Trukhacheva TV, Zhebentyaev AI, Petrov PT: HPLC study of chlorin e6 and its molecular complex with polyvinylpyrrolidone. *Biomed Chromatogr* 2007, 21:318-325.
 115. Hanley JA, McNeil BJ: A method of comparing the areas under receiver operating characteristic curves derived from the same cases. *Radiology* 1983, 148:839-843.
 116. Bellnier DA, Greco WR, Parsons JC, Oseroff AR, Kuebler A, Dougherty TJ: An assay for the quantitation of Photofrin in tissues and fluids. *Photochem Photobiol* 1997, 66:237-244.
 117. Kirchner LM, Schmidt SP, Gruber BS: Quantitation of angiogenesis in the chick chorioallantoic membrane model using fractal analysis. *Microvasc Res* 1996, 51:2-14.
 118. Copley L, van der Watt P, Wirtz KW, Parker MI, Leaner VD: Photolontrade mark, a chlorin e6 derivative, triggers ROS production and light-dependent cell death via necrosis. *Int J Biochem Cell Biol* 2007, 40(2):227-35.
 119. Simon GA, Maibach HI: Relevance of hairless mouse as an experimental model of percutaneous penetration in man. *Skin Pharmacol Appl Skin Physiol* 1998, 11:80-86.
 120. Moffitt EA: Blood substitutes. *Can Anaesth Soc J* 1975, 22:12-19.
 121. Young SW, Muller HH, Marincek B: Contrast enhancement of malignant tumors after intravenous polyvinylpyrrolidone with metallic salts as determined by computed tomography. *Radiology* 1981, 138:97-105.
 122. Kodaira H, Tsutsumi Y, Yoshioka Y, Kamada H, Kaneda Y, Yamamoto Y, Tsunoda S-i, Okamoto T, Mukai Y, Shibata H, et al: The targeting of anionized polyvinylpyrrolidone to the renal system. *Biomaterials* 2004, 25:4309-4315.
 123. Allen JC, Baxter JH, Goodman HC: Effects of dextran, polyvinylpyrrolidone and gamma globulin on the hyperlipidemia of experimental nephrosis. *J Clin Invest* 1961, 40:499-508.
 124. Sanbar SS, Smet G: Hypolipidemic effect of polyvinylpyrrolidone in man. *Circulation* 1968, 38:771-776.

-
125. Dougherty TJ: Photosensitizers: therapy and detection of malignant tumors. *Photochem Photobiol* 1987, 45:879-889.
 126. Chin WW, Lau WK, Heng PW, Bhuvanewari R, Olivo M: Fluorescence imaging and phototoxicity effects of new formulation of chlorin e6-polyvinylpyrrolidone. *J Photochem Photobiol B* 2006, 84:103-110.
 127. Brayton CF: Dimethyl sulfoxide (DMSO): a review. *Cornell Vet* 1986, 76:61-90.
 128. Ris HB, Giger A, Hof VI, Mettler D, Stewart JC, Althaus U, Altermatt HJ: Experimental assessment of photodynamic therapy with chlorins for malignant mesothelioma. *Eur J Cardiothorac Surg* 1997, 12:542-548.
 129. Moghissi K, Dixon K: Is bronchoscopic photodynamic therapy a therapeutic option in lung cancer? *Eur Respir J* 2003, 22:535-541.
 130. Maziak DE, Markman BR, MacKay JA, Evans WK: Photodynamic therapy in nonsmall cell lung cancer: a systematic review. *Ann Thorac Surg* 2004, 77:1484-1491.
 131. Moghissi K: Role of bronchoscopic photodynamic therapy in lung cancer management. *Curr Opin Pulm Med* 2004, 10:256-260.
 132. Sutedja TG, Venmans BJ, Smit EF, Postmus PE: Fluorescence bronchoscopy for early detection of lung cancer: a clinical perspective. *Lung Cancer* 2001, 34:157-168.
 133. Piotrowski WJ, Gorski P: Photodynamic diagnosis and treatment of bronchial cancer. *Int J Occup Med Environ Health* 2003, 16:105-112.
 134. Levy JG: Photosensitizers in photodynamic therapy. *Semin Oncol* 1994, 21:4-10.
 135. Lam S: Photodynamic therapy of lung cancer. *Semin Oncol* 1994, 21:15-19.
 136. Nyman ES, Hynninen PH: Research advances in the use of tetrapyrrolic photosensitizers for photodynamic therapy. *J Photochem Photobiol B* 2004, 73:1-28.
 137. Pandey RK, Bellnier DA, Smith KM, Dougherty TJ: Chlorin and porphyrin derivatives as potential photosensitizers in photodynamic therapy. *Photochem Photobiol* 1991, 53:65-72.
 138. Pandey RK, Goswami LN, Chen Y, Gryshuk A, Missert JR, Oseroff A, Dougherty TJ: Nature: a rich source for developing multifunctional agents. Tumor-imaging and photodynamic therapy. *Lasers Surg Med* 2006, 38:445-467.
 139. Usuda J, Kato H, Okunaka T, Furukawa K, Tsutsui H, Yamada K, Suga Y, Honda H, Nagatsuka Y, Ohira T, et al: Photodynamic therapy (PDT) for lung cancers. *J Thorac Oncol* 2006, 1:489-493.
 140. Lam S, Kennedy T, Unger M, Miller YE, Gelmont D, Rusch V, Gipe B, Howard D, LeRiche JC, Coldman A, Gazdar AF: Localization of bronchial intraepithelial neoplastic lesions by fluorescence bronchoscopy. *Chest* 1998, 113:696-702.
 141. Chin W, Lau W, Lay SL, Wei KK, Olivo M: Photodynamic-induced vascular damage of the chick chorioallantoic membrane model using perylenequinones. *Int J Oncol* 2004, 25:887-891.
 142. Kubota K, Furuse K, Kawaguchi T, Kawahara M, Ogawara M, Yamamoto S: A case of long-term survival with stage IV small cell lung cancer and early-stage central-type squamous cell lung cancer treated by photodynamic therapy. *Jpn J Clin Oncol* 1999, 29:45-48.
 143. Salgia R, Skarin AT: Molecular abnormalities in lung cancer. *J Clin Oncol* 1998, 16:1207-1217.
 144. Scagliotti GV, Novello S, Selvaggi G: Multidrug resistance in non-small-cell lung cancer. *Ann Oncol* 1999, 10 Suppl 5:S83-86.

-
145. Modok S, Mellor HR, Callaghan R: Modulation of multidrug resistance efflux pump activity to overcome chemoresistance in cancer. *Curr Opin Pharmacol* 2006, 6:350-354.
 146. Kawabata S, Oka M, Soda H, Shiozawa K, Nakatomi K, Tsurutani J, Nakamura Y, Doi S, Kitazaki T, Sugahara K, et al: Expression and functional analyses of breast cancer resistance protein in lung cancer. *Clin Cancer Res* 2003, 9:3052-3057.
 147. Robey RW, Steadman K, Polgar O, Bates SE: ABCG2-mediated transport of photosensitizers: potential impact on photodynamic therapy. *Cancer Biol Ther* 2005, 4:187-194.
 148. Robey RW, Steadman K, Polgar O, Morisaki K, Blayney M, Mistry P, Bates SE: Pheophorbide a is a specific probe for ABCG2 function and inhibition. *Cancer Res* 2004, 64:1242-1246.
 149. Liu W, Baer MR, Bowman MJ, Pera P, Zheng X, Morgan J, Pandey RA, Oseroff AR: The tyrosine kinase inhibitor imatinib mesylate enhances the efficacy of photodynamic therapy by inhibiting ABCG2. *Clin Cancer Res* 2007, 13:2463-2470.
 150. Donnelly RF, McCarron PA, Woolfson AD: Drug delivery of aminolevulinic acid from topical formulations intended for photodynamic therapy. *Photochem Photobiol* 2005, 81:750-767.
 151. Parkhots MV, Knyukshto VN, Isakov GA, Petrov PT, Lepeshkevich SV, Khairullina AY, Dzhagarov BA: Spectral-luminescent studies of the "photolon" photosensitizer in model media and in blood of oncological patients. *J of Applied Spectroscopy* 2003, 70:921-926.
 152. Drulis-Kawa Z, Bednarkiewicz A, Bugla-Ploskonska G, Strek W, Doroszkiewicz W: The susceptibility of anaerobic bacteria isolated from periodontal diseases to photodynamic inactivation with Fotolon (chlorin e6). *Pol J Microbiol* 2005, 54:305-310.
 153. Drulis-Kawa Z, Bednarkiewicz A, Bugla G, Strek W, Doroszkiewicz W: Bactericidal effects of the Fotolon (chlorin e6) on gram-negative and gram-positive strains isolated from wound infections. *Advances in Clinical and Experimental Medicine* 2006, 15:279-283.
 154. Chin WW, Ramaswamy B, Thong PSP, Heng PWS, Gan YY, Olivo M, Soo KC: Preclinical and pilot clinical cancer studies using fluorescence-guided photodynamic therapy with chlorin e6-polyvinylpyrrolidone and hypericin. *Singapore General Hospital Proceedings* 2007, 16:118-126.
 155. Chin WW, Heng PW, Bhuvanewari R, Lau WK, Olivo M: The potential application of chlorin e6-polyvinylpyrrolidone formulation in photodynamic therapy. *Photochem Photobiol Sci* 2006, 5:1031-1037.
 156. Simonelli AP, Mehta SC, Higuchi WI: Dissolution rates of high energy sulfathiazole-povidone coprecipitates II: characterization of form of drug controlling its dissolution rate via solubility studies. *J Pharm Sci* 1976, 65:355-361.
 157. Vargas A, Zeisser-Labouebe M, Lange N, Gurny R, Delie F: The chick embryo and its chorioallantoic membrane (CAM) for the in vivo evaluation of drug delivery systems. *Adv Drug Deliv Rev* 2007, 59:1162-1176.
 158. Hammer-Wilson MJ, Akian L, Espinoza J, Kimel S, Berns MW: Photodynamic parameters in the chick chorioallantoic membrane (CAM) bioassay for topically applied photosensitizers. *J Photochem Photobiol B* 1999, 53:44-52.

-
159. Richardson M, Singh G: Observations on the use of the avian chorioallantoic membrane (CAM) model in investigations into angiogenesis. *Curr Drug Targets Cardiovasc Haematol Disord* 2003, 3:155-185.
 160. Kunzi-Rapp K, Genze F, Kufer R, Reich E, Hautmann RE, Gschwend JE: Chorioallantoic membrane assay: vascularized 3-dimensional cell culture system for human prostate cancer cells as an animal substitute model. *J Urol* 2001, 166:1502-1507.
 161. Malik E, Meyhofer-Malik A, Berg C, Bohm W, Kunzi-Rapp K, Diedrich K, Ruck A: Fluorescence diagnosis of endometriosis on the chorioallantoic membrane using 5-aminolaevulinic acid. *Hum Reprod* 2000, 15:584-588.
 162. Zenzen V, Zankl H: Protoporphyrin IX-accumulation in human tumor cells following topical ALA- and h-ALA-application in vivo. *Cancer Lett* 2003, 202:35-42.
 163. Waidelich R, Beyer W, Knuchel R, Stepp H, Baumgartner R, Schroder J, Hofstetter A, Kriegmair M: Whole bladder photodynamic therapy with 5-aminolevulinic acid using a white light source. *Urology* 2003, 61:332-337.
 164. Gronlund-Pakkanen S, Pakkanen TM, Talja M, Kosma VM, Ala-Opas M, Alhava E: The morphological changes in rat bladder after photodynamic therapy with 5-aminolaevulinic acid-induced protoporphyrin IX. *BJU Int* 2000, 86:126-132.
 165. Van Staveren HJ, Beek JF, Verlaan CW, Edixhoven A, De Reijke TM, Brutel De La Rivi EG, Star WM: Comparison of normal piglet bladder damage after PDT with oral or intravesical administration of ALA. *Lasers Med Sci* 2002, 17:238-245.
 166. Vaucher L, Jichlinski P, Lange N, Ritter-Schenk C, van den Bergh H, Kucera P: Hexyl-aminolevulinic acid-mediated photodynamic therapy: how to spare normal urothelium. An in vitro approach. *Lasers Surg Med* 2007, 39:67-75.
 167. Jones SA, Martin GP, Brown MB: Determination of polyvinylpyrrolidone using high-performance liquid chromatography. *J Pharm Biomed Anal* 2004, 35:621-624.
 168. Valenta C, Auner BG: The use of polymers for dermal and transdermal delivery. *Eur J Pharm Biopharm* 2004, 58:279-289.
 169. Petrov P, Trukhachova T, Isakau H, Stawinski T, Adamkiewicz M, Mirek S: Novel association, a method of its preparation and its uses. In <http://www.freepatentsonline.com/20050265954.html>; 2005.
 170. Kongshaug M: Distribution of tetrapyrrole photosensitizers among human plasma proteins. *Int J Biochem* 1992, 24:1239-1265.
 171. Sasnouski S, Kachatkou D, Zorin V, Guillemin F, Bezdetsnaya L: Redistribution of Foscan from plasma proteins to model membranes. *Photochem Photobiol Sci* 2006, 5:770-777.
 172. Mojzisoava H, Bonneau S, Vever-Bizet C, Brault D: The pH-dependent distribution of the photosensitizer chlorin e6 among plasma proteins and membranes: a physico-chemical approach. *Biochim Biophys Acta* 2007, 1768:366-374.
 173. Rosenberger V, Margalit R: Thermodynamics of the binding of hematoporphyrin ester, a hematoporphyrin derivative-like photosensitizer, and its components to human serum albumin, human high-density lipoprotein and human low-density lipoprotein. *Photochem Photobiol* 1993, 58:627-630.
 174. Sasnouski S, Zorin V, Khludayev I, D'Hallewin MA, Guillemin F, Bezdetsnaya L: Investigation of Foscan interactions with plasma proteins. *Biochim Biophys Acta* 2005, 1725:394-402.
 175. Yamaguchi M, Tanabe S, Nakajima S, Takemura T, Ogita K, Kuwayama H, Sakata I, Miyaki S, Suzuki K, Namiki H, et al: Comparison of nonmetal and metal

-
- hydrophilic photosensitizer, ATX-S10 (Na) and ATN-2, binding with human serum proteins using spectrophotometry. *Photochem Photobiol* 2004, 80:262-266.
176. Beltramini M, Firey PA, Ricchelli F, Rodgers MA, Jori G: Steady-state and time-resolved spectroscopic studies on the hematoporphyrin-lipoprotein complex. *Biochemistry* 1987, 26:6852-6858.
177. Verchere-Beaur C, Mikros E, Perree-Fauvet M, Gaudemer A: Structural studies of metalloporphyrins. Part XIa: Complexes of water-soluble zinc(II) porphyrins with amino acids: influence of ligand-ligand interactions on the stability of the complexes. *J Inorg Biochem* 1990, 40:127-139.
178. Vermathen M, Vermathen P, Simonis U, Bigler P: Time-dependent interactions of the two porphyrinic compounds chlorin e6 and mono-L-aspartyl-chlorin e6 with phospholipid vesicles probed by NMR spectroscopy. *Langmuir* 2008, 24:12521-12533.
179. Cohen S, Margalit R: Binding of porphyrin to human serum albumin. Structure-activity relationships. *Biochem J* 1990, 270:325-330.
180. Verma S, Watt GM, Mai Z, Hasan T: Strategies for enhanced photodynamic therapy effects. *Photochem Photobiol* 2007, 83:996-1005.
181. Korbelik M: Low density lipoprotein receptor pathway in the delivery of Photofrin: how much is it relevant for selective accumulation of the photosensitizer in tumors? *J Photochem Photobiol B* 1992, 12:107-109.
182. Misawa J, Moriwaki S, Kohno E, Hirano T, Tokura Y, Takigawa M: The role of low-density lipoprotein receptors in sensitivity to killing by Photofrin-mediated photodynamic therapy in cultured human tumor cell lines. *J Dermatol Sci* 2005, 40:59-61.
183. Nakamura Y, Yamamoto M, Kumamaru E: Very low-density lipoprotein receptor in fetal intestine and gastric adenocarcinoma cells. *Arch Pathol Lab Med* 2000, 124:119-122.
184. Webb DJ, Nguyen DH, Sankovic M, Gonias SL: The very low density lipoprotein receptor regulates urokinase receptor catabolism and breast cancer cell motility in vitro. *J Biol Chem* 1999, 274:7412-7420.
185. Kessel D, Whitcomb KL, Schulz V: Lipoprotein-mediated distribution of N-aspartyl chlorin-E6 in the mouse. *Photochem Photobiol* 1992, 56:51-56.
186. Allison BA, Pritchard PH, Levy JG: Evidence for low-density lipoprotein receptor-mediated uptake of benzoporphyrin derivative. *Br J Cancer* 1994, 69:833-839.
187. England IG, Naess L, Blomhoff R, Berg T: Uptake, intracellular transport and release of ¹²⁵I-poly(vinylpyrrolidone) and [¹⁴C]-sucrose-asialofetuin in rat liver parenchymal cells. Effects of ammonia on the intracellular transport. *Biochem Pharmacol* 1986, 35:201-208.
188. Ogura S, Yazaki K, Yamaguchi K, Kamachi T, Okura I: Localization of poly-L-lysine-photosensitizer conjugate in nucleus. *J Control Release* 2005, 103:1-6.
189. Sherif A, Jonsson MN, Wiklund NP: Treatment of muscle-invasive bladder cancer. *Expert Rev Anticancer Ther* 2007, 7:1279-1283.
190. Sim HG, Lau WK, Cheng CW: A twelve-year review of radical cystectomies in Singapore General Hospital. *Ann Acad Med Singapore* 2002, 31:645-650.
191. Pinthus JH, Bogaards A, Weersink R, Wilson BC, Trachtenberg J: Photodynamic therapy for urological malignancies: past to current approaches. *J Urol* 2006, 175:1201-1207.
192. Jichlinski P: Photodynamic applications in superficial bladder cancer: facts and hopes! *J Environ Pathol Toxicol Oncol* 2006, 25:441-451.
193. Nseyo UO: Photodynamic therapy in the management of bladder cancer. *J Clin Laser Med Surg* 1996, 14:271-280.

-
194. Kausch I, Doehn C, Jocham D: Recent improvements in the detection and treatment of nonmuscle-invasive bladder cancer. *Expert Rev Anticancer Ther* 2006, 6:1301-1311.
 195. Szeimies RM, Landthaler M: Photodynamic therapy and fluorescence diagnosis of skin cancers. *Recent Results Cancer Res* 2002, 160:240-245.
 196. Thong PS, Ong KW, Goh NS, Kho KW, Manivasager V, Bhuvanewari R, Olivo M, Soo KC: Photodynamic-therapy-activated immune response against distant untreated tumors in recurrent angiosarcoma. *Lancet Oncol* 2007, 8:950-952.
 197. Roberts WG, Smith KM, McCullough JL, Berns MW: Skin photosensitivity and photodestruction of several potential photodynamic sensitizers. *Photochem Photobiol* 1989, 49:431-438.
 198. Chin WW, Heng PW, Thong PS, Bhuvanewari R, Hirt W, Kuenzel S, Soo KC, Olivo M: Improved formulation of photosensitizer chlorin e6 polyvinylpyrrolidone for fluorescence diagnostic imaging and photodynamic therapy of human cancer. *Eur J Pharm Biopharm* 2008.
 199. Thong PS, Olivo M, Kho KW, Bhuvanewari R, Chin WW, Ong KW, Soo KC: Immune response against angiosarcoma following lower fluence rate clinical photodynamic therapy. *J Environ Pathol Toxicol Oncol* 2008, 27:35-42.
 200. Kopriva I, Persin A, Zorc H, Pasic A, Lipozencic J, Kostovic K, Loncaric M: Visualization of basal cell carcinoma by fluorescence diagnosis and independent component analysis. *Photodiagnosis and Photodynamic Therapy* 2007, 4:190-196.
 201. Nseyo UO, Shumaker B, Klein EA, Sutherland K: Photodynamic therapy using porfimer sodium as an alternative to cystectomy in patients with refractory transitional cell carcinoma in situ of the bladder. Bladder Photofrin Study Group. *J Urol* 1998, 160:39-44.
 202. Gronlund-Pakkanen S, Wahlfors J, Talja M, Kosma VM, Pakkanen TM, Ala-Opas M, Alhava E, Moore RB: The effect of photodynamic therapy on rat urinary bladder with orthotopic urothelial carcinoma. *BJU Int* 2003, 92:125-130.
 203. Shackley DC, Briggs C, Whitehurst C, Betts CD, O'Flynn KJ, Clarke NW, Moore JV: Photodynamic therapy for superficial bladder cancer. *Expert Rev Anticancer Ther* 2001, 1:523-530.
 204. Kessel D: Pharmacokinetics of N-aspartyl chlorin e6 in cancer patients. *J Photochem Photobiol B* 1997, 39:81-83.
 205. D'Hallewin MA, Kamuhabwa AR, Roskams T, De Witte PA, Baert L: Hypericin-based fluorescence diagnosis of bladder carcinoma. *BJU Int* 2002, 89:760-763.
 206. Jichlinski P, Wagnieres G, Forrer M, Mizeret J, Guillou L, Oswald M, Schmidlin F, Graber P, Van den Bergh H, Leisinger HJ: Clinical assessment of fluorescence cytometry during transurethral bladder resection in superficial bladder cancer. *Urol Res* 1997, 25 Suppl 1:S3-6.
 207. Harty JI, Amin M, Wieman TJ, Tseng MT, Ackerman D, Broghamer W: Complications of whole bladder dihematoporphyrin ether photodynamic therapy. *J Urol* 1989, 141:1341-1346.
 208. Kubin A, Meissner P, Wierrani F, Burner U, Bodenteich A, Pytel A, Schmeller N: Fluorescence Diagnosis of Bladder Cancer with New Water Soluble Hypericin Bound to Polyvinylpyrrolidone: PVP-Hypericin. *Photochem Photobiol* 2008, 84:1560-1563.
 209. Syrigos KN, Harrington KJ, Pignatelli M: Role of adhesion molecules in bladder cancer: an important part of the jigsaw. *Urology* 1999, 53:428-434.
 210. Taniguchi K, Koga S, Nishikido M, Yamashita S, Sakuragi T, Kanetake H, Saito Y: Systemic immune response after intravesical instillation of bacille Calmette-

-
- Guerin (BCG) for superficial bladder cancer. *Clin Exp Immunol* 1999, 115:131-135.
211. Elsasser-Beile U, Gutzeit O, Bauer S, Katzenwadel A, Schultze-Seemann W, Wetterauer U: Systemic and local immunomodulatory effects of intravesical BCG therapy in patients with superficial urinary bladder carcinomas. *J Urol* 2000, 163:296-299.
212. Nseyo UO, Whalen RK, Duncan MR, Berman B, Lundahl SL: Urinary cytokines following photodynamic therapy for bladder cancer. A preliminary report. *Urology* 1990, 36:167-171.
213. Zhang Y, Mahendran R, Yap LL, Esuvaranathan K, Khoo HE: The signalling pathway for BCG-induced interleukin-6 production in human bladder cancer cells. *Biochem Pharmacol* 2002, 63:273-282.
214. Leibovici D, Grossman HB, Dinney CP, Millikan RE, Lerner S, Wang Y, Gu J, Dong Q, Wu X: Polymorphisms in inflammation genes and bladder cancer: from initiation to recurrence, progression, and survival. *J Clin Oncol* 2005, 23:5746-5756.
215. Shackley DC, Briggs C, Gilhooley A, Whitehurst C, O'Flynn KJ, Betts CD, Moore JV, Clarke NW: Photodynamic therapy for superficial bladder cancer under local anaesthetic. *BJU Int* 2002, 89:665-670.

APPENDIX A

LIST OF PUBLICATIONS

This thesis is based on the following original publications:

1. Ramaswamy B, Manivasager V, Chin WW, Soo KC, Olivo M. Photodynamic diagnosis of a human nasopharyngeal carcinoma xenograft model using the novel Chlorin e6 photosensitizer Fotolon. *Int J Oncol*. 2005 Jun;26(6):1501-6.
2. Chin WW, Lau W, Heng PWS, Ramaswamy B, Olivo M. Chlorin e6-polyvinylpyrrolidone as a fluorescent marker for fluorescence diagnosis of human bladder cancer implanted on the chick chorioallantoic membrane model. *Cancer Lett*. 2007 Jan 8;245(1-2):127-33. Epub 2006 Mar 3.
3. Chin WW, Lau W, Heng PWS, Ramaswamy B, Olivo M. Fluorescence imaging and phototoxicity effects of new formulation of chlorin e6-polyvinylpyrrolidone. *Photochem Photobiol B*. 2006 Aug 1;84(2):103-10. Epub 2006 Mar 20.
4. Chin WW, Heng PW, Bhuvanewari R, Lau WK, Olivo M. The potential application of chlorin e6-polyvinylpyrrolidone formulation in photodynamic therapy. *Photochem Photobiol Sci* Nov;5(11):1031-7. Epub 2006 Sep 21.
5. Chin WW, Heng PW, Thong SP, Bhuvanewari R, Kuenzel S, Hirt W, KC Soo, Olivo M. Improved formulation of photosensitizer chlorin e6-polyvinylpyrrolidone for fluorescence diagnostic imaging and photodynamic therapy of human cancer. *European Journal of Pharmaceutics and Biopharmaceutics*, 2008 Aug;69(3):1083-93. Epub 2008 Mar 10.
6. Chin WW, Ramaswamy B, Thong PSP, Heng PWS, Gan YY, Soo KC, Olivo M. Fluorescence guided photodynamic therapy of cancer using biophotonics strategies: Preclinical and early clinical studies. *SGH Proceedings*, Vol 16, No 3: 118-126, 2007.

-
7. Chin WW, Heng PWS, Olivo M. Chlorin e6 – polyvinylpyrrolidone mediated photosensitization is effective against human non-small cell lung carcinoma compared to small cell lung carcinoma xenografts. *BMC Pharmacol.* 2007 Dec 1;7(1):15
 8. Chin WW, Heng PWS, Lau WK, Lim PL, Olivo M. Membrane transport enhancement of chlorin e6 - polyvinylpyrrolidone and its photodynamic efficacy on the chick chorioallantoic model. *Journal of Biophotonics*, 1–13 (2008) / DOI 10.1002/jbio.200810005.
 9. Chin WW, Thong PSP, Lau WK, Bhuvanewari R, Soo KC, Heng PW, Olivo M. Fluorescence imaging and spectroscopy of the photosensitizer chlorin e6-polyvinylpyrrolidone for cancer tissue differentiation. *BMC Med Imaging.* 2009 Jan 8;9(1):1. [Epub ahead of print]
 10. Thong PS, Olivo M, Kho KW, Bhuvanewari R, Chin WW, Ong KW, Soo KC. Immune response against angiosarcoma following lower fluence rate clinical photodynamic therapy. *J Environ Pathol Toxicol Oncol.* 2008;27(1):35-42.
 11. Chin WW, Thoniyot P, Heng PWS, Olivo M. Effect of polyvinylpyrrolidone on the interaction of chlorin e6 with plasma proteins and its subcellular localization. Manuscript submitted to *European Journal of Pharmaceutics and Biopharmaceutics*, 2010

APPENDIX B

LIST OF CONFERENCE PARTICIPATION

In addition to the above papers, the content of the thesis was also presented in the following conferences and proceeding:

1. Chin WW, Thong PSP, Bhuvanewari R, KC Soo, Heng PW, Olivo M. Chlorin e6-polyvinylpyrrolidone induced fluorescence endoscopy and spectroscopy for in vivo cancer diagnostics. Optics Within Life Sciences –10th Biophotonics Asia, 2 – 4 July, 2008, Singapore. *Poster presentation*
2. Chin WW, Heng PW, Lau WK, Lim PL, Bhuvanewari R, Thong PSP, Olivo M. Fluorescence kinetics and drug transport of chlorin e6 – polyvinylpyrrolidone for photodynamic applications of urological cancer. American Society for Photobiology (ASP) 2008, Burlingame, CA, June 20 – 25, 2008. *Oral presentation. Recipient of Frederick Urbach Travel Award for 34th Meeting of the American Society for Photobiology 2008*
3. Chin WW, Lau WK, Heng PWS, Lim PL, Olivo M. Membrane transport enhancement of chlorin e6 - polyvinylpyrrolidone and its photodynamic efficacy on the chick chorioallantoic model. SGH 17th Annual Scientific Meeting, 25th – 26th April 2008, Singapore. *Oral presentation. Awarded as Best Scientist Oral Paper*
4. Chin WW, Heng PWS, Lau WK, Lim PL, Bhuvanewari R, Gulam Razul S, Olivo M. Chlorin e6 – polyvinylpyrrolidone selectively accumulates and causes photodynamic damage in human bladder carcinoma: From chick chorioallantoic membrane model to clinical patients. 12th European Society for Photobiology 2007 - University of Bath, U.K., September 1-6, 2007. *Poster presentation. Recipient of European Society for Photobiology Travel Fellowship for 12th Congress of the European Society for Photobiology*
5. Chin WW, Heng PWS, Ramaswamy B, Lau KO, Thong PSP, Soo KC, Lim PL, Olivo M. A dual-modality photosensitizer for fluorescence diagnosis and

photodynamic therapy: A biophotonic application in oncology. SGH 16th Annual Scientific Meeting, 27th – 28th April 2007, Singapore. *Oral presentation. Finalist for Best Scientist Oral Paper*

6. Chin WW, Heng PWS, Lau WKO, Dill O, Kuenzel S, Hirt W, Soo KC, Olivo M. Effect of polyvinylpyrrolidone on the trisodium salt of chlorin e6 for in vitro and in vivo photodynamic application in human carcinoma cells. 11th World Congress of the International Photodynamic Association 2007, March 28-31, 2007, Shanghai, China. *Oral presentation. Recipient of Prof. Thomas J. Dougherty Oncologic Foundation of Buffalo Travel Fellowship for 11th World Congress of the International Photodynamic Association*
7. Chin WW, Heng PWS, Bhuvanewari R, Dill O and Olivo M. Investigation of antitumor efficacy using chlorin e6-polyvinylpyrrolidone in cancer models. The 33rd Meeting of the American Society for Photobiology and the Photostability of Drug and Drug Products Group. Rio Grande, Puerto Rico. July 8-12, 2006. *Oral presentation*
8. Chin WW, Olivo M, and Heng PWS. Chlorin e6-polyvinylpyrrolidone as a fluorescent marker for photodynamic diagnosis of human bladder cancer using the chick chorioallantoic membrane model. Inaugural American Association of Pharmaceutical Science-NUS Student Chapter Symposium, 16 September 2005, Singapore. *Oral presentation*
9. Chin WW, Lau W, Ramaswamy B, Heng PWS, Olivo M. Assessment of photodynamic diagnosis and therapy of human bladder cancer on the chick chorioallantoic membrane (CAM) using Fotolon. 10th World Congress of the International Photodynamic Association, June 22–25, 2005, Munich, Germany. *Poster presentation*
10. Chin WW, Olivo M, Ramaswamy B, Heng PWS, Lau W. Therapeutic efficacy of chlorin e6 conjugated with polyvinyl pyrrolidone (Fotolon[®]) as a novel sensitizer for phototherapy. 10th World Congress of the International Photodynamic

Association, June 22–25, 2005 Munich, Germany. *Oral presentation. Recipient of Singapore Urological Association Travel Fellowship*

11. Chin WW, Olivo M, Heng PWS, Cheng C, Lau W. Assessment of Fotolon mediated photodynamic therapy. Urology Fair 2005, Singapore Urological Association, Singapore, 25-28 February 2005. *Oral presentation*

APPENDIX C

VITA

William Chin Wei Lim was born on April 7, 1979 in Kuala Lumpur, Malaysia. After attending public schools in Kuala Lumpur, he attended the University Malaysia Sabah, and received his B.Sc. (Hons) in Biotechnology in 2002. He was also awarded with the Dean's List Award for meritorious performance in that year. Upon graduation, he then went to Singapore and joined the Department of Urology at the Singapore General Hospital and worked as a Medical Technologist under the supervision of Associate Prof. Weber Lau Kam On (Senior Consultant and Director of Uro-Oncology of Singapore General Hospital) for 3 years. The following year, he joined National Cancer Centre Singapore as a Research Officer under the leadership of Prof. Malini Olivo. In 2005, William then pursued a part time PhD from the National University of Singapore at the Department of Pharmacy under the supervision of Prof. Malini Olivo and Associate Prof. Paul Heng. Throughout his 6 years of research career, he has published a total of 21 papers in peer-reviewed journals and 26 conference proceedings in the area of photobiology and photomedicine. In the period of Jul-Sept 2006, his paper published in the Journal of Photochemistry and Photobiology B: Biology was selected as top 25 most read article, counted by article downloads on ScienceDirect. In 2008, his paper published in BioMed Central Pharmacology was cited as highly accessed article within the journal. He was also invited as an ad-hoc reviewer for Journal of Signal Processing Systems (Biomedical Imaging) and Journal of Veterinary Science. In addition, he has successfully obtained a total amount of SGD 1.01 million grant support from the Singapore General Hospital and National Medical Research Council of Singapore to initiate research projects at the National Cancer Centre Singapore and the Department of Pharmacy, NUS. He has won numerous travel and fellowship awards from Singapore Urological Association, International Photodynamic Association and the American Society for Photobiology that supported his trip to international conferences. In April 2007, he was selected as one of the finalists in the oral presentation in Basic Science category at the Singapore General Hospital 16th Annual Scientific Meeting for his presentation entitled: A dual-modality photosensitizer for fluorescence diagnosis and photodynamic therapy: A biophotonic application in oncology. In June 2007, he was awarded with a highly prestigious Singapore Millennium Foundation Scholarship (<http://www.smf-scholar.org/>). In February 2008, he has mentored Mr Lin Yingbo from Raffles Junior College and their presentation entitled "Transport enhancement and improved selectivity of chlorin e6 – polyvinylpyrrolidone on the chorioallantoic tumor model" won a Silver Award in the Singapore Science and Engineering Fair 2008, a national competition organised by the Ministry of Education (MOE), the Agency for Science, Technology & Research (A*STAR) and the Science Centre Singapore (SCS). In April 2008, he was awarded with the Best Scientist Oral Paper at the Singapore General Hospital 17th Annual Scientific Meeting where he presented his work along with other prominent researchers within the Singhealth Medical Cluster. Subsequently, in May 2008, he was awarded with the European Society for Photobiology (ESP) Fellowship (Visits of Young Photobiologist in European Photobiology Laboratories). He has been chosen among several candidates on the basis of his scientific curriculum vitae by the ESP Education Committee (Miguel Angel Miranda Alonso (Chair), Spain; Thierry Douki, France; Paola Taroni, Italy). He is scheduled to complete his Ph.D. at the National University of Singapore in early 2009.